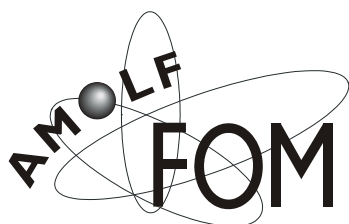


**Electrospray ionisation FT-ICR mass
spectrometry of linear and hyperbranched
polymers**

Cover design: Iliya Cerjak



The work described in this thesis was performed at the FOM-Institute for Atomic and Molecular Physics (AMOLF), Kruislaan 407, 1098 SJ Amsterdam, The Netherlands. It is part of the research program nr. 28 "Mass Spectrometry of Macromolecular systems" of the "Stichting voor Fundamenteel Onderzoek der Materie (FOM)" a subsidiary of the "Nederlandse organisatie voor Wetenschappelijke Onderzoek (NWO)". This project is financially supported by FOM, DSM Research (Geleen, the Netherlands) and Akzo Nobel Chemicals Research Arnhem (Arnhem, the Netherlands).

© Sander Koster, 2002.

Electrospray ionisation FT-ICR mass spectrometry of linear and hyperbranched polymers

ACADEMISCH PROEFSCHRIFT

ter verkrijging van de graad van doctor
aan de Universiteit van Amsterdam
op gezag van de Rector Magnificus
prof. mr. dr. P.F. van der Heijden

ten overstaan van een door het college voor promoties ingestelde
commissie, in het openbaar te verdedigen in de Aula der Universiteit
op vrijdag 15 februari 2002, te 12:00 uur

door

Sander Koster

geboren te Amsterdam

Promotiecommissie

Promotoren: prof. dr. J.J.Boon
 prof. dr. ing. R.M.A.Heeren

Overige leden: prof. dr. C.G. de Koster
 dr. M.W.F. Nielen
 dr. ing. H.J.A. Philipsen
 prof. dr. P.G. Kistemaker
 prof. dr. P.J. Schoenmakers
 prof. dr. H. Poppe

Faculteit der Natuurwetenschappen, Wiskunde en Informatica.

This thesis is based on the following publications:

Chapter 4

Endgroup Determination of Synthetic Polymers by Electrospray Ionisation Fourier Transform Ion Cyclotron Resonance Mass Spectrometry, S. Koster; M.C. Duursma; J.J. Boon; R.M.A. Heeren, *J. Am. Soc. Mass Spectrom.* **2000**, *11*, 536-543

Chapter 5

Quantitative Analysis of Copolymers: The Influence of the Structure of the Monomer on the Ionisation Efficiency in Electrospray Ionisation FTMS, S. Koster; B. Mulder; M.C. Duursma; J.J. Boon; H.J.A. Philipsen; J.W. v. Velde; M.W.F. Nielen; C.G. de Koster; R.M.A. Heeren, Submitted to *Macromolecules*

Chapter 6

Structural Analysis of Synthetic Homo- and Copolyesters by Electrospray Ionisation on a Fourier Transform Ion Cyclotron Resonance Mass Spectrometer, S. Koster; M.C. Duursma; J.J. Boon; M.W.F. Nielen; C.G. de Koster; R.M.A. Heeren, *J. Mass Spectrom.* **2000**, *35*, 739-748

Chapter 7

Structural Characterisation of Hyperbranched Polyesteramides: MSⁿ and the Origin of Species, S. Koster; C.G. de Koster; R.A.T.M. van Benthem; M.C. Duursma; J.J. Boon; R.M.A. Heeren, *Int. J. Mass Spectrom.*, **2001**, *210/211*, 591-602

Chapter 8

Isomer separation of hyperbranched polyesteramides with gasphase H/D exchange and a novel MSⁿ approach: DoDIP, S. Koster; M.C. Duursma; X. Guo; J.J.Boon; R.M.A. Heeren, C.G. Submitted to *JMS*

Chapter 9

Electron capture dissociation of hyperbranched polyesteramides S. Koster; S. Ingemann; C.G. de Koster; M.C. Duursma; J.J. Boon; R.M.A. Heeren, Submitted to *JASMS*

Other publications

Quantitative Analysis of Copolymers Based on Bayesian Probability Theory Applied to MS/MS Spectra, S. Koster; C.G. de Koster; R.M.A. Heeren; J.J. Boon; B. Mulder. In preparation.

Surface Characterization of Industrial Fibres with Inverse Gas Chromatography', A. Van Asten; N. Veenendaal; S. Koster *J. Chromatography A*, **2000**, *888*, 175-196.

Contents

1	General Introduction	1
1.1.	Polymer properties	2
1.1.1.	The molecular weight distribution (MWD)	2
1.1.2.	Endgroup and monomer composition	8
1.1.3.	Copolymer sequence	10
1.1.4.	Chemical composition distribution	14
1.2.	Scope of this thesis	15
2	Basics and experimental set-up of the ESI FT-ICR MS	17
2.1.	Electrospray ionisation (ESI)	17
2.2.	Fourier transform ion cyclotron resonance mass spectrometry (FT-ICR MS)	19
2.2.1.	The cyclotron motion	20
2.2.2.	Excitation and detection	23
2.2.3.	Collisional excitation for fragmentation	25
2.2.4.	Instrumental layout and experimental procedures for ESI FT-ICR MS analysis	27
3	Characterisation of the molecular weight distribution of polyoxyalkylenes	33
3.1	Introduction	33
3.2.	Experimental	35
3.3.	Results and discussion	35
3.3.1.	Charge state dependence of M_p , M_n and M_w	37
3.3.2.	Dependence of the monomer length/structure on the observed charge states	39
3.3.3.	Reconstruction of the molecular weight distribution	40
3.4.	Conclusion	42

4	Accurate determination of the polymer endgroup and monomer mass of polyoxyalkylenes	43
4.1.	Introduction	43
4.2.	Experimental	44
4.3.	Results and discussion	45
	4.3.1. Theory of the endgroup determination using the linear regression and averaging methods with ESI	46
	4.3.2. Results of the endgroup determination using the linear regression and averaging methods	49
	4.3.3. Endgroup determination combining all charge states	53
	4.3.4. Comparison of the endgroup accuracy determined with ESI and MALDI FT-ICR MS	54
4.4.	Conclusions	56
5	Quantitative analysis of copolymers: The influence of the monomers on the ionisation efficiency in ESI	59
5.1.	Introduction	59
5.2.	Methods and materials	61
	5.2.1. ESI FT-ICR MS analysis	61
	5.2.2. GPEC ESI TOF analysis	62
	5.2.3. Materials	62
	5.2.4. Copolymerisation models	63
	5.2.4.1. Markovian chain statistical model	63
	5.2.4.2. Bernoullian chain statistical model	67
5.3.	Results and discussion	68
	5.3.1. ESI FT-ICR MS spectra of copolyesters	68
	5.3.2. Copolymerisation statistics applied to mass spectra	69
	5.3.3. Polyester quantification with GPEC	72
	5.3.4. Electrospray ionisation efficiency (IE)	74
5.4.	Conclusions	78

6	Sequence analysis of synthetic copolyesters by ESI FT-ICR MS	81
6.1.	Introduction	81
6.2.	Methods and materials	83
6.2.1.	Methods	83
6.2.2.	Materials	84
6.3.	Results and discussion	84
6.3.1.	MS/MS of homopolyesters with two alcohol endgroups; (DA) ₂ D and (DI) ₂ D	86
6.3.2.	MS/MS of homopolyesters with one alcohol and one acid endgroup; (DA) ₃ and (DI) ₃	91
6.3.3.	MS/MS of copolyesters with one alcohol and one acid endgroup; (DA) ₂ (DI) and (DA)(DI) ₂	94
6.4.	Conclusions	97
7	Structural characterisation of hyperbranched polyesteramides: MSⁿ and the origin of species	99
7.1.	Introduction	99
7.2.	Methods and materials	101
7.2.1.	ESI FT-ICR MS analysis	101
7.2.2.	Hyperbranched polyesteramides	101
7.3.	Results and discussion	103
7.3.1.	The glutaric acid anhydride based polymer	105
7.3.2.	The succinic and 1,2-cyclohexane dicarboxylic acid anhydride based polymers	110
7.3.3.	The phthalic acid anhydride based polymer	110
7.3.3.	Origin of the oligomers P ₃ D ₄ -H ₂ O, S ₃ D ₄ -H ₂ O, G ₃ D ₄ -H ₂ O and C ₃ D ₄ -H ₂ O	112
7.4.	Conclusion	115

8	Isomer separation of hyperbranched polyesteramides with gas phase H/D exchange and a novel MSⁿ approach: DoDIP	117
8.1.	Introduction	118
8.2.	Experimental	119
8.3.	Results and discussion	120
8.3.1.	Dissociation of depleted ion populations (DoDIP) for isomer analysis	121
8.3.2.	Combined hydrogen/deuterium (H/D) exchange and MS ² for isomer analysis	128
8.3.3.	Combined MS ² and H/D exchange for the study of the fragmentation mechanism	133
8.3.4.	Other hyperbranched polyesteramides	135
8.4.	Conclusions	136
9	Electron capture dissociation of hyperbranched polyesteramides	139
9.1.	Introduction	139
9.2.	Experimental	141
9.3.	Results and discussion	142
9.3.1.	CAD	142
9.3.2.	ECD	149
9.4.	Comparison of CAD with ECD of doubly charged hyperbranched polymers and concluding remarks	163
	Bibliography	165
	Glossary of symbols and abbreviations	177
	Summary	181
	Samenvatting	185
	Dankwoord	189

Chapter 1

General introduction

Research and development performed on synthetic polymers during the last century has led to many classes of different polymers for specific applications. New types of synthetic polymers with tailor-made properties are still being introduced for new applications or as an alternative for materials, like glass and metals. The challenge for polymer chemists is to control and alter the polymerisation conditions such that the final product has a well-defined structure with desired properties. The complex structure of polymers requires continued analytical chemical efforts to understand the polymerisation process and the relationships between the molecular structure and material properties. Actually, the research performed during the last century did not lead to a complete understanding of the microstructure of polymers. For many decades, research on the polymer composition has been performed primarily with techniques such as NMR, light scattering, IR, titration techniques and viscometry. These techniques provide a wealth of information on a large number of polymer characteristics. However, the main limitation of these techniques is that the result of the characterisation is an average over the entire molecular weight distribution (MWD). In order to obtain a complete picture of the molecular structure of synthetic polymers, techniques must be developed that enable the study of the individual components in the MWD separately.

Several liquid chromatographic separation techniques have been explored in order to obtain more detailed information about the molecular architecture and microstructure of individual polymer molecules in a MWD. Although it is possible to separate and quantify low molecular weight polymer molecules from a MWD and study their structure, molecules with a relatively high molecular weight (> 5000 Da) are still difficult to separate. Detailed analysis of the MWD is also possible using mass spectrometry, which measures the mass over charge ratio of ions rather than chemical shifts or the absorption/scattering of light. Especially, the soft ionisation techniques of matrix-assisted laser desorption/ionisation (MALDI) and electrospray ionisation (ESI) are of significant importance for polymer characterisation. These techniques allow the transfer of intact molecules into the

gas phase and their (subsequent) ionisation through cation transfer. In the next sections we will review the many polymer characteristics that can be studied by coupling these ionisation techniques with advanced mass analysers such as time-of-flight (TOF) and Fourier transform ion cyclotron resonance mass spectrometry (FT-ICR MS).

In this thesis, the soft ionisation nature of ESI is combined with FT-ICR MS for polymer analysis. One of the advantageous features of FT-ICR MS is that ions can be stored for a longer period of time in the ICR cell. This allows doing experiments for structural analysis with an unsurpassed resolution and mass accuracy. The analysis of micro-structural characteristics with mass spectrometry will be reviewed in section 1.1. Fundamental aspects of ESI and FT-ICR MS will be discussed in sections 2.1 and 2.2, respectively.

1.1. *Polymer properties*

Mass spectrometry has many advantages over other polymer characterisation techniques, because it measures the mass over charge ratio of ions allowing the study of the individual polymer molecules. Mass spectrometry also has its limitations. For example, a mass spectrometric analysis is seldom quantitative. In addition, a mass spectrometric analysis requires ions that have to be generated from the sample. Some polymers, such as polyolefins, are difficult or even impossible to ionise, because the binding energy of a cation with these apolar polymers is too small to survive the conditions in the ion source.¹

The most important polymer micro-structural characteristics that are studied with mass spectrometry are summarised in figure 1.1 and include the MWD, endgroup and monomer composition, copolymer sequence, copolymer chemical composition distribution and branching. These micro-structural characteristics will be reviewed in the next sections that focus mainly on MALDI and ESI coupled with TOF and FT-ICR MS because these ionisation techniques and mass analysers have revolutionised the characterisation of synthetic polymers.

1.1.1. *The molecular weight distribution (MWD)*

Most polymerisation reactions generate a molecular weight distribution (MWD) of structurally similar molecules that differ in their degree of polymerisation n , defined as the number of building blocks (monomers) in a polymer molecule. These structurally similar molecules are called oligomers when the degree of polymerisation is below 10. Larger molecules are called polymer

molecules. The MWD is a result of the statistical nature of the polymerisation process. Three parameters are often used to define the MWD: the number average molecular weight (M_n), the weight average molecular weight (M_w) and the polydispersity (D).²⁻⁴ The M_n , M_w and D are defined as follows:

$$M_n = \frac{\sum_i n_i m_i}{\sum_i n_i} \quad (1.1)$$

$$M_w = \frac{\sum_i n_i m_i^2}{\sum_i n_i m_i} \quad (1.2)$$

$$D = \frac{M_w}{M_n} \quad (1.3)$$

where n_i is the number of polymer molecules and m_i the molecular weight. The molecular weight and shape of the MWD formed in the polymerisation reaction can be controlled by, for example, the variation of the monomer feed.

Mass spectrometry can be used to obtain information about M_n , M_w and D for a large variety of polymer classes. The ionisation techniques that have been used for this purpose include fast atom bombardment,^{5,6} field desorption,⁶⁻⁹ potassium ionisation of desorbed species (K^+IDS),^{10,11} laser desorption ionisation,¹²⁻¹⁵ electrohydrodynamic ionisation,¹⁶ secondary ion mass spectrometry,^{6,17} ²⁵²Cf fission fragment ionisation,¹⁸ matrix-assisted laser desorption/ionisation (MALDI) and electrospray ionisation (ESI). MALDI and ESI are currently the most important ionisation techniques used for polymer analysis as will be discussed in the next two sections.

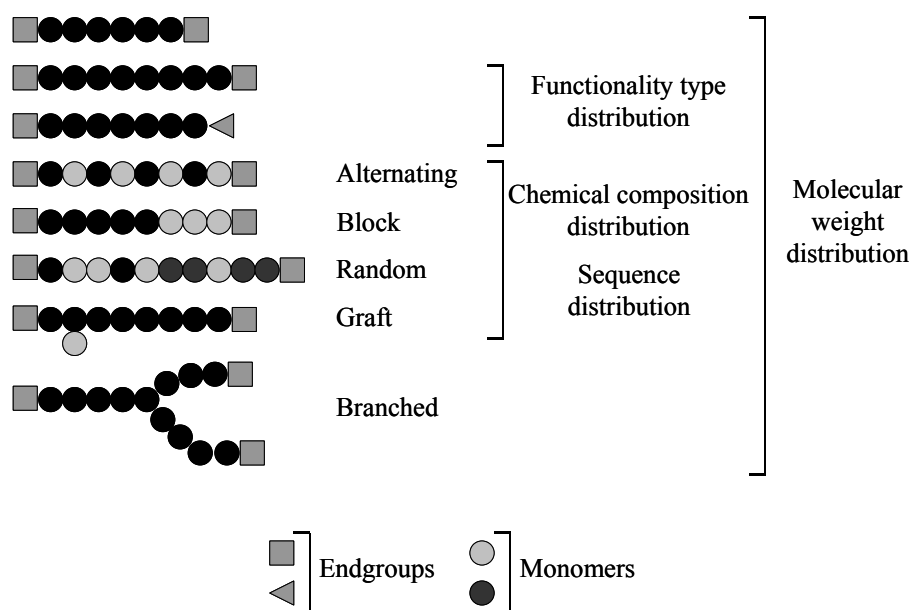


Figure 1.1 *Molecular architecture and microstructure of synthetic polymers.*

1.1.1.1. Analysis of the molecular weight distribution with MALDI MS

MALDI was first used for the characterisation of the synthetic polymers poly(ethylene glycol), poly(propylene glycol), poly(methyl methacrylate) and poly(styrene) by Hillenkamp and coworkers in 1992.¹⁹ Since then, numerous studies have appeared in the literature in which polymers with a molecular weight exceeding 1.500.000 Da could be ionised and detected without observed fragmentation.²⁰⁻²⁴

The study of Hillenkamp and coworkers¹⁹ suggested that mass spectrometry was superior to size exclusion chromatography (SEC) for polymer MWD analysis. SEC is a widely used technique for MWD analysis that measures the hydrodynamic volume of polymers. Mass spectrometry provides an absolute mass analysis in contrast to SEC, which is difficult to calibrate. Good agreement of the M_w measured with SEC and mass spectrometry is generally obtained for polymers with a polydispersity lower than 1.1.^{19-21,25,26} However, polymers with a polydispersity larger than 1.1 analysed with MALDI TOF-MS yield molecular weight distributions that deviate dramatically from the distributions obtained with SEC.^{22,23,25,27-32} Note that a fundamental difference exists between SEC and mass spectrometry. SEC measures the weight fraction versus the logarithm of the molar mass while mass spectrometry measures the number fraction versus the mass over

charge ratio (m/z). These differences must be corrected in order to obtain MWD values that can be compared.^{4,31}

The discrepancies in the measured MWD between SEC and MALDI MS are, among others, caused by instrumental parameters and the preparation of the sample. The M_n and M_w of a polystyrene sample depended significantly on the lab where the polymer was studied.³³ The matrix,^{22,27,34-37} matrix/analyte ratio,³⁸ type of cation,^{22,35,37,39-44} cation concentration,³⁸ pH, and solvents^{40,45} have a large influence on the observed MWD of a sample. Electrospray or pneumatically assisted matrix deposition can be performed for a good co-crystallisation of the matrix, analyte, and cation.⁴⁶ This enhances the S/N, shot-to-shot and spot-to-spot reproducibility. The laser power,^{27,28,35,36,47,48} ionisation efficiency, transmission,⁴⁹ and detection efficiency^{28,49} are instrumental parameters that influence the measured MWD.

Accurate MWD analysis can only be performed with mass spectrometry if the mass discrimination effects mentioned above are absent and the response of the detector is quantitative. Shimada and coworkers were able to study these effects for a polystyrene sample with MALDI TOF. They fractionated a low molecular weight polystyrene sample with supercritical fluid extraction. Polymer molecules up to a degree of polymerisation 25 were fractionated. This allowed them to perform experiments with equimolar and equiweight mixtures of these polymer molecules and to study the MS response. They observed that oligomers smaller than $n=5$ were systematically lowest in intensity which they attributed to evaporation in the mass spectrometer due to the low boiling point of small oligomers. Mass discrimination effects increased for large polymer molecules with increasing laser power. These effects made it impossible to perform an accurate MWD analysis.⁴⁸

The experimental and instrumental parameters mentioned above, with the exception of the evaporation of small oligomers of PS, result primarily in a decreased sensitivity for higher molecular weight polymer molecules. To prevent discrimination, the sample can be fractionated into monodisperse fractions with SEC prior to the analysis with MALDI TOF. The fractions are collected off-line into fractions with a polydispersity lower than 1.1. An on-line study with aerosol MALDI has also been performed.⁵⁰ Fractionation allows the determination of the average mass of the fractions with MALDI TOF and is used to calibrate the SEC system.^{22,23,29,36}

For some polymers, a higher resolution than TOF is required to resolve all polymer molecules. An example is the copolymer poly(ethylene glycol/propylene glycol) (EO/PO) for which only FT-ICR MS provides enough resolution to resolve the polymer molecules in the MWD.⁵¹ One has to take into account that the MALDI process leads to ions with a broad, mass independent velocity distribution.

Consequently, the polymer molecules of the MWD will enter the ICR cell at a different time due to the mass dependent kinetic energy. This time-of-flight effect can be corrected by acquiring mass spectra at different trapping times. The spectra acquired should be superimposed to yield the correct molecular weight distribution.⁵²⁻⁵⁷ Note that this is only true for external ion sources.

It has been discussed that MALDI is very useful for polymer MWD analysis although a combination with liquid chromatographic techniques like SEC gives the best results. However, a more facile MWD determination with SEC and mass spectrometry becomes possible when ESI is used as ionisation technique since ESI can be coupled online to most mass analysers as will be discussed in the next section.

1.1.1.2. Analysis of the molecular weight distribution with ESI MS

Dole and coworkers reported in 1968 the electrospray ionisation of polystyrene with a molecular weight up to 411,000 Da using a Faraday cage detector.⁵⁸ Their conclusions have been subject to discussion because it was uncertain whether singly or multiply charged ions were formed.^{59,60} Fenn and coworkers coupled ESI with mass spectrometry two decades later^{60,61} and were able to ionise poly(ethylene glycol) (PEG) samples with a molecular weight of 400 up to 5,000,000 Da.^{62,63} Charge states up to 4200+ were estimated for PEG5,000,000. The maximum charge state that they could distinguish was 6+ for PEG3350 based on the spacing between the polymer ions in the mass spectrum. PEG has a monomer mass of 44 Da. For singly charged ions, the peaks in the mass spectrum will be separated by 44. For charge state 6 the spacing is $44/6=7.3$. Their results clearly demonstrate that the polymer MWD could be measured in the mass range of their quadrupole mass analyser because of the multiply charged nature of ions generated by ESI. The peak density in the mass spectrum, however, became too high to resolve the peaks of PEG samples with a molecular weight higher than 3350 Da. A resolved analysis of all polymer molecules is a prerequisite for the calculation of M_n and M_w with ESI MS. A fairly good agreement of M_n and M_w , obtained with SEC and ESI, was observed for ethoxylated polymers (Surfonyl) with a molecular weight below 1300 Da.⁶

To determine the M_n and M_w of polymers with a high molecular weight, a mass spectrometer with sufficient resolution is required for isotopic resolved analysis. Alternatively, distinguishing between the different polymer molecules is sufficient. The analysis of poly(ethylene glycol) with a molecular weight of 24,000 Da was performed with isotopic resolution by coupling ESI with FT-ICR MS.⁶⁴ The mass spectrum observed allowed to determine the charge state by measuring

the spacing between the isotopic peaks. The M_n and M_w were calculated and found to increase with increasing charge state. When the MWD's observed in the different charge states were summed, a fairly good comparison with SEC was obtained.⁶⁴ The same effect has been observed for PMMA.⁶⁵ The polymer molecules of a dendrimer with a molecular weight of 1.000.000 Da could not be resolved with ESI FT-ICR MS making the determination of M_n and M_w of such polymers difficult.⁶⁶

An important factor that has to be taken into account for an accurate determination of the MWD is the ionisation efficiency of the different polymer molecules. A linear response independent of the polymeric structure over the entire m/z range is a prerequisite for an accurate MWD determination with mass spectrometry. The appearance of the MWD is determined by the type of polymer (polar/apolar),^{67,68} polydispersity, spray solvent composition, pH or cation used,^{69,70} counter ion,⁷¹ nozzle skimmer potential,^{65,68,72-75} and charge state. The tacticity of isotactic and syndiotactic PMMA did not influence the instrumental response and charge state.⁶⁵ The response was linear for a mixture of the 25 and 50-mer of PMMA after the signal was corrected for charge state compression.⁶⁵ Maziarz and coworkers observed a preferential ionisation of poly(ethylene glycol) in a mixture of poly(ethylene glycol) and poly(dimethylsiloxane). They also observed differences in ionisation efficiency for a mixture of two poly(dimethylsiloxanes) differing only in their endgroups.⁶⁷ These results showed that differences in ionisation efficiency have to be tested and corrected for to obtain accurate information about the MWD and the relative composition in polymer blends with mass spectrometry.

Probably the most convenient and accurate method of measuring the MWD with mass spectrometry is by coupling size exclusion chromatography (SEC) online with ESI, although off-line coupling with SEC has also been performed.^{36,76} Differences in the ionisation efficiency between various polymer molecules are less relevant when SEC is coupled with mass spectrometry because the polymer concentration is recorded with, for example, a UV detector. The main function of the mass spectrometer is to convert the measured hydrodynamic volume to a molecular weight. Mass analysers that have been used for the coupling of SEC with ESI include quadrupoles,⁷⁷⁻⁷⁹ TOF,^{80,81} and FT-ICR MS.^{82,83} Gradient polymer elution chromatography (GPEC) and liquid chromatography at the critical point of adsorption (LCCC) have been coupled with ESI as well.^{81,84}

Chapter 1

1.1.2. Endgroup and monomer composition

A polymer molecule consists of a chain of n monomers and, in case of linear polymer molecules, two endgroups. For example, a linear poly(ethylene glycol) $\text{HO}(\text{CH}_2\text{CH}_2\text{O})_n\text{H}$ contains the endgroups $-\text{OH}$ and $-\text{H}$. Cyclic polymer molecules do not contain endgroups. For branched polymers, the number of endgroups depends on the degree of branching. Polymer molecules with only one branching point will contain three endgroups. Dendrimers are highly branched structures and can contain more than 1000 endgroups.⁶⁶ The study of endgroups and monomeric composition with mass spectrometry became relatively easy since the beginning of the 1980's when ionisation techniques were used for polymer analysis that allowed the conversion of intact large polymer molecules into the gas phase. Ionisation techniques that have been used for endgroup analysis include electrohydrodynamic ionisation,¹⁶ ^{252}Cf fission fragment ionisation,¹⁸ laser desorption ionisation,^{12,13} potassium ionisation of desorbed species (K^+IDS),^{10,11} field desorption,^{7,9,59,85,86} FAB,^{5,87-91} and SIMS.¹⁷ Although these ionisation techniques are 'soft' in nature, fragmentation could not always be excluded making an unequivocal determination of the endgroup and monomer difficult. With the introduction of MALDI and ESI, fragmentation became minimal. The accurate determination of the endgroup and monomer composition became possible by coupling MALDI and ESI with high resolution mass spectrometers as discussed in the sections below.

1.1.2.1. Endgroup and monomer mass determined with MALDI MS

A linear regression method was introduced by de Koster and van Rooij, making it possible to determine the mass of the monomer and endgroup with a high accuracy.^{92,93} The measured mass of a polymer molecule, m_{meas} , consists of n monomers with mass m_{mon} , the mass of the endgroup m_{end} and the mass of the cation m_{cat} . The mass of an electron m_{elec} has to be considered when measuring with FT-ICR MS and must be subtracted from the neutral atom or molecule mass that is responsible for the charge to obtain the cation mass (e.g. $m_{atom}-m_{elec}$). The necessity of this correction was illustrated by the successful separation of a mixture of two peptides with a mass difference of 0.00045 Da, which is smaller than the mass of an electron.⁹⁴

$$m_{meas} = n \times m_{mon} + m_{end} + m_{cat} \quad (1.4)$$

By plotting the measured mass m_{meas} as a function of the degree of polymerisation n , the combined mass of the endgroups and cation can be determined from the intercept of the regression line. The mass of the monomer follows from the slope. The method has been applied successfully to linear and hyperbranched polymers.^{56,92,93,95,96} Unfortunately, the procedure depends heavily on the calibration of the instrument. An interlaboratory comparison of a polystyrene sample measured with MALDI TOF in 23 different laboratories has shown that calibration of the TOF MS is often a source of error. Endgroup masses were obtained which differed over 40 Da from the real endgroup mass.³³

One cannot distinguish between the composition of the endgroups from the head and tail from the chain with the linear regression procedure described above, because the method provides only the combined endgroup and cation mass. The identity of the endgroup composition from the head and tail can be obtained by performing MS/MS.^{59,97-104} Each peak in the MS/MS spectrum corresponds to a cleavage somewhere in the polymer backbone. A cleavage resulting in two cationised fragments provides the information on the elemental composition of both endgroups separately.

1.1.2.2. Endgroup and monomer mass determination with ESI

The elemental composition of polymer endgroups can be studied directly from the ESI mass spectrum⁷⁸ or by the MS/MS method as described for MALDI in the previous section.^{59,97-101} Linear regression methods, as used for MALDI generated ions (section 1.1.2.1), have not been reported for multiply charged ions generated by ESI. Linear regression was used in one ESI study on singly charged ions.¹⁰⁵ The endgroup composition of polysulfides,¹⁰⁶ aliphatic polyesters,^{107,108} and polypropylene glycols¹⁰⁹ has been studied using MSⁿ (n=2-4). Maziarz *et al.* used another approach, which did not require the isolation of a parent ion. They performed nozzle skimmer dissociation on the entire MWD of poly(dimethylsiloxane) to induce fragmentation. The fragments that were formed upon dissociation had m/z values intermediate to the original polymer distribution and were used to obtain endgroup information.¹¹⁰ Yalcin and coworkers also performed nozzle skimmer dissociation of the entire MWD and combined this with additional MS/MS on small fragments. A positive identification of the endgroup structure was obtained by comparing the fingerprint of the MS/MS spectrum with reference compounds.¹¹¹ McLafferty and coworkers used electron capture dissociation (ECD) on multiply charged polyethylene glycol and polypropylene glycol polymer molecules. This dissociation method provided direct endgroup

Chapter 1

information contrary to collisionally activated dissociation (CAD) where internal monomer losses and secondary dissociations were observed.¹¹²⁻¹¹⁴

1.1.3. Copolymer sequence

Copolymers are formed in a polymerisation reaction if two or more different monomers react together. The *intramolecular* arrangement of the monomers, the sequence, is determined by the reactivity of the monomers towards each other during the polymerisation process. The most frequently occurring sequences of the copolymer molecules formed are:

Random:

the monomers are distributed in a random fashion on each polymer molecule, -A-A-B-A-A-B-B-A-B-A-B-A-A-.

Block:

all A monomers are bound with other A's. The B monomers are bound with other B's with the exception of the central A-B bond, -A-A-A-A-A-B-B-B-B-B-B-.

Partly random/block:

the A monomers preferentially bind with other A's but have a slight tendency to connect to B monomers. This type of sequence is often called a statistical copolymer, -A-B-A-A-A-B-B-B-B-A-.

Alternating:

the A and B monomers are distributed in an alternating fashion on the polymer molecule, -A-B-A-B-A-B-A-B-A-B-.

Branched:

the copolymer sequences mentioned above are made by the polymerisation of monomers with a functionality of two. Each monomer can react with two other monomers leading to linear polymer chains. Branched copolymers on the contrary are made by the polymerisation of two (or more) monomers of which at least one contains a functionality higher than two, which results in a branched polymer.

Graft: the copolymer is branched where the branches consist of different monomers (e.g. A) as the polymer backbone (e.g. B). For example, the polymer backbone consists of monomers A only and the branches contain only monomers B.

1.1.3.1. Linear copolymers

The methodologies to determine the sequence of copolymers with mass spectrometry are similar for MALDI and ESI and will therefore be discussed together. Block copolymers have been observed by performing MS/MS or post source decay (PSD) after ionisation with FAB, MALDI, and ESI.¹¹⁵⁻¹¹⁸ A confirmation of the block structure is fairly straightforward. The monomeric composition of the polymer molecule can be determined from the m/z i.e. n A monomers and m B monomers. The sequence of the polymer molecule on the contrary does not follow from the measured m/z but requires MS/MS. The MS/MS spectrum will contain fragments with blocks of n A's and a couple of B's and blocks of m B's and a couple of A's. Fragments containing, for example, one A and one B would indicate the presence of another type of sequence.

Distinguishing alternating copolymer sequences from other sequences is straightforward because the mass spectrum should only contain polymer molecules A_nB_m with $|n-m|$ is 0 or 1. Polymer molecules with $|n-m|$ higher than 1 indicate the presence of another type of sequence. An exception is a branched polymer which can be alternating with a $|n-m|$ higher than 1. The alternating sequence of a linear polymer molecule can be confirmed by performing MS/MS. The MS/MS spectrum of an alternating polymer molecule A_nB_n must contain fragments $A_{n-x}B_{n-y}$ with $|x-y|$ is 0 or 1. An alternating polymer molecule A_nB_m with an $|n-m|$ of 1 gives the fragments $A_{n-x}B_{m-y}$ with $|(n-x)-(m-y)|$ of 0 or 1. A value of $|n-m|$ or $|(n-x)-(m-y)|$ larger than 1 will indicate the presence of another sequence.

The determination of the sequence becomes more complex when the MS/MS spectrum does not show the features of a block or alternating copolymer. The sequence must be random or partly random/block for such polymer molecules. Urakami *et al.* were able to determine the sequence of copolymers up to a degree of polymerisation 4 by performing MS³ experiments. One of the endgroups was acetylated prior to the MS analysis making the interpretation of the MS/MS spectra more facile. Their experiments demonstrate that a full elucidation of the sequence of large polymer molecules requires a large number of MSⁿ steps. Although their conclusion was that the copolymers have a random sequence, it might also be possible that the copolymer is a statistical copolymer and has a partly random/block structure.⁹¹ The sequence of statistical copolymers could so far not be distinguished from random copolymers based on their MS/MS spectra.

All methodologies described above assume that internal fragments do not appear in the MSⁿ spectra. Internal fragments originate from multiple cleavages of a molecule and make the interpretation of MSⁿ spectra even more complex. Sequencing of biomolecules by MSⁿ is less complex than the sequencing of copolymers because generally biomolecules contain a unique sequence. Each

fragment in the MSⁿ spectrum of biomolecules gives direct information about the sequence whereas the fragments of copolymers can originate from different polymer molecules.

Montaudo and coworkers introduced a method to obtain information about statistical copolymers with mass spectrometry^{119,120} by applying chain statistics to the mass spectra. The statistical methods, originally developed for NMR,^{121,122} are based on Bernoullian and Markovian chain statistics that can distinguish between random and partly random/block copolymers without performing MSⁿ. The Bernoullian chain statistics hold for random copolymers where the addition of a monomer during the polymerisation is independent of the previous addition (no penultimate effects). Markovian chain statistics are used for partly random/block copolymers where penultimate effects are present. In several studies, mainly concerning condensation polymers, Montaudo and coworkers observed predominantly random sequence distributions.^{119,123} Chen *et al.* observed a block sequence in copolymers based on fluorinated and nonfluorinated isocyanates using Markovian chain statistics.¹²⁴ In most studies, the chain statistics are directly applied to the mass spectrum^{125,126} although partial degradation by methanolysis,^{119,126,127} hydrolysis,⁸⁹ aminolysis,^{125,127} and pyrolysis^{119,124,128-132} prior to statistical analysis has also been performed.

Another approach to determine the sequence of a copolymer is by chemical degradation of the copolymer followed by mass spectrometric analysis. Hercules and coworkers chemically degraded the urethane bonds of copolymers consisting of a polyether and a polyurethane block and a copolymer consisting of a polyester and polyurethane block. The mass spectrum obtained after degradation revealed a MWD of the polyether and polyester,¹³³ which gave direct information about the block structure of the copolymers.

The complexity of the copolymer mass spectra becomes in general more complex than the spectra of the homopolymers. Mass spectrometers with a high resolution are necessary for such polymers to resolve all polymer peaks. Shi and coworkers successfully used an ESI FT-ICR MS to resolve the copolymer glycidyl methacrylate/butyl methacrylate. Only FT-ICR MS provides enough resolution to distinguish between the polymer molecules of this copolymer that is made of two monomers that have the same nominal mass but differ in exact mass by 0.036 Da (CH₄ vs O). The resolution of the FT-ICR MS ($m/\Delta m_{50\%}=500000$) was sufficient to resolve the different polymer molecules up to a molecular weight of 7000 Da. They concluded on the basis of the co-polymer intensity profiles that butyl methacrylate is more reactive than glycidyl methacrylate.⁷⁶

1.1.3.2. Branched copolymers

Branched polymers, e.g. dendrimers and hyperbranched polymers, are in general complex materials, which contain at least three endgroups in contrast to linear polymers with only two endgroups. Dendrimers have a well-defined branched structure with a central core. These polymers are produced in a labour intensive process. Their functionalisation involves a controlled multistep polymerisation process to obtain monodisperse structures. The production of dendrimers is usually costly. Hyperbranched polymers, on the other hand, are made in a one-step polymerisation procedure and do not have a central core. The synthesis of these polymers typically leads to a polydisperse MWD and the manufacturing costs are low.^{2,134}

The structure of dendrimers and (hyper)branched polymers has been studied with MALDI^{95,135-141} and ESI.^{66,95,142} Most dendrimer studies involve the analysis of the M_n and polydispersity that are in agreement with the theoretical values. Confirmation of the structure of dendrimers from the first to third generation has been achieved with post-source decay analysis.¹³⁶

A difficulty in the characterisation of branched polymers is the fact that branching does not directly follow from the m/z value.¹⁴³ For example, a condensation of a diacid (A) with a dialcohol (C) and a small amount of a triol (T) will result in polymer molecules with a composition of, for example, $A_xC_yT_z$ in which $z \ll x$ and $z \ll y$. Linear and branched polymer molecules $A_xC_yT_z$ can be synthesised with the same monomeric composition and the same m/z value. The linear and branched polymer molecules can therefore not be distinguished by their m/z . A mass spectrometric procedure exist that provides a means to determine whether a polymer is branched or not. Hercules and coworkers performed a transesterification with trifluoroacetic acid (TFA) of the ester bonds of branched polymers.¹⁴⁴ Ester bonds are broken upon transesterification forming diesters of TFA for linear polymer molecules and (n+2)-esters of TFA for branched polymer molecules depending on the number of branches n that the polymer molecules contains. The main disadvantage is however that the transesterification reactions utilised are destructive.

Post-source decay can reveal the alternating sequence of copolymers although it was not possible to demonstrate whether the polymer molecules were branched or linear.⁹⁵ With SEC-DV (viscometric detection) and SANS (small-angle neutron scattering) it was possible to demonstrate that the polymers were randomly branched.¹⁴⁵ Muscat and coworkers observed extensive in-source decay of FD and MALDI generated ions of hyperbranched polyesteramides made by the polycondensation of di-isopropanolamine and hexahydrophthalicacid anhydride.

Minimal fragmentation was observed with ESI when compared with MALDI and FD. This indicates that ESI is a softer ionisation technique than MALDI and FD in this case.⁹⁵

1.1.4. Chemical composition distribution

The *intramolecular* arrangement of the monomers, the sequence, is an important aspect of copolymers that is difficult to study with mass spectrometry as discussed in the previous section. Apart from the monomer sequence the *intermolecular* arrangement of the polymer molecules is an important issue also. The polymer molecules of a copolymer, made of A and B, with degree of polymerisation n can contain a number of A's and B's. For example: $n=5$, AABAB, ABBAB, BBBBA, AABBA, AAABA etc. The variation of the chemical composition with the degree of polymerisation n is called the *intermolecular* or chemical composition distribution.

Wilczek-Vera and coworkers synthesised two block copolymers by sequential anionic polymerisation of α -methylstyrene and styrene showing that the chemical composition distribution of the block copolymer formed upon copolymerisation obeys the random coupling hypothesis and is best described by the Schulz Zimm model. The random coupling hypothesis states that the molecular weight distributions of the individual blocks are not correlated, i.e., x and y are not correlated for a polymer molecule A_xB_y . They showed that NMR analysis of the copolymer was necessary for the interpretation of the mass spectrometric results.^{146,147} The random coupling hypothesis was also obeyed for a block copolymer of poly(oxyethylene) (EO) and poly(oxypropylene) (PO) measured with MALDI FT-ICR MS. However, the observed intensity profile had to be corrected for:

- 1) TOF effects in the external MALDI source (see section 1.1.1.1.).
- 2) The intensity of the monoisotopic peak.
- 3) Overlapping isotopic peaks of different polymer molecules.

The intensity of the monoisotopic peak (peak due to ^{12}C , ^1H , ^{14}N , ^{16}O etc. only) decreases with increasing number of carbon atoms in the polymer molecules. If the intensity is not corrected for this effect, the intensity of large polymer molecules will be underestimated. The monoisotopic peak of the homo-polymer PO overlaps with the second isotopic peak (containing two ^{13}C) of polymer molecules containing a given number of EO and PO units. This overlap will result in an overestimation of the intensity of the homo-polymer molecules PO in the spectrum. The random coupling hypothesis is only valid when these effects are

corrected.⁵¹ The chemical composition distribution of a tri-block copolymer of polyethylene glycol (PEG) and polypropylene glycol (PPG) was found to be more difficult to interpret because of the increasing complexity of the mass spectra. Mass spectrometers with a higher resolution such as FT-ICR MS compared to a TOF could simplify this problem.¹⁴⁸

1.2. Scope of this thesis

The current status of ESI and MALDI mass spectrometry in the field of polymer characterisation has been reviewed in the previous sections. It has been shown that a mass spectrometric analysis of some polymer characteristics deviate from the results obtained with other, more conventional, polymer characterisation methods. This thesis describes, in chapter 2, the advantage of coupling ESI with FT-ICR MS for the study of several polymer characteristics. Emphasis is placed on the analysis of various polymer characteristics rather than focusing on, for example, the determination of the MWD only. The MWD is the first polymer characteristic that will be studied. The influence of the charge state on the observed M_n and M_w of a series of polyoxyalkylenes with each a different monomeric structure and molecular weight is studied and discussed in chapter 3.

Chapter 4 explores the scope of multiply charged polymer ions generated by ESI for monomer and endgroup analysis. The combined use of the multiple charge states observed with ESI leads to an increase in the precision of the endgroup and monomer mass determination compared to the single charge state observed with MALDI FT-ICR MS.

Mass spectrometry is used in several studies for the quantitative analysis of sequence distributions in copolymers. However, no study exists where a linear response over the entire m/z range of the mass analyser is reported independent of the structure of the monomers. The influence of the monomeric structure in copolymers and mixtures of homopolymers on the ionisation efficiency is tested and described in chapter 5. This chapter clearly demonstrates that differences in ionisation efficiency make the quantification of the polymers studied very difficult or even impossible. The sequence analysis of copolymers with MS/MS is described in chapter 6. The chapter describes the MS/MS experiments and the procedure for the sequence determination of copolymers from sequence specific fragmentations, a procedure that is often used in biomolecular sequence analysis.

Chapter 7 describes the fragmentation behaviour of a series of hyperbranched polyesteramides. This study was performed to determine whether

Chapter 1

the origin of a series of oligomeric ions in the spectra is a result of the polymerisation process or the dissociation processes in the ion source.

The presence of isomeric structures of hyperbranched polyesteramides is investigated with a novel MS^n approach and gas phase hydrogen/deuterium (H/D) exchange described in chapter 8. It is investigated whether H/D exchange combined with MS^2 provides additional structural information and information about the fragmentation process itself. The same set of hyperbranched polymers is studied with electron capture dissociation (ECD). It is tested whether ECD is a complementary dissociation technique for hyperbranched polymers as reported in the literature for biomolecules.

This thesis will demonstrate that the combination of ESI with FT-ICR MS contributes significantly to an improved characterisation of synthetic polymers. The unsurpassed resolution and mass accuracy of FT-ICR MS enables the determination of structural characteristics of polymers with a molecular weight up to 10,000 Da. The ion storage possibilities of the technique can be used to perform MS^n , H/D exchange and ECD experiments for structural elucidation of the sequence of polymers.

Chapter 2

Basics and experimental set-up of the ESI FT-ICR MS

The basics of electrospray ionisation and Fourier transform ion cyclotron resonance mass spectrometry are discussed in this chapter. A detailed description of the instrument and experimental set-up is given. All experiments discussed in this thesis were performed with a modified Bruker ESI FT-ICR MS.

2.1. Electrospray ionisation (ESI)

Magnetic and electrical fields, time-of-flight and ion cyclotron resonance are the most commonly used mass spectrometric techniques to separate ions by their m/z ratio. One of the most crucial steps in mass spectrometry is the generation and transfer of ions from a sample to the gas phase. Until recently, the most common ionisation technique was electron impact ionisation, which is based on the irradiation of vaporised sample molecules with electrons resulting in ionised fragments. The most important advantage of electron impact is that structural information of many classes of compounds is obtained. However, polymers are not volatile. Also, the technique is not the best choice if one desires to obtain structural information of one molecule in a mixture of molecules, for example, one polymer molecule in a MWD. A fragment that appears in the mass spectrum upon electron impact can originate from different polymer molecules making the interpretation of the mass spectra difficult.

During the last decades, new ionisation techniques have been developed to transfer the molecules *intact* to the gas phase and produce *intact* molecular ions (see section 1.1.1). Fragmentation during the ionisation was absent or minimised with the introduction of the soft ionisation techniques matrix-assisted laser desorption/ionisation (MALDI) and electrospray ionisation (ESI).

Electrospray ionisation is based on the dispersion of a dilute solution of (macro)molecules as a fine spray of charged droplets at atmospheric pressure. The

spray is produced by applying a potential of 2-5 kV between the spray needle and inlet of the mass spectrometer, as shown in figure 2.1. The solution to which a salt or acid is added is pumped through the spray needle where a Taylor cone¹⁴⁹ is formed due to the electrical field. Charge separation takes place in the Taylor cone through the electrophoretic mechanism and a nebula of positively charged droplets is formed when operated in the positive ion mode. Since the overall number of charges must be constant, some negative ions (e.g. OH⁻) have to be oxidised at the surface of the spray tip or alternatively the metal surface of the spray tip is oxidised. For example, Zn²⁺ ions were formed and detected when a spray tip was used made of Zinc.¹⁵⁰

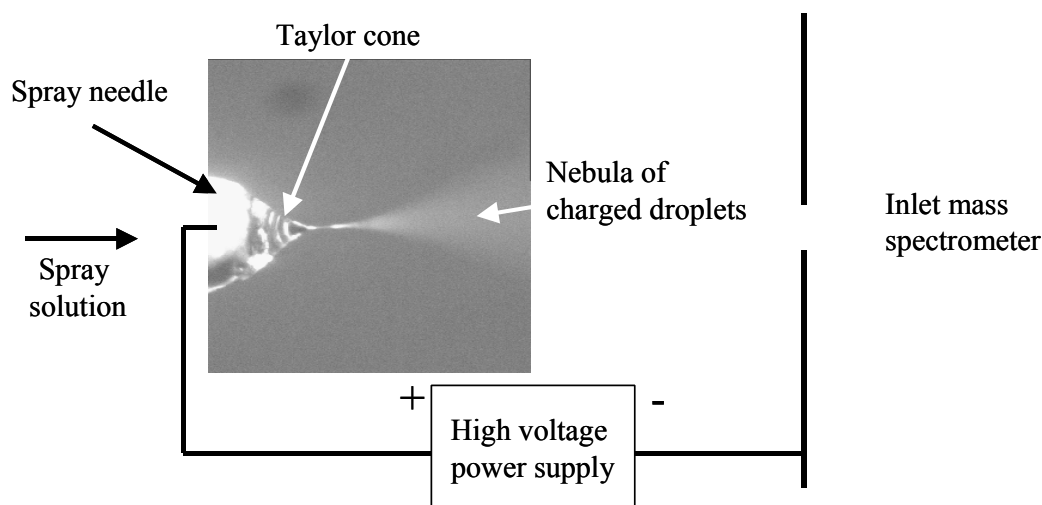


Figure 2.1 *Schematic representation of the ESI process.*

The charged droplets are directed to the inlet of the mass spectrometer. On their way to the mass spectrometer the solvent of the droplets is made to evaporate leading to an increase of the charge density on the surface of the droplets. The evaporation of the solvent can be enhanced by directing the droplets through a heated capillary. It is assumed that the number of charges on the droplets remains constant because the evaporation of a cation (e.g. sodium) is very endothermic. When the electrostatic repulsion between the charges becomes equal to the force resulting from the surface tension, the droplet will explode into smaller charged droplets. This can theoretically be described by the Rayleigh stability limit.¹⁵¹ This process continues several times until ionised (macro)molecules enter the gas phase.

The final stage in electro-spray ionisation, the transfer of an ion from the droplets to the gas phase, is not well understood but can be described by two models. The first is the Charged Residue Model (CRM) developed by Dole⁵⁸ and holds that gaseous ions are formed from droplets containing a single analyte

molecule bound to a certain number of electrolyte ions. When all solvent molecules evaporate, a charged molecule remains. The second model, the Ion Evaporation Model (IEM),^{152,153} developed by Iribarne and Thomson states that the field on the surface of the droplet increases due to the shrinkage of the droplet by evaporation. The field can become so high that an ion ‘desorbs’ from the surface of the droplet entering the gas phase, which is a similar process as in field desorption. The main advantages of electrospray ionisation are:

- The detection of high mass compounds at relative low m/z values due to multiply charging.
- Conventional solutions can be sprayed.
- Minimal fragmentation.
- Combination with separation methods.

Multiply charging can also be a disadvantage for some applications. When samples are measured that consist of different molecules, like synthetic polymers, the peak density in the mass spectrum can become too high to resolve all polymer molecules. This disadvantage can be overcome with high resolution mass analysers like time-of-flight and Fourier transform mass spectrometry. Another disadvantage is that only molecules with polar groups, necessary for the interaction with cations, can be sprayed. A more detailed description of the electrospray process can be found elsewhere.¹⁵⁴⁻¹⁵⁸

2.2. Fourier transform ion cyclotron resonance mass spectrometry (FT-ICR MS)

The cyclotron motion of ions in a magnetic field was first used in 1932 to accelerate protons to high kinetic energies for nuclear physics experiments.¹⁵⁹ It took however four decades before image charge detection of the cyclotron motion of ions in combination with Fourier transformation algorithms was introduced.¹⁶⁰⁻¹⁶² This development resulted in a new mass spectrometric technique: Fourier transform ion cyclotron resonance mass spectrometry (FT-ICR MS). The basics of this technique will be discussed briefly in the next paragraphs. More detailed introductions of the technique can be found elsewhere.¹⁶³⁻¹⁶⁶

2.2.1. *The cyclotron motion*

The heart of the Fourier transform ion cyclotron resonance mass spectrometer (FT-ICR MS) is the ICR cell, which is a Penning trap and is positioned in the centre of a (super-conducting) magnet. Several ICR cell designs have been investigated in the literature including rectangular,¹⁶⁷ cubic^{168,169} and cylindrical¹⁷⁰ cells. The main disadvantage of these cells is the undesirable loss of ions along the z-axis. The loss of ions was minimised with the introduction of the ‘infinity’ trap.¹⁷¹ However, the main disadvantage of this cell is that ions are introduced through a small hole in the front trap electrode making the trapping of ions difficult. With the introduction of the open-ended cell,¹⁷²⁻¹⁷⁴ ions were easier to trap because the front trap electrode has a diameter of typically 6 cm. Trapping with an open cell requires a gas pulse during the ion introduction. This reduces the kinetic energy of the ions allowing ions to be trapped.

Ions are trapped radially, in the x-y direction, by the magnetic field and axially (z-axis) by an electrostatic potential applied to the two trapping electrodes as is shown in figure 2.2. An ion with charge q and velocity \mathbf{v} moving in magnetic and electrical fields \mathbf{B} and \mathbf{E} experiences a Lorentz force F_L

$$F_L = q\mathbf{E} + q(\mathbf{v} \times \mathbf{B}) \quad (2.1)$$

Only q , \mathbf{v} and the strength of the magnetic field influence the magnitude of the Lorentz force if the electrical field is considered negligible. The magnetic field is homogenous and uniform in the volume of the ICR cell. The Lorentz force becomes $qv_{xy}B$ and is compensated by a centripetal force F_C opposite to the Lorentz force as shown in figure 2.3, which is given mathematically by the following equation

$$qv_{xy}B = \frac{mv_{xy}^2}{r} \quad (2.2)$$

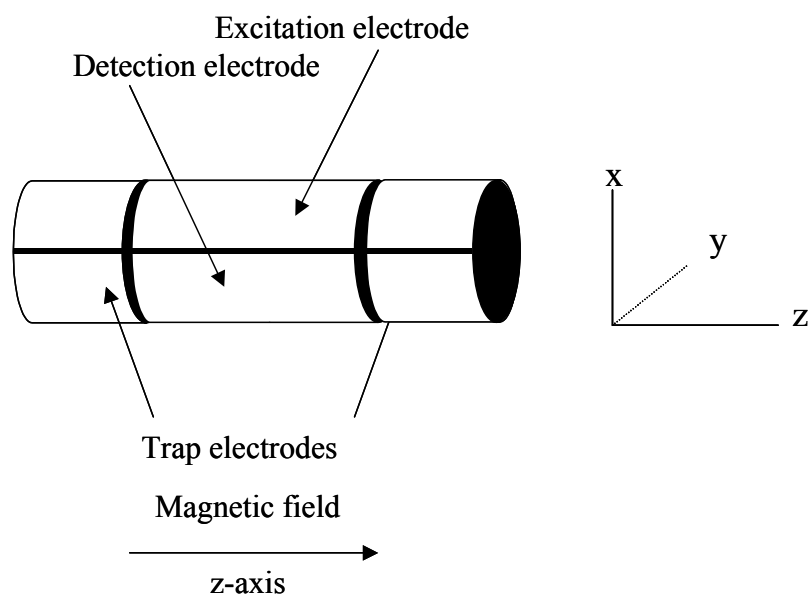


Figure 2.2 Schematic of an FT-ICR analyser open cell. The cell is positioned in the centre of a 7-T super-conducting magnet. The open ICR cell contains two trapping electrodes, two excitation electrodes and two detection electrodes. The trapping electrodes are divided in four segments. The excitation electrodes are capacitively coupled to the trapping electrodes

where r is the orbit radius of the ion in the ICR cell. In the absence of collisions the orbit radius is constant. By introducing the angular velocity $\omega = v_{xy}/r$, equation (2.2) becomes the well known cyclotron frequency ω_c of ions in a magnetic field

$$\omega_c = \frac{qB}{m} \quad (2.3)$$

It is important to point out two important advantages that follow from equation (2.3). First, the cyclotron frequency is a function of the mass, charge and the strength of the magnetic field (which is constant in time and space). Moreover, the frequency of the ions is independent of the orbit radius. Secondly, mass resolution and frequency resolution are the same (except for a minus sign) as can be seen by taking the derivative d/dm of equation (2.3) ($\omega_c/d\omega_c = -m/dm$).

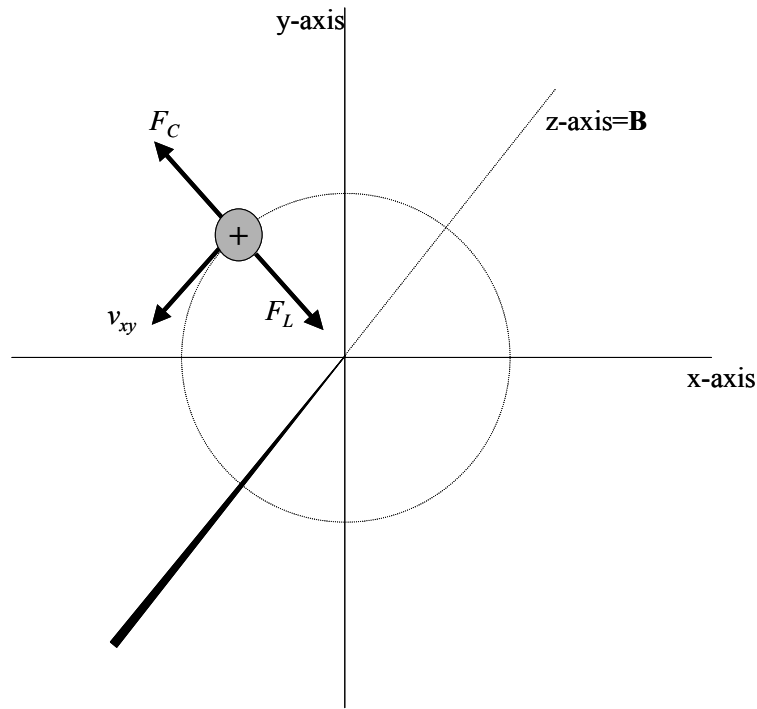


Figure 2.3 Motion of the ions with velocity v_{xy} in an FT-ICR in the presence of a magnetic field \mathbf{B} . The Lorentz force F_L is opposed by the centripetal force F_C .

The electrical field of the trapping electrodes has been neglected in equation (2.3) but can have a significant contribution on the cyclotron motion and must therefore not be disregarded. Most Fourier transform mass spectrometers operate with an external ion source requiring that the ions have a kinetic energy along the z-axis to enter the ICR cell. The potential on the trapping electrodes makes sure that the ions are trapped along the z-axis. Consequently, the ions oscillate along the z-axis with a trapping frequency ω_T given by

$$\omega_T = \sqrt{\frac{qV_T}{md^2}} \quad (2.4)$$

where V_T is the potential applied to the trapping electrodes and d the diameter of the ICR cell. The trapping potential induces an axial electric field $\mathbf{E}=V_T r/2d^2$ that opposes the Lorentz force. Equation (2.2) has to be extended with $q\mathbf{E}$ to correct the cyclotron frequency for the trapping potential according to equation (2.1) and can be written as $m\omega^2 r=q\mathbf{B}\omega r-q(V_T r/2d^2)$. It can be shown that two solutions exist for ω

$$\omega^+ = \frac{1}{2} \left(\omega_c + \sqrt{\omega_c^2 - 2\omega_T^2} \right) \quad (2.5a)$$

$$\omega^- = \frac{1}{2} \left(\omega_c - \sqrt{\omega_c^2 - 2\omega_T^2} \right) \quad (2.5b)$$

where ω^+ is the cyclotron frequency and ω^- the frequency of the magnetron motion.

2.2.2. Excitation and detection

It was shown in the previous paragraph that ions have a cyclotron motion in a magnetic and electrical field. The mass and charge of the ions can be determined with high accuracy by detection of the cyclotron frequency ω_c . To detect the cyclotron frequency and to calculate the corresponding mass and charge of the ions, the ions must be excited into a coherent motion. An ion population that is excited without a coherent motion is not detected. Ions can be coherently excited by applying an RF electric field between two opposite excitation electrodes (see figure 2.2) of the form

$$\mathbf{E}(\mathbf{t}) = E_0 \cos \omega_c t \mathbf{j} = \frac{\alpha V_{pp}}{d} \cos \omega_c t \mathbf{j} \quad (2.6)$$

where α is the geometry constant of the ICR cell, V_{pp} is the peak-to-peak amplitude of the excitation RF signal. The geometry constant α is 0.897 (5% accuracy)¹⁷⁵ for the Infinity Cell and 2.26 for the home build open cell (based on a comparison of breakdown diagrams measured with the Infinity and open cell).

The electrical field $\mathbf{E}(\mathbf{t})$ consists of two counter rotating components $\mathbf{E}_1(\mathbf{t}) + \mathbf{E}_2(\mathbf{t})$ that continuously push the ions coherently to a higher orbit in the ICR cell.

$$\mathbf{E}_1(\mathbf{t}) = \frac{E_0}{2} (\sin \omega_c t + \cos \omega_c t) \quad (2.7a)$$

$$\mathbf{E}_2(\mathbf{t}) = \frac{E_0}{2} (\sin \omega_c t - \cos \omega_c t) \quad (2.7b)$$

Only the component, which rotates with the same frequency and in the same direction as the ion of interest, will increase the kinetic energy of the ions. The counter-rotating component does not influence the kinetic energy but ensures the coherent motion of the ions. If it is assumed that all power absorbed by the ions ($A(t) = E_0^2 q^2 t / 4m$) is converted into kinetic energy, the radius r of the ions becomes

$$r = \frac{E_0 t_{exc}}{2B} \quad (2.8)$$

The nice feature of this equation is that all ions are excited to the same radius in the ICR cell independent of the mass and charge of the ions. However, most excitation methods provide an excitation power that is not completely independent of the frequency. These methods include rectangular pulse or impulse excitation, single frequency excitation and a frequency chirp.¹⁶⁰⁻¹⁶² A method that does excite the ions to the same radius is called stored waveform inverse Fourier transform (SWIFT) and was introduced by Marshall *et al.* in 1985.^{176,177} The frequency range for excitation is specified followed by an inverse Fourier transformation to obtain the time domain excitation waveform. Quadratic phase scrambling is used to spread the power of the time domain signal.

The coherent motion of the ions is detected with the detection electrodes after kinetic excitation of the ions to an orbit with a radius smaller than the diameter of the ICR cell. The two detection electrodes are opposite to each other and positioned next to the excitation electrodes as shown in figure 2.2. An alternating image current is induced each time the ions pass the detection electrodes. The frequency of the alternating image current matches the cyclotron frequency of the ions. After conversion of the alternating current to an alternating voltage the time domain voltage signal $f(t)$ is obtained

$$f(t) = \sum_{i=1}^M N_i e^{-t/\tau_i} \cos(\omega_i t + \varphi_i) \quad (2.9)$$

where t is the length (in seconds) of the transient, N_i is the number of ions i and φ_i the phase of the ions. The intensity of the time domain signal decreases with damping constant τ_i due to collisions with background gas and space charge effects.¹⁷⁸⁻¹⁸⁰ These effects result in a dephasing of the coherent motion of the ions, magnetron expansion and a decrease of the orbit radius.

An example of a time domain signal of an ion with a cyclotron frequency ω of 114.179 Hz (m/z of 940.6933) is shown in figure 2.4a (see insert). The beating pattern that is observed originates from the presence of other ions with cyclotron frequencies 114.057 Hz and 113.936 Hz (m/z 941.6967 and 942.7001). These ions are the isotopic peaks of the ion with a cyclotron frequency of 114.179 Hz due to the natural abundance of isotopes (^2H , ^{13}C , ^{15}N and ^{18}O). Another feature of equation 2.9 that becomes clearly visible in figure 2.4a is that the intensity of the time domain signal decays in time, which can be described by τ_i . After Fourier transformation of the time domain spectrum the frequency spectrum is obtained. The mass spectrum (figure 2.4b) is calculated by equation (2.3).

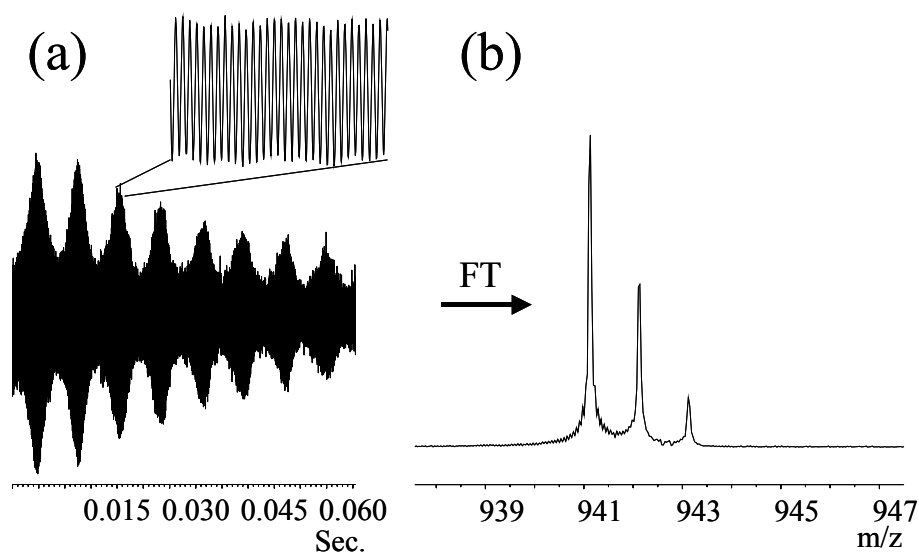


Figure 2.4 Time domain signal of a synthetic hyperbranched oligomer made by the polycondensation of di-isopropanolamine and phthalic acid (a). Mass spectrum of the Fourier transformed time domain signal (b).

2.2.3. Collisional excitation for fragmentation

A frequently used method to obtain structural information of ions is by collisionally activated dissociation (CAD). The ion of interest is kinetically excited in the ICR cell and collided with a collision gas. A part of the collision energy is converted into internal energy until the dissociation threshold is reached and fragmentation occurs. Kinetic excitation is performed by applying a well-defined RF voltage on the excitation electrodes. The two most common methods to activate the ions are on-resonance excitation and sustained-off resonance irradiation (SORI). The alternating field in on-resonance excitation has the same frequency as

the cyclotron frequency of the ion of interest. The laboratory frame kinetic energy $E_{kin,lab}$ at time t_{exc} can be controlled by t_{exc} and E_0 and is given by the following relation

$$E_{kin,lab} = \frac{q\omega_c E_0^2 t_{exc}^2}{8B} = \frac{q^2 E_0^2 t_{exc}^2}{8m} \quad (2.10)$$

Note that the orbit radius r in equation (2.8) is independent of the *mass* and *charge* of the ions. The increase of the orbit radius during the excitation is schematically shown in figure 2.5a.

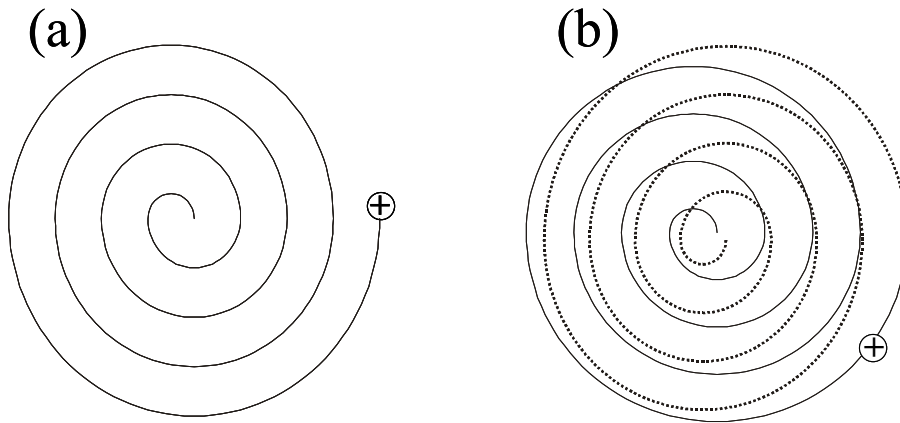


Figure 2.5 Increase of the orbit radius during the excitation upon on-resonance excitation (a) and increase of the orbit radius during sustained off resonance irradiation (SORI) (b). Solid line represents acceleration of the ions, dotted line deceleration. Note that the radius of the ion trajectory in the ICR cell during the SORI excitation is much smaller.

An electrical field that is off resonance with the cyclotron frequency of the ions is applied on the excitation electrodes in SORI. The radius is continuously modulated as is shown in figure 2.5b. The following relation gives the laboratory frame kinetic energy and orbit radius.

$$E_{kin,lab} = \frac{q\omega_c E_0^2}{2B} \left[\frac{\sin((\omega_i - \omega_{eff})t_{exc}/2)}{\omega_i - \omega_c} \right]^2 \quad (2.11a)$$

$$r = \frac{E_0}{B} \frac{\sin((\omega_i - \omega_c)t_{exc}/2)}{\omega_i - \omega_c} \quad (2.11b)$$

The main difference with on-resonance excitation is that the ions are continuously (sustained) accelerated and decelerated. In on-resonance excitation the ions are accelerated to a relatively high kinetic energy in approximately 100 – 300 μ s. The kinetic energy of the ions relaxes in \sim 0.1 second after acceleration due to multiple collisions.¹⁸¹ In SORI, the kinetic energy can be modulated for seconds. The collision energy of each collision is typically lower than in on-resonance excitation, which allows the study of the lowest energetic fragmentation pathways.

2.2.4. Instrumental layout and experimental procedures for ESI FT-ICR MS analysis

The electrospray ionisation Fourier transform ion cyclotron resonance mass spectrometry (ESI FT-ICR MS) experiments are performed with a modified Bruker-Spectrospin (Fällanden, Switzerland) APEX 7.0e FT-ICR MS equipped with a 7T super-conducting magnet. The heart of the system, the ICR cell, is positioned in the centre of the super-conducting magnet and is held at $10^{-9} - 10^{-10}$ mbar.

A polymer solution to be electrosprayed is made that contains \sim 1 mg/ml polymer. Several types of solvents can be chosen for this purpose but the polymer must be soluble in the solvent and the solvent must be electrospray compatible. Commonly used solvents are THF, methanol and propanol. The ‘magic’ solvent hexafluoroisopropanol (HFI) can often be used for polymers that are difficult to dissolve. Depending on the type of cations that is desired, \sim 1 mM NaI (for sodium cationised ions) or \sim 2% acetic acid (for protonated ions) is added to the solution.

Ions are generated in an in-house constructed ESI source shown in figure 2.6. The sample is pumped with a Harvard syringe pump model 55-1111 (Kent, U.K.) at a flowrate of 0.1 ml/hr through a fused silica capillary (0.18 mm internal diameter). Positively charged electrosprayed droplets are generated by applying a 3000-5000 V potential difference between a stainless steel spray needle and the stainless steel capillary, which is the inlet of the mass spectrometer. The stainless steel capillary is at a distance of \sim 0.5 cm from the spray needle. The capillary has

an internal diameter of 0.75 mm, length of ~20 cm (Alltech Assoc., Inc., Deerfield, IL) and is placed in a ceramic heater tube. To aid the evaporation of the solvent, the stainless steel capillary is held at approximately 170 °C by passing a current of 1.8 A (~12 W) through a metal wire woven in the ceramic heater tube.

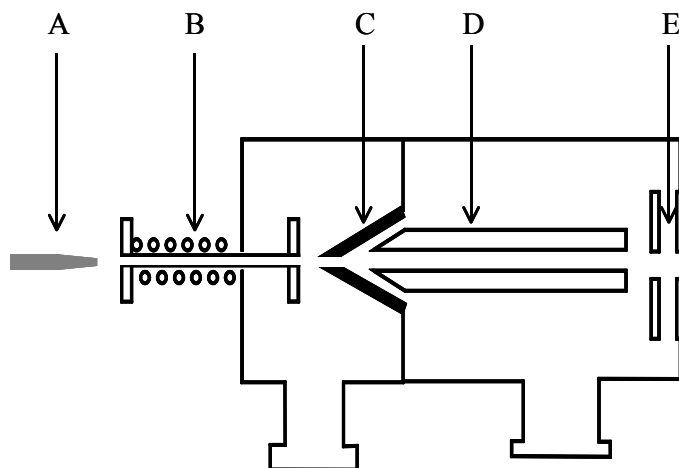


Figure 2.6 Schematic representation of the ESI source with spray needle (A), heated capillary (B), skimmer (C), quadrupole (D), and extraction lenses (E).

Five stages of differential pumping are employed to bridge between the atmospheric pressure conditions in the ESI source to the FT-ICR cell at 10^{-9} - 10^{-10} mbar. In the first pumping stage, the nozzle skimmer region, the pressure is approximately 1 mbar. Ions are focused by a tube lens (not shown) through a copper skimmer with an orifice diameter of 1 mm. Excess neutrals are removed by the skimmer. Typical nozzle skimmer voltage differences are about 5 V to minimise fragmentation in the ion source. The second pumping stage contains a RF-only quadrupole at a pressure of 10^{-5} mbar. Electrostatic ion optics is used (at a pressure of 10^{-7} mbar) in the third region to guide the ions from the exit of the quadrupole in the direction of the ICR cell. Ions are accelerated to 3000 eV in the intermediate region ($\sim 10^{-8}$ mbar) at the exit of the quadrupole to prevent radial ejection by the magnetic field. Before entering the ICR cell the ions are decelerated to approximately 1 eV to facilitate trapping in the ICR cell at $10^{-9} - 10^{-10}$ mbar.

Two ICR cells have been used in this thesis. The analysis described in chapter 3 and 4 were performed with a Bruker Infinity™ ICR Cell. All other experiments were performed with an in-house constructed capacitively coupled open cell shown in figure 2.7. The copper electrodes of the open cell are mounted in an Al_2O_3 cylinder with an internal diameter of 6 cm and an outer diameter of 8 cm. The 1 cm thick Al_2O_3 wall contains sixteen channels with a diameter of 3 mm.

In these channels 12 electrically shielded heater elements are placed. The coaxial heater elements consist of a closed rigid copper cylinder, a UHV compatible coaxial isolation material and a central heater wire. These elements were chosen as they can be electrically shielded from the ICR cell electrodes to prevent the introduction of noise from the heater current and to keep the heater current sufficiently low to have only a minimal effect on the magnetic field homogeneity. A Pt100 temperature sensor was mounted on the outside of the Al₂O₃ cylinder to measure and control the cell temperature. A Shinyo thermostat was used to readout the Pt100 sensor and controls the temperature of the open cell.¹⁸²

A standard ESI FT-ICR MS experimental time sequence is shown in figure 2.8a. The experiment starts with a quench on the rear trapping electrode to make sure that all ions are ejected from the ICR cell. In the next step the emptied ICR cell is filled with the ion population. Argon gas is pulsed ($\sim 10^{-6}$ mbar) during the introduction of the ions to kinetically cool down the ions and enhance trapping. Kinetic excitation and detection of the ion population takes place after a delay of several seconds to pump down to a pressure of $\sim 10^{-8}$ - 10^{-9} mbar. Collisional cooling is only required if the experiments are performed with the open cell. Data acquisition (128k datapoints) and control is performed using XMASS (Bruker-Daltonics, Billerica MA) running on an SGI Indigo R4000 (Silicon Graphics, Mountain View, CA) UNIX-based workstation. The total duration of one experiment is in the order of seconds.

The experimental time sequence of a mass spectrometry/mass spectrometry (MS/MS) experiment is shown in figure 2.8b. After the ions are trapped and the Argon pressure is reduced to $\sim 10^{-8}$ - 10^{-9} mbar the precursor ion is selected. Isolation of the ions is performed with an in-house constructed arbitrary waveform generator (AWG) with a memory of 192 Mb.¹⁸³ Tailor made isolation pulses can be generated including single frequency excitation, frequency chirp and SWIFT. These pulses have in common that the cyclotron motion of all ions, except the ion of interest, is kinetically excited to make sure that these ions collide with the electrodes of the ICR cell. The ion of interest remains in the ICR cell for further study. The AWG can also be used for detection. A factor of 1500 more data points are available by detecting with the AWG compared with the 128 Kb of the Bruker hardware. This allows detecting the coherent motion of ions for a longer period and hence an increase of the resolution can be obtained. MS/MS experiments are started with an Argon pulse in the ICR cell after isolation of the ion. A delay of ~ 0.5 s is implemented before the ions are excited by on-resonance or sustained off resonance collisionally activation as described in paragraph 2.2.3. Collisions of the ions with Argon take place in approximately 2 seconds for on-resonance excitation. The collision time can be longer or shorter for SORI. After the collision experiment a pumping delay of 5 seconds is introduced followed by the regular

excitation and detection event. In a similar way other experiments can be designed. For example, MS/MS/MS experiments can be performed with an additional isolation and MS/MS step. MS^n experiments were performed in chapters 6 and 7.

A typical time sequence of a H/D exchange experiment is depicted in figure 2.8 c. The experiment is very similar to the previous two experiments. The only difference is that the ion excitation/activation event of figure 2.8 b is replaced by a D_2O gas pulse ($\sim 5 \cdot 10^{-7}$ mbar) via a pulsed valve. The pulsed valve is in-between a reservoir containing liquid D_2O and the ICR cell. A combination of gas phase H/D exchange experiments and MS^n was used in chapter 8 for the study of the isomeric structures of hyperbranched polyesteramides. The electron capture dissociation (ECD) experiments described in chapter 9 for the study of hyperbranched polyesteramides have been performed in a similar manner as the experiment described in figure 2.8c. The only difference is that an electron pulse for ECD is used instead of the D_2O pulse. A Rhenium filament is positioned in the back of the ICR cell centred on the z-axis of the cell. The filament is heated by a current of 2.95 A, which is sufficient to generate electrons. During the ECD event the electrons are accelerated to ~ 1.5 eV and allowed to be captured by the ions.

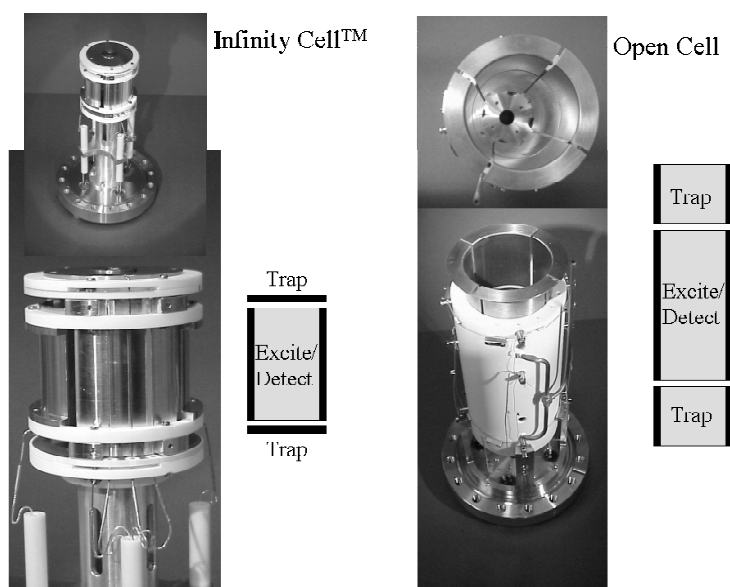


Figure 2.7 The two ICR cells used in this thesis. *InfinityTM Cell (a) and in house constructed capacitively coupled open cell (b).*

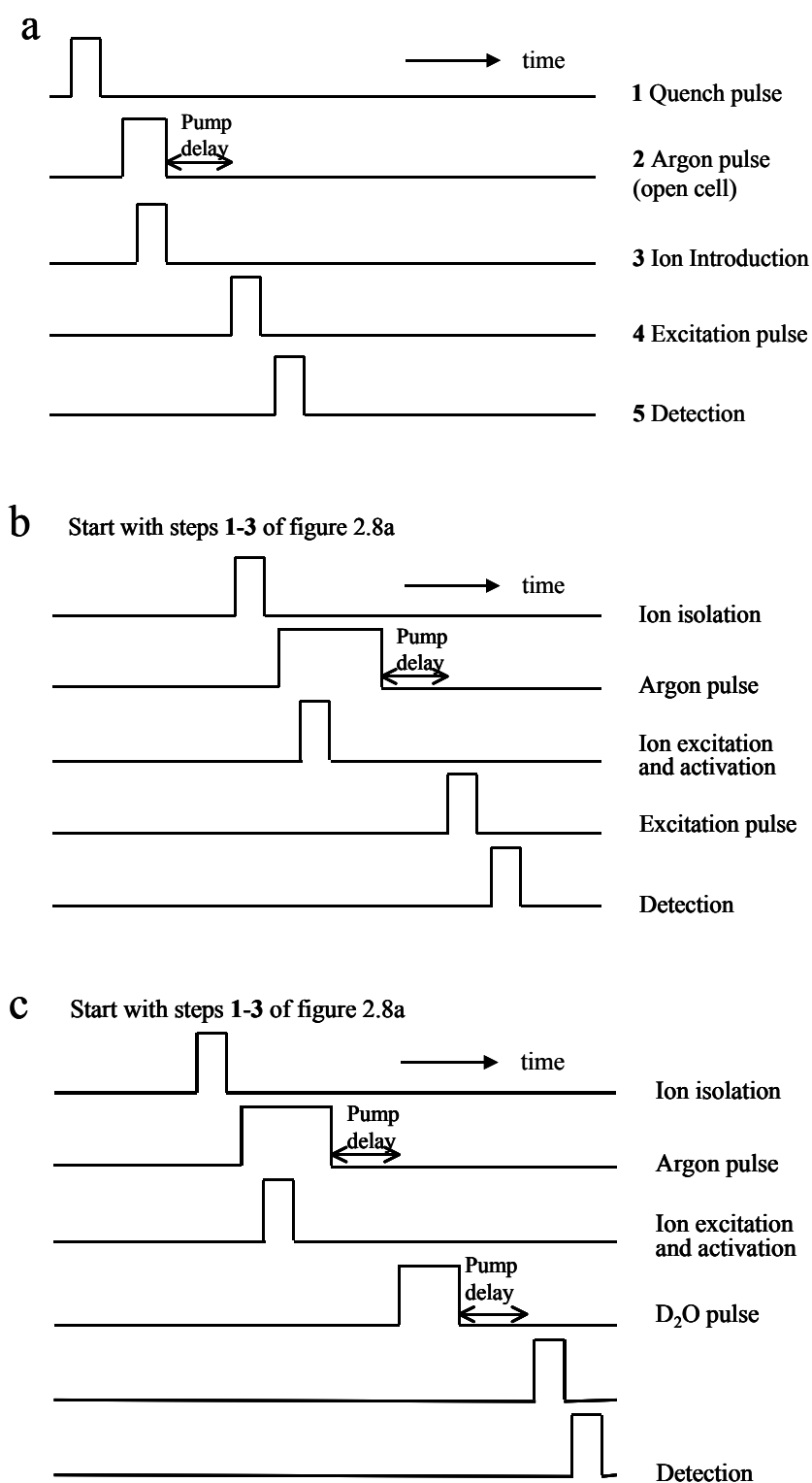


Figure 2.8 Time sequence of a standard ESI FT-ICR MS experiment (a), MS/MS experiment (b) and H/D exchange experiment (c).

Chapter 3

Characterisation of the molecular weight distribution of polyoxyalkylenes

Electrospray ionisation (ESI) Fourier transform ion cyclotron resonance mass spectrometry (FT-ICR MS) was used for the study of charge state effects on the measured molecular weight distribution of three poly(oxyalkylene)s in the mass range of 400-8000 Da. A linear increase of the number average molecular weight (M_n) as a function of the charge state is observed for all poly(oxyalkylene)s. An explanation of the increasing M_n as a function of the charge state is given on the basis of the available number of charge sites (oxygen atoms) on a polymer molecule. Large polymer molecules, which contain more oxygen atoms than small polymer molecules, can accommodate more cations. A method is introduced that uses all charge states from the ESI FT-ICR mass spectrum to reconstruct the molecular weight distribution. The method is based on a summation of the polymer molecules observed in all charge states. The obtained reconstructed molecular weight distributions are in good agreement with the distributions observed with MALDI TOF-MS.

3.1. Introduction

The molecular weight distribution is often characterised using four parameters: the number (M_n), weight (M_w) and z (M_z) average molecular weights and polydispersity ($D=M_w/M_n$). Conventional techniques used to measure M_n and M_w are based on osmotic pressure and lightscattering, respectively.¹⁸⁴ Neither technique is able to provide detailed information about the shape of the distribution, which is often required. A technique that measures the shape of the molecular weight distribution is size exclusion chromatography (SEC). The retention of the polymer molecules depends on their hydrodynamic volume: small polymer molecules will be retained longer than large polymer molecules, which will elute earlier from the column. In this way, a hydrodynamic volume versus

concentration curve is obtained. From the shape of the distribution M_n , M_w and D can be calculated. The main drawback of SEC is that the hydrodynamic volume is strongly dependent on the type of polymer and branching of the main chain. As a result, analysis of a polymer requires calibration with a well-defined standard of the same polymer class/type, which is not always available. A universal calibration method for SEC can be obtained with the Mark-Houwink equation ($[\eta]=kM^a$).¹⁸⁴ M is the molar mass of the polymer, $[\eta]$ the intrinsic viscosity, and k and a are polymer specific constants, respectively. Constants k and a are solvent and temperature dependent. The viscosity is measured using a viscometric detector allowing the molecular weight to be calculated.

Mass spectrometry can provide the necessary additional molecular information for a large variety of polymer classes. However, polymers with a polydispersity larger than 1.1 analysed with matrix-assisted laser desorption/ionisation time-of-flight mass spectrometry (MALDI TOF-MS) yield molecular weight distributions which deviate dramatically from the distributions obtained with SEC.^{25,31,185} Fractionation with SEC prior to the analysis with MALDI TOF is required to sample the entire distribution.^{22,23,29,50,80} Electrospray ionisation (ESI) is another ionisation technique for mass spectrometry that has a high potential in polymer molecular weight distribution (MWD) characterisation. Only a limited number of publications have appeared so far mainly because overlapping distributions of polymeric ions are observed in the mass spectra due to the multiple charging nature of ESI. Mass spectrometers such as quadrupoles^{62,68,79} and sector instruments⁶⁵ do often not provide sufficient resolution to distinguish between the isotopic peaks. The combination of ESI and FT-ICR MS provides enough resolution to distinguish the isotopic peaks of the polymer molecules in the different charge states. For example, the isotopic peaks of a poly(ethylene glycol) (PEG) sample with a molecular weight of 23,000 were resolved.⁶⁴ Only a few research groups have used ESI FT-ICR MS for the characterisation of synthetic polymers.^{64,67,76,82,110,113} Most groups use FT-ICR MS in combination with MALDI.^{51-53,56,93,102,186-190} Given the single charge state observed with MALDI, the technique is limited to relatively low-molecular weight polymeric systems (typically <10,000 Da) since high mass ions (high m/z) are more difficult to trap, a problem that can be overcome with ESI.^{52,53}

In this chapter ESI FT-ICR MS is used for the characterisation of the MWD of a series of monodisperse poly(oxyalkylene)s. The influence of the charge state on the measured polymer parameters M_n and M_w is studied. A method is introduced to derive the MWD of monodisperse poly(oxyalkylene)s from the analysis.

3.2. Experimental

The electrospray ionisation Fourier transform ion cyclotron resonance mass spectrometry (ESI FT-ICR MS) experiments were performed with a modified Bruker-Spectrospin (Fällanden, Switzerland) APEX 7.0e FT-ICR MS equipped with a 7T super-conducting magnet and a Bruker InfinityTM Cell¹⁷¹ (see Chapter 2).

The MALDI TOF spectra were acquired using a Bruker BIFLEX (Bruker-Franzen Analytik, Bremen, Germany) system equipped with a SCOUT ion source and a 337 nm nitrogen laser VLS-337i (Laser Science, Newton MA). All analysis shown here were carried out in the reflectron mode with an acceleration voltage of 20 kV. The system was externally calibrated using phtalocyanine (C₃₂N₈Cl₁₆) and a mixture of PEG1000, PEG2000 and PEG3000.

The poly(ethylene glycol) (PEG): PEG3000 and PEG6000 and poly(propylene glycol) (PPG): PPG1150 and PPG3250 standards were obtained from Fluka Chemical (Buchs, Switzerland). PEG1000 was obtained from Serva (Heidelberg, Germany). The poly(tetrahydrofurane) PTHF2000 sample was supplied by DSM (Geleen, The Netherlands). PTHF2000 has a polydispersity of ~1.05-1.1 and the other polymers have a polydispersity of ~1.01-1.04. The numbers in the names denote the average molecular weight of the sample. All samples contained sodium and were used without further purification. The PEG samples were sprayed in an ~ 1 µM solution with a solvent composition of 70:30 MeOH:H₂O. PPG and PTHF were sprayed at concentrations of ~5 and 100 µM, respectively. The average molecular weight of the polymer standards (e.g. 3000 g/mol for PEG3000) was used for the calculation of the polymer molar concentration. Approximately 10 µM NaI (Aldrich) was added to the polymer solutions via a concentrated NaI stock solution in H₂O to enhance the ionisation.

The matrix used for the MALDI TOF experiments was 2,5-dihydroxybenzoicacid (2,5-DHB) from Sigma Chemical Co. (St. Louis, MO). The samples were mixed with the matrix using a molar ratio of 1000:1 matrix:sample. All samples and the DHB were dissolved in ethanol, mixed and deposited manually on the stainless steel MALDI target.

3.3. Results and discussion

The ESI FT-ICR MS spectra of PEG3000 and PTHF2000 are shown in figure 3.1. Several distributions are observed each corresponding to a particular charge state of the same molecular weight distribution. Charge states of 2+ to 7+ are observed for PEG3000. PPG3250 and PTHF2000 are found in charge states

1+ to 5+ and 1+ to 3+, respectively. From the maximum charge state observed for each polymer it becomes clear that PEG3000 accommodates more charges than PPG3250 although the average molecular weight is about the same.

If conformational effects do not play a role in the cationisation of the different polymer molecules, we can assume that the observation of a certain charge state distribution is statistical of nature. The normalised intensity of M_p is plotted as a function of the charge state in figure 3.2. M_p is the most intense peak in the mass spectrum for a given charge state. Normalisation was performed with the M_p in the most intense charge state ($z=5$ for PEG3000). The comparison of the charge state distributions of PEG3000 and PEG6000 reveals that large polymer molecules (PEG6000) accommodate more charges than small polymer molecules (PEG3000). The intensities of the peaks in figure 3.2 are corrected for the charge state (section 3.3.3.).

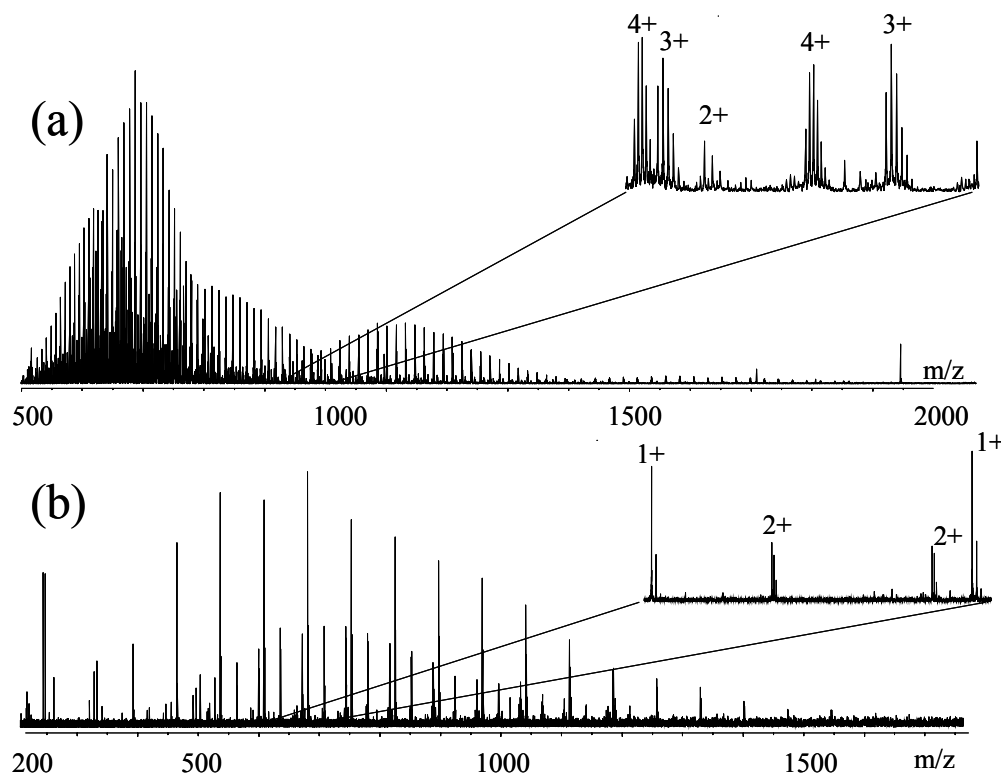


Figure 3.1 ESI FT-ICR MS spectra of PEG3000 (a) and PTHF2000 (b) with sodium iodide added to the spray solution (70:30 MeOH:H₂O).

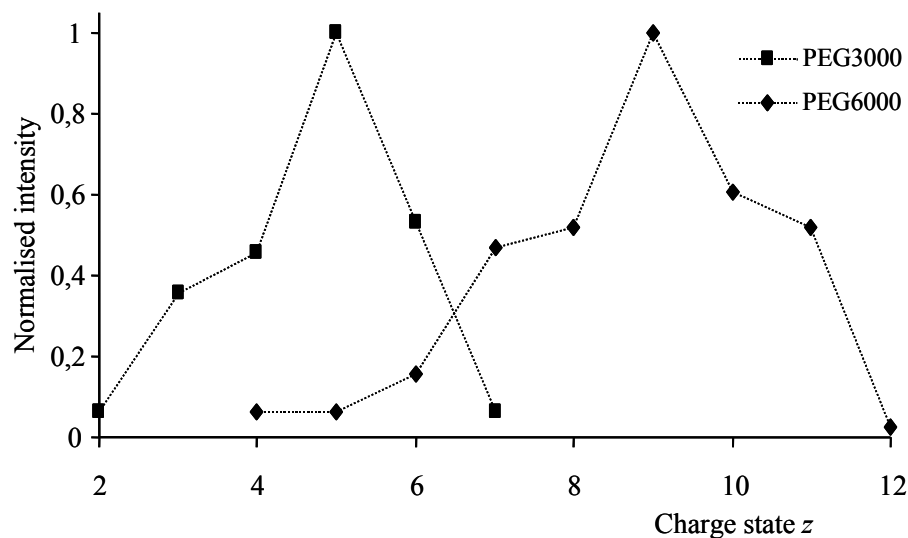


Figure 3.2 Normalised intensity of M_p plotted for all charge states observed for PEG3000 and PEG6000.

3.3.1. Charge state dependence of M_p , M_n and M_w

If the ionisation probability would be independent of the chain length of the polymer molecules, the distributions corresponding to different charge states should be similar and yield unique values for M_p , M_n and M_w . The mass values (m_i) used for the determination of M_n and M_w (equation 1.1) in charge state z are calculated by subtracting the mass of z cations (m_{cat}) from z times the measured m/z of each individual mono-isotopic peak ($m_i = z \cdot (m/z) - z \cdot m_{cat}$). In this manner the masses of the neutral polymer chains are obtained. The calculations were performed for all charge states observed for PEG1000/3000/6000, PPG1150/3250 and PTHF2000.

The dependence of the measured M_n on the charge state is presented in figure 3.3. A linear increase of the measured M_n as a function of the charge state is observed for all poly(oxyalkylene)s. M_p and M_w (not shown) exhibit a similar behavior and are not discussed in detail. The molecular weight of the poly(oxyalkylene) influences the slope of the lines in figure 3.3, which decreases with increasing average molecular weight.

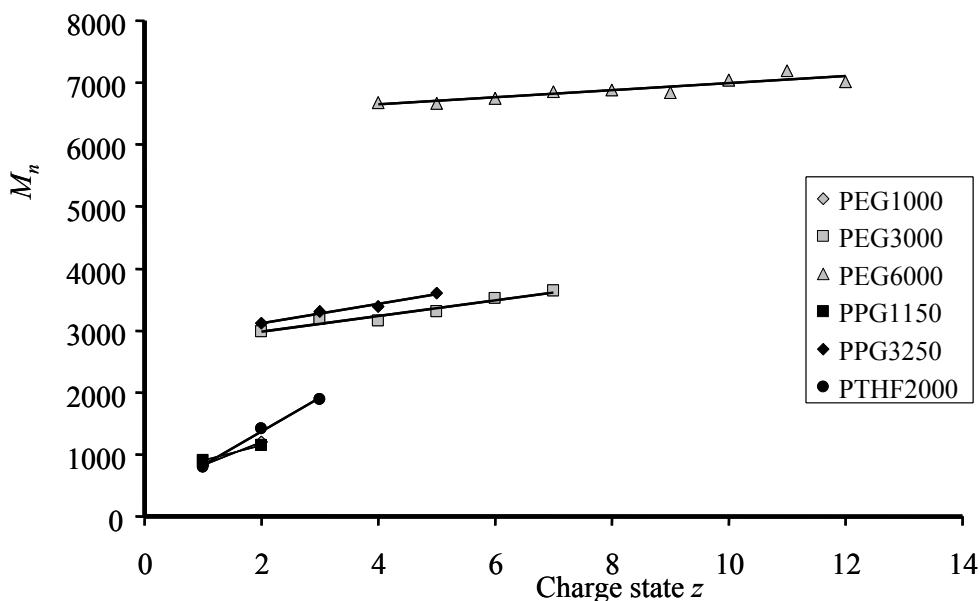


Figure 3.3 Influence of the measured number average molecular weight M_n on the charge state of PEG, PPG and PTHF with different average molecular weights.

An increase in the measured M_n value of PEG with the charge state has been observed earlier with electrohydrodynamic ionisation MS.^{16,191} With ESI, a linear increase in the *maximum* number of accommodated sodium cations with the molecular weight of PEG has been observed.^{62,63} These findings and the results presented here indicate that a strong correlation exists between the number of oxygen atoms that a PEG molecule contains, and the charge states observed, because the charging sites on PEG, PPG and PTHF are the oxygen atoms.^{62,192-194} Molecular modelling has demonstrated that up to eight oxygen atoms are involved in the formation of a singly sodiated PEG ion with MALDI^{192,193} and seven and six for PPG and PTHF, respectively.¹⁹⁴ An explanation for the increasing M_n with the charge state for all poly(oxyalkylene)s is based on the length of the molecules. Relatively long molecules contain more available charge sites (oxygen atoms) than short polymer molecules. Consequently, small molecules are preferably observed in low charge states because of a lack of available sites. Large polymer molecules can accommodate more charges and are mainly observed in high charge states. An increase of calculated M_n with the observed charge state z results.

3.3.2. Dependence of the monomer length/structure on the observed charge states

The relation between the number of oxygen atoms and the charge state can be visualised by plotting M_n/m_{mon} , which is the number average degree of polymerisation P_n , versus the charge state (figure 3.4). Here, m_{mon} denotes the monomer mass. The ratio M_n/m_{mon} yields the average number of oxygen atoms it takes to accommodate a certain number of charges provided that the monomer unit contains only one oxygen atom. By plotting M_n/m_{mon} versus z , the three poly(oxyalkylene)s with a different monomer composition but with oxygen as charge site can be compared. We have seen earlier that the slope of the line in figure 3.3 decreases with increasing molecular weight (or number of available charging sites) of the polymer samples. The same is true for figure 3.4. This is because a large PEG6000 molecule/cation complex will experience only a slight conformational distortion if an additional charge is added to the complex. A relatively small PEG1000 molecule/cation complex will experience a much larger conformational distortion. If it is assumed that the number of oxygen atoms is the only parameter that influences the slope of the line in figure 3.4, then PPG3250 should have a larger slope than PEG3000 since PPG3250 contains fewer oxygen atoms. PEG3000 and PPG3250 contain an average of ~ 75 and ~ 60 oxygen atoms, respectively. The slopes of the lines in figure 3.4 are however almost the same. A tentative explanation for this effect is that the addition of a methyl group to the polymer chain (PPG vs. PEG) leads to a different conformation of the sodium cation/polymer chain complex as was shown by Gidden *et al.*¹⁹⁴ using ion mobility methods and molecular mechanics/dynamics. The methyl groups point away from the sodium cation but create enough hindrance to distort the complex. Gidden *et al.* showed that the sodium cation interacts with seven PPG oxygen atoms and eight PEG oxygen atoms.¹⁹⁴ The slope of the lines in figure 3.4 decreases with the available number of oxygen atoms (e.g. PEG3000 vs. PEG6000) but increases with the number of oxygens involved in the cation/polymer chain complex (e.g. PEG vs. PTHF). For example, if one oxygen atom were required for a stable complex, the slope of the line in figure 3.4 would be 1 (if no other parameters influence the slope) whereas a slope of 10 would be obtained if 10 oxygens were involved in the formation of a stable complex. These two effects contribute to the similar slopes observed for PEG3000 and PPG3250.

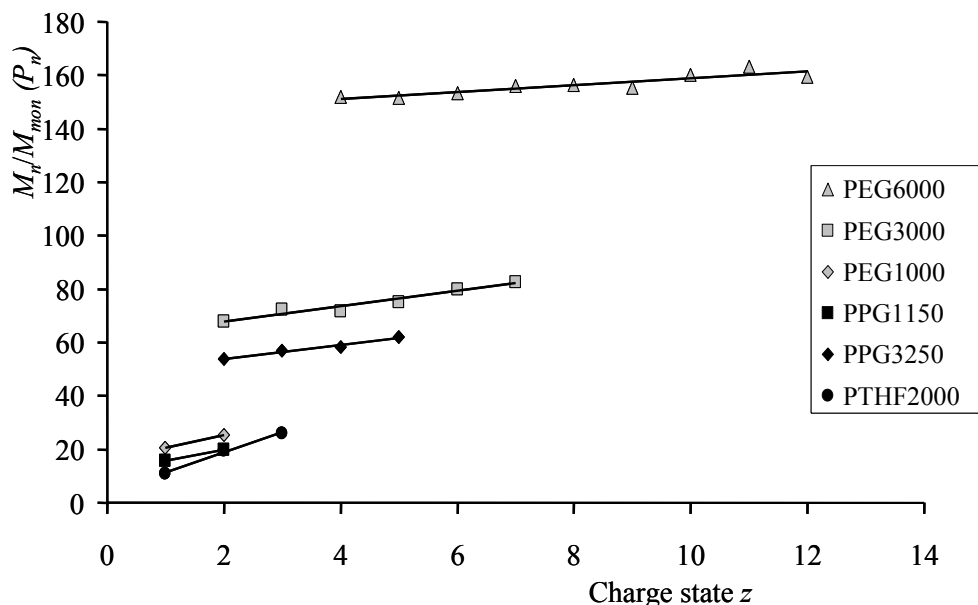


Figure 3.4 $M_n/m_{mon} (P_n)$ versus charge state for PEG, PPG and PTHF with different molecular weights. $M_n/m_{mon} (P_n)$ is correlated to the number of charging sites (oxygen atoms).

For PTHF2000 a slope two times larger than the slope of PEG1000 and PPG1150 is observed although the molecules contain a comparable number of oxygen atoms. This can be due to the relatively high polydispersity of PTHF (~ 1.05 - 1.10) compared with the other samples studied in this chapter (~ 1.01 - 1.04). A difference in the M_n values between two distributions of different charge state can therefore be higher than for a less polydisperse sample. PEG and PPG have, however, a similar polydispersity. Differences in the slope between PEG and PPG can therefore not be explained by a difference in the polydispersity.

Figures 3.3 and 3.4 demonstrate that the characterisation of the molecular weight distribution with ESI FT-ICR MS introduces a large error if an arbitrary charge state is used for the calculation of M_n . The difference in M_n between the highest and lowest charge state of PEG3000 is about 650 Da! In the next section a method is introduced that combines all charge states for the calculation of the molecular weight distribution.

3.3.3. Reconstruction of the molecular weight distribution

It was shown that the analysis of the molecular weight distribution with ESI FT-ICR MS can introduce a large error in the calculated M_n . The question is addressed if it is possible to reconstruct the molecular weight distribution

representative for the polymer of interest using all the different charge states. Therefore all distributions are combined taking the charge state and isotopic distribution of the polymer molecules into account using equation (3.1).

$$I_n^{corr} = \sum_z \frac{I_{n,z}}{z \cdot P(n)} \quad (3.1)$$

All ions are excited to the same radius in the ICR cell during the excitation event¹⁶³ independent of m/z . An ion charged by z cations will induce z times more current on the detection electrodes than a singly charged ion. Therefore the peak intensity of a polymer molecule with degree of polymerisation n in charge state z ($I_{n,z}$) has to be corrected for the number of charges z . As the chance of finding an molecule containing only ^{12}C isotopes, $P(n)$, decreases with increasing number of carbon atoms, the intensities used have to be corrected as was shown by others.⁵¹ The isotopic correction is carried out for all polymer molecules present in all charge states. In figure 3.5 the reconstructed molecular weight distribution of PEG3000 is compared with the distribution as obtained with MALDI TOF. The two distributions are in good agreement, $M_n(\text{MALDI TOF}) = 3250$ Da and $M_n(\text{ESI FT-ICR MS}) = 3350$ Da. For PEG6000 these values are $M_n(\text{MALDI TOF}) = 6530$ Da and $M_n(\text{ESI FT-ICR MS}) = 6980$ Da. This illustrates that the molecular weight distribution can be reconstructed using all charge states with a reasonable accuracy (~7%). The distributions of the polymers have not been verified using SEC but several authors have shown that accurate MWD analysis can be performed with MALDI when the polydispersity is lower than 1.1, which is the case for the polymers studied here.^{22,23,29,50,80} Similar reconstructions have been performed before with electrohydrodynamic ionisation^{16,191} MS and ESI FT-ICR MS.⁶⁴

The peak height was used in the previous part for the calculation of M_n and M_w because peak areas are relatively difficult to determine with the data acquisition program XMASS. Another reason for using the peak height was that some peaks in the spectrum of PEG6000 overlap with peaks of other polymer molecules in other charge states. Therefore it is not possible to determine the exact area of all the peaks. We have studied whether the peak area is a better parameter for the reconstruction since peaks are broadened at higher masses in the same charge state, which is inherent to FT-ICR MS. The difference in reconstructed M_n values using peak heights and areas of PEG3000 is less than 1%. Larger differences are only expected for polymers with a broad molecular weight distribution. When polymers of low polydispersity are investigated, the m/z range in which a distribution of a certain charge state is found is small e.g. the peaks of PEG3000 in the 3+ charge state are observed in the m/z range of 900-1400. The higher the charge state, the

narrower the m/z range of the distribution and peak broadening effects become very small. Since the poly(oxyalkylene)s investigated in this report are of low polydispersity and for PEG3000 no differences are found for M_n calculated using the peak area and peak height, the peak height can be used for the calculations.

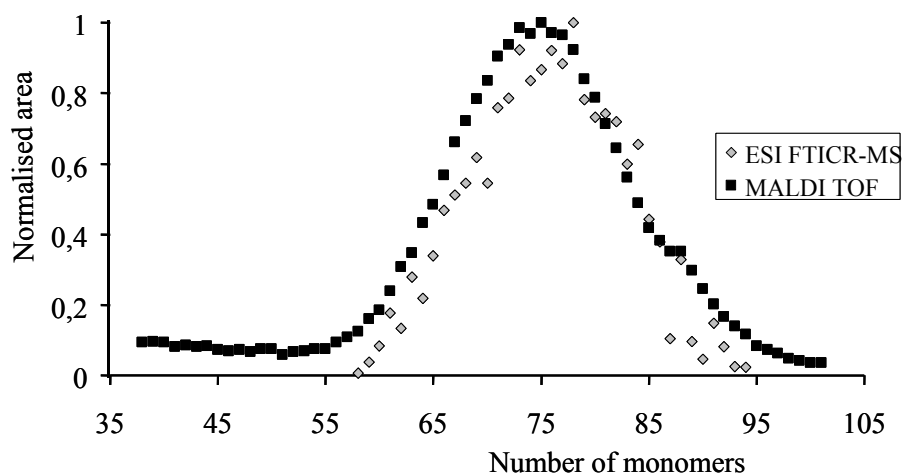


Figure 3.5 Calculated molecular weight distribution of PEG3000 using all charge states observed with ESI FT-ICR MS compared with the MALDI TOF distribution.

3.4. Conclusions

The combination of ESI with FT-ICR MS for the characterisation of the molecular weight distribution of a series of poly(oxyalkylene)s yields apparent M_n values that increase with the charge state. This effect is due to the number of available charging sites (oxygen atoms) that the polymer molecules contain. Small polymer molecules have fewer charging sites than large polymer molecules and are preferentially observed in low charge states whereas large molecules are preferentially observed in higher charge states. The shielding effect of the methyl groups of the PPG molecules lead to a cation/PPG complex that involves an interaction with fewer oxygen atoms than a cation/PEG complex. A smaller increase of the M_n value of PPG with the charge state (compared with PEG) results.

A method is introduced that combines all charge states in order to reconstruct the molecular weight distribution. Isotopic effects and the charge state are taken into account. The reconstructed distributions are in good agreement with the distributions observed with MALDI TOF-MS. This illustrates that such corrections must always be performed for polymers with a polydispersity > 1.01 .

Chapter 4

Accurate determination of the polymer endgroup and monomer mass of polyoxyalkylenes

Accurate monomer and endgroup masses were measured of three polyoxyalkylenes in the mass range of 400-8000 Da using electrospray ionisation (ESI) Fourier transform ion cyclotron resonance mass spectrometry (FT-ICR MS). Use of all multiple charge states observed with ESI lead to a threefold increase in precision of the endgroup and monomer mass determination when compared with MALDI. The improvement is attributed to the increased number of data points used for the regression procedure. Endgroup masses are determined with a mass error better than 5 and 75 millimass units for the molecular weight range of 400-4200 Da and 6200-8000 Da, respectively. A mass error of better than 1 millimass unit was observed for all monomer mass determinations. With ESI, endgroup and monomer masses have been determined for PEG molecules with a mass higher than 8000 Da. This is almost two times larger than observed with MALDI on the same instrument.

4.1. Introduction

One of the most commonly used techniques to obtain quantitative endgroup information is titration. However, this technique fails to provide information about the structure of the endgroup. NMR can provide information on both the endgroup and monomer structure but only yields an average of these polymer characteristics. Mass spectrometry provides detailed molecular information on the composition and structure for a large variety of polymer classes using only minute amounts of sample. Matrix-assisted laser desorption/ionisation time-of-flight mass spectrometry (MALDI TOF) has proven to be a good technique for the characterisation of the molecular weight distribution and the monomer/endgroup composition up to a molecular weight of $\sim 50,000$ Da.^{22,25,29} However, the mass resolution is not sufficient to distinguish the different isotopic peaks at high m/z .

Isotopic resolution is not necessary for the determination of the molecular weight distribution but it is required for an accurate endgroup and monomer mass determination as will be shown in this chapter.

MALDI Fourier transform ion cyclotron resonance mass spectrometry (FT-ICR MS) has been explored for the characterisation of synthetic polymer endgroups.^{92,93} However, given the single charge state generated with MALDI, the technique is limited to relatively low-molecular weight polymer systems (typically <10,000 Da) since ions with a high mass (high m/z) are difficult to trap.^{52,53} A technique that overcomes this problem is electrospray ionisation (ESI). The main advantage of ESI compared to other ionisation techniques is that multiply charged polymer ions are formed that are easier to trap and enables an analysis at lower m/z values. ESI also provides a low internal energy deposition, like MALDI, resulting in minimal fragmentation of the polymer ions. ESI can be used online with SEC, spraying conventional solutions.^{77,79} Solubility properties and the inability to interact with cations of for example polyolefins can be a limitation for polymer analysis with ESI.¹

Due to the multiple charge states created by ESI, overlapping distributions of polymeric ions are observed in the mass spectra. Mass spectrometers such as quadrupoles,^{62,68,79} sector⁶⁵ and TOF instruments do often not provide enough mass resolution to distinguish between the isotopic peaks. The combination of ESI and FT-ICR MS provides enough mass resolution to distinguish the isotopic peaks of the polymer molecules in the different charge states of a molecular weight up to 23,000.⁶⁴ Only a few research groups have used ESI FT-ICR MS for the characterisation of synthetic polymers,^{64,67,76,82,110,113} while most groups use MALDI.^{51-53,56,93,102,186-190}

We have combined the advantages of ESI and FT-ICR MS for the characterisation of polyethylene glycol (PEG), polypropylene glycol (PPG) and polytetrahydrofuran (PTHF) on monomer and endgroup mass. A novel method is introduced that uses all charge states in one linear regression procedure. We will demonstrate how this method can be used to improve the endgroup characterisation substantially compared to the linear regression procedure using a single charge state, as done with MALDI.

4.2. Experimental

The electrospray ionisation Fourier transform ion cyclotron resonance mass spectrometer (ESI FT-ICR MS) experiments are performed with a modified Bruker-Spectrospin (Fällanden, Switzerland) APEX 7.0e FT-ICR MS equipped

with a 7-T super-conducting magnet and a Bruker InfinityTM Cell¹⁷¹ (see chapter 2).

The polyethylene glycol (PEG): PEG3000 and PEG6000 and polypropylene glycol (PPG): PPG1150 and PPG3250 standards are obtained from Fluka Chemical (Buchs, Switzerland). PEG1000 is obtained from Serva (Heidelberg, Germany). The polytetrahydrofuran PTHF2000 sample is supplied by DSM (Geleen, The Netherlands). The numbers in the names denote the average molecular weight of the samples. All samples contain sodium from origin and are used without further purification. The PEG samples are sprayed in an $\sim 1 \mu\text{M}$ solution with a solvent composition of 70:30 MeOH:H₂O. PPG and PTHF are sprayed with concentrations of ~ 5 and $100 \mu\text{M}$, respectively. The average molecular weight of the polymer standards (e.g. 3000 g/mol for PEG3000) is used for the calculation of the polymer concentration. Approximately $10 \mu\text{M}$ NaI (Aldrich) was added to the polymer solutions to be sprayed via a concentrated stock solution in H₂O to increase the S/N ratio.

4.3. Results and discussion

A series of polyoxyalkylenes with different average molecular weights in the range 400-8000 Da was used for endgroup determination. Charge states of 1+ to 12+ are generated depending on the average molecular weight of the polymer standards. In figure 3.1 the spectra of PEG3000 and PTHF2000 are shown. All polymer peaks are isotopically resolved (see insert of figure 3.1) with a resolution $(m/\Delta m)_{50\%}$ of ~ 25.000 at $m/z \sim 1000$ in broadband mode.

The spectrum of PEG6000 is more complex than the spectrum of PEG3000 although the samples contain approximately an equal number of polymer molecules. This difference is caused by three factors. First, higher mass molecules are observed in more charge state distributions. Second, the spacing between the molecules and isotopic peaks becomes smaller for higher charge states. Third, the number of isotopic peaks increases with the degree of polymerisation. Figure 4.1 shows a simulation of the isotopic distribution of three polymer molecules (upper figures) with degrees of polymerisation 25, 75 and 150, which are comparable to the size of a molecule in PEG1000, PEG3000 and PEG6000, respectively. Four isotopic peaks are observed for PEG1000 while for a PEG6000 molecule, about 10 isotopic peaks show up in the spectrum. Another feature in figure 4.1 is that the intensity of the mono isotopic peak decreases with increasing molecular weight. The intensity has become almost zero for PEG6000. This is because the probability to observe a molecule containing only ¹²C atoms decreases with an increasing number of carbon atoms. Some of the experimentally observed isotopic peaks of

PEG6000 (lower figure) show deviations from the simulated isotopic pattern. This is probably caused by an overlap with peaks of other polymer molecules. In general, the experimentally observed isotopic patterns correspond well with the simulated pattern.

4.3.1. Theory of the endgroup determination using the linear regression and averaging methods with electrospray ionisation

Two methods have been introduced by others for the calculation of the endgroup mass, monomer mass and mass accuracy of synthetic polymers from MALDI FT-ICR mass spectra.⁹³ The method has been applied successfully to linear and hyperbranched polymers.^{56,92,93,95,105} The multiple charge states observed with ESI require a linear regression procedure similar to the procedure applied to the MALDI mass spectrum in which only singly charged ions are observed. In ESI, an ion in charge state z will contain z cations. The charge state is determined from the m/z spacing between the isotopic peaks. Since z can be very large, and the mass accuracy of the FT-ICR MS is very high, the mass of z electrons is taken into account. Fenn *et al.* estimated more than 4200 charges on a PEG with a molecular weight of 5 million,⁶³ which will result in an error of ~ 2.3 Da if a correction for the electron is not performed. The mass of an electron m_{elec} has to be subtracted from the mass of the neutral atom or molecule that is responsible for the charge, to obtain the cation mass (for example $m_{atom} - m_{electron}$). The measured mass over charge ratio, $(m/z)^{z+}_{meas}$, for the monoisotopic polymer molecule is given by

$$\left(\frac{m}{z}\right)^{z+}_{meas} = \frac{n \cdot m_{mon} + m_{end} + z \cdot m_{cat}}{z} = \quad (4.1)$$

$$n \cdot \frac{m_{mon}}{z} + \frac{m_{end}}{z} + m_{cat}$$

where m_{mon} is the mass of the monomer unit, n is the number of monomers, m_{end} is the endgroup mass and m_{cat} is the mass of the cation. Equation (4.1) has to be extended with the term $x \cdot (mass^{13C} - mass^{12C})/z$ if the selected molecules contains x ^{13}C atoms. We have considered the masses of the cation and electron to be known exactly. Later in this chapter we will describe a method that enables the determination of the identity of an unknown cation.

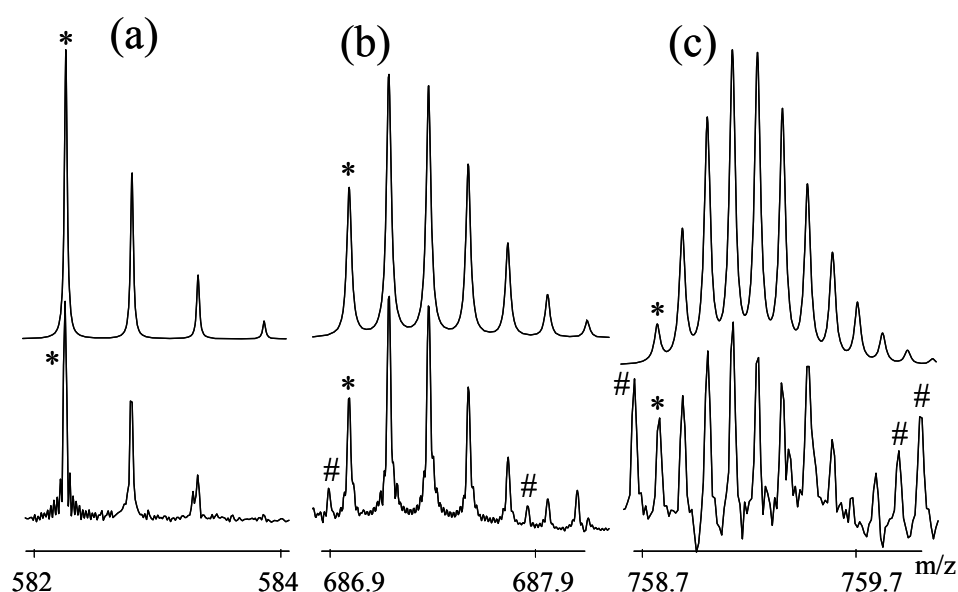


Figure 4.1 Simulated (upper) and experimentally observed isotopic pattern of PEGs with $n=25$, $z=2$ (a), $n=75$, $z=5$ (b) and $n=150$, $z=9$ (c). Peaks marked with an asterisk (*) are the mono isotopic peaks. Peaks marked with an # originate from other polymer molecules.

A more manageable way to determine the endgroup and monomer masses is by plotting the mass m_{meas} (by multiplying $(m/z)^{z+}$ with the charge state) as a function of n (equation (4.2)) assuming that z is known. In this equation the monomer mass and the sum of the endgroup and z cation(s) follow immediately from the intercept and slope, respectively

$$m_{meas} = n \cdot m_{mon} + m_{end} + z \cdot m_{cat} \quad (4.2)$$

In order to determine the degree of polymerisation n of an ion, all possible combinations, $m_{end} = m_0 + n_i \cdot m_{mon}$, have to be considered. Here, m_0 is the smallest possible endgroup mass for $n_i = 0, 1, 2, \dots$ ⁹³ The calculated endgroup mass must be consistent with the information that is known about the polymer system (synthesis etc).

Note that for unknown polymers only isotopic peaks may be visible in the mass spectrum that contains an unknown number of ^{13}C atoms. The resulting m_0 , which is calculated with linear regression is the sum of the endgroup and this unknown number of ^{13}C atoms. To determine the number of ^{13}C atoms the following procedure is followed. First, the monomer mass is the slope of

equation (4.2), which is accurately determined (see further). Second, the elemental composition of the monomer is determined using the monomer mass. Third, by comparing the theoretical isotopic pattern of a given molecule with the experimentally observed pattern, as done in figure 4.1, the number of ^{13}C atoms that a given ion contains can be estimated. Note that for relatively large monomer masses, e.g. > 100 Da, various elemental compositions can correspond with the determined monomer mass. This requires additional information about the polymer from techniques such as NMR.

For large n , the distance between the measured points and the intercept becomes large. As a result, small deviations in the slope will introduce a large error in the endgroup mass. This can easily be seen from the expression for the precision of the endgroup mass σ_{end}^2 that results from the propagation of errors in the extrapolation procedure

$$\sigma_{end}^2 = \sigma_b'^2 + \bar{n}^2 \sigma_a'^2 = \frac{\sigma_{data}^2}{N} + \bar{n}^2 \frac{\sigma_{data}^2}{\sum_{i=1}^N n_i'^2} \quad (4.3)$$

Where $\sigma_b'^2$, $\sigma_a'^2$ and σ_{data}^2 are respectively the uncertainties at the centre of gravity in the fit procedure, the slope and the mass measurements, \bar{n} is the transformed average degree of polymerisation as described by van Rooij and coworkers⁹³, N is the number of data points, n_i is a polymer molecule with degree of polymerisation i and $n_i' = n_i - \bar{n}$. A more detailed description of equation (4.3) can be found elsewhere.⁹³

A method which is unaffected by small fluctuations in the slope has been evaluated by van Rooij *et al.* for MALDI FT-ICR MS.⁹³ This method, 'the averaging method', requires a known elemental composition of the monomer. The method does not involve an extrapolation procedure to $n=0$. By subtracting n times the mass of the monomer from the mass of the singly charged ions formed by MALDI, the endgroup plus cation mass is obtained. This procedure is followed by an averaging of the results of all polymer molecules. For multiply charged ions, as formed by ESI, the same result is obtained by subtracting n times the mass of the monomer from m_{meas}^{z+} . The charge state follows from the spacing between the isotopic peaks. Hence isotopic resolution is absolutely necessary.

4.3.2. Results of the endgroup determination using the linear regression and averaging methods

The results for the determination of the endgroup and monomer masses of PEG1000, PEG3000 and PEG6000 determined with linear regression ($m_{end,regression}$ and $m_{mon,regression}$) and the averaging method ($m_{end,average}$) are shown in tables 4.1 and 4.2. The endgroup masses have been calculated for all observed charge states separately. Only peaks with S/N >3 were used for the endgroup calculations.

The elemental composition of the monomers of PEG, PPG and PTHF is confirmed with linear regression as C₂H₄O ($m_{mon,exact}$ =44.0262 Da, $m_{mon,regression}$ ≈44.025 Da), C₃H₆O ($m_{mon,exact}$ =58.0419 Da, $m_{mon,regression}$ ≈58.042 Da) and C₄H₈O ($m_{mon,exact}$ =72.0575 Da, $m_{mon,regression}$ ≈72.058 Da), respectively. The mass accuracy resulting from linear regression is very high ($\Delta m_{mon,regression}$ <<0.1%) as can be seen from tables 4.1 and 4.2. Note that $m_{mon,regression}$ is determined for all charge states separately.

The endgroup mass $m_{end,regression}$ calculated with equation (4.2) includes the mass of the cation(s) as well (similar to the method used by van Rooij *et al.*⁹³) and therefore increases with the charge state. When the mass of the cations and ¹³C atoms is subtracted from the calculated endgroup, $m_{end-cation,regression}$ in tables 4.1 and 4.2, the elemental composition of the endgroups is confirmed as –H and –OH ($m_{end,exact}$ =18.0106) for all polymers studied. This corresponds to what is known about the synthesis of polyoxyalkylene polymers. A comparison of the theoretical and the experimentally observed endgroup masses is described in more detail later in this chapter.

The $\sigma_{mon,regression}$ and $\sigma_{end,regression}$ values are the uncertainties of the monomer and endgroup mass respectively as determined with the linear regression method. The $\sigma_{end,average}$ value is the uncertainty of the endgroup mass as determined with the averaging method. Note that $\sigma_{mon,average}$ =0 because the average method assumes the monomer mass to be known exactly. The determination of the accuracy in the experimental data (σ_{data}) has been done for all charge states separately. We have taken the maximum observed experimental mass error in the measurements as σ_{data} . The σ_{data} value is considered for all charge states separately since the mass error increases with decreasing charge state (see below). Large fluctuations of σ_{data} for the highest charge states have not been observed, e.g. for 3+ to 7+ of PEG3000.

Chapter 4

Masses (Da) and deviations	PEG1000			PEG3000					
	z	1+	2+	2+	3+	4+	5+	6+	7+
$n (N)$		10-26 (17)	20-32 (13)	58-80 (22)	59-92 (34)	60-92 (33)	60-93 (32)	63-94 (28)	72-89 (16)
$m_{mon, regression}$		44.0266	44.0267	44.0244	44.0255	44.0263	44.0264	44.0262	44.0261
$\Delta m_{mon, regression}$		0.0004	0.0005	-0.0018	-0.0007	0.0001	0.0002	<0.0001	-0.0001
$\sigma_{mon, regression}$		0.0006	0.0008	0.0020	0.0005	0.0006	0.0006	0.0003	0.0005
$m_{end, regression}$		40.9963	63.9788	64.0979	87.0287	109.9672	132.9421	155.9484	178.9434
$m_{end-cation, regression}$		18.0071	18.0003	18.1194	18.0610	18.0104	17.9960	18.0131	18.0189
$\Delta m_{end, regression}$		-0.0035	-0.0102	0.1089	0.0504	-0.0002	-0.0145	0.0025	0.0083
$\sigma_{end, regression}$		0.0108	0.0197	0.1365	0.0399	0.0470	0.0487	0.0207	0.0429
$m_{end, average}$		41.0031	63.9926	63.9768	86.9757	109.9699	132.9571	155.9453	178.9350
$m_{end-cation, average}$		18.0139	18.0141	17.9983	18.0080	18.0130	18.0110	18.0106	18.0105
$\Delta m_{end, average}$		0.0033	0.0036	-0.0122	-0.0025	0.0025	0.0005	-0.0005	-0.0001
$\sigma_{end, average}$		0.0028	0.0028	0.0127	0.0051	0.0058	0.0060	0.0024	0.0028
σ_{data}		0.0117	0.0101	0.0597	0.0300	0.0336	0.0340	0.0126	0.0110

Table 4.1 Calculated monomer and endgroup masses (Da) and accuracy for PEG1000 and PEG3000 of all observed charge states determined with the regression and averaging method. Only the monoisotopic peaks have been used for the determination of the monomer and endgroup masses. The Δ values denote the difference between the theoretical and measured masses. The σ values are the corresponding standard deviations, which follow from linear regression or equation 4.3 (average method). $m_{end-cation, regression}$ is the endgroup mass as calculated by equation 4.2 minus the mass of the cation(s). $m_{end-cation, average}$ is similar to $m_{end-cation, regression}$ but determined by the averaging method. σ_{data} is considered for all charge states separately and is the maximum observed experimental mass error.

Masses (Da) and deviations	z	PEG6000								
		4+	5+	6+	7+	8+	9+	10+	11+	12+
n (N)		143-161 (17)	140-167 (26)	139-168 (26)	137-178 (37)	143-174 (32)	140-169 (30)	151-167 (16)	143-174 (32)	148-166 (14)
$m_{mon, regression}$		44.0198	44.0243	44.0254	44.0258	44.0256	44.0264	44.0260	44.0263	44.0265
$\Delta m_{mon, regression}$		-0.0064	-0.0019	-0.0009	-0.0004	-0.0006	0.0002	-0.0002	0.0001	0.0003
$\sigma_{mon, regression}$		0.0076	0.0052	0.0024	0.0024	0.0028	0.0024	0.0056	0.0020	0.0048
$m_{end, regression}$		114.8888	137.1809	160.0199	182.9255	205.9571	228.8091	251.8789	274.8222	297.7904
$m_{end-cation, regression}$		18.9185	18.2214	18.0712	17.9876	18.0299	17.8927	17.9733	17.9274	17.9063
$\Delta m_{end, regression}$		0.9079	0.2108	0.0606	-0.0230	0.0193	-0.1178	-0.0373	-0.0832	-0.1042
$\sigma_{end, regression}$		1.1499	0.7911	0.3758	0.3847	0.4429	0.3759	0.8956	0.3111	0.7460
$m_{end, average}$		113.9175	136.8852	159.8877	182.8646	205.8609	228.8458	251.8402	274.8335	297.8283
$m_{end-cation, average}$		17.9472	17.9257	17.9390	17.9267	17.9338	17.9294	17.9346	17.9386	17.9443
$\Delta m_{end, average}$		-0.0634	-0.0849	-0.0716	-0.0839	-0.0768	-0.0812	-0.0760	-0.0719	-0.0663
$\sigma_{end, average}$		0.0404	0.0404	0.0195	0.0267	0.0258	0.0210	0.0284	0.0181	0.0288
σ_{data}		0.1664	0.2062	0.0993	0.1623	0.1457	0.1152	0.1136	0.1023	0.1078

Table 4.2 Calculated monomer and endgroup masses (Da) and accuracy for PEG6000 of all observed charge states determined with the regression and averaging method. For the determination of the exact masses, only the peaks containing 4 ^{13}C isotopes were used. The Δ values denote the difference between the theoretical and measured masses. The σ values are the corresponding standard deviations, which follow from linear regression or equation 4.3 (average method). $m_{end-cation, regression}$ is the endgroup mass as calculated by equation 4.2 minus the mass of the cation(s) and ^{13}C atoms. $m_{end-cation, average}$ is similar to $m_{end-cation, regression}$ but determined by the averaging method. σ_{data} is considered for all charge states separately and is the maximum observed experimental mass error.

The range of polymer molecules n and the corresponding number of datapoints N observed for each charge state z and used for the calculations are given in the tables. In most cases N is determined by the range of polymer molecules n observed in the mass spectrum. However, for some polymer molecules it was difficult to locate the peak due to peak overlap with other polymer molecules. Therefore, N and the range of polymer molecules n do not correspond in all cases.

The $m_{end-cation, regression}$ values of PEG1000 and PEG3000 are ~ 18.01 Da which is less than 0.08% difference with the theoretical endgroup mass for $-\text{OH}$ and $-\text{H}$. For PEG6000 this value is smaller than 0.7%. The 2+ charge state of PEG3000 and 4+ - 5+ charge states of PEG6000 are the only exceptions due to the decreasing mass accuracy at higher m/z (see further). For PEG6000 and PPG3250 only the peaks containing 4 and 1 ^{13}C isotopes were used for the endgroup and

monomer calculations, respectively. This is necessary since the intensity of the monoisotopic peaks becomes too low.

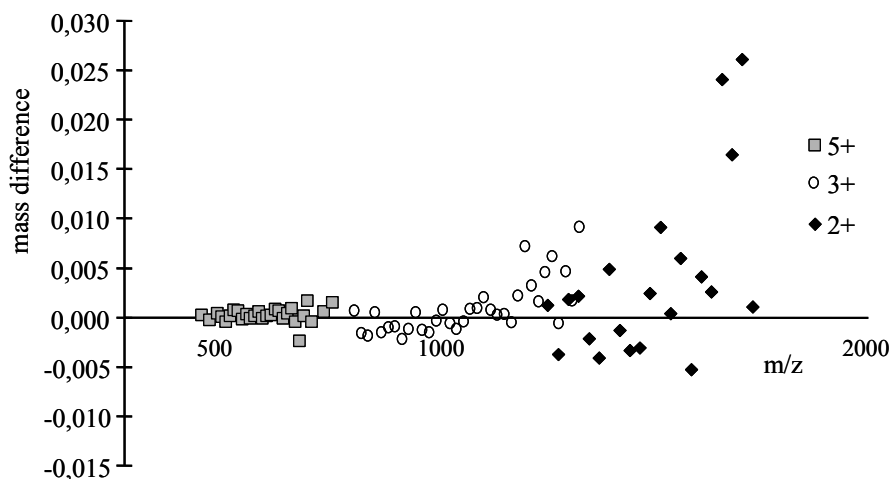


Figure 4.2 Mass error ($m_{exact}-m_{meas}$) for PEG3000 (2+, 3+ and 5+ charge states) as a function of m/z for the observed charge states.

The $\sigma_{mon,regression}$ and $\sigma_{end,regression}$ values are highest for the ions which are observed in the m/z range of ~ 1300 to 1800 , such as the 2+ charge state for PEG3000, and the 4+ and 5+ charge states of PEG6000. This is illustrated in figure 4.2 where the difference between exact and measured mass ($m_{exact} - m_{meas}$) is given for PEG3000 as a function of m/z . Only the 2+, 3+ and 5+ charge states have been plotted in figure 4.2 to prevent an overlap of different data points from different charge states. The average mass error fluctuates around zero if m/z is between 500 and 1200. An increase in the mass error is observed for m/z values above 1200. This increase is attributed to the decreasing number of data points that constitutes a peak. Ions of higher m/z have a lower cyclotron frequency and are therefore reconstructed with fewer data acquisition points. This decrease in accuracy at higher m/z partially explains the higher $\sigma_{mon,regression}$ and $\sigma_{end,regression}$ values. Another consequence of the increasing mass error with m/z is that the slope of the fitted line (equation (4.2)) will decrease, which results in lower $m_{mon,regression}$ and higher $m_{end,regression}$ values. This can easily be seen from the tables where the $\Delta m_{mon,regression}$ value becomes more negative for lower charge states while $\Delta m_{end,regression}$ increases. In general, the best mass accuracy is achieved at the highest charge states.

The linear regression procedure requires an extrapolation from about $n=60$ to $n=0$ for PEG3000. Small deviations in the slope of the line will dramatically

alter the extrapolated endgroup mass. This does not hold for the average method since this method does not require an extrapolation. For PEG1000, PPG1150, PPG3250 and PTHF2000 higher $\sigma_{mon, regression}$ and $\sigma_{end, regression}$ values at lower charge states, compared to higher charge states, are not observed. PEG1000 and PPG1150 are observed below m/z 1300 where the mass accuracy is relatively high. The lowest charge states (2+ and 3+) observed for PPG3250 contain at least twice as many data points as the higher charge states and increase the endgroup accuracy according to equation (4.3). For PTHF2000 a similar reasoning can be held. The $\Delta m_{end-cation, average}$ values of PEG1000 and PEG3000 have a relative error of less than 0.02% with the 2+ and 3+ charge states of PEG3000 being the only exceptions. For PEG6000 these values have a relative error of $\sim 0.4\%$. The σ values determined with the averaging method are about one order of magnitude lower than the σ values determined with the linear regression procedure.

The magnitude of the σ values discussed in this chapter is determined by the number of data points N used for the calculations, the distance between the measured points and the intercept (not for the averaging method) and the m/z range in which the polymer molecules are observed (see figure 4.2). Other effects that might influence the magnitude of the σ values such as space charge effects have not been considered.

4.3.3. Endgroup determination combining all charge states

Taking advantage of the generation of multiple charge states in ESI can increase the mass precision in the endgroup determination. According to equation (4.2), the mass of z cations can be subtracted from the m_{meas} values observed in all charge states. The resulting mass values only account for the monomer and endgroup mass. Since the mass of the cation can be considered exact, all mass values can be combined in one linear regression procedure. The advantage of this method is that the number of data points N for the linear regression procedure increases. This results in an endgroup determination with a higher precision (equation (4.3)). The σ^2_{data} value introduced in equation (4.3) is different for each charge state. In order to combine all charge states, $\sigma^2_{data, all}$ is introduced which is the weighted average of the σ^2_{data} values over the different charge states

$$\sigma^2_{data, all} = \frac{\sum_{z=1}^z \sigma^2_{data}(z) \cdot \nu(z)}{\sum_{z=1}^z \nu(z)} \quad (4.4)$$

Where $\sigma^2_{data}(z)$ is the σ^2_{data} value in charge state z and $\nu(z)$ is the statistical degree of freedom of the number of data points N observed in charge state z .

The charge carrying cation is sodium in all cases. This is confirmed by the addition of different alkali salts to the solution (spectra not shown). A major disadvantage of this method for cation identification is that additional analysis with other cations have to be carried out. A faster and less laborious confirmation is obtained from figure 4.3 for PEG3000. In this figure the measured masses (m_{meas}) in all charge states are plotted as a function of n . We have used the same m_{meas} values as we have used for the endgroup determination. The vertical spacing between the different lines gives the mass of the cation. This can also be seen from equation (4.2) if z is increased by one charge. For PEG3000 a cation mass of 22.989 ± 0.001 is determined from figure 4.3.

The results of the method that combines the data of all charge states are shown in table 4.3. In general, the endgroup precision increases when all charge states are combined instead of considering them separately. This is explained as due to the increasing number of datapoints N that is used in the linear regression procedure (equation (4.3)). For PEG1000 a $\sigma_{end,average}$ of 0.0020 is observed after combining the two observed charge states. When considering the charge states separately, a 1.4 times higher value of 0.0028 is found. For PEG3000 a value of 0.0026 is observed which is on average 2.2 times higher than the $\sigma_{end,average}$ values of the separate charge states. For PEG6000 a factor of approximately three is observed. Similar results are obtained for PPG1150 and PPG3250.

4.3.4. Comparison of the endgroup accuracy determined with ESI and MALDI FT-ICR MS

The mass accuracies for the endgroup determination of PEG1000 and PEG4000 found by van Rooij *et al.*⁹³ with MALDI FT-ICR MS are compared with the results for the PEGs reported in this chapter (see summary of the MALDI results⁹³ in the last two columns of table 4.3). The σ values for PEG1000 determined with MALDI FT-ICR MS are in good agreement with the values found in this chapter with ESI FT-ICR MS when all charge states are considered separately. The σ values of PEG4000 are of the same order of magnitude as those of PEG3000 and PEG6000. This demonstrates that the σ values generated with ESI data are of the same order as the MALDI data. Note that the number of data points used with MALDI FT-ICR MS described by van Rooij *et al.*⁹³ is lower than the number of data points used in this chapter with ESI FT-ICR MS. This influences the σ values. Therefore, the endgroup and monomer mass calculations have been done with a similar number of data points as used by van Rooij *et al.*⁹³ for several

charge states of PEG3000 and PEG6000. As expected, the resulting σ values are lower. However, the σ values are still of the same order of magnitude as the results found with MALDI for PEG4000.

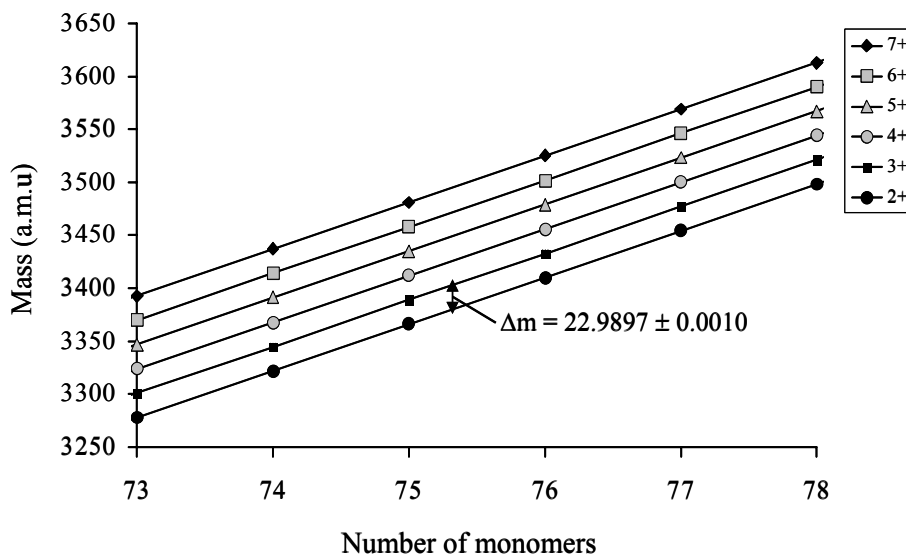


Figure 4.3 Determination of the mass of the cation for PEG3000. Plot of an enlarged mass scale of all observed charge states. The distance between two adjacent parallel lines determines the mass of the cation.

The σ values of PEG6000 have improved by a factor of about two compared to those of PEG4000 when all charge states are combined in one linear regression procedure (fourth column of table 4.3). This is in spite of the fact that the molecular weight of PEG6000 is larger than PEG4000. Large polymer molecules can be measured more accurately using ESI compared to MALDI because ESI yield lower m/z values, which can be measured more accurately using FT-ICR MS.

Chapter 4

Masses (Da) and deviations	PEG1000	PEG3000	PEG6000	PPG1150	PPG3250	PTHF2000	PEG1000	PEG4000
			(+4 ¹³ C)		(+1 ¹³ C)			
<i>n</i> (<i>N</i>)	10-32 (30)	58-94 (165)	137-178 (230)	6-25 (29)	16-72 (134)	4-29 (41)	13-30 (18)	85-102 (18)
<i>m</i> _{mon, regression}	44.0265	44.0261	44.0256	58.0421	58.0419	72.0577	44.0260	44.0285
Δm _{mon, regression}	0.0002	-0.0001	-0.0006	0.0002	<0.0001	0.0002	-0.0002	0.0023
σ _{mon, regression}	0.0003	0.0003	0.0010	0.0003	0.0001	0.0003	0.0004	0.0025
<i>m</i> _{end-cation, regression}	18.0087	18.0164	18.0273	18.0085	18.0088	18.0117	18.0120	17.7941
Δm _{end, regression}	-0.0019	0.0059	0.0167	-0.0021	-0.0018	0.0011	0.0014	-0.2200
σ _{end, regression}	0.0076	0.0217	0.1631	0.0046	0.0058	0.0053	0.0080	0.2400
<i>m</i> _{end-cation, average}	18.0140	18.0089	17.9338	18.0117	18.0112	18.0153	18.0079	18.0081
Δm _{end, average}	0.0034	-0.0017	-0.0768	0.0012	0.0006	0.0047	-0.0027	-0.0030
σ _{end, average}	0.0020	0.0026	0.0093	0.0014	0.0017	0.0019	0.0019	0.0140
σ _{data,all}	0.0111	0.0339	0.1413	0.0074	0.0193	0.0124	0.0080	0.0600

Table 4.3 Calculated monomer and endgroup masses (Da) and precision for PEG1000, PEG3000, PEG6000, PPG1150, PPG3250 and PTHF2000 combining all charge states. The values of PEG1000 and PEG4000 displayed in the last two columns are obtained with MALDI FT-ICR MS from reference ⁹³ (mass of cation and ¹³C subtracted).

The largest polymer molecule observed with MALDI has a degree of polymerisation of 105. For ESI a polymer molecule with 178 monomeric units (PEG6000) has been observed on the same FT-ICR MS. This demonstrates clearly that when ESI is used instead of MALDI the mass range is extended by almost a factor of 2. Note that for other polymers, like polyolefins, multiply charging is difficult and an extension of the mass range will not be obtained. Polyethylene glycol samples with molecular weights of up to 20,000 Da have also been measured successfully using ESI. Accurate endgroup determinations for polyethylene glycol samples with a molecular weight larger than 20,000 Da require a mass resolving power only provided by a high field FT-ICR MS.

4.4. Conclusions

Two methods, a linear regression and an averaging method, have been developed and evaluated for the accurate analysis of the monomer and endgroup composition of synthetic polymers using ESI FT-ICR MS. All charge states of a

polymer, observed with ESI, are combined in one linear regression or averaging procedure, in order to increase the precision of the endgroup determination. The charge states can be combined under condition that the mass of the cation is known. By plotting $(m/z)^{z+}$ multiplied by the charge state as a function of the degree of polymerisation the identity of the cation is easily determined. This procedure prevents multiple experiments in which different cations have to be added to the polymer sample.

The endgroup accuracy determined from a single charge state with ESI FT-ICR MS is of the same order of magnitude as determined by MALDI FT-ICR MS on the same instrument. However, when all charge states measured with ESI are combined in one procedure, the endgroup precision increases up to threefold. This demonstrates that more accurate monomer and endgroup masses are obtained using ESI instead of MALDI. ESI exceeds MALDI in the study of larger polymeric systems due to the multiple charging nature of ESI. Multiply charging results in a lower m/z value, which are measured with a higher accuracy in the FT-ICR MS. However, multiply charging of polymers like polyolefins is difficult, which will not result in more accurate monomer and endgroup masses and an extension of the mass range.

Chapter 5

Quantitative analysis of copolymers: The influence of the monomers on the ionisation efficiency in electrospray ionisation

The influence of the ionisation efficiency on the measured copolymer sequence distribution is discussed. Large differences in ionisation efficiency were observed for mixtures of homopolyesters containing dipropoxylated bisphenol-A/adipic acid and dipropoxylated bisphenol-A/isophthalic acid and the corresponding copolyester dipropoxylated bisphenol-A/isophthalic acid/adipic acid. The adipic acid structure has a higher affinity for the sodium cation, which results in more intense peaks for adipic acid containing oligomers. Relative sodium affinities of the oligomers were found to increase with an increasing number of acid endgroups in favour of adipic acid containing oligomers. The ESI response of the oligomers depends on the polymer concentration in the sprayed mixture and other parameters. This makes it impossible to correct for the ionisation efficiency necessary for copolymer analysis. If differences in ionisation efficiency are not corrected, the ion intensities in the copolymer mass spectra will show large deviations from the real composition and no conclusion can be drawn about the chemical (in)homogeneity of the MWD nor the random or block structure of the copolymer. This will also be valid for other cationisation techniques like MALDI and FAB.

5.1. Introduction

Copolymers consist of a complex mixture of molecules that differ in size, chemical composition and sequence. Complete characterisation of such complex materials demands new analytical approaches. A technique that has become increasingly popular for copolymer analysis during the last ten years is mass spectrometry. Soft ionisation techniques like matrix-assisted laser desorption/ionisation (MALDI) and electrospray ionisation (ESI) have been

successfully used to ionise intact polymer molecules,^{4,20,31,62,64,77} which made it possible to study the chemical composition distribution of the copolymer directly from the mass spectrum.^{51,146,147,195,196}

The sequence of copolymers can be studied using Bernoullian and Markovian chain statistics applied to the intensity profile of the polymer distribution.^{119,120,124,197} The Bernoullian chain statistics are used to model random copolymerisation reactions. Markovian statistics allow the modelling of both random and non-random copolymerisation reactions. Non-random polymerisation reactions in step (radical) polymerisation normally result in the formation of block copolymers.

The chain statistical models rely on a uniform mass spectrometric response i.e. an equal ionisation efficiency (IE) for the various components in the molecular weight distribution (MWD), but this uniformity is questionable because the overall efficiency of a molecule to become charged in electrospray ionisation is influenced by several processes. Ions with relatively low solvation energy or a high surface tension will be situated preferentially on the surface of the droplets and are desolvated more easily during ESI. Ions with larger solvation energies will be distributed throughout the entire droplet and will be ionised less easily.^{67,152,198-202} Other factors that influence the ionisation efficiency of an analyte are the polarity of the solvent, the structure of the ion (i.e. the organic functionalities in the molecule), the flexibility of the chain (for example cyclic versus linear molecules), pH or the nature of the cation,^{69,70} charge state, counter ion effects,⁷¹ drying gas flow rate and the ESI source temperature (selective nozzle skimmer ion activation).^{65,68,72-75} Several studies have been reported in the literature in which ionisation efficiencies of mixtures of different cyclic compounds like crown ethers and peptides with a variety of cations were studied using FAB MS,^{203,204} MALDI MS²⁰⁵ and ESI MS.^{70,200,205-211} Most studies indicate that a good correlation exists between the selectivity of analytes towards metal ions in the liquid phase and the intensity in the mass spectrum, which allows a correction for differences in ionisation efficiency. Synthetic polymer mass spectrometric studies carried out so far do not take the ionisation efficiency (or response factors) of the different components in copolymers into account. This is probably because synthetic polymers are not single molecules but consist of mixtures with a distribution of different molecules, which are impossible to quantify with NMR. Liquid Chromatography (LC) allows only a quantification of the low molecular weight part of the MWD. Besides, the determination of the ionisation efficiency of all individual polymer molecules would be a very laborious process.

In this chapter Bernoullian and Markovian chain statistics are applied to the ESI FT-ICR MS spectra of the copolyester poly(di-propoxylated bisphenol-A/adipic acid/isophthalic acid). Table 5.1 presents the structures of the different monomers. The copolymer composition determined with the chain statistics will be different from the real copolymer composition if differences in ionisation efficiency (IE) between the adipic and isophthalic acid structures exist. The relative IE of the adipic and isophthalic acid structures are determined with well defined mixtures of the homopolyesters poly(di-propoxylated bisphenol-A/adipic acid) and poly(di-propoxylated bisphenol-A/isophthalic acid). Gradient polymer elution chromatography (GPEC) was used to quantify the weight fractions of the oligomers in the low molecular weight part of the molecular weight distribution of the homopolyesters, a necessary requirement for the determination of the relative IE. This is the first time synthetic polymers were measured with GPEC for quantitative analysis with ESI FT-ICR MS.

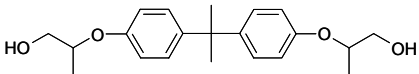
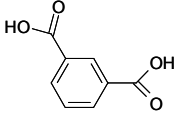
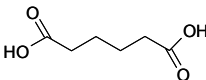
Monomer	Notation	Molar mass (Da)	Structure
Di-propoxylated bisphenol-A	D	344.1987	
Isophthalic acid	I	166.0266	
Adipic acid	A	146.0579	

Table 5.1 *Notation, mass and structure of the monomers used in this chapter.*

5.2. *Methods and materials*

5.2.1. *ESI FT-ICR MS analysis*

The ESI FT-ICR MS (Bruker-Spectrospin APEX 7.0e, Fällanden, Switzerland) used in this work has been described in chapter 2 and elsewhere.^{54,212} The cell is an in-house constructed open cell.¹⁸² The electrospray generated ions

Chapter 5

were trapped for 2-4 s. Argon gas is introduced through a pulsed valve to enhance trapping ($P_{Ar}=5*10^{-6}$ mbar).

5.2.2. GPEC ESI TOF analysis

GPEC analyses were performed at Akzo Nobel Chemicals Research Arnhem as described elsewhere.⁸¹ The Hewlett Packard LC system model 1050 (Palo Alto, CA, USA) was operated with an autoinjector model Basic Marathon (Spark Holland, Emmen, The Netherlands) with a loop volume of 10 μ l. Solution A contained unstabilised THF:H₂O 5:95 and solution B unstabilised THF:H₂O 95:5 (v/v). To both solutions 0.1 % glacial acetic acid was added. The applied gradient ran from 45% of solution A at t=0 to 10% of solution A at t=35 min, at a flow of 1 ml/min. The column was a Waters Symmetry C18 (5 μ m particle size), 150 mm x 4.6 mm ID. Approximately 30 μ l/min of the eluent from the column was split with a 0.01 inch i.d. stainless steel T-piece (Valco, Houston, TX, USA) that was allowed to flow to the Z-spray TOF instrument (Micromass, Manchester, UK). The eluent stream was compatibilised with a NaI solution (10 μ l/min of a 250 μ M NaI solution in THF/iso-propylalcohol). The remaining eluent was eluted through an UV diode array detector model 1000S (Applied Biosystem, San Jose, Ca, USA).

5.2.3. Materials

The unstabilised THF was obtained from Fluka (Buchs, Switzerland). The polymers used for this study are the homopolyesters poly(di-propoxylated bisphenol-A/adipic acid) and poly(di-propoxylated bisphenol-A/isophthalic acid) and the copolyester poly(di-propoxylated bisphenol-A/adipic acid/isophthalic acid). These polymers were a gift from Océ Technologies (Venlo, The Netherlands) and are from the same batch as the polyesters described in a previous publication.²¹³ The structures are shown in table 5.1. Di-propoxylated bisphenol-A, adipic acid and isophthalic acid will be abbreviated by D, A and I throughout the chapter, respectively. The copolyesters studied have the composition DAI31, DAI21, DAI11, DAI12 and DAI13 where the numbers denote the molar ratio of adipic acid and isophthalic acid. DAI31, DAI21, DAI11, DAI12 and DAI13 contain a molar ratio D:A:I of 0.5:0.37:0.13, 0.51:0.33:0.16, 0.5:0.26:0.24, 0.51:0.16:0.33 and 0.51:0.12:0.37, respectively as was determined with NMR. Since identification of the oligomers was not performed using mass spectrometry,²¹³ the GPEC experiments were repeated with online ESI TOF for identification.

5.2.4. Copolymerisation models

The copolymerisation models and their link with mass spectrometry have first been used by Montaudo and coworkers.^{119,120} In their work the entire mass spectrum is used to determine the composition and ‘blockiness’ of the copolymers. Here, we investigate the copolymer composition for each endgroup class separately and subsequently as a function of the degree of polymerisation and charge state. For example, the composition of the pentamer with two alcohol endgroups in charge state 2 was studied by searching for the best fit of the experimentally observed intensity profile with the chain statistical models. This allows studying the chemical inhomogeneity as a function of the degree of polymerisation, endgroup class and charge state. The Markovian and Bernoullian models used were implemented in Matlab 5.3 (The MathWorks, Inc.) and are described below.

5.2.4.1. Markovian chain statistical model

Consider a system composed of linear copolymers constructed from N different types of monomers, which we will label by the letters $\tau=A, B, \dots$. Each polymer molecule consists of $M=1, 2, 3, \dots$ monomers whose position within the chain is labelled by lowercase letters m, k, l, n, \dots . Note that we allow bare monomers as ‘chains’ of length $M=1$. We denote the probability for an M -mer to have a specific monomer sequence by $P^{(M)}(\tau_1, \tau_2, \dots, \tau_M)$. Let us further define the probability of finding a certain initial segment of length m in a polymer of total length M

$$P_m^{(M)}(\tau_1, \tau_2, \dots, \tau_m) = \sum_{\tau_{m+1}, \dots, \tau_M} P^{(M)}(\tau_1, \tau_2, \dots, \tau_M) \quad (5.1)$$

The Markovian assumption now states that the conditional probability of finding the next monomer τ_{m+1} of a chain to be of a certain type only depends on the type of the immediately preceding monomer τ_m , the penultimate effect, i.e.

$$P_{m+1}^{(M)}(\tau_{m+1} | \tau_1, \tau_2, \dots, \tau_m) = \frac{P_{m+1}^{(M)}(\tau_1, \tau_2, \dots, \tau_m, \tau_{m+1})}{P_m^{(M)}(\tau_1, \tau_2, \dots, \tau_m)} = P(\tau_m \rightarrow \tau_{m+1}) \quad (5.2)$$

where we adopt the arrow notation to stress the order of the two monomers in the sequence. Each probability $P(\tau_m \rightarrow \tau_{m+1})$ corresponds to a matrix element P_{ij} from the probability matrix \mathbf{P} as described by Montaudo and coworkers.^{119,120} Note that

$$\sum_{\tau'} P(\tau \rightarrow \tau') = 1 \quad (5.3)$$

Under this assumption we find that

$$P_M^{(M)}(\tau_1, \tau_2, \dots, \tau_{M-1}, \tau_M) = P_{M-1}^{(M)}(\tau_1, \tau_2, \dots, \tau_{M-1}) \cdot P(\tau_{M-1} \rightarrow \tau_M) \quad (5.4)$$

which upon iteration yields

$$P_M^{(M)}(\tau_1, \tau_2, \dots, \tau_{M-1}, \tau_M) = P_1^{(M)}(\tau_1) \cdot \prod_{m=2}^M P(\tau_{m-1} \rightarrow \tau_m) \quad (5.5)$$

The probability $P_1^{(M)}(\tau_1)$ is the probability that a polymer molecule starts with τ_1 (an A, B, ...). However, since the choice of the start of a chain is arbitrary, one could just as well start at the other end to obtain

$$\begin{aligned} P_M^{(M)}(\tau_1, \tau_2, \dots, \tau_{M-1}, \tau_M) &= P_M^{(M)}(\tau_M, \tau_{M-1}, \dots, \tau_2, \tau_1) \\ &= P_{M-1}^{(M)}(\tau_M, \tau_{M-1}, \dots, \tau_2) \cdot P(\tau_2 \rightarrow \tau_1) \end{aligned} \quad (5.6)$$

or

$$P_M^{(M)}(\tau_1, \tau_2, \dots, \tau_{M-1}, \tau_M) = P_1^{(M)}(\tau_M) \cdot \prod_{m=2}^M P(\tau_m \rightarrow \tau_{m-1}) \quad (5.7)$$

Next, we also assume the probability that a chain starts with a specific type of monomer does not depend on the length of the chain i.e. $P_1^{(M)}(\tau_1) = P_1(\tau_1)$ so that equation (5.6) simplifies to

$$P_M^{(M)}(\tau_1, \tau_2, \dots, \tau_{M-1}, \tau_M) = P_{M-1}^{(M-1)}(\tau_M, \dots, \tau_3, \tau_2) \cdot P(\tau_2 \rightarrow \tau_1) \quad (5.8)$$

Note that by definition

$$\sum_{\tau} P_1(\tau_1) = \sum_{\tau} P_1(\tau_M) = 1 \quad (5.9)$$

This relation can be used to obtain a self-consistency condition on $P_1(\tau_1)$ (or $P_1(\tau_M)$) as follows

$$\begin{aligned} P_1(\tau_1) &= \sum_{\tau_2, \dots, \tau_M} P_M^{(M)}(\tau_M, \tau_{M-1}, \dots, \tau_2, \tau_1) \\ &= \sum_{\tau_2, \dots, \tau_M} P_{M-1}^{(M-1)}(\tau_M, \tau_{M-1}, \dots, \tau_2) \cdot P(\tau_2 \rightarrow \tau_1) \\ &= \sum_{\tau_2} \sum_{\tau_3, \dots, \tau_M} P_{M-1}^{(M-1)}(\tau_M, \tau_{M-1}, \dots, \tau_2) \cdot P(\tau_2 \rightarrow \tau_1) \\ &= \sum_{\tau_2} P_1(\tau_2) \cdot P(\tau_2 \rightarrow \tau_1) \end{aligned} \quad (5.10)$$

This equation together with the two normalisation constraint equations (5.9) and (5.3) allow $P_1(\tau_1)$ to be expressed in terms of the transition probabilities $P(\tau_m \rightarrow \tau_{m-1})$. Consider a copolymer made of monomers A and B. The probability a sequence starts with an A is given by equation (5.10) or

$$P_1(A) = \sum_{\tau_2} P_1(\tau_2) \cdot P(\tau_2 \rightarrow \tau_A) = P_1(A) \cdot P(A \rightarrow A) + P_1(B) \cdot P(B \rightarrow A) \quad (5.11)$$

Using the notation of Montaudo and coworkers, equation (5.11) becomes $S_A = S_A P_{AA} + S_B P_{BA}$.

Note that equation (5.8) is the basis of the Markovian model applied to copolymer mass spectra. By correlating this equation to the measured intensity $I_M^{(M)}(\tau_1, \tau_2, \dots, \tau_{M-1}, \tau_M)$ in a mass spectrum, equation (5.8) becomes

$$\begin{aligned} I_M^{(M)}(\tau_1, \tau_2, \dots, \tau_{M-1}, \tau_M) &= \\ &= IE^{(M)}(\tau_1, \tau_2, \dots, \tau_{M-1}, \tau_M) \cdot P_1^{(M)}(\tau_1) \cdot \prod_{m=2}^M P(\tau_{m-1} \rightarrow \tau_m) \end{aligned} \quad (5.12)$$

Chapter 5

where $IE^{(M)}(\tau_1, \tau_2, \dots, \tau_{M-1}, \tau_M)$ is the ionisation efficiency of the co-polymer with monomer composition and sequence $(\tau_1, \tau_2, \dots, \tau_{M-1}, \tau_M)$. For example, the mass spectrometric intensity for the specific oligomer with sequence AABBA is given by

$$I_5^{(5)}(A, A, B, B, A) =$$

$$IE^{(5)}(A, A, B, B, A) \cdot P_1^{(5)}(A) \cdot P(A \rightarrow A) \cdot P(A \rightarrow B) \cdot P(B \rightarrow B) \cdot P(B \rightarrow A) \quad (5.13)$$

The ionisation efficiency $IE^{(M)}(\tau_1, \tau_2, \dots, \tau_{M-1}, \tau_M)$ has until now always assumed to be 1.^{119,120} This chapter will demonstrate that this assumption is not valid.

The models used by Montaudo and coworkers assume that the probability that a chain starts with τ_1 is proportional to the molar fraction of the monomer in the copolymer. Here we provide a simple proof of this assertion based on the Markovian assumption itself. Consider thereto the probability $P_m(\tau_m)$ that a given monomer at position $1 \leq m \leq M$ within the chain is of a certain type

$$\begin{aligned} P_m(\tau_m) &= \sum_{\tau_1, \tau_2, \dots, \tau_{m-1}} \sum_{\tau_{m+1}, \tau_{m+2}, \dots, \tau_M} P^{(M)}(\tau_1, \tau_2, \dots, \tau_M) \\ &= \sum_{\tau_1, \tau_2, \dots, \tau_{m-1}} \sum_{\tau_{m+1}, \tau_{m+2}, \dots, \tau_M} P_1(\tau_1) \prod_{i=1}^{M-1} P(\tau_i \rightarrow \tau_{i+1}) \\ &= \sum_{\tau_1, \tau_2, \dots, \tau_{m-1}} P_1(\tau_1) \prod_{i=1}^{m-1} P(\tau_i \rightarrow \tau_{i+1}) \sum_{\tau_{m+1}, \tau_{m+2}, \dots, \tau_M} \prod_{j=m}^{M-1} P(\tau_j \rightarrow \tau_{j+1}) \\ &= \sum_{\tau_2, \tau_3, \dots, \tau_{m-1}} P_1(\tau_2) \prod_{i=1}^{m-1} P(\tau_i \rightarrow \tau_{i+1}) \sum_{\tau_{m+1}, \tau_{m+2}, \dots, \tau_{M-1}} \prod_{j=m}^{M-2} P(\tau_j \rightarrow \tau_{j+1}) \\ &= \{repeat\ the\ same\ steps\} \\ &= P_1(\tau_m) \end{aligned} \quad (5.14)$$

where we repeatedly employ Eqs. (5.3) and (5.10). As the position m is arbitrary we can simply define the probability that an arbitrary monomer has a given type to be $P(\tau) = P_m(\tau) = P_1(\tau)$.

5.2.4.2. *Bernoullian chain statistical model*

In case of Bernoullian chain statistics the addition of a new monomer does not depend on the nature of the previous monomer and it is assumed that it also does not depend on the chain length

$$P(\tau_m \rightarrow \tau_{m-1}) = P(\tau_m) \quad (5.15)$$

The intensity of an ion in the mass spectrum becomes

$$I_M^{(M)}(\tau_1, \tau_2, \dots, \tau_{M-1}, \tau_M) = IE^{(M)}(\tau_1, \tau_2, \dots, \tau_{M-1}, \tau_M) \cdot \prod_{m=1}^M P(\tau_m) \quad (5.16)$$

or for the oligomer with sequence AABBA

$$I_5^{(5)}(A, A, B, B, A) = IE^{(5)}(A, A, B, B, A) \cdot P(A)^3 \cdot P(B)^2 \quad (5.17)$$

where P(A) and P(B) are the molar fractions of A and B, respectively. The Bernoullian model (random copolymerisation) uses the molar fraction as determined by NMR and the degree of polymerisation as input. The output of the model is the theoretical intensity profile. The Markovian model (non-random copolymerisation) has as input the mass spectrometric relative intensity profile for an oligomer intensity distribution with a degree of polymerisation n . The program searches for the best fit using two variables: the molar fraction of the monomers and the probability to find two monomers A after each other. The probability to find two monomers A after each other can be used to calculate the ‘blockiness’ of the copolymer.^{119,120}

5.3. Results and discussion

5.3.1. ESI FT-ICR MS spectra of copolyesters

The ESI FT-ICR MS spectrum of the copolyester poly(di-propoxylated bisphenol-A/adipic acid/isophthalic acid) DAI11 is presented in figure 5.1. The polymer molecules observed are sodium cationised and contain two alcohol endgroups $(DI)_n(DA)_mD$, one alcohol and one acid endgroup $(DI)_n(DA)_m$ or two acid endgroups $A(DI)_n(DA)_m$, $I(DI)_n(DA)_m$. Cyclic molecules, $c(DI)_n(DA)_m$, were also observed. D denotes the dialcohol di-propoxylated bisphenol-A, A and I the diacids adipic acid and isophthalic acid, respectively, n and m the degree of polymerisation and c denotes cyclic structure of the molecules.

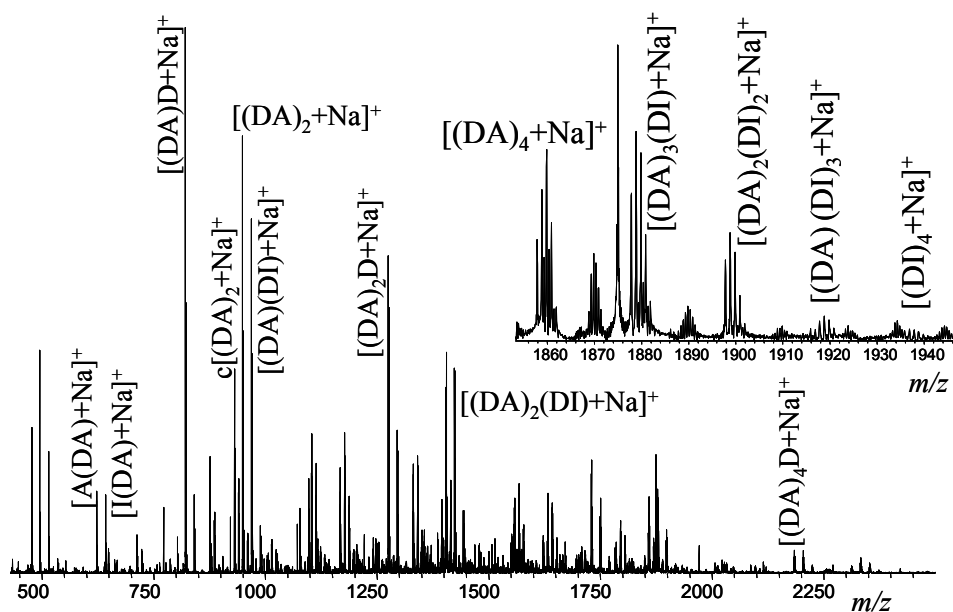


Figure 5.1 ESI FT-ICR MS spectrum of DAI11 (1 mg/ml, 5 mM NaI, sprayed in THF). The insert shows the intensity profile of the tetramer with one alcohol and one acid endgroup.

The insert of figure 5.1 shows a typical intensity profile of the composition of the tetramer with one alcohol and one acid endgroup. Bernoullian and Markovian chain statistics were used to fit the oligomer intensity profile in the mass spectra using the model described earlier and first applied to copolymer mass spectra by Montaudo *et al.*^{119,120} Here we have determined separately the

copolymer composition as a function of the degree of polymerisation and the charge state for each endgroup class.

5.3.2. Copolymerisation statistics applied to mass spectra

The experimentally observed intensities, denoted by an open square, of the tetramer with two acid endgroups electrosprayed in acetone is plotted in figures 5.2a-c for three copolymers with different molar ratios of adipic and isophthalic acid. The intensity profiles in figures 5.2a-c originate from copolymers containing a molar ratio of 3:1, 1:1 and 1:3 adipic(A):isophthalic acid(I) denoted by DAI31, DAI11 and DAI13, respectively. The oligomer intensities presented in figures 5.2a-c correspond with $A(DA)_3$, $A(DA)_2(DI)$, $A(DA)(DI)_2$, $A(DI)_3$ and $I(DI)_3$. The measured m/z values and normalised intensities are presented in table 5.2. Random copolymerisation (Bernoullian) chain statistics were used to calculate the theoretical intensity profile (denoted by a closed circle ●). The molar fraction of adipic acid and isophthalic acid in the bulk determined by NMR were used for the calculations. The results of the Bernoullian calculations are presented in table 5.2. It can be seen from figures 5.2a-c that the intensity profile (open squares) observed with mass spectrometry and the intensity profile as calculated by random copolymerisation statistics ● do not agree. In all cases the experimental intensity profiles are shifted in favour of adipic acid. A better agreement between experiment and the Bernoullian intensity profile for copolymer DAI11 is obtained when ~ 10% more adipic acid (A) is used in the calculation. The calculated molar fractions of adipic acid and isophthalic acid $P(A)$ and $P(I)$, presented in table 5.2, suggest that the copolymers contain more adipic acid than determined by NMR. The disagreement between the intensity profiles obtained with mass spectrometry and the Bernoullian calculation is more prominent for copolymers with a high molar ratio of isophthalic acid.

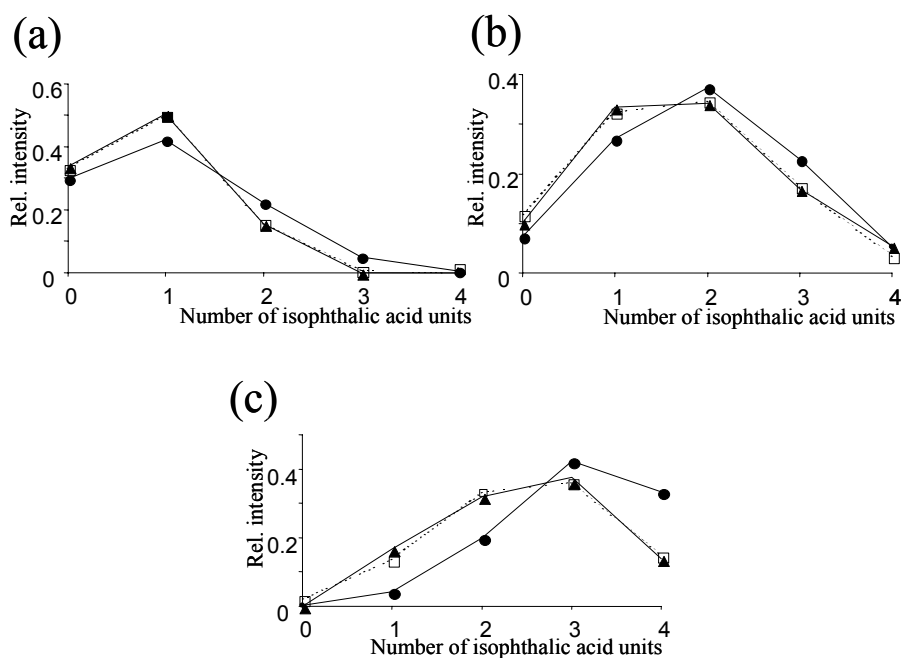


Figure 5.2 Experimental relative intensity profiles (open square with dotted line) of the tetramers with two acid endgroups for the copolyesters DAI31 (a), DAI11 (b) and DAI13 (c) sprayed in acetone. The numbers denote the molar ratio of adipic acid and isophthalic acid. The figures also display the theoretical Bernoullian (●) and Markovian intensity profiles (▲).

A better agreement between experiment and theory is obtained using Markovian chain statistics, denoted in figure 5.2 by a closed triangle ▲, resulting in a calculated molar fraction of adipic acid $P(A)$ that is $\sim 10\%$ higher as determined by NMR^{213,214} for the copolymer DAI11. This is similar to the results of the Bernoullian model, but with a slight block formation of the monomers. The calculated molar fraction adipic acid and isophthalic acid with the Markovian chain statistics is presented in table 5.2. Oligomers with another degree of polymerisation and with other endgroups give similar results compared to those obtained from the analysis of the tetramer with two acid endgroups. When the ESI experiments are performed in THF under the same experimental conditions approximately 5% more adipic acid is found with the Markovian calculation (results not shown).

The average molar fraction of adipic acid determined by NMR is plotted in figures 5.3a-b as a function of the molar fraction determined by a Markovian fit of the ESI FT-ICR MS spectrum (sprayed in THF). The curves represent the oligomers of five copolyesters with two alcohol endgroups in charge states 1 and 2, respectively. The molar fraction of adipic acid as calculated with the Markovian

model increases with increasing charge state and decreases with increasing degree of polymerisation.

		A(DA) ₃	A(DA) ₂ (DI)	A(DA)(DI) ₂	A(DI) ₃	I(DI) ₃	Calculated P(A)	P(I)
Measured <i>m/z</i>		1531.754	1551.723	1571.691	1591.660	1611.629		
NMR	DAI31						0.74	0.26
	DAI11						0.52	0.48
	DAI13						0.24	0.76
Experimental □	DAI31	0.339	0.505	0.156	0.000	0.000	-	-
	DAI11	0.101	0.335	0.342	0.168	0.054	-	-
	DAI13	0.000	0.166	0.320	0.376	0.138	-	-
Bernoullian theory ● with NMR data	DAI31	0.300	0.421	0.222	0.052	0.005	-	-
	DAI11	0.073	0.270	0.374	0.230	0.053	-	-
	DAI13	0.003	0.042	0.200	0.421	0.334	-	-
Bernoullian fit with ~10% more A	DAI31	0.355	0.420	0.186	0.037	0.003	0.772	0.228
	DAI11	0.113	0.328	0.356	0.172	0.031	0.580	0.420
	DAI13	0.022	0.140	0.336	0.359	0.144	0.384	0.616
Markovian fit ▲	DAI31	0.333	0.501	0.159	0.007	0.000	0.790	0.210
	DAI11	0.119	0.324	0.348	0.174	0.034	0.580	0.420
	DAI13	0.021	0.136	0.333	0.362	0.148	0.380	0.620

Table 5.2 Experimentally observed *m/z* (open square) and intensity profile for the tetramer with two acid endgroups. The experimentally observed intensity profile has been used for the calculation of the molar ratio of adipic *P(A)* and isophthalic acid *P(I)* with Bernoullian (●) and Markovian (▲) chain statistical models. The molar ratio of adipic and isophthalic acid determined by NMR has also been used for the calculation of the Bernoullian theoretical intensity profile.

The ~10% higher molar fraction of adipic acid as calculated with the Bernoullian and Markovian models for the copolyesters can be explained in two ways. One possibility is that the molecular weight distribution is chemically inhomogeneous, a feature that cannot be determined by NMR since it is impossible to make a distinction between the different polymer molecules. In that case the low part of the MWD would contain more adipic acid than isophthalic acid, while the high part of the MWD would contain more isophthalic acid than adipic acid. Another explanation is that the ionisation efficiency of adipic acid is higher than isophthalic acid in the ESI process. This will result in a shift of the intensity profile in favour of adipic acid.

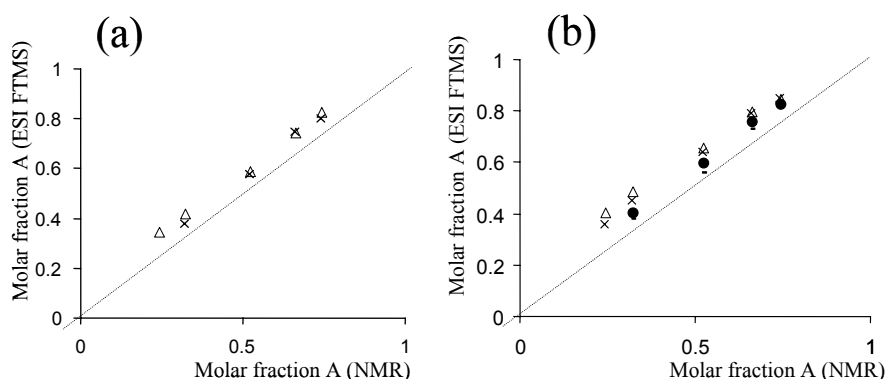


Figure 5.3 Molar fraction of adipic acid determined by NMR versus molar fraction as determined by the Markovian fit of the ESI FT-ICR MS intensity profiles of the oligomers with two alcohol endgroups sprayed in THF for charge states 1 (a) and 2 (b). Degrees of polymerisation shown are $n=3$ (Δ), 4 (\times), 6 (\bullet) and 7 (-).

The chemical inhomogeneity of the copolymer MWD can only be studied quantitatively with ESI FT-ICR MS if the relative ionisation efficiency of the individual components in the MWD is known. Therefore the remaining part of this chapter will focus on the relative ionisation efficiency of adipic and isophthalic acid in the ESI process. Quantification of the oligomers with Gradient polymer elution chromatography (GPEC) is required to test for the presence of relative ionisation efficiency differences.

5.3.3. Polyester quantification with GPEC

GPEC was applied using an UV diode array detector for quantification and online ESI TOF for identification of the oligomers in the MWD. GPEC is based on a combination of precipitation/redissolution, sorption and exclusion processes.^{213,215} The technique requires a gradient LC system with at least two solvents. One of the solvents, which is often a bad solvent for the polymer of interest, promotes the precipitation of the polymer after injection on the column. The other solvent is a good solvent that enables the redissolution of the polymer. Because most components from the MWD have different solubilities, the components will not redissolve at the same time. The LC column enhances the separation of the eluting molecules. Oligomers of various homo-polyesters were endgroup separated with this technique up to the 7-mer (~ 3500 Da).²¹³ The technique fails to separate larger homo-oligomers due to smaller differences in

solubility and hydrodynamic volumes. Quantification of copolymers with GPEC is difficult because the number of oligomers with different compositions increases dramatically with increasing degree of polymerisation n , which results in co-elution.

The GPEC chromatogram of DAI31 is presented in figure 5.4a. The oligomers are endgroup separated to $n=2$. This limited amount of information does not allow the quantification of the oligomers in the MWD, which is a requirement for the determination of the relative ionisation efficiency (IE) in the ESI process. Therefore, we did not further consider the GPEC separations of the copolyesters.

The homopolyesters poly(di-propoxylated bisphenol-A/adipic acid) (polyDA) and poly(di-propoxylated bisphenol-A/isophthalic acid) (polyDI) are better candidates for IE studies because the low molecular weight part of the MWD can be separated with GPEC (see figure 5.4b and c). The oligomers in the MWD are endgroup separated up to $n=6$ and $n=7$ for polyDA and polyDI, respectively, providing quantitative information.

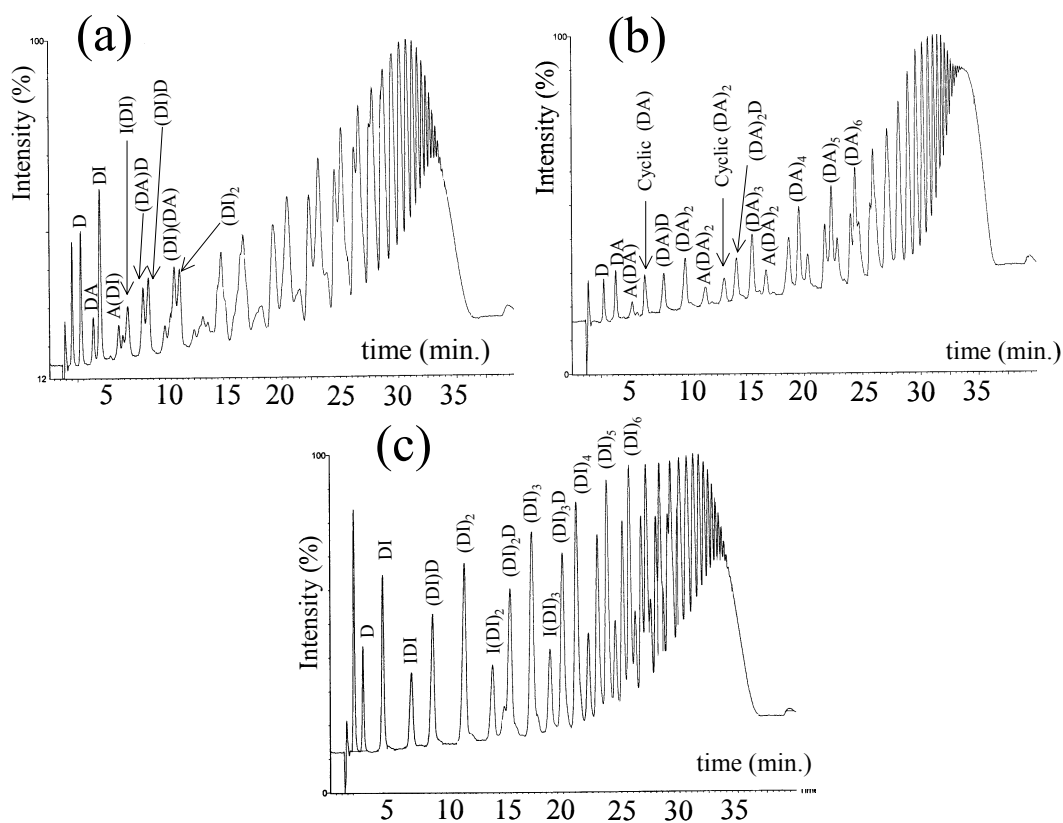


Figure 5.4 Gradient polymer elution chromatograms of polyDAI (a), polyDA (b) and polyDI (c).

5.3.4. Electrospray ionisation efficiency (IE)

Mixtures of the homopolyesters were analysed to determine whether differences in IE between the adipic acid and isophthalic acid structures occur in ESI. The concentration of one of the polymers was held constant while the concentration of the other one was increased. The intensity ratio of oligomers from polyDA:polyDI in the mass spectra should vary proportionally with the molar ratio of homopolyesters present in the sample, when differences in IE are absent. Differences in the relative IE between adipic acid and isophthalic acid containing polyesters should become apparent when comparing structurally similar oligomers. For example, (DA)₃ and (DI)₃ are of the same degree of polymerisation and both have one acid and one alcohol endgroup. If we compare (DA)₃ and (DI)₃ the relative IE is only influenced by the adipic and isophthalic acid structures. It is assumed that the difference between the acid endgroups does not influence the IE.

The ESI FT-ICR MS spectra of polyDA and polyDI show polymer molecules up to a degree of polymerisation of 14 in charge states 1-4 (spectra not shown). The polymer molecules are isotopically resolved with a resolution of 20,000 at m/z 1.000 (128kB data points, bandwidth 500 kHz). The M_w measured with SEC is approximately 3000 Da higher than the M_w measured with ESI. This demonstrates that the low part of the MWD is preferably ionised resulting in a discrimination against the higher molecular weight polymer molecules (see chapter 3). The comparison of the intensity of an oligomer with, for example, $n=2$ with an oligomer of $n=5$, is therefore not performed because they are ~1500 Da separated, for the polymers studied in this chapter. A difference in the response between these oligomers will be influenced by the size of the molecule and the chemical composition. The influence of the size of the oligomers is negligible if we assume that the intensity of an oligomer of $n=3$ of polyDA can be compared with an oligomer of $n=3$ of polyDI since they are separated by only 3·19.97 Da.²¹¹ Note that the M_w measured with SEC is based on a calibration of the SEC system with polystyrene samples. The real M_w is approximately 5000 Da.

The peak intensities in the ESI FT-ICR MS spectra will correlate with the number fraction $n(M)$ of a certain oligomer with molar mass M if all oligomers have the same IE. The number fraction according to mass spectrometry is $n(M)_{DI} = I_{DI} / I_{total}$, in which I_{DI} and I_{total} are the peak intensity of oligomer DI and the integrated intensity of the MWD, respectively. However, the relative IE of the different oligomers during ESI is not known and therefore $n(M)_{DI}$ has only a limited meaning. The ratio $N(M)$ is introduced which allows the comparison of the relative IE of structurally similar oligomers. This ratio is given for the trimer with one acid and one alcohol endgroup by $N(M)_{(DI)3} = I_{(DI)3} / (I_{(DI)3} + I_{(DA)3})$.

The GPEC analysis are used to determine the weight fraction $w(M)$ of a certain oligomer e.g. for DI: $w(M)_{DI} = A_{DI}/A_{total}$, in which A_{DI} and A_{total} are the peak areas of DI and of the entire molecular weight distribution (MWD), respectively. The number ratio $N(M)$ determined with ESI FT-ICR MS must be converted into the weight ratio $W(M)$ to compare the ESI results with GPEC. The weight ratio is calculated for ESI FT-ICR MS by $W(M)_{(DA)3}^{ESIFTMS} = I_{(DA)3} \cdot M_{(DA)3} / (I_{(DA)3} \cdot M_{(DA)3} + I_{(DI)3} \cdot M_{(DI)3})$. However, the intensity of the monoisotopic peak decreases with increasing number of carbon atoms. Therefore the peak intensity in the mass spectrum should be corrected for this effect with $P(n)_{(DA)n}$ and $P(n)_{(DI)n}$.

$$W(M)_{(DA)n}^{ESIFTMS} = \frac{\frac{I_{(DA)n} \cdot M_{(DA)n}}{P(n)_{(DA)n}}}{\frac{I_{(DA)n} \cdot M_{(DA)n}}{P(n)_{(DA)n}} + \frac{I_{(DI)n} \cdot M_{(DI)n}}{P(n)_{(DI)n}}} \quad (18)$$

For GPEC, $W(M)_{(DA)n}^{GPEC}$ is given by

$$W(M)_{(DA)n}^{GPEC} = \frac{w(M)_{(DA)n} \cdot m_{polyDA}}{w(M)_{(DA)n} \cdot m_{polyDA} + w(M)_{(DI)n} \cdot m_{polyDI}} \quad (19)$$

where m_{polyDA} and m_{polyDI} are the amounts of homopolyesters in the mixtures (in gram). In figure 5.5a a plot is presented of $W(M)_{(DA)n}^{ESIFTMS}$ (sprayed in acetone) as a function of $W(M)_{(DA)n}^{GPEC}$ for oligomers with one acid and one alcohol endgroup (n=1-3). Note that each series of peaks corresponds to the concentration dependence (by changing the mixing ratio polyDA:polyDI) of two structurally similar oligomers e.g. DA₃ and DI₃. In the absence of differences in IE a linear relation between $W(M)_{(DA)n}^{ESIFTMS}$ and $W(M)_{(DA)n}^{GPEC}$ with a slope of 1 and intercept of 0 should be obtained (see dotted line in figure 5.5a). However, more adipic acid is detected with ESI FT-ICR MS than is present in the mixture as can be seen by the curved lines in figure 5.5a that all lie above the dotted line. Similar but less dramatic results were observed when THF was used as solvent. This is probably due to the lower permittivity of THF (compared with acetone) resulting in ESI generated droplets with a smaller radius and higher surface area from which ions can desorb more efficiently.^{216,217} These results demonstrate that oligomers with adipic acid are more efficiently ionised than the oligomers with isophthalic acid.

The relative difference in IE has not been quantified here because too many parameters influence the IE.

The relative difference in IE can be attributed to a difference in solvation energy of polyDA and polyDI. If PolyDA has lower solvation energy than polyDI, this will lead to a relatively high surface activity and therefore an efficient ion desorption from the surface of an electrosprayed droplet. Unfortunately the solvation energies of the molecules studied in this work are unknown and an explanation based on a difference in the solvation energy will remain an inference. Several authors have shown a large influence of the surface activity on IE.^{152,198-202} An additional indication that the solvation energy of polyDA is relatively low is seen by comparison of different charge states. The intensity of PolyDI in charge state 2 has a negligible abundance compared to the intensity of polyDA. PolyDI has not been observed in charge states 3 and 4, although polyDA has been observed in charge states 1-4. This is probably because most charges are located on the surface of the droplets together with polyDA making it more probable for polyDA to be multiply charged than polyDI.

The $W(M)^{ESIFTMS}$ values of the oligomers with two alcohol and two acid endgroups are plotted as a function of $W(M)^{GPEC}$ in figures 5.5b-c, respectively. The results demonstrate that relative differences in IE become larger with an increasing number of acid endgroups. The intensity of the isophthalic acid containing oligomers has almost become zero for the oligomers with two acid endgroups. Differences in IE for the cyclic oligomers are in-between that of the oligomers with two acid endgroups and oligomers with one acid and one alcohol endgroup. The difference in IE increases in favour of adipic acid with increasing degree of polymerisation n as can be seen in figures 5.5a-b.

The increasing difference in IE with increasing number of acid endgroups can be explained by a higher sodium affinity of adipic acid compared to isophthalic acid. Oligomers with two adipic acid endgroups will have a higher chance to interact with the sodium cation than oligomers with one acid and one alcohol endgroup.

The results presented in figures 5.5a-c were performed at relatively high polyDA concentration. To exclude possible concentration effects induced by the high polyDA concentration a new series of experiments was performed. Dilutions of a 1:1 mixture of polyDA and polyDI (w/w) were made in acetone and THF to which 5 mM NaI was added. The stock solution contained 2 mg/ml polyDA and 2 mg/ml polyDI and was diluted to samples with 0,01 – 2 mg/ml of each polymer.

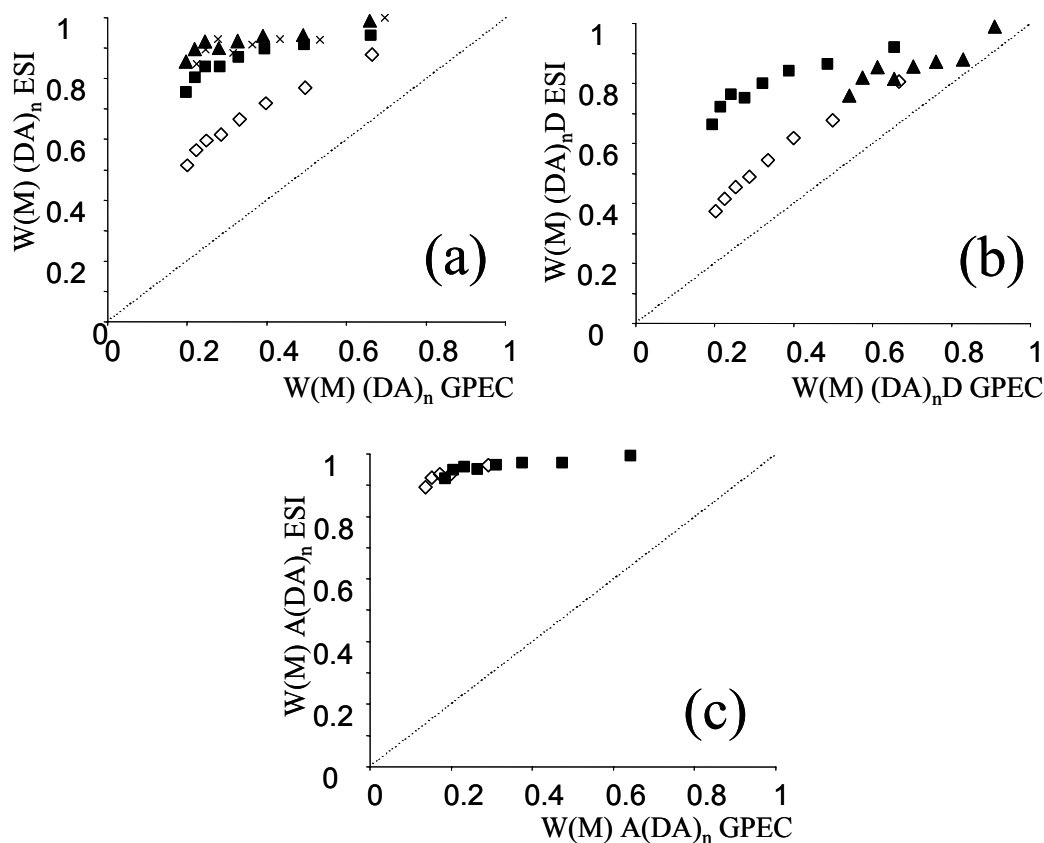


Figure 5.5 $W(M)^{ESI \text{ FT-MS}}$ sprayed in acetone is plotted as a function of $W(M)^{GPEC}$ for the oligomers with one acid and one alcohol endgroup (a), for oligomers with two alcohol endgroups (b) and for oligomers with two acid endgroups (c). Degrees of polymerisation shown are $n=1$ (\diamond), 2 (\blacksquare), 3 (\blacktriangle) and 4 (\times). The blends contain 0.5-2 mg/ml polymer.

Figure 5.6 shows the molar ratio polyDA:polyDI for the structurally similar dimers observed in the FT-ICR MS spectra sprayed in THF. A molar ratio of 1 indicates that the oligomers in polyDA and polyDI are present in equimolar amounts. The differences in relative IE show similar effects as observed in figures 5.5a-c. As can be seen clearly, the effects decrease significantly at low homopolymer concentration, which points to concentration effects. The measured molar ratio has become lower than one for most of the oligomers at the detection limit of the experiment. This indicates that polyDI is more efficiently ionised at low concentration. Note that this effect can have a different offset when the same mixture is measured with other mass spectrometers. The detection limit was approximately 3 fmol for $A(DA)_2$ (m/z 1077) in the electrospray source not taking losses due to ion transport into account. The strongest concentration effects were observed for the oligomers with two acid endgroups $A(DA)_n$ and $I(DI)_n$ ($n=1-2$)

sprayed in acetone (results not shown). The molar ratio $A(\text{DA})_n/I(\text{DI})_n$ was 2.5 at 0.01 mg/ml and increased to 60 at 2 mg/ml. It is unclear why the relative IE becomes larger for polyDI, or lower for polyDA, at concentrations near the detection limit.

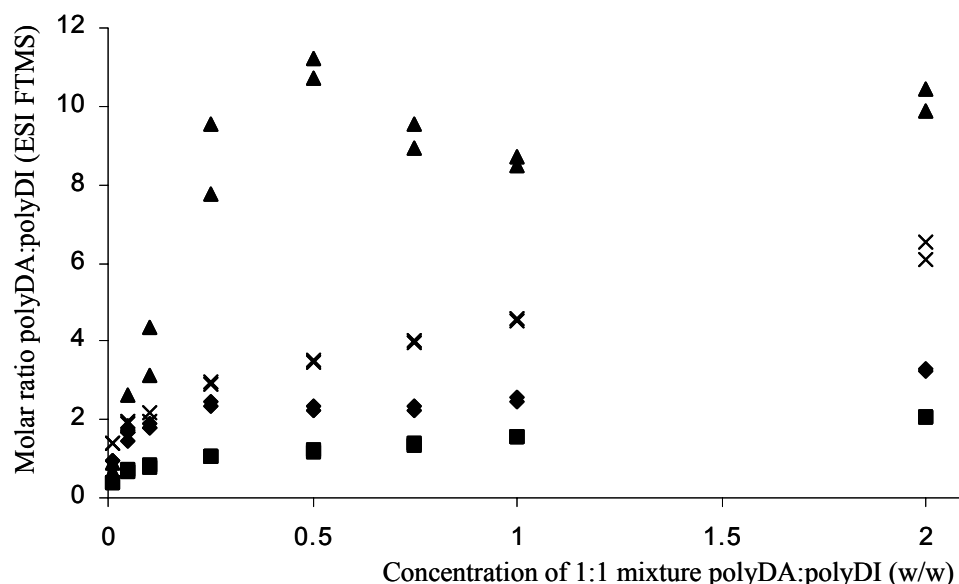


Figure 5.6 Molar ratio polyDA and polyDI for the structurally similar dimers observed in the spectra sprayed in THF. The mixtures contain 1:1 polyDA and polyDI (w/w). The 1 on the x-axis corresponds to a mixture of 1 mg/ml polyDA and 1 mg/ml polyDI. The symbols denote $(\text{DA})_2/(\text{DI})_2$ (◆), $(\text{DA})_2\text{D}/(\text{DI})_2\text{D}$ (■), $A(\text{DA})_2/I(\text{DI})_2$ (▲) and cyclics $(\text{DA})_2/(\text{DI})_2$ (×).

5.4. Conclusions

Our results demonstrate that differences in IE between the monomeric structures of copolymers can influence the copolymer composition as measured with electrospray ionisation mass spectrometry. The concentration and nature of the solvent influence the relative IE of the oligomer ions in the ESI process. Other important parameters that may influence the ionisation efficiency of co-oligomers are the chemical composition (i.e. the number of A's and B's in the oligomers), the sequence of the monomers, the polydispersity (D) but also spray conditions (SC) and instrumental parameters (IP). To deal with some of these variables, the ionisation efficiency $IE^{(M)}(\tau_1, \tau_2, \dots, \tau_{M-1}, \tau_M)$ was introduced in equation (5.12). When all parameters are taken into account that can influence the ionisation efficiency, the ionisation efficiency should in principle be written as

$IE^{(M)}(D, SC, IP)(\tau_1, \tau_2, \dots, \tau_{M-1}, \tau_M)$. It will however be very difficult to determine the $IE^{(M)}(D, SC, IP)(\tau_1, \tau_2, \dots, \tau_{M-1}, \tau_M)$ for each component separately but should be performed for a good characterisation of the copolymer chemical composition and sequence distribution using ESI (FT-ICR) MS.

Differences in IE have also been demonstrated for the copolymer poly(ethylene glycol/propylene glycol) studied with MALDI by Chen and coworkers.²¹⁸ The study of Chen and the work presented here demonstrate that the statistical copolymerisation models can only be used to model the mass spectra successfully when differences in IE have been quantified. Hence, earlier published copolymer sequence studies have become questionable.^{119,120}

Chapter 6

Sequence analysis of synthetic copolyesters by ESI FT-ICR MS

The molecular structure of a series of homo- and copolyesters has been studied using sustained off-resonance irradiation (SORI) collisionally activated dissociation (CAD) on a Fourier transform ion cyclotron resonance mass spectrometer (FT-ICR MS). Electrospray ionisation (ESI) was used as ionisation technique. The most important fragmentation pathways of the homopolyesters poly(di-propoxylated bisphenol-A/adipic acid) and poly(di-propoxylated bisphenol-A/isophthalic acid) were studied. Six different dissociation mechanisms were observed which are very similar to the mechanisms found to occur during pyrolysis of these compounds. Four of these mechanisms are a result of cleavages of the ester bond. The others are due to cleavages of the ether bond and bisphenol-A unit. Some of the fragments expected are not present in the spectrum indicating that each fragment has a specific sodium affinity. Sequence specific fragments of two of the three copolyester sequences that theoretically can exist were experimentally observed. Fragments that originate from the third sequence are not unique and can be formed from other sequences as well. Therefore it was not possible to determine the presence of the third sequence. Block sequences of larger co-oligomers can be distinguished from random sequences by studying whether block structured fragments appear in the MS/MS spectra. The method fails in making a distinction between random and partially random/block monomer sequences.

6.1. Introduction

Polymers are often complex systems consisting of a broad molecular weight distribution of polymer molecules with a variety of endgroups and monomeric units. Information on the intramolecular microstructure of synthetic copolymers is often obtained by nuclear magnetic resonance spectroscopy (NMR).

However, NMR only provides an average of the molecular weight distribution (MWD).²¹⁹ The individual polymer molecules in the MWD cannot be studied with NMR because isolation of one polymer molecule from the MWD is difficult if not impossible. Liquid chromatographic techniques like gradient polymer elution chromatography (GPEC) in combination with an UV detector provide information about the chemical composition of the polymer molecules but the determination of the sequence of copolymers is impossible (see also chapter 5).^{213,214,220}

Mass spectrometry can provide additional information about the monomer sequence of a copolymer. Matrix-assisted laser desorption/ionisation time-of-flight mass spectrometry (MALDI TOF-MS) is now frequently used for the determination of the chemical composition of the polymer molecules.^{29,126,196} The sequence of individual polymer molecules can be studied using post-source decay (PSD) or collisionally activated dissociation (CAD).^{98,101,221}

The number of theoretical sequences for a co-polymer with a particular chemical composition increases dramatically with increasing degree of polymerisation n .¹⁸⁴ Consider a random polymerisation reaction of two monomers A and B. An oligomer with degree of polymerisation 3 can have four compositions (A_3 , A_2B , AB_2 and B_3) which can all have different m/z values if the mass of $A \neq B$. The same oligomer with $n=3$ can have 6 different sequences (if $AAB=BAA$). An oligomer with $n=5$ can have five oligomer compositions with in total 20 sequences! The sequence of copolymers formed in a step polymerisation reaction such as polycondensation is random and the probability to observe a given oligomer with a block sequence is low. If the reactivity of monomer A is higher than the reactivity of monomer B, the probability that an oligomer will be observed with a block sequence increases.¹⁸⁴ A high resolution technique such as Fourier transform ion cyclotron resonance mass spectrometry (FT-ICR MS) is necessary to separate all co-polymer molecules in the mass spectrum.

In this chapter, the fragmentation behaviour of several homopolyesters and copolyesters is studied using sustained off-resonance irradiation collisionally activated dissociation (SORI CAD).²²² MS/MS studies with FT-ICR MS on synthetic polymers have been performed by others on the homopolymers poly(ethylene glycol), polystyrene and polyisoprene using MALDI.¹⁰² The selected molecular ions undergo multiple low energetic collisions near the centre of the ICR cell upon SORI. This results in a relatively slow increase of the internal energy so that the lowest energetic fragmentation pathways are sampled. Fragment ions are formed near the centre of the cell leading to a minimal loss of ions.

In order to acquire sequential information from the copolymer mass spectrum, a thorough knowledge of the fragmentation processes is a prerequisite. Insight in the fragmentation processes was obtained by studying the fragmentation

behaviour of various oligomers of the homopolyesters poly(di-propoxylated bisphenol-A/adipic acid) (DA) and poly(di-propoxylated bisphenol-A/isophthalic acid) (DI) (see table 5.1 for their structures). Oligomers of the copolyester poly(di-propoxylated bisphenol-A/adipic acid/isophthalic acid) with a degree of polymerisation 3 and 5 were studied in order to find out whether sequence information of the copolyester oligomers can be obtained.

6.2. Methods and materials

6.2.1. Methods

The electrospray ionisation Fourier transform ion cyclotron resonance mass spectrometry (ESI FT-ICR MS) experiments were performed with a modified Bruker-Spectrospin (Fällanden, Switzerland) APEX 7.0e FT-ICR MS equipped with a 7T super-conducting magnet and open cell. The system is described in detail in chapter 2.

Ions generated in the ESI source (3-4 kV) were trapped in the ICR cell and were left to equilibrate thermally for 5 seconds. Typical nozzle skimmer voltages were 10 V. Nozzle-skimmer dissociation was not observed. Ions were m/z isolated using a 262 kB (1.25 MHz) SWIFT pulse^{176,177} generated by a home build 200 Mb arbitrary waveform generator (AWG).¹⁸³ Xenon gas was pulsed into the ICR cell to perform collisionally activated dissociation (CAD) experiments. A delay of 1 second after the start of the Xenon gas introduction was employed to stabilise the Xenon pressure in the ICR cell ($2 \cdot 10^{-6}$ mbar). After 1 second, the parent ion was excited using sustained off-resonance irradiation (SORI) with an excitation frequency that was approximately 1500 Hz lower than the resonance frequency. The pulsed gas valve was closed one second after the SORI excitation event ended. A delay of 15 seconds was used to reduce the Xenon pressure to approximately $1 \cdot 10^{-8}$ mbar and followed by excite/detect. The duration of the SORI excitation pulse and the average kinetic energies of the oligomers studied in this chapter were: 10 s with 2.6 eV for $[(DA)_2D]Na^+$, 10 s with 2.5 eV for $[(DI)_2D]Na^+$, 10 s with 2.3 eV for $[(DA)_3]Na^+$, 13 s with 2.2 eV for $[(DI)_3]Na^+$, 13 s with 2.6 eV for $[(DA)_2(DI)]Na^+$ and 7 s with 2.3 eV for $[(DA)(DI)_2]Na^+$. The SORI excitation time was chosen such that the survival yield was lower than 50%.

6.2.2. Materials

The homopolyester and copolyester samples poly(di-propoxylated bisphenol-A/adipic acid); DA, poly(di-propoxylated bisphenol-A/isophthalic acid); DI and poly(di-propoxylated bisphenol-A/adipic acid/isophthalic acid); DAI used in this study were a gift of Océ Technologies, the Netherlands. The D denotes di-propoxylated bisphenol-A, A adipic acid and I isophthalic acid, see table 5.1 for the structures. Numbers added to the abbreviations, e.g. DAI13 denote the molar ratio A:I. Di-propoxylated bisphenol-A is always present in a molar ratio of approximately 50% because the polymers were made by a polycondensation reaction. The reactivity ratio for ester bond formation k_A/k_I (A = adipic acid, I = isophthalic acid) of the reactants in the copolymerisation reaction is 4 indicating a larger reactivity for adipic acid than isophthalic acid.²¹³ The number average molecular weight (M_n) of all polymers used in this chapter was about 3500 Da (polystyrene equivalent molar masses) with a polydispersity of ~2.2. The polymers were sprayed in a 1 mg/ml solution of acetone (Merck). Approximately 500 μ M NaI (Aldrich) was added to the solution to promote cationisation.

All polymers studied in this chapter have previously been characterised by the liquid chromatographic (LC) techniques size exclusion chromatography (SEC) and gradient polymer elution chromatography (GPEC).²¹³ The homopolyester poly(di-propoxylated bisphenol-A/adipic acid) (DA) consists of oligomers containing 0, 1 and 2 acid endgroups, denoted as $(DA)_nD$, $(DA)_n$ and $A(DA)_n$ respectively, and cyclic oligomers. The subscript n is the degree of polymerisation and ranges from 1 to more than 25. Similar oligomers were observed for the homopolyester poly(di-propoxylated bisphenol-A/isophthalic acid) (DI), and the copolyester poly(di-propoxylated bisphenol-A/adipic acid/isophthalic acid) (DAI). The copolyester sample contains co- and homopolyester oligomers formed during the polymerisation reaction.

6.3. Results and discussion

The ESI FT-ICR MS spectra of the homopolyester DA and the copolyester DAI12 are shown in figure 6.1 (a) and (b). All peaks are isotopically resolved as is shown in the insert of figure 6.1 (b) with a resolution of 20,000 at m/z 1000 (128 kB data points, bandwidth 500 kHz). Approximately 150 and 200 different ions are present in the spectra of DA and DAI12, respectively, of which most have been identified. For reasons of clarity only a few peaks have been labelled. The oligomers observed for the homo- and copolyesters are sodium cationised and

contain 0, 1 or 2 acid endgroups. This confirms the observations by GPEC. Cyclic oligomers were also detected (denoted by C in figure 6.1a). Table 6.1 displays the main series of oligomers observed for DA, DA12 (figures 6.1 (a) and (b)) and DI (spectrum not shown). The n and m denote the number of (DA) and (DI) units, respectively. The spectrum of the copolyester shows the presence of both homo- and copolyester oligomers. Charge states up to +3 were observed.

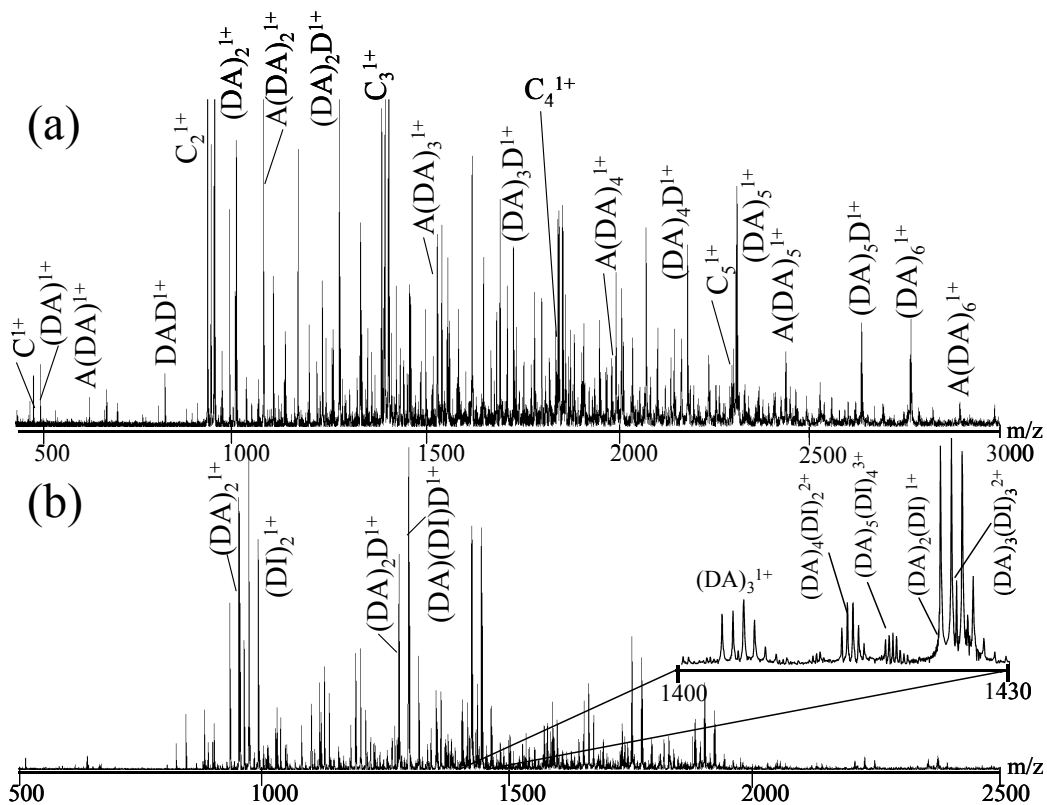


Figure 6.1 ESI FT-ICR MS spectra of the homopolymer di-propoxylated bisphenol-A/adipic acid (DA) (a) and the copolymer di-propoxylated bisphenol-A/adipic acid/isophthalic acid (DA12) (b). All ions observed are sodium cationised.

	m/z	n	m
$(DA)_n$	$454.2292 n + 41.0119$	1-14	
$(DA)_nD$	$454.2305 n + 367.1985$	1-13	
$A(DA)_n$	$454.2251 n + 169.0685$	1-12	
$(DA)_n$ cyclic	$454.2260 n + 23.0083$	1-5	
$(DI)_m$	$474.1920 m + 41.0196$		1-10
$(DI)_mD$	$474.1911 m + 367.2040$		1-9
$I(DI)_m$	$474.2002 m + 189.0188$		1-7
$(DI)_m$ cyclic	$474.2002 m + 22.9930$		2-5
$(DA)_n(DI)_m$	$454.2306 n + 474.1963 m + 41.0075$	1-7	0-7
$(DA)_n(DI)_mD$	$454.2346 n + 474.2045 m + 367.1871$	1-6	0-7
$I(DA)_n(DI)_m$	$454.2129 n + 474.1945 m + 189.0106$	1-5	0-5

Table 6.1 Main series of oligomers observed for DA, DAI12 and DI. n and m denote the number of DA and DI units, respectively.

Cyclic oligomers appear in the spectra in charge state +1 only with a maximum degree of polymerisation of 5. The largest linear polymer molecule measured has a degree of polymerisation of 14, with a mass of ~6500 Da ($[(DA)_{14}]Na_3^{3+}$). This is much smaller than the largest polymer molecule detected with GPEC indicating that only the low molecular weight part of the MWD is detected in the MS experiment. This effect has been observed earlier in the comparison of SEC with ESI FT-ICR MS.²²³ Fractionation of the polyesters with SEC, in order to get more mono-disperse molecular weight distributions, might solve this problem.⁷⁷ Another solution to this problem is the hyphenation of LC with mass spectrometry.^{81,82}

The measured MWD shifts to higher masses with increasing charge state. For example, $(DA)_n$ has been observed in charge state 1 for $n=1-6$ and increases to $n=4-12$ and $n=7-14$ for charge states 2 and 3, respectively. This is probably due to the number of oxygen atoms in the oligomers as discussed in chapter 3.

6.3.1. MS/MS of homopolyesters with two alcohol endgroups; $(DA)_2D$ and $(DI)_2D$

Figure 6.2 (a) and (b) display the SORI CAD spectra of $[(DA)_2D]Na^+$ with m/z 1275 and $[(DI)_2D]Na^+$ with m/z 1315, respectively. The formation of the collisionally induced fragment ions observed for $[(DA)_2D]Na^+$ and $[(DI)_2D]Na^+$ can almost all be explained by ester bond cleavages of the parent ion. In

mechanism 6.1 a 1,4-hydrogen rearrangement is proposed, that leads to the dissociation of the ester bond between di-propoxylated bisphenol-A and adipic acid. The proton bound to the tertiary C atom of the di-propoxylated bisphenol-A is transferred to the carbonyl oxygen atom of the ester bond in course of the rearrangement. Cleavage yields two possible reaction products. One fragment contains an adipic acid endgroup. The other fragment ion contains an unsaturated di-propoxylated bisphenol-A endgroup. This mechanism is analogous to the mechanisms proposed by several authors to explain the thermally induced dissociation of aliphatic and aromatic polyesters analysed by pyrolysis mass spectrometry.²²⁴⁻²²⁶ The major difference with these studies is that collisionally activated dissociation processes of sodiated ions using SORI do not necessarily involve the formation of sodiated radicals, while radicals are formed upon EI pyrolysis of neutral molecules. The mechanism explains the most abundant peaks in the CAD mass spectra (labelled as '1'). Table 6.2 lists the measured and theoretical masses of all fragment ions formed upon CAD.

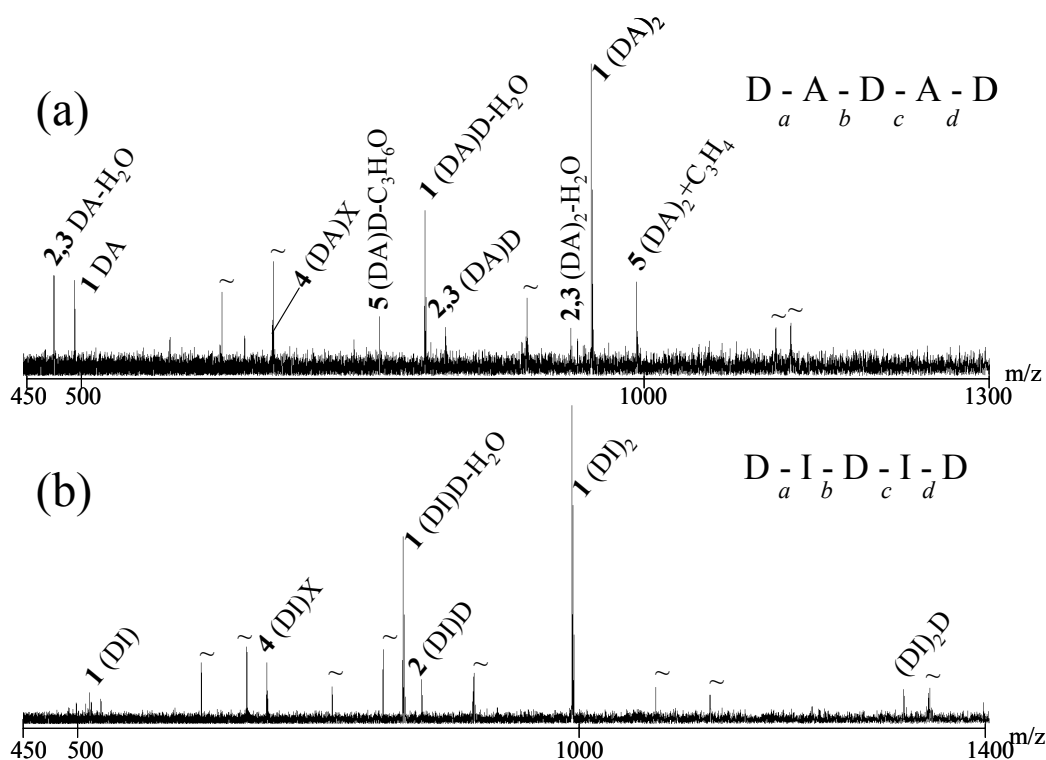
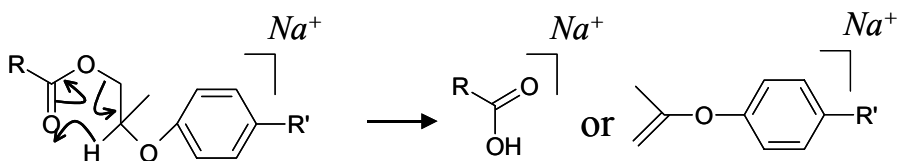


Figure 6.2 SORI CAD spectra with Xenon at 293K of the sodiated cationised homo-oligomers $(DA)_2D$ (a) and $(DI)_2D$ (b). The $[(DA)_2D]Na^+$ oligomer was excited for 10 s with an average kinetic energy of 2.6 eV. $[(DI)_2D]Na^+$ was excited for 10 s with an average kinetic energy of 2.5 eV. The symbols ~ denote electronic noise.



Mechanism 6.1 *1,4-hydrogen rearrangement of the ester bond results in a fragment with an alcohol endgroup or a fragment with an unsaturated bisphenol-A endgroup.*

The oligomers in figure 6.2 (a) and (b) have two D endgroups and are therefore symmetric. This results in uncomplicated MS/MS spectra. A 1,4-H rearrangement of ester bonds *b* and *c*, see insert in figure 6.2 (a) and (b), yields exactly the same fragmentation products. A similar argument is valid for the 1,4-H rearrangement of ester bonds *a* and *d*.

Three fragment ions are formed from the collisionally activation of $[(DA)_2D]Na^+$ that can not be explained by a 1,4-H rearrangement of the ester bond, i.e. $[(DA)_2-H_2O]Na^+$, $[(DA)D]Na^+$ and $[(DA)-H_2O]Na^+$. With the exception of $[(DA)-H_2O]Na^+$, the intensity of these peaks is relatively low. The presence of these fragmentation products indicates that another reaction channel is operational for the cleavage of the ester bonds. Two plausible mechanisms of this fragmentation reaction are given in mechanisms 6.2 and 6.3. In mechanism 6.2 an intramolecular transesterification is proposed. The hydroxyl oxygen of the di-propoxylated bisphenol-A endgroup reacts with the carbonyl carbon of the ester bond by a nucleophilic substitution, which yields a ring-closed intermediate. The positively charged hydroxyl oxygen in the formed ring rearranges the proton towards the hydroxyl oxygen of the leaving group followed by a cleavage. The reaction products are a stable cyclic ion or an ion with a di-propoxylated bisphenol-A endgroup. These peaks are marked with '2' in figures 6.2 (a) and (b). Cyclic esters have been observed by Buxbaum in the thermal degradation of polyethylene terephthalate²²⁴ and later by Montaudo *et al.*²²⁷ The rate of formation of cyclic ions by transesterification will be low because the alcohol endgroup has to be close to the ester bond. However, the time scale of SORI in FT-ICR MS is in the order of seconds which supports the chance that transesterification can take place during an FT-ICR MS experiment.

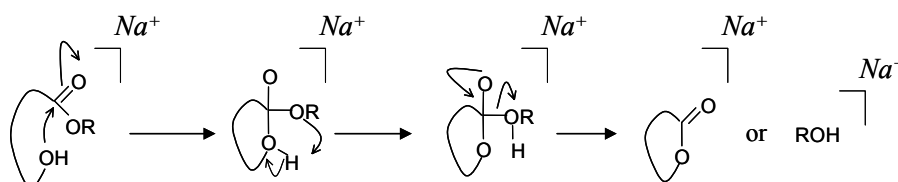
Fragment	measured m/z	exact m/z	$\Delta m/z$	Fragmentation mechanism(s)
(DA)	495.2245	495.2353	0.0108	1,2,3,6
(DA)-H ₂ O	477.2158	477.2248	0.0003	1,2,3
(DA)D	821.3946	821.4236	0.0428	2,3
(DA)D-H ₂ O	803.3808	803.4130	0.0322	1
A(DA)	623.2661	623.2827	0.0166	1
(DA) ₂	949.4298	949.4709	0.0411	1,2,3
(DA) ₂ -H ₂ O	931.4218	931.4603	0.0385	1,2,3
A(DA) ₂	1077.4667	1077.5182	0.0515	1
(DA) ₂ D	1275.5839	1275.6591	0.0752	3
(DA) ₂ D-H ₂ O	1257.5710	1257.6485	0.0775	1
(DA)X	669.3146	669.3398	0.0252	4
(DA)D-C ₃ H ₆ O	763.3497	763.3817	0.0320	5
(DA) ₂ +C ₃ H ₄	989.4550	989.5022	0.0472	5
A(DA)+C ₃ H ₄	663.2905	663.3140	0.0235	5
A(DA) ₂ +C ₃ H ₄	1117.4830	1117.5495	0.0665	5
(DI)	515.1913	515.2040	0.0127	1,2,6
(DI)-H ₂ O	497.1807	497.1935	0.0128	1,2,6
(DI)D	841.3561	841.3923	0.0362	2,6
(DI)D-H ₂ O	823.3404	823.3817	0.0413	1
I(DI)	663.2004	663.2201	0.0197	1
(DI) ₂	989.3552	989.4083	0.0531	1,2,6
(DI) ₂ -H ₂ O	971.3499	971.3977	0.0478	1,2,6
I(DI) ₂	1137.3499	1137.4243	0.0744	1
(DI) ₂ D	1315.4961	1315.5965	0.1004	6
(DI) ₂ D-H ₂ O	1297.4992	1297.5860	0.0868	1
(DI)X	689.2839	689.3085	0.0246	4
(DI) ₂ X	1163.4360	1163.5128	0.0768	4
I(DA)	643.2305	643.2514	0.0209	1
(DA)(DI)	969.3894	969.4396	0.0502	1,2,3
(DA)(DI)-H ₂ O	951.3755	951.4290	0.0535	1,2,3,6
I(DA) ₂	1097.4190	1097.4869	0.0679	1
A(DI) ₂	1117.3883	1117.4556	0.0673	1
(DA)(DI)D-H ₂ O	1277.5311	1277.6173	0.0862	1
(DA)(DI)-C ₃ H ₆ O	911.3510	911.3978	0.0468	5
A(DA)(DI)+C ₃ H ₄	1137.4508	1137.5182	0.0674	5

Table 6.2 Measured and theoretical masses of all fragment ions observed in this chapter and the mechanisms, which explain the fragment ions.

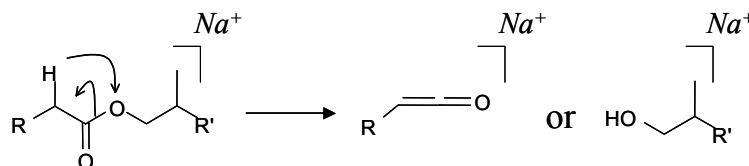
In mechanism 6.3, the methylene hydride adjacent to the carbonyl C-atom is transferred via a 1,3-hydrogen rearrangement to the ether oxygen of the ester bond followed by a cleavage of the ester bond. Two reaction products are formed. One product ion contains a di-propoxylated bisphenol-A endgroup and one product ion an adipic acid minus H₂O endgroup (see table 6.2 for their measured and theoretical masses). These peaks are marked with '3' in figure 6.2 (a). Distinguishing mechanism 6.2 from 6.3 by the m/z values of the product ions is not possible because the product ions have the same elemental composition.

The 1,4-H rearrangement and transesterification mechanisms described in mechanisms 6.1 and 6.2 were applied to the homopolyesters containing isophthalic

acid to rationalise product ion formation (figure 6.2(b)). Only one product ion, $[(DI)D]Na^+$, is observed that can be assigned to the transesterification of $[(DI)_2D]Na^+$. The fragment can be formed by mechanism 6.6 as well which will be shown later. Mechanism 6.3 cannot be applied to the isophthalic acid containing homopolyesters because of structural dissimilarities with adipic acid.



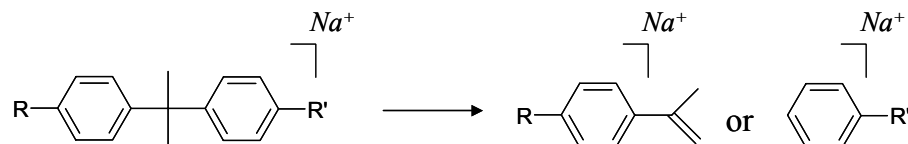
Mechanism 6.2 *Intramolecular transesterification of a polyester oligomer requires an alcohol endgroup. A cyclic ester and an alcohol are the resulting reaction products.*



Mechanism 6.3 *1,3-hydrogen rearrangement of the ester bond between adipic acid and di-propoxylated bisphenol-A. One product ion contains a di-propoxylated bisphenol-A endgroup and the other one an adipic acid minus H_2O endgroup.*

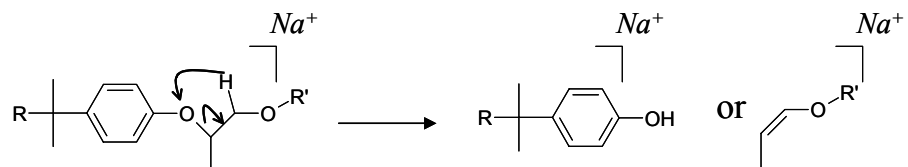
A fragment ion, $[(DA)X]Na^+$ with m/z 669, labelled as '4' in figure 6.2 (a), observed upon SORI CAD of $[(DA)_2D]Na^+$ is explained by the cleavage of the bisphenol-A unit (see mechanism 6.4). The elemental composition of X is $C_{12}H_{14}O$. The mechanism is not fully understood. Two molecules are formed of which one contains a newly formed phenyl endgroup and the other an isopropenyl phenyl endgroup (see table 6.2 for their measured and theoretical masses). Their appearance in the MS/MS spectrum upon collisional activation is thought to depend on the relative sodium cation affinities of the various organic functionalities of the product ion. If one of the two candidate reaction products has a substantially higher relative sodium affinity, then the sodium cation is retained by this fragment. The other reaction product will then be neutral and is not observed in the mass spectrum. The fragment with the isopropenyl benzene endgroup has been observed in the MS/MS spectrum indicating a higher sodium affinity

compared to the other fragment. The formation of this product ion has been observed as an M^{++} before by Montaudo *et al.* using EI pyrolysis mass spectrometry.²²⁸ The same phenomenon was observed for $[(DI)_2D]Na^+$.



Mechanism 6.4 *Cleavage of the bisphenol-A unit resulting in one product ion with a phenyl endgroup or another one with an isopropenyl phenyl endgroup.*

The last fragmentation pathway is unique for $[(DA)_2D]Na^+$. Two fragment ions, $[(DA)D-C_3H_6O]Na^+$ and $[(DA)_2C_3H_4]Na^+$, from the activated adipic acid containing homopolyester are due to the cleavage of the ether bond between the bisphenol-A and propoxyl group (see mechanism 6.5). The peaks are labelled with '5' in figure 6.2 (a). The secondary methylene hydride of the isopropoxyl group is transferred via a 1,3-hydrogen rearrangement to the ether oxygen between the bisphenol-A and propoxyl group followed by a cleavage of the ether bond. This results in fragment ions with a bisphenol-A endgroup and a propylene endgroup.



Mechanism 6.5 *1,3-hydrogen rearrangement of the ether bond between bisphenol-A and the isopropoxy group. One fragment ion contains a bisphenol-A endgroup and the other a propylene endgroup.*

6.3.2. MS/MS of homopolyesters with one alcohol and one acid endgroup;

$(DA)_3$ and $(DI)_3$

Figures 6.3 (a) and (b) display the SORI CAD spectra of the homopolyesters m/z 1403 $[(DA)_3]Na^+$ and m/z 1463 $[(DI)_3]Na^+$, respectively. Most fragment ions of $[(DA)_3]Na^+$ and $[(DI)_3]Na^+$ are produced by a 1,4-H rearrangement (labelled as '1') of the ester bond (see mechanism 6.1). The oligomers $[(DA)_3]Na^+$ and $[(DI)_3]Na^+$ are not symmetric because they have two different endgroups. Therefore more fragmentation products could be formed. The

1,4-H rearrangement of ester bond *b* of $[(DA)_3]Na^+$ for example, results in the fragments $[DA]Na^+$ and $[(DA)_2 - H_2O]Na^+$ while the 1,4-H rearrangement of ester bond *d* results in the fragments $[DA-H_2O]Na^+$ and $[(DA)_2]Na^+$ (see figure 6.3 (a)). Two fragments, $[(DA)D]Na^+$ and $[(DA)_2D]Na^+$, of the sodium cationised $(DA)_3$ can be explained by the 1,3-hydrogen rearrangement in mechanism 6.3 (see table 6.2 for their measured and theoretical masses). The product ions cannot originate from a transesterification because this requires the unlikely nucleophilic substitution of an alcohol endgroup to an ester bond. A transesterification of $[(DA)_3]Na^+$ can only result in the cyclic fragments $[(DA)-H_2O]Na^+$ and $[(DA)_2-H_2O]Na^+$.

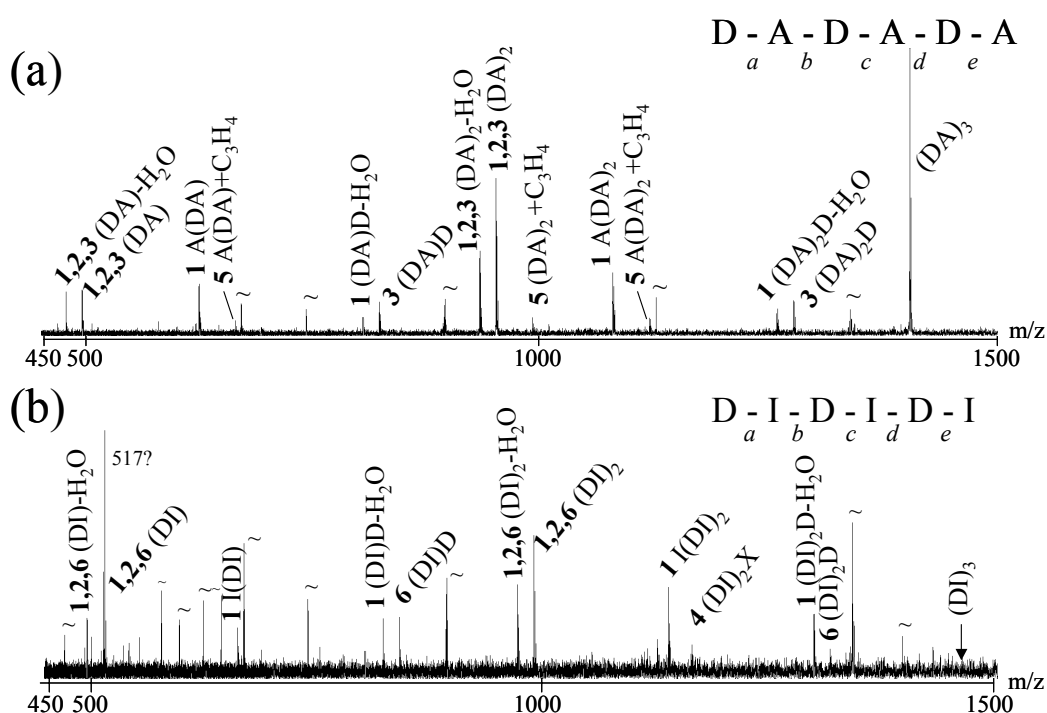
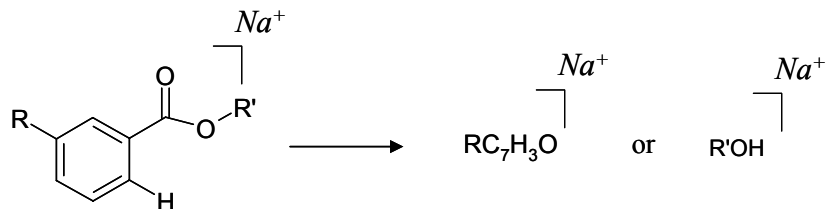


Figure 6.3 SORI CAD spectra of the sodium cationised homo-oligomers $(DA)_3$ (a) and $(DI)_3$ (b) with Xenon at 293K. $[(DA)_3]Na^+$ was excited for 10 s with an average kinetic energy of 2.3 eV. $[(DI)_3]Na^+$ was excited for 13 s with an average kinetic energy of 2.2 eV. The symbols ~ denote electronic noise.

The ester bonds of the isophthalic acid containing polyester can be cleaved by mechanisms 6.1 and 6.2. Two of the $[(DI)_3]Na^+$ fragments, $[(DI)D]Na^+$ and $[(DI)_2D]Na^+$, can not be explained by one of the mechanisms described so far but a hydrogen rearrangement can be proposed (mechanism 6.6). Two product ions are formed in course of the hydrogen rearrangement. One of these contains a di-propoxylated bisphenol-A endgroup ($[(DI)D]Na^+$ or $[(DI)_2D]Na^+$). The other

product ion has not been observed but should have a composition of $[C_7H_3O]Na^+$ or $[IDC_7H_3O]Na^+$. The exact structure of this ion is not known.



Mechanism 6.6 *Hydrogen rearrangement of the ester bond between isophthalic acid and bisphenol-A. One fragment ion contains a di-propoxylated bisphenol-A endgroup and the other an endgroup with elemental composition $[C_7H_3O]Na^+$ or $[IDC_7H_3O]Na^+$.*

The formation of fragment ions $[(DA)D]Na^+$ and $[(DA)D-H_2O]Na^+$ suggest that ions $[A(DA)-H_2O]Na^+$ and $[A(DA)]Na^+$ should also be present in the MS/MS spectrum. However, $[A(DA)-H_2O]Na^+$ was not observed. This indicates that fragment (DA)D has a much stronger sodium affinity than $[A(DA)-H_2O]$. The loss of a D endgroup from the parent ion can be explained by a 1,4-H rearrangement leading to $[A(DA)_2]Na^+$. Fragment ion $[D-H_2O]Na^+$ is not present in the spectrum. Similar results have been found upon collisional activation of $[(DI)_3]Na^+$.

Most of the mechanisms proposed in this chapter have been reported earlier in the pyrolysis literature.²²⁴⁻²²⁸ This suggests that pyrolysis and SORI processes in the timescale of the FT-ICR MS experiment are similar for polyesters. The most frequently observed fragmentation pathway is the cleavage of the ester bond. From the literature²²⁹ is known that the sodium cations preferentially bind by electrostatic forces to the carbonyl and free hydroxyl oxygen atoms of poly(ethylene terephthalate) (PET) which has structural similarities to poly(di-propoxylated bisphenol-A/adipic acid) and poly(di-propoxylated bisphenol-A/isophthalic acid). Thus, we assume a similar interaction of the sodium cation with our polyesters. The electrostatic interaction of the sodium cation with the carbonyl oxygen atom delocalises the electrons of the ester bond. This interaction weakens the ester bond and might promote fragmentation of the ester bond.

6.3.3. MS/MS of copolyesters with one alcohol and one acid endgroup;

 $(DA)_2(DI)$ and $(DI)_2(DA)$

Two oligomers of the copolyester poly(di-propoxylated bisphenol-A/adipic acid/isophthalic acid) with a degree of polymerisation 3 were selected for fragmentation using SORI CAD. The oligomers are m/z 1423 $[(DA)_2(DI)]Na^+$ and m/z 1443 $[(DA)(DI)_2]Na^+$. Figure 6.4 (a) and (b) displays the SORI CAD spectra of $[(DA)_2(DI)]Na^+$ and $[(DA)(DI)_2]Na^+$, respectively. The MS/MS spectra were interpreted using mechanisms 6.1 to 6.6 proposed for the homopolyesters.

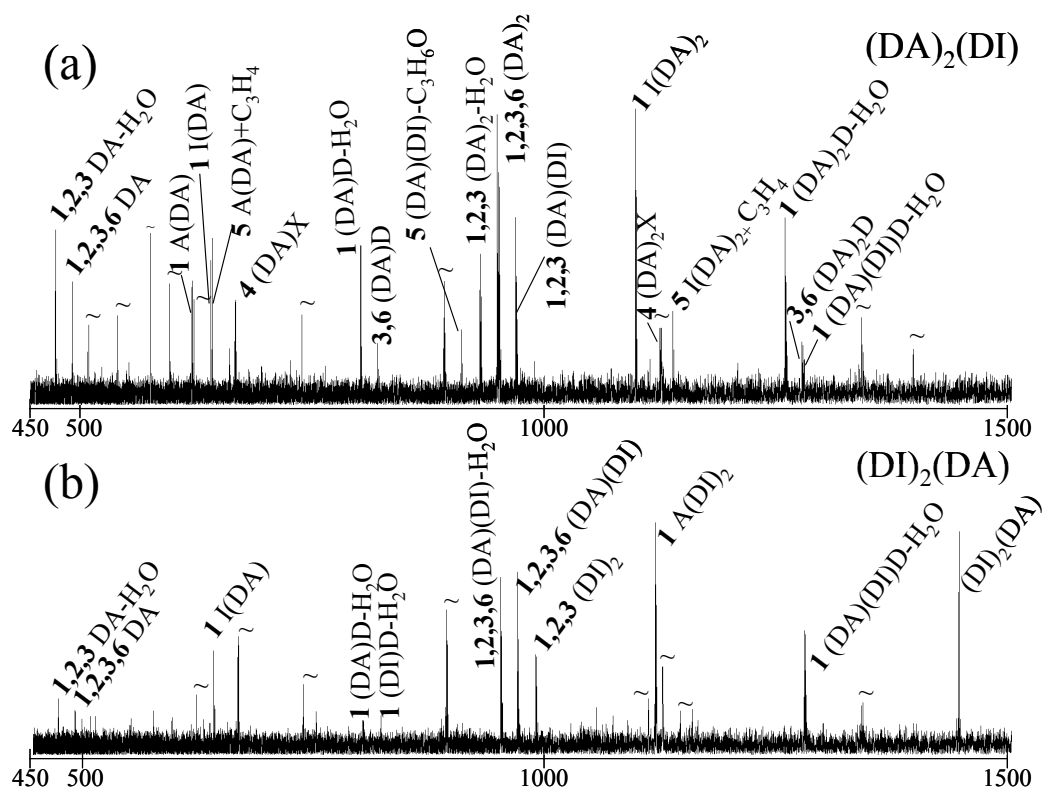


Figure 6.4 SORI CAD spectra of the co-oligomers $(DA)_2(DI)$ (a) and $(DA)(DI)_2$ (b) with Xenon at 293K. $[(DA)_2(DI)]Na^+$ was excited for 13 s with an average kinetic energy of 2.6 eV. $[(DA)(DI)_2]Na^+$ was excited for 7 s with an average kinetic energy of 2.3 eV. The symbols ~ denote electronic noise.

The fragmentation products of $[(DA)_2(DI)]Na^+$ can be explained by all mechanisms proposed so far for the homopolyesters. Product ions of $[(DA)(DI)_2]Na^+$ are formed according to mechanisms 6.1, 6.2, 6.3 and 6.6 (see table 6.2 for their measured and theoretical masses). Mechanisms 6.4 and 6.5 were not observed for the fragmentation of $[(DA)_2(DI)]Na^+$.

Both oligomers can be formed in the polymerisation reaction with three different sequences. The $(DA)_2(DI)$ sequences are: I) DIDADA II) DADIDA and III) DADADI and for $(DA)(DI)_2$: I) DADIDI, II) DIDADI and III) DIDIDA. Five fragments of $[(DA)_2(DI)]Na^+$ have been observed that are sequence specific. The fragments $[A(DA)]Na^+$ and $[(A(DA)C_3H_4)]Na^+$ can only be formed from sequence I through mechanisms 6.1 and 6.5, respectively. Fragments $[(DA)_2D]Na^+$ (mechanism 6.3 and 6.6), $[(DA)_2D-H_2O]Na^+$ (mechanism 6.1) and $[(DA)_2X]Na^+$ (mechanisms 6.4) can only be formed from sequence III. The other fragmentation products observed are not sequence specific but can be formed from 2 or 3 different sequences.

For $[(DA)(DI)_2]Na^+$ only one sequence specific fragment, $[(DA)D - H_2O]Na^+$, has been observed which can only be formed from sequence I through mechanism 6.1. However, fragments $[IDA]Na^+$ and $[(DI)D-H_2O]Na^+$ can be formed from sequences II or III through mechanism 6.1. This indicates that at least two sequences of $(DA)(DI)_2$ are present in the polymer sample.

Only fragments from sequences I and III of $(DA)_2(DI)$ were positively identified in the polymer sample. Fragments were observed that might have originated from sequence II, but could be formed from sequences I and/or III as well. A similar reasoning can be given for $(DA)(DI)_2$. Although the copolyesters are not very complex molecules (they consist of only two different building blocks), obtaining sequence information from their MS/MS spectra is complicated. By comparison, the determination of the amino acid sequence of peptides is generally less complicated because almost all amino acids have a specific mass and peptides have a unique sequence. Exact mass analysis of the fragment ions excludes many sequences.

For larger oligomers the number of sequences becomes very large and the question: 'which sequences are present in the copolyester sample' becomes less relevant. A more relevant question is: 'does our copolyester sample have a random or block sequence'. It can be expected that the interpretation of the MS/MS spectra for large oligomers becomes less complicated. For example, when a block oligomer containing a block of 5 A's and a block of 5 B's is fragmented, the fragments will contain blocks of five A's and a couple of B's or five B's and a couple of A's. Or the fragments will only contain A's or B's. Fragments containing e.g. one A and one B will indicate the presence of other types of sequences. This methodology has recently been used to confirm the block structure of a methyl methacrylate/butyl methacrylate copolymer.¹¹⁶

The MS/MS spectrum of a larger co-oligomer $[(DA)_3(DI)_2]2Na^+$ in charge state 2 ($m/z=1187.55$) is presented in figure 6.5. The parent ion $(DA)_3(DI)_2$ can have 10 sequences of which two have a block structure: DADADADIDI and

DIDIDADADA. Singly charged fragments with an m/z lower and higher than the m/z of the parent ion are observed. Doubly charged fragments with an m/z lower than the parent ion are observed as well. Fragments $[(DA)_3]Na^+$ and $[(DI)_2]Na^+$ that are indicative for block copolymers are *not* observed, indicated with an arrow in figure 6.5. All fragments that are observed, for example $[(DA)_2(DI)]Na^+$, $[ADI]Na^+$ and $[DADI]Na^+$, point toward a random copolymer.

Two methodologies are described above which both are based on MS/MS experiments to determine whether the polymer has a block or random sequence. The second methodology, searching for block-structured fragments, does give information about the random or block structure of the copolymer. However, it is not possible to distinguish a pure random copolymer from a copolymer with a partial random and partial block structure with MS/MS experiments. All three copolyester sequences would have sequence specific fragments if the bonds could be broken more selectively. For example, the sequence can be clarified if the DI ester bond is selectively broken. This might be achieved by photo dissociation or electron capture dissociation.

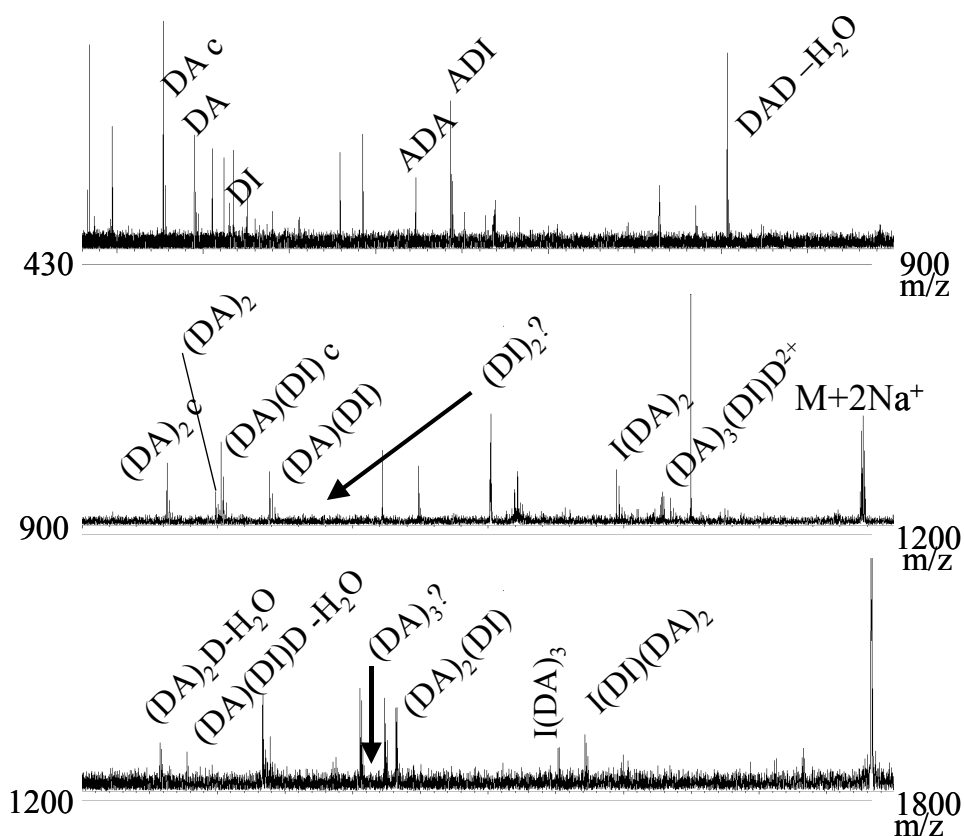


Figure 6.5 MS/MS of $[(DA)_3(DI)_2]2Na^+$ in charge state 2.

6.4. Conclusions

Electrospray ionisation on a Fourier transform ion cyclotron resonance mass spectrometer (ESI FT-ICR MS) is used to selectively isolate and fragment oligomers of the homopolyesters of poly(di-propoxylated bisphenol-A/isophthalic acid) and poly(di-propoxylated bisphenol-A/adipic acid) and the copolyester poly(di-propoxylated bisphenol-A/isophthalic acid/adipic acid) using sustained off-resonance irradiation collisionally activated dissociation (SORI CAD). Six different mechanisms can explain the fragmentation products. Four mechanisms involve the cleavage of the ester bond and two others involve cleavages of the ether bond and bisphenol-A unit.

For each cleavage two fragment ions are expected to appear in the MS/MS spectrum. However, the cleavage of some of the bonds yields only one fragment ion. This indicates that large differences exist in the sodium affinity of the fragment ions or that local sodium affinities are present in the parent ion.

Only the presence of two sequences of $(DA)_2(DI)$ and $(DA)(DI)_2$ have experimentally been observed by means of sequence specific fragments. The third theoretical sequence might be present in the polymer sample but does not contain sequence specific fragments. Another MS/MS based approach can be used to study whether the copolymer has a random or block sequence. The methodology is based on studying whether block structured fragments appear in the MS/MS spectra. This procedure is especially of use for large oligomers. However, the method fails to distinguish fully random from partially random/block copolymers. Other dissociation techniques like photon induced dissociation or electron capture dissociation might be more selective in the cleavage of specific bonds of the molecule necessary for sequence analysis.

Chapter 7

Structural characterisation of hyperbranched polyesteramides: MS^n and the origin of species

Four synthetic hyperbranched polyesteramides were analysed with electrospray ionisation Fourier transform ion cyclotron resonance mass spectrometry. The polymers were polycondensation products of the trifunctional di-isopropanolamine (D) and difunctional anhydrides (X) of succinic acid, glutaric acid, 1,2-cyclohexane dicarboxylic acid and phthalic acid. The most intense oligomer series observed was X_nD_{n+1} containing di-isopropanolamine endgroups as expected from the polycondensation conditions. A series of oligomers $X_nD_{n+1}-H_2O$ was observed as well, which can have its origin in the polymerisation process or alternatively could result from in-source fragmentation of X_nD_{n+1} . Breakdown diagrams of the protonated parent ions X_3D_4 and additional MS^n ($n=1,2,3$) measurements gave insight in the fragmentation behaviour of the polymers. Three main fragmentation pathways have been observed for all polymers of which the loss of H_2O to oxazonium ions has the lowest appearance energy followed by the rearrangement of the amide and ester bonds also leading to oxazonium ions. The loss of a second H_2O to allylic or morpholine endgroups has the highest appearance energy. MS^3 experiments demonstrated that the presence of oligomers $X_nD_{n+1}-H_2O$ can be attributed to the polymerisation process. Most probably an allylic endgroup has formed from one of the alcohol endgroups. The formation of allylic endgroups partly terminates the polymerisation reaction and results in a change of the composition of the molecular weight distribution and decrease of the number average molecular weight compared with theoretical polymerisation models.

7.1. Introduction

Soft ionisation techniques for synthetic polymer characterisation like matrix-assisted laser desorption/ionisation (MALDI) and electrospray ionisation

(ESI) have become widely used in mass spectrometry mainly because intact protonated or cationised molecular ions are generated.^{4,20,51,64,77,196} Most studies concern linear polymers, although some branched polymers have been successfully analysed.^{95,138,139,141,143} An example of a recent mass spectrometric study of a branched polymer concerns a hyperbranched polyesteramide synthesised by the polycondensation of the trifunctional di-isopropanolamine (D)²³⁰ and the difunctional 1,2-cyclohexane dicarboxylic acid anhydride (C).^{95,231} Extensive in-source decay was observed for ions generated by field desorption (FD) and MALDI for this particular branched polymer. These fragments appear in the spectra as $C_nD_{n+m}-H_2O$ ($m=0-2$) ions. Metastable decay of the parent ion without a collision gas was also observed for the MALDI generated ions. This resulted in the rearrangement of the amide and ester bonds to oxazolonium ions, which appear in the spectra as $C_nD_{n+m}-H_2O$ ($m=0-1$) ions. For ESI generated ions, the intensity of the oligomeric ions $C_nD_{n+m}-H_2O$ ($m=0-1$) relative to the intensity of the intact molecular ions C_nD_{n+m} ($m=0-1$) was lowest. It was however not possible to determine whether the low intensity ions $C_nD_{n+m}-H_2O$ ($m=0-2$) were generated in the ESI source or during the polymerisation reaction. The ions observed in ESI can hence have a mixed origin that cannot be distinguished exclusively by the determination of their m/z values.

From a polymer synthesis point of view, it is important to know whether the $C_nD_{n+m}-H_2O$ ($m=0-2$) series is formed in the polymerisation reaction or by in-source fragmentation upon ESI. The generation of this oligomer series $C_nD_{n+m}-H_2O$ ($m=0-2$) during the polymerisation implies that some of the functional groups of the oligomers have terminated by allylic endgroup formation which influences the molecular weight distribution. The origin of the oligomer $C_3D_4-H_2O$ has been determined using MS^n studies. First, the fragmentation behaviour of the protonated oligomer C_3D_4 was studied by energy resolved MS^2 collisionally activated dissociation experiments. The information obtained from this study is used to interpret MS^3 experiments, which are necessary to determine the origin of the oligomer $C_3D_4-H_2O$. This study has been performed for four hyperbranched polyesteramides, which were synthesised by the polycondensation of an excess of the trifunctional di-isopropanolamine and the difunctional anhydrides of succinic acid, glutaric acid, 1,2-cyclohexane dicarboxylic acid and phthalic acid.

7.2. Methods and materials

7.2.1. ESI FT-ICR MS analysis

The analyses were performed with a modified FT-ICR MS (Bruker-Spectrospin APEX 7.0e, Fällanden, Switzerland). The cell was an in house constructed open cell. The system is described in chapter 2. Pulsed gas trapping with Argon at $P_{Ar}=5.2\cdot 10^{-6}$ mbar for 2 seconds was used to enhance trapping of the ions in the open cell. On-resonance excitation collisionally activated dissociation in the ICR cell was used to activate the parent ions generated by electrospray ionisation. Argon was used as collision gas ($P_{Ar}=5.2\cdot 10^{-6}$ mbar). The geometry factor α of the open cell necessary for the calculation of the excitation potentials on the excitation electrodes was estimated to be 2.26 based on a comparison between room temperature breakdown diagrams of several peptides measured with the Infinity cell and the open cell. The peak-to-peak voltage of the RF excitation signal was 17.6 V in all CAD experiments. The procedure followed for the construction of breakdown diagrams and calculation of the laboratory frame kinetic energy $E_{kin,lab}$ has been described in chapter 2 by equation (2.10).¹⁸¹ For the energy resolved experiments, three scans were summed at each collision energy.

7.2.2. Hyperbranched polyesteramides

The hyperbranched polyesteramides used in this study are polycondensation products of the trifunctional di-isopropanolamine (D) and a difunctional dicarboxylic acid anhydride provided by DSM (Geleen, the Netherlands).²³⁰ The difunctional dicarboxylic acid anhydrides used in the polymerisations are succinic acid anhydride (S), glutaric acid anhydride (G), phthalic acid anhydride (P) and 1,2-cyclohexane dicarboxylic acid anhydride (C). Figure 7.1 shows the structures of these monomers.

A dynamic equilibrium exists between the ester and amide bond formed during the polymerisation as shown in figure 7.2. This equilibrium results in the polymerisation of a mixture of AB_2 and ABB' monomers where A represents the acid group, B the hydroxyl and B' the amine.^{2,134,232} The polycondensation proceeds via oxazolonium ions. The desired pathway (A) is presented in figure 7.3 where a carboxylic acid group reacts with an oxazolonium ion (AB_2 type of polymerisation). Mainly alternating X_nD_{n+1} oligomers are formed although alternating cyclic oligomers X_nD_n have also been observed.⁹⁵ X is a diacid and D the di-isopropanolamine. The oxazolonium ion can react with the amine group as

well as shown in figure 7.3 pathway B. These reactions result in a bond between two di-isopropanolamine groups via a tertiary amine and lead to oligomers X_nD_{n+2} , X_nD_{n+3} , These oligomers contain defects of the alternating polymer structure (ABB' type of polymerisation). The synthesis is described in more detail by van Bentem et al. for 1,2-cyclohexane dicarboxylic acid anhydride.²³¹ The other polymers were synthesised in a similar manner.

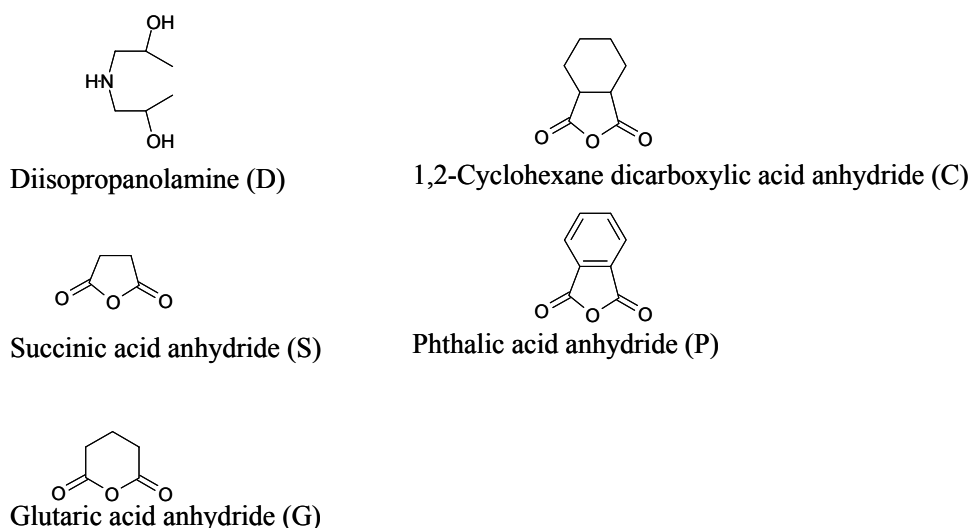


Figure 7.1 Structure of the di- and trifunctional monomers used in the synthesis of the hyperbranched polyesteramides.

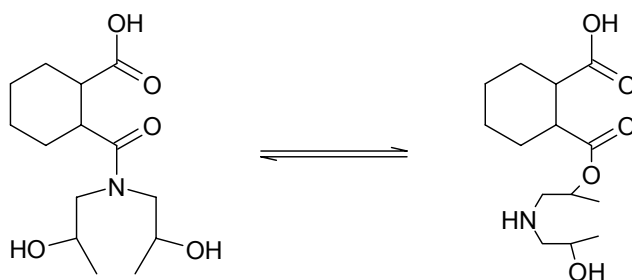


Figure 7.2 Dynamic equilibrium between amide and ester bond.

The products of the polycondensation reactions of the anhydrides of succinic acid, glutaric acid, phthalic acid and 1,2-cyclohexane dicarboxylic acid have a designed number average molecular weights of 1200, 1200, 1000 and 925, respectively.²³¹ The electrospray ionisation solutions consist of 74:24:2 Methanol (Merck, Darmstadt, Germany):H₂O:HAc (Biosolve, Valkenswaard, the

Netherlands) in which approximately 300 µg/ml of the hyperbranched polymers is dissolved.

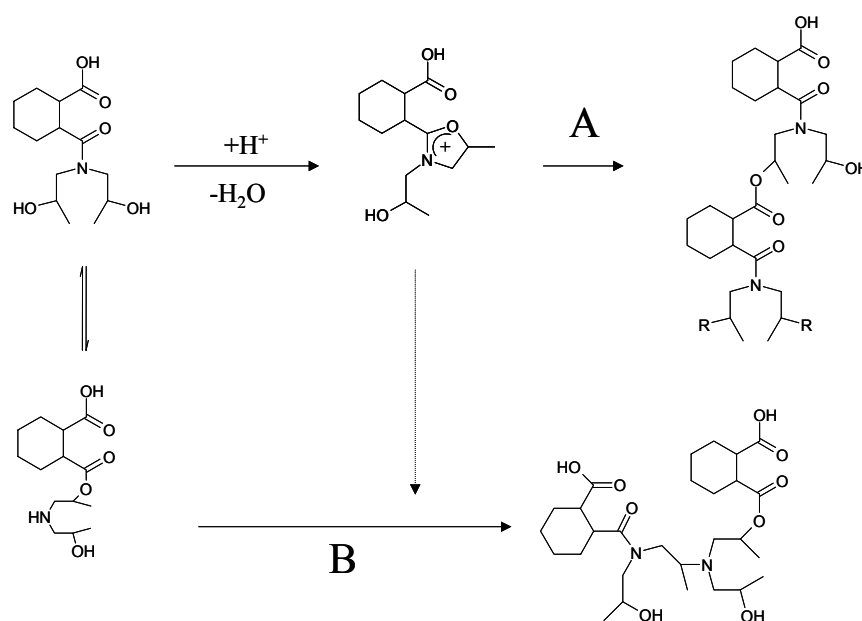


Figure 7.3 Polycondensation of trifunctional di-isopropanolamine and difunctional 1,2-cyclohexane dicarboxylic acid proceeds via AB₂ (A) and ABB' (B) type of polymerisation.

7.3. Results and discussion

The hyperbranched polyesteramides were all produced by the same synthetic route, in which the trifunctional monomer di-isopropanolamine (D) was added in excess to the dicarboxylic acid anhydride. The notation used to denote the dicarboxylic acid anhydrides is S, G, C and P for the anhydrides of succinic acid, glutaric acid, 1,2-cyclohexane dicarboxylic acid and phthalic acid, respectively. Figure 7.4 shows the mass spectrum of the phthalic acid based polymer. The spectrum reveals the presence of a series of protonated and sodiated polyesteramide oligomers, although sodium salts were not added to the spray solution. Endgroup analysis with linear regression (see also chapter 4) shows that the most intense oligomers P_nD_{n+1} and P_nD_{n+2}, contain di-isopropanolamine endgroups. The n denotes the number of monomers in a given oligomer. Cyclic oligomers P_nD_n were also observed. The oligomer series P_nD_{n+2} are formed by the reaction of an oxazolonium ion, created in the polymerisation reaction,⁹⁵ with an amine. The polymerisation conditions were chosen such that the concentration of amine groups during the polymerisation was low⁹⁵ and the concentration of P_nD_{n+2}

in the final polymer was lower than the concentration of P_nD_{n+1} . The oligomer series observed in the mass spectra of the other hyperbranched polyesteramides are very similar to figure 7.4 (spectra not shown).

Series of oligomers $P_nD_{n+1}-H_2O$, $P_nD_{n+2}-H_2O$ and $P_nD_n-H_2O$ have been observed for all polymers. The ions may be molecular ions of oligomers formed in the polymerisation process or may be due to fragmentation in the mass spectrometer as a result of internal energy uptake in the ion source, ion transport section or ion trap. It is known from the literature, however, that the 1,2-cyclohexane dicarboxylic acid anhydride based polymer undergoes metastable fragmentation for MALDI generated ions.⁹⁵ Whether similar processes are possible during ESI is not known and is the aim of the research described in this chapter.

The most important fragmentation pathways of the hyperbranched polyesteramides and the energetics involved were studied by MS^n of the protonated oligomers containing three diacid anhydrides and four di-isopropanolamines (S_3D_4 , G_3D_4 , C_3D_4 and P_3D_4). The insight obtained from these experiments was used to determine whether the oligomers $P_3D_4-H_2O$, $S_3D_4-H_2O$, $G_3D_4-H_2O$ and $C_3D_4-H_2O$ have their origin in the polymerisation process or result from mass spectrometric fragmentation.

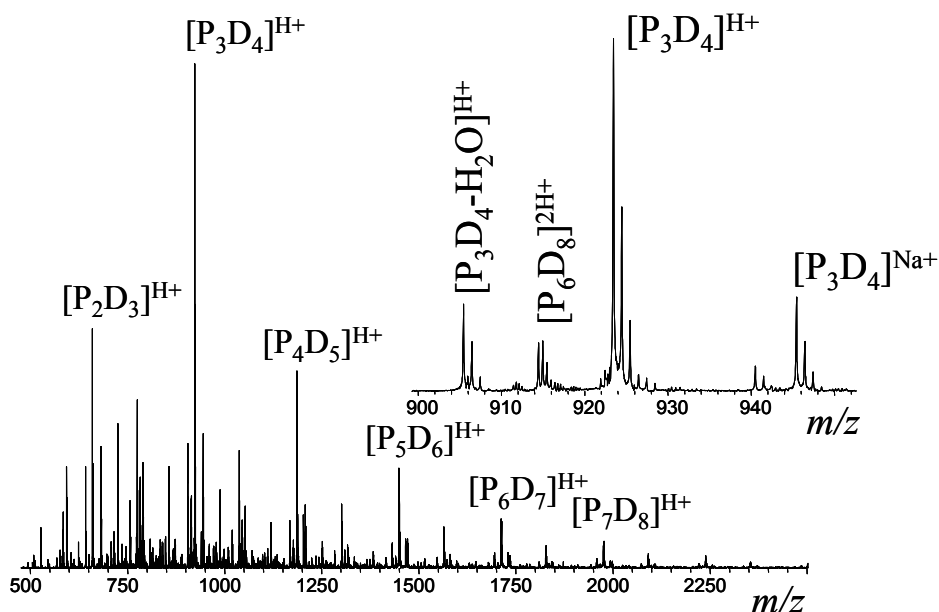
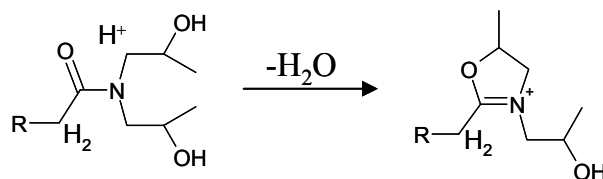


Figure 7.4 ESI FT-ICR MS mass spectrum of the phthalic acid based hyperbranched polyesteramide.

7.3.1. The glutaric acid anhydride based polymer

Only the loss of H₂O from [G₃D₄]^{H+} (*m/z* 821) is observed at a relatively low laboratory frame collision energy (*E*_{kin,lab}) of 32 eV (spectrum not shown). The notation [G₃D₄]^{H+} is used in stead of the more conventional [G₃D₄+H]⁺ notation because this allows to distinguish protonated ions from oxazolonium ions (see further). The proposed mechanism for H₂O loss is the intramolecular transfer of the proton to one of the OH endgroups, which results in the loss of H₂O and the formation of an oxazolonium ion as shown in scheme 7.1.²³³ Note that the positive charge of the parent ion is a proton. The positive charge becomes a quaternary ammonium ion stabilised by oxazolonium ion formation for the fragment ion. In figure 7.5 the MS/MS spectrum obtained at a higher collision energy (*E*_{kin,lab}= 209 eV) is shown. Ten fragments are observed. Ions resulting from the loss of two water molecules are of low abundance and cannot be explained by the formation of two oxazolonium ions, since the parent ion is charged by only one proton. Ions due to the loss of the second water molecule possibly originate from another OH endgroup on the parent ion leading to an allylic or 2,6-dimethyl morpholine endgroup.



Scheme 7.1 *Intramolecular transfer of the proton to one of the OH endgroups resulting in the loss of H₂O and the formation of an oxazolonium ion.*

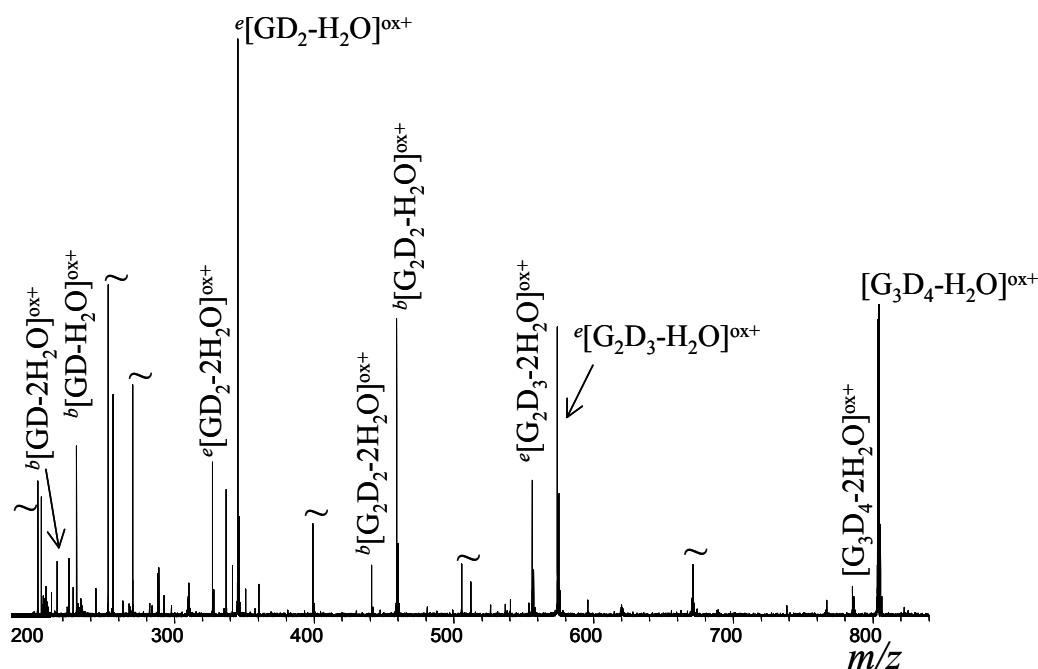
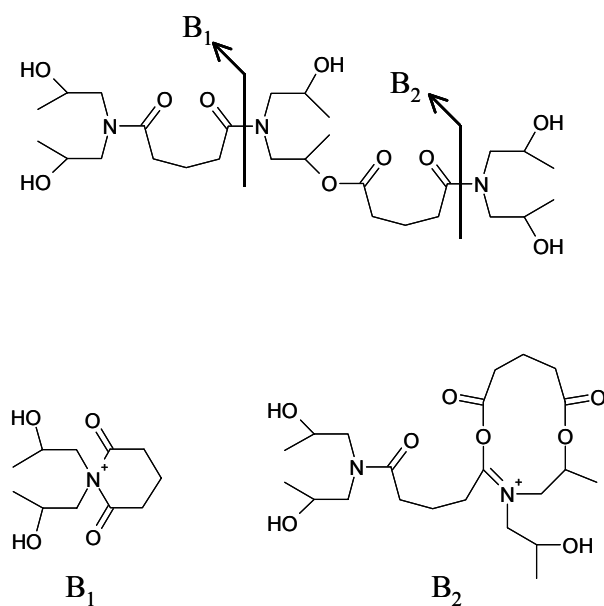


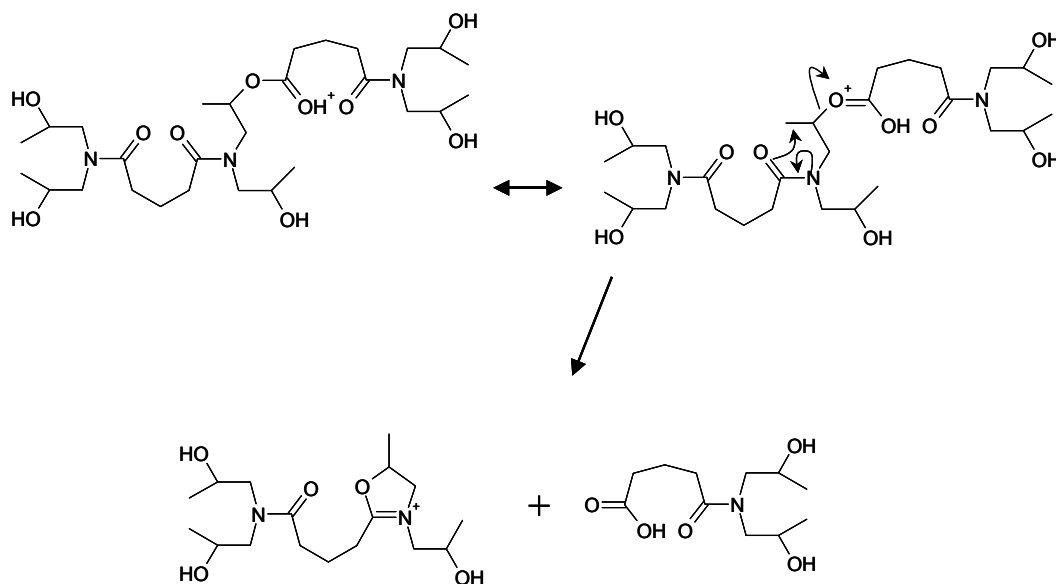
Figure 7.5 MS/MS spectrum of $[G_3D_4]^{H+}$ at relatively high collision energy $E_{kin,lab} = 209$ eV. The \sim symbols denote electronic noise.

Two mechanisms are proposed by Muscat and coworkers⁹⁵ that explain the unimolecular rearrangement of the amide and ester bonds. The rearrangement of the amide and ester bonds are shown for the glutaric acid based polyesteramide in schemes 7.2 and 7.3, respectively. Most fragments observed in figure 7.5 can be explained by these mechanisms. Stable oxazolonium ions, denoted by the addition of $^{ox+}$, are formed due to the rearrangement of the amide or the ester bond $^e[G_2D_3-H_2O]^{ox+}$, $^b[G_2D_2-2H_2O]^{ox+}$, $^e[GD_2-2H_2O]^{ox+}$ and $^b[GD-H_2O]^{ox+}$. Rearrangements of the amide and ester bonds are denoted by b and e superscripts, respectively. The b notation that indicates the rearrangement of the amide has its origin in the peptide literature where such b ions are very common. The nomenclature is also introduced for polyesteramides although the structure of these molecules is very different from peptides.⁹⁵ A series of fragments is observed that is due to oxazolonium ion formation followed by an additional H_2O loss. This results in the singly charged fragments $^e[G_2D_3-2H_2O]^{ox+}$, $^b[G_2D_2-2H_2O]^{ox+}$, $^e[GD_2-2H_2O]^{ox+}$ and $^b[GD-2H_2O]^{ox+}$. These fragments cannot be explained by the loss of a water molecule by oxazolonium ion formation and subsequent rearrangement according to one of the two mechanisms shown in schemes 7.2 and 7.3, because the charge state is one. It is therefore more probable that an ester or amide bond is rearranged to an oxazolonium ion followed by the loss of H_2O from one of the endgroups to an allylic endgroup.



Scheme 7.2 *Unimolecular rearrangement of the amide bond.*⁹⁵

Note that only one fragment is observed as oxazolonium ion during the rearrangements and the other one is always a neutral fragment. This is usually not observed for molecular ions of polyesters with only ester bonds nor for peptides containing only amide bonds, where the intensity in the MS/MS spectrum depends on the proton or cation affinity of the fragments.²³⁴⁻²³⁶



Scheme 7.3 *Unimolecular rearrangement of the ester bond.*⁹⁵

The MS/MS spectrum at $E_{\text{kin,lab}}=32$ eV is very different from the MS/MS spectrum at $E_{\text{kin,lab}}=209$ eV. Therefore the energy dependence of the dissociation of the parent ion is studied to gain insight in the relative strengths of the amide and ester bonds in the protonated polyesteramide oligomer. The collision energy dependence of the fragmentation process is studied by constructing the breakdown diagram for the parent ion and fragments as shown in figure 7.6a. The survival yield of the parent ion and the most intense fragments due to rearrangements of the ester and amide bonds, ${}^e[\text{G}_2\text{D}_3\text{-H}_2\text{O}]^{\text{ox}+}$, ${}^b[\text{G}_2\text{D}_2\text{-H}_2\text{O}]^{\text{ox}+}$, ${}^e[\text{GD}_2\text{-H}_2\text{O}]^{\text{ox}+}$, ${}^b[\text{GD-H}_2\text{O}]^{\text{ox}+}$ and ions due to the loss of H_2O are plotted as a function of the laboratory frame collision energy $E_{\text{kin,lab}}$. The survival yield of the parent ion is defined as the intensity of the parent ion divided by the sum of the intensities of the parent ion and all fragments. To obtain the survival yield of the fragments, the intensity of a particular fragment is divided by the sum of the parent ion and all fragment ions. Although only five fragment ions are shown in figure 7.6a, all fragments observed have been used in the calculation of the survival yield. The reproducibility of the survival yield of the parent ion was about 5%. Fragments with an m/z of lower than 107 are not detected, but could influence the breakdown diagram.

Figure 7.6a clearly demonstrates that the lowest energetic fragmentation pathway is the loss of H_2O , which has an appearance energy of $E_{\text{kin,lab}}\sim 32$ eV. The breakdown diagram shows that the fragments due to rearrangement of the amide and ester bonds do not appear at the same collision energies. The lines in the figure are used to guide the eyes. Rearrangements of the ester bonds, fragments ${}^e[\text{G}_2\text{D}_3\text{-H}_2\text{O}]^{\text{ox}+}$ and ${}^e[\text{GD}_2\text{-H}_2\text{O}]^{\text{ox}+}$, are observed at an appearance energy of $E_{\text{kin,lab}}\sim 80$ eV, while the amide bonds start rearranging at ~ 126 eV (fragments ${}^b[\text{G}_2\text{D}_2\text{-H}_2\text{O}]^{\text{ox}+}$ and ${}^b[\text{GD-H}_2\text{O}]^{\text{ox}+}$). The intensity ratio of the fragments in the spectra changes significantly with the collision energy. For example, at laboratory frame collision energy $E_{\text{kin,lab}}=209$ eV the intensity of fragment ${}^e[\text{G}_2\text{D}_3\text{-H}_2\text{O}]^{\text{ox}+}$ is approximately the same as the intensity of fragment ${}^e[\text{GD}_2\text{-H}_2\text{O}]^{\text{ox}+}$. At a higher collision energy $E_{\text{kin,lab}}=400$ eV the intensity of ${}^e[\text{GD}_2\text{-H}_2\text{O}]^{\text{ox}+}$ becomes 3 times higher than ${}^e[\text{G}_2\text{D}_3\text{-H}_2\text{O}]^{\text{ox}+}$.

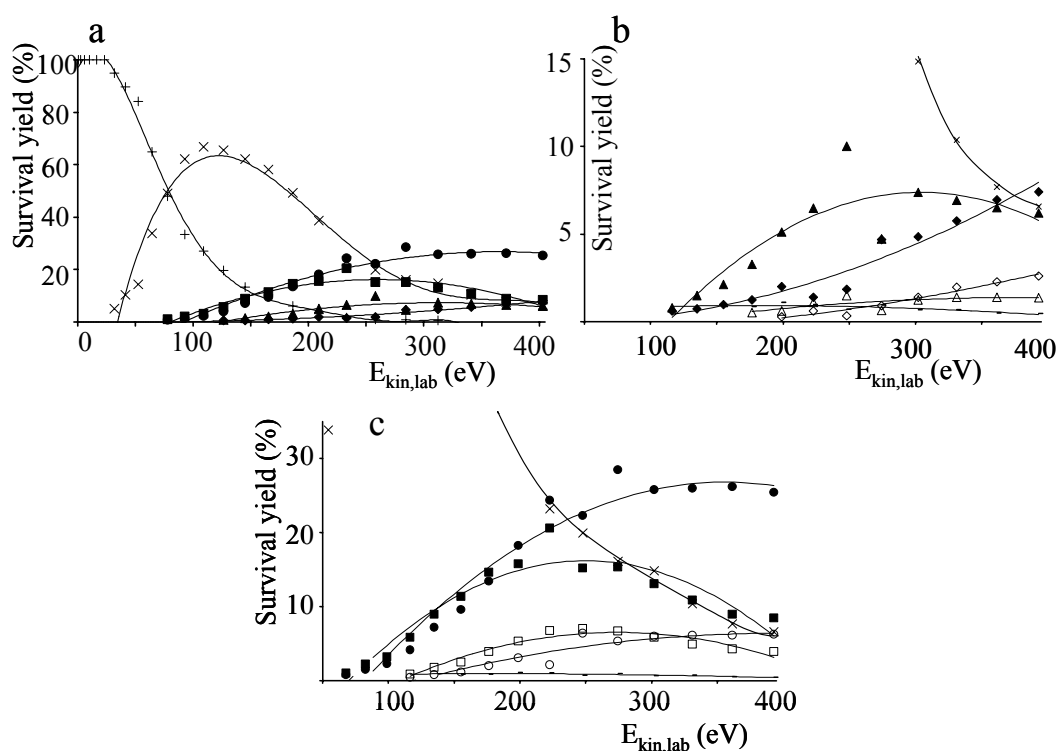


Figure 7.6 Breakdown diagrams of $[G_3D_4+H]^+$. For the most intense fragments $^e[G_2D_3-H_2O]^{ox+}$, $^b[G_2D_2-H_2O]^{ox+}$, $^e[GD_2-H_2O]^{ox+}$, $^b[GD-H_2O]^{ox+}$ and ions due to the loss of H_2O (a). Enlargements of breakdown diagram concerning amide bond rearrangements (b) and ester bonds (c). The fragments are denoted by \times $[G_3D_4-H_2O]^{ox+}$, $-$ $[G_3D_4-2H_2O]^{ox+}$, \blacksquare $^e[G_2D_3-H_2O]^{ox+}$, \square $^e[G_2D_3-2H_2O]^{ox+}$, \blacktriangle $^b[G_2D_2-H_2O]^{ox+}$, \triangle $^b[G_2D_2-2H_2O]^{ox+}$, \bullet $^e[GD_2-H_2O]^{ox+}$, \circ $^e[GD_2-2H_2O]^{ox+}$, \blacklozenge $^b[GD-H_2O]^{ox+}$ and \diamond $^b[GD-2H_2O]^{ox+}$ and parent ion $+ [G_3D_4]^{H+}$. The lines are used to guide the eyes.

In figure 7.6b the breakdown diagram for the same parent ion $[G_3D_4]^{H+}$ is presented. Only fragments due to the loss of two H_2O molecules and amide bond rearrangements are shown for reasons of clarity. Figure 7.6c shows the results obtained for the ester bond. Ions due to the loss of two H_2O molecules (fragment ion $[G_3D_4-2H_2O]^{ox+}$) from the parent ion appear at significantly higher collision energy ($E_{kin,lab} \approx 145$ eV) than ions due to the loss of the first H_2O $[G_3D_4-H_2O]^{ox+}$. At approximately the same collision energy where the second H_2O loss is observed, four fragments appear in the MS/MS spectra, which are due to rearrangements of the ester and amide bond with an additional loss of an H_2O . This results in singly charged fragment ions $^e[G_2D_3-2H_2O]^{ox+}$, $^b[G_2D_2-2H_2O]^{ox+}$, $^e[GD_2-2H_2O]^{ox+}$ and $^b[GD-2H_2O]^{ox+}$.

It is concluded from figures 7.4a-c that the three different fragmentation pathways observed can be distinguished by their appearance energies. The

formation of oxazolonium ions by the loss of H₂O has the lowest appearance energy followed by the formation of oxazolonium ions by amide and ester rearrangement. The loss of the second H₂O, most probably by formation of allylic or 2,6-dimethyl morpholine endgroups, has the highest appearance energy.

7.3.2. The succinic and 1,2-cyclohexane dicarboxylic acid anhydride based polymers

In the same way as the glutaric acid anhydride based polymer, the lowest energetic fragmentation pathway of the polyesteramides based on succinic acid anhydride is the loss of H₂O at $E_{\text{kin,lab}} \sim 25$ eV. The MS/MS spectra of [S₃D₄]^{H+} (not shown) contain fragments due to the same mechanisms as observed in figure 7.5 for [G₃D₄]^{H+}. The main difference between the breakdown diagrams of [S₃D₄]^{H+} and [G₃D₄]^{H+} is that the difference in appearance energy of the rearrangement of the ester ($E_{\text{kin,lab}} \sim 68$ eV) and amide ($E_{\text{kin,lab}} \sim 50$ eV) bonds is reversed for [S₃D₄]^{H+} with the exception of fragment ion ^b[SD-H₂O]^{ox+} with an $E_{\text{kin,lab}} \sim 180$ eV.

For the 1,2-cyclohexane dicarboxylic acid anhydride based polymer a loss of one D unit by amide rearrangement to ^b[C₃D₃-H₂O]^{ox+} is observed as the lowest energetic fragmentation pathway together with the loss of H₂O to form [C₃D₄-H₂O]^{ox+} at $E_{\text{kin,lab}} \sim 36$ eV. The appearance energies for the rearrangement of the ester and other amide bonds have approximately the same values as the collision energy of the ester bonds ($E_{\text{kin,lab}} \sim 56-110$ eV).

These results demonstrate that the appearance energy for the ester and amide rearrangement strongly depends on the structure of the diacid anhydride and that these energy resolved experiments can be used to study the structure of the diacid anhydride. However, as observed for the glutaric acid anhydride based polymer, the appearance energies for the three main fragmentation pathways are of the following order: H₂O loss < ester and amide rearrangement < 2nd H₂O loss.

7.3.3. The phthalic acid anhydride based polymer

The MS/MS spectrum of [P₃D₄]^{H+} with m/z 923 in figure 7.7 shows two remarkable features. The first feature is an intense peak due to the loss of one diisopropanolamine resulting from an amide rearrangement, which forms ^b[P₃D₃-H₂O]^{ox+}. This fragment was not observed for the polymers based on succinic acid anhydride and glutaric acid anhydride, although these are connected by amide or ester bonds too. The fragment was low in intensity in the case of the

polymer based on 1,2-cyclohexane dicarboxylic acid anhydride. A second feature is an intense peak at m/z 660, which cannot be explained by a rearrangement of the amide or ester bond. The mass difference between this fragment and fragment $^c[\text{P}_2\text{D}_3\text{-H}_2\text{O}]^{\text{ox}+}$ corresponds with the mass H_2O indicating that the parent ion $[\text{P}_3\text{D}_4]^{\text{H}+}$ has lost one PD monomer to $[\text{P}_2\text{D}_3]^{\text{H}+}$. Such depolymerising fragmentations were observed earlier for the copolyester poly(di-propoxylated bisphenol-A/isophthalic acid/adipic acid) for which a γ -hydrogen rearrangement was proposed as described in chapter 6. Such a γ -hydrogen rearrangement can be used to explain the formation of $[\text{P}_2\text{D}_3]^{\text{H}+}$ also. This rearrangement must however lead to a protonated species $^{\gamma}[\text{P}_2\text{D}_3]^{\text{H}+}$ because the formation of an oxazolonium ion with composition P_2D_3 is structurally prohibited. The appearance of the fragments in the MS/MS spectra upon γ -hydrogen rearrangement depends on the proton affinity of the fragments. The protonated $^{\gamma}[\text{PD-H}_2\text{O}]^{\text{H}+}$, the counterpart of $^{\gamma}[\text{P}_2\text{D}_3]^{\text{H}+}$, has the same m/z value as $^b[\text{PD-H}_2\text{O}]^{\text{ox}+}$ because they are isomers. The γ -hydrogen and amide rearrangements can therefore not be distinguished with these fragment ions.

The rearrangement of the amide and ester bonds appears at approximately the same collision energy of $E_{\text{kin,lab}} = 70$ eV. The ions resulting from the loss of two H_2O molecules and the fragments due to rearrangement of the amide and ester bonds with an additional loss of H_2O appear, as observed for the other polymers, at a higher collision energy of 112-207 eV. The fragment $^{\gamma}[\text{P}_2\text{D}_3]^{\text{H}+}$ appears at the same collision energy as the fragments due to ester and amide bond rearrangement indicating that γ -hydrogen and ester/amide rearrangements of $[\text{P}_3\text{D}_4]^{\text{H}+}$ have similar appearance energies.

The 50% survival yields, indicative for the mean of the internal energy distribution, of the parent ions $[\text{G}_3\text{D}_4]^{\text{H}+}$, $[\text{S}_3\text{D}_4]^{\text{H}+}$, $[\text{C}_3\text{D}_4]^{\text{H}+}$ and $[\text{P}_3\text{D}_4]^{\text{H}+}$ were compared. For all parent ions a 50% survival yield is observed at approximately 95 eV laboratory frame collision energy. This is because all polymers show similar fragmentation behaviour due to the amide and ester bonds that are rearranged by the same mechanisms leading to similar fragments (oxazolonium ions).

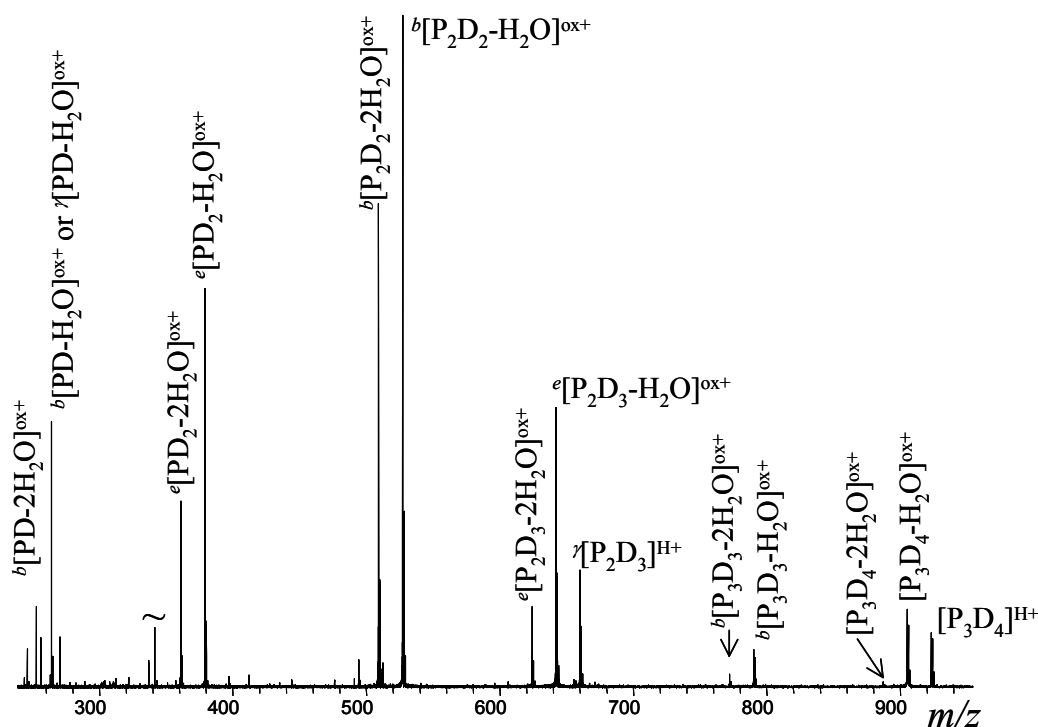


Figure 7.7 MS/MS spectrum of $[P_3D_4]^{H+}$ m/z 923 at $E_{kin,lab} = 150$ eV

7.3.4. Origin of the oligomers $P_3D_4-H_2O$, $S_3D_4-H_2O$, $G_3D_4-H_2O$ and $C_3D_4-H_2O$

The observations described in the previous paragraphs show that the lowest energetic fragmentation pathway observed for the hyperbranched polymers is the loss of H_2O . Nozzle skimmer activation in the ESI source will most likely lead to a loss of H_2O , or alternatively an amide or ester rearrangement to oxazolonium ions. Two MS^n experiments are performed in order to determine whether the oligomeric ions $P_3D_4-H_2O$, $S_3D_4-H_2O$, $G_3D_4-H_2O$ and $C_3D_4-H_2O$ observed in the mass spectra (see figure 7.4 for the phthalic acid anhydride based polymer) are formed during the polymerisation process or are the result of in-source fragmentation processes. The first experiment is an MS^3 experiment where MS^2 of protonated $[P_3D_4]^{H+}$ is followed by MS^3 of the isolated oxazolonium fragment $[P_3D_4-H_2O]^{ox+}$. The MS^3 of fragment $[P_3D_4-H_2O]^{ox+}$ is expected to show a different fragmentation behaviour than observed for protonated species because the oxazolonium ion is not protonated. The second experiment is MS^2 of the oligomer $P_3D_4-H_2O$. If the oligomer is formed during the polymerisation process it will appear as a protonated species in the mass spectrum, $[P_3D_4-H_2O]^{H+}$. When the oligomeric ion is the result of in-source fragmentation, the ion is already a fragment ion and will appear in the mass spectrum as the oxazolonium ion

$[\text{P}_3\text{D}_4\text{-H}_2\text{O}]^{\text{ox}+}$ with the same elemental composition as $[\text{P}_3\text{D}_4\text{-H}_2\text{O}]^{\text{H}+}$. The origin of the $\text{P}_3\text{D}_4\text{-H}_2\text{O}$ oligomer can be determined by comparison of the MS³ spectrum of the oxazolonium ion $[\text{P}_3\text{D}_4\text{-H}_2\text{O}]^{\text{ox}+}$ obtained from the MS² spectrum of $[\text{P}_3\text{D}_4]^{\text{H}+}$ with the MS² spectrum of $[\text{P}_3\text{D}_4\text{-H}_2\text{O}]^{\text{H}+}$ or $[\text{P}_3\text{D}_4\text{-H}_2\text{O}]^{\text{ox}+}$. The same set of experiments was also performed with parent ions S_3D_4 , G_3D_4 and C_3D_4 .

Figure 7.8 shows the MS³ spectrum of the $[\text{P}_3\text{D}_4\text{-H}_2\text{O}]^{\text{ox}+}$ fragment ion obtained by MS² of $[\text{P}_3\text{D}_4]^{\text{H}+}$ (figure 7.7). The MS³ spectrum contains fragment ions, which can all be explained by γ -hydrogen rearrangements. Note that rearrangements of the amide and ester bonds to oxazolonium ions are not possible, because free protons are not available. Most interesting about figure 7.8 is the absence of a fragment due to the loss of a H_2O molecule, which would have resulted in a fragment $[\text{P}_3\text{D}_4\text{-2H}_2\text{O}]^{\text{ox}+}$. The loss of H_2O has been observed for all protonated parent ions in the previous section.

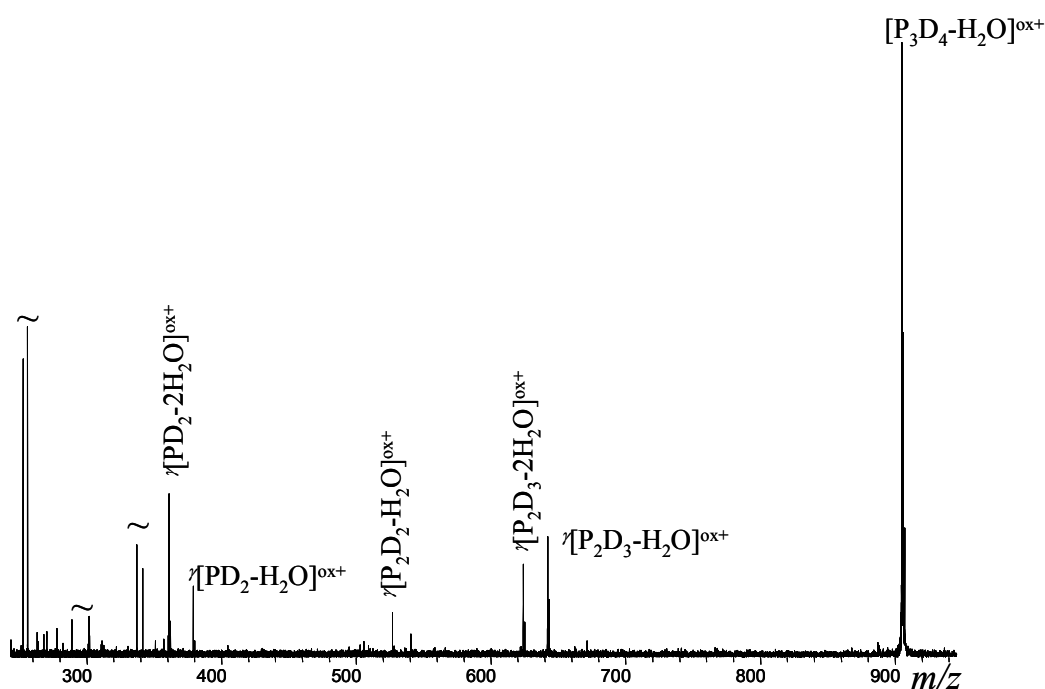


Figure 7.8 MS³ spectrum of the oxazolonium ion $[\text{P}_3\text{D}_4\text{-H}_2\text{O}]^{\text{ox}+}$ obtained from MS² from $[\text{P}_3\text{D}_4]^{\text{H}+}$ (figure 7.7). $E_{\text{kin,lab}}(\text{MS}^2) = 129 \text{ eV}$, $E_{\text{kin,lab}}(\text{MS}^3) = 129 \text{ eV}$.

Figure 7.9 shows the MS² spectrum of $[\text{P}_3\text{D}_4\text{-H}_2\text{O}]^{\text{H}+}$ or $[\text{P}_3\text{D}_4\text{-H}_2\text{O}]^{\text{ox}+}$. Two important differences with figure 7.8 are observed. First, an intense loss of H_2O is observed resulting in fragment $[\text{P}_3\text{D}_4\text{-2H}_2\text{O}]^{\text{ox}+}$, which is not observed in figure 7.8. This indicates that the parent ion must be protonated. Furthermore a fragment $[\text{P}_2\text{D}_3]^{\text{H}+}$ is observed in figure 7.9 but not in the MS³ spectrum of $[\text{P}_3\text{D}_4\text{-H}_2\text{O}]^{\text{ox}+}$. Only a γ -hydrogen rearrangement of the ester bond of a protonated

parent ion $[P_3D_4-H_2O]^{H^+}$ can explain the formation of this fragment. This is because the positive charge is fixed on the oxazolonium ion which must result in fragment $[P_2D_3-H_2O]^{ox+}$. For the protonated species a rearrangement of the ester bond leads to fragment $^{\gamma}[P_2D_3]^{H^+}$. With the exception of γ -hydrogen rearrangements, the same fragmentation behaviour has been observed for $S_3D_4-H_2O$, $G_3D_4-H_2O$ and $C_3D_4-H_2O$.

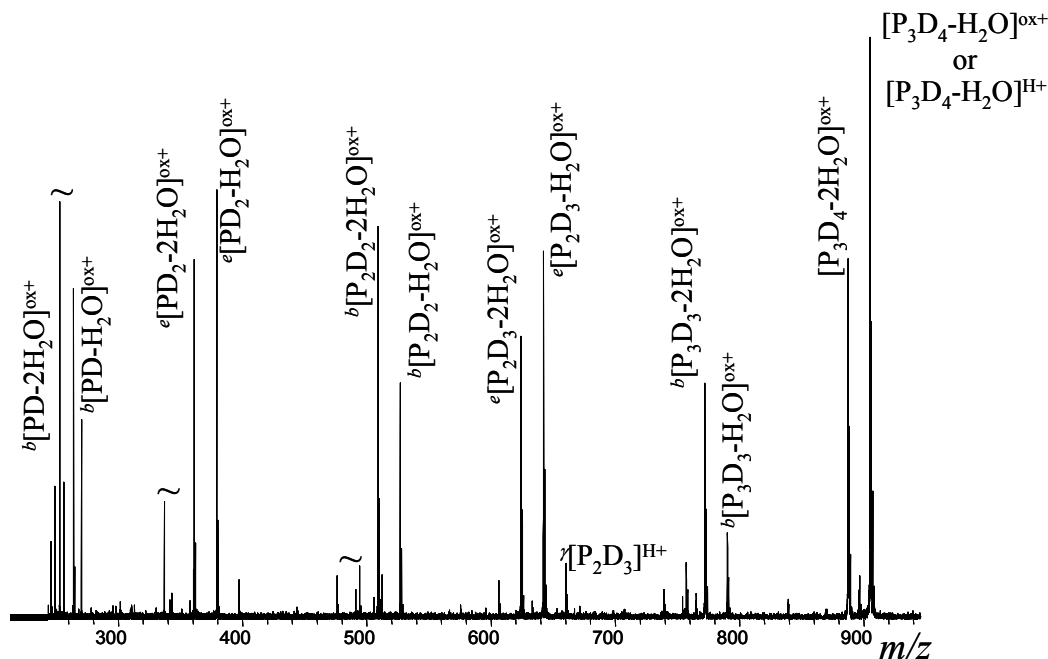


Figure 7.9 MS^2 of $[P_3D_4-H_2O]^{ox+}$ or $[P_3D_4-H_2O]^{H^+}$ at $E_{kin,lab} = 129$ eV.

The observations described above show that some of the fragments observed for MS^2 of $[P_3D_4-H_2O]^{H^+}$ can not be formed by MS^2 of $[P_3D_4-H_2O]^{ox+}$, which demonstrates that the oligomeric ions $P_3D_4-H_2O$, $S_3D_4-H_2O$, $G_3D_4-H_2O$ and $C_3D_4-H_2O$ observed in the mass spectra are protonated parent ions and must therefore originate from the polymerisation process. These findings have been confirmed with NMR and titration experiments that have revealed a very low concentration of allylic endgroups in the MWD, which are assumed to be due to elimination processes for which ester bonds are rearranged.²³⁷ The insert of figure 7.4 shows that oligomer $[P_3D_4-H_2O]^{H^+}$ is present in a high intensity, approximately 20% of $[P_3D_4]^{H^+}$. It is however not possible to quantify the contribution of the oligomers $P_3D_4-H_2O$, $S_3D_4-H_2O$, $G_3D_4-H_2O$ and $C_3D_4-H_2O$ in the molecular weight distributions with ESI FT-ICR MS. A part of the oligomers $P_3D_4-H_2O$, $S_3D_4-H_2O$, $G_3D_4-H_2O$ and $C_3D_4-H_2O$ can still originate from in-source fragmentation. Quantification of the polymer related species is difficult for two reasons. (1) Differences in ionisation efficiency between $P_nD_{n+1}-H_2O$ and P_nD_{n+1} ions can exist

but have not been quantified. Significant differences in ionisation efficiency have for example been observed for mixtures of the homopolyesters poly(di-propoxylated bisphenol-A/adipic acid) and poly(di-propoxylated bisphenol-A/isophthalic acid) (see chapter 5). (2) The fact that fragments of $[P_3D_4-H_2O]^{H+}$ can be distinguished from the fragments of $[P_3D_4-H_2O]^{ox+}$ but not the other way around further complicates quantification. It is therefore possible to demonstrate the presence of protonated species i.e. the species are formed in the polymerisation reaction but it is not possible to quantify them.

7.4. Conclusions

The fragmentation behaviour of hyperbranched polyesteramides made by the polycondensation of the trifunctional di-isopropanolamine (D) with the difunctional anhydrides of succinic acid (S), glutaric acid (G), 1,2-cyclohexane dicarboxylic acid (C) and phthalic acid (P) was studied by ESI FT-ICR MS. The breakdown diagrams of parent ions $[G_3D_4]^{H+}$, $[S_3D_4]^{H+}$, $[C_3D_4]^{H+}$ and $[P_3D_4]^{H+}$ were constructed using energy resolved on-resonance collisionally activated dissociation in the FT-ICR MS. Three main fragmentation pathways were observed that could be distinguished by the appearance energy. The lowest energetic fragmentation pathway is the loss of H₂O leading to oxazolonium ions. The rearrangements of the ester and amide bonds, also leading to oxazolonium ions, were observed at a higher collision energy. The loss of a second H₂O was observed at highest collision energies and most probably results in fragments with allylic or 2,6-dimethyl morpholine endgroups.

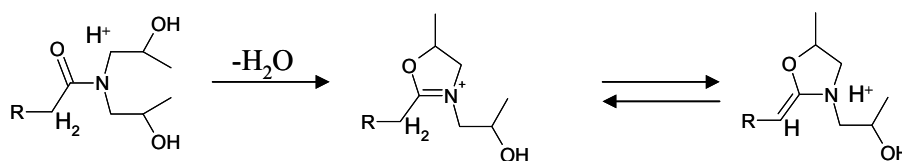
The origin of an oligomeric ions P₃D₄-H₂O, S₃D₄-H₂O, G₃D₄-H₂O and C₃D₄-H₂O observed in the mass spectra was determined with MSⁿ experiments. By comparing MS³ experiments of $[P_3D_4-H_2O]^{ox+}$ generated by the MS² of $[P_3D_4]^{H+}$ with MS² experiments of P₃D₄-H₂O, it was concluded that P₃D₄-H₂O is present in the polymer sample. An intense loss of H₂O was observed from MS² of $[P_3D_4-H_2O]^{H+}$ but not from MS³ of the oxazolonium ion $[P_3D_4-H_2O]^{ox+}$ obtained from the MS² of $[P_3D_4]^{H+}$. This demonstrates that P₃D₄-H₂O is formed during the polymerisation reaction. This phenomenon was observed for all four hyperbranched polyesteramides. The oligomeric ions P₃D₄-H₂O, S₃D₄-H₂O, G₃D₄-H₂O and C₃D₄-H₂O are probably due to the formation of allylic endgroups. This partly terminates the polymerisation reaction, which influences the composition of the molecular weight distribution. These findings have been confirmed with NMR and titration experiments.

Addendum

The work presented in this chapter has been published in the International Journal of Mass Spectrometry.²⁷⁸ Scheme 7.1 has however been subject of discussion after the publication.²³⁸ The oxazolonium ion, which is an immonium ion, can have a protonated isomer as shown in scheme 7.4.^{239,240} The discussion in section 7.3.4 would not be valid if this ion were formed under the conditions of our experiments.

The fact that an MS³ experiment of [C₃D₄-H₂O]^{ox+} fragment ion obtained from MS² of [C₃D₄]^{H+} does not lead to the loss of a water molecule, makes it unlikely that the protonated ion is formed. If [C₃D₄-H₂O]^{ox+} were a protonated cyclic amine as shown in scheme 7.4, an additional loss of H₂O should be observed because a proton is required to expel a water molecule. This observation has been confirmed by the MS² of multiply protonated ions where the maximum number of water losses depends on the number of protons. Additionally, the loss of a water molecule was not observed for the MS² of sodiated ions. The same results were obtained with the succinic and glutaric acid containing polymers. Note that the protonated cyclic amine cannot be formed for the phthalic acid containing polymer because a hydrogen for an intramolecular hydrogen shift is not available. These observations indicate that protonated cyclic amines are not formed under the conditions of the FT-ICR MS experiments described in this chapter.

There is however a possibility that the protonated species are formed after low energy CAD, but are not observed in the experiment. This is because such protonated amines have a relatively high proton affinity as will be discussed in chapter 8. The proton has a relatively strong interaction with the amine that does not lead to a loss of a water molecule upon CAD.



Scheme 7.4 Loss of H₂O to the oxazolonium ion and the protonated isomer of the oxazolonium ion.

Chapter 8

Isomer separation of hyperbranched polyester-amides with gas phase H/D exchange and a novel MSⁿ approach: DoDIP

Two approaches are introduced that provide information about the isomeric composition of hyperbranched polyesteramides. The first approach is based on a novel MSⁿ approach that allows studying different types of isomeric structures by a separation based on their difference in appearance energy. The method is called DoDIP: Dissociation of Depleted Ion Populations. A first MS/MS step is used to fragment isomers with relatively low appearance energy. The isomers with higher appearance energy are fragmented in a second MS/MS step. The second approach is based on gas phase H/D exchange experiments that result in a bimodal isotopic distribution for oligomers X_nD_{n+1} of which one distribution corresponds to a type of isomeric structure that exhibit H/D exchange behaviour and the other one to an isomeric structure that does not exhibit H/D exchange behaviour. X is a difunctional anhydride of phthalic acid, 1,2-cyclohexane dicarboxylic acid, succinic acid, or glutaric acid, D is a trifunctional diisopropanolamine and n the degree of polymerisation. The type of isomeric structure that does not exhibit H/D exchange behaviour has a non-alternating monomer sequence that contains an amine bond with a relatively high proton affinity. The other isomeric structure that does exhibit H/D exchange behaviour has an alternating monomer sequence containing only amide and ester bonds with relatively low proton affinity. Oligomer structures were confirmed with additional MS² experiments after H/D exchange. H/D exchange experiments on the fragments obtained after MS² of the parent ion disprove two postulated mechanisms (mechanisms 7.2 and 7.3) for the cleavage of the ester and amide bond.⁹⁵ A new mechanism is introduced to explain the H/D exchange behaviour of the fragments that requires a cleavage of the amide bonds only. Two types of fragments are formed by this mechanism. One type is protonated due to the cleavage of the amide bond whereas the other type has an oxazolonium ion structure due to the loss of an additional H₂O.

8.1. Introduction

Ion-molecule reactions have long been used to obtain detailed structural information of organic compounds. The first studies involved small molecules like amino acids.²⁴¹⁻²⁴⁴ Studies of large molecules have become popular in the last decade after the soft ionisation techniques electrospray ionisation (ESI) and matrix-assisted laser desorption/ionisation (MALDI) were introduced. These ionisation techniques allow the transfer of large molecules *intact* into the gas phase to study their chemical structure. Most ion-molecule reactions reported on large molecules concern biomolecules.²⁴⁵⁻²⁵⁵ Isomer identification poses a special problem for mass spectrometry as isomers have the same m/z value. Isomeric structures of small molecules, for example xylenes, can be distinguished with hydrogen/deuterium (H/D) exchange experiments due to a difference in the number of exchangeable hydrogens and exchange rate.^{256,257} For larger molecules, mainly biomolecules, different rates of deuterium incorporation have also been observed. This is however not a result of differences in isomeric structures but caused by differences in the gas phase conformation of the biomolecules.^{246,248,250,253} Different conformations have a different proton accessibility along the chain responsible for the H/D exchange. Other important factors in the reaction kinetics of deuterium incorporation during the H/D exchange events are the proximity of functional groups, differences in the proton affinity between analyte and reagent gas and temperature.²⁵⁷

Beauchamp and coworkers proposed the relay mechanism for the H/D exchange activity of biomolecules.^{247,252} This mechanism requires a proton transfer from the site of protonation in the hydrogen bonded complex to gas phase D_2O . At the same time, a deuteron is transferred from D_2O to a distant, slightly less basic site on the molecule. A nice feature of this mechanism is that only protonated ions exhibit H/D exchange activity. This phenomenon provides a tool to study fragmentation mechanisms that may lead to non-protonated ions.

The hyperbranched polymers studied in this chapter are made by the polycondensation of a trifunctional (D) and a difunctional (X) monomer (see chapter 7). Alternating oligomer sequences with amide and ester bonds only are ideally formed during the polymerisation reaction leading to mainly oligomer series X_nD_{n+1} because D was added in excess to the polymerisation. Such oligomers contain OH endgroups. Oligomer series X_nD_{n+1} can also consist of a non-alternating sequence, although this is less likely, when two D monomers are connected by an amine. Such oligomers contain at least one carboxylic acid endgroup, which might influence the cross-linking properties of these polymers when applied as cross-linkers in powder coatings. It is therefore important to determine which type of oligomer is present. Note that when doing a single mass

spectrometric analysis of such polymers the alternating and non-alternating monomer sequences cannot be distinguished because they are isomeric structures. We describe here two approaches that allow the distinction between isomeric structures of hyperbranched polyesteramides. The first approach is a novel MSⁿ methodology using a two-step collisionally activated dissociation (CAD) process called Dissociation of Depleted Ion Populations (DoDIP). The second approach is based on gas phase H/D exchange. CAD is a widely used technique to obtain structural information of biomolecules and synthetic polymers.^{91,115-118,258-260} To the knowledge of the authors, dissociation techniques have never been used to determine whether the oligomers in synthetic polymers consist of mixture of different isomers.

8.2. Experimental

The analyses were performed with a modified FT-ICR MS (Bruker-Spectrospin APEX 7.0e, Fällanden, Switzerland). The cell was an in house constructed open cell. Pulsed gas trapping with Argon at $P_{Ar}=5.2 \cdot 10^{-6}$ mbar for 2 seconds was used to enhance trapping of the ions in the open cell. On-resonance excitation collisionally activated dissociation in the ICR cell was used to activate the parent ions generated by electrospray ionisation. Argon was used as collision gas ($P_{Ar}=5.2 \cdot 10^{-6}$ mbar). The geometry factor α of the open cell necessary for the calculation of the excitation potentials on the excitation electrodes was 2.26. The peak-to-peak voltage of the RF excitation signal was 17.6 V in all CAD experiments. For the energy resolved experiments, three scans were summed at each collision energy. H/D exchange experiments were performed by pulsing D₂O in the ICR cell using a pulsed needle valve. See chapter 2 for a more detailed description of the experimental set-up.

The hyperbranched polyesteramides used for this study are polycondensation products of the trifunctional di-isopropanolamine (D) and a difunctional dicarboxylic acid anhydride provided by DSM (Geleen, the Netherlands).²³¹ The difunctional dicarboxylic acid anhydrides used in the polymerisations are succinic acid anhydride (S), glutaric acid anhydride (G), phthalic acid anhydride (P) and 1,2-cyclohexane dicarboxylic acid anhydride (C). Figure 7.1 shows the structures of the monomers.

8.3. Results and discussion

The mass spectrum of the phthalic acid anhydride based polymer with an average molecular weight of 1000 Da is presented in figure 8.1. The spectrum reveals the presence of a series of protonated and sodiated oligomers that were observed earlier in FD, MALDI and ESI studies of these polymers.^{95,145} The most intense oligomer series, P_nD_{n+1} , contains di-isopropanolamine (D) endgroups and are all expected to have an alternating structure.⁹⁵ The n denotes the number of monomers in a given oligomer. Cyclic alternating oligomers P_nD_n were also observed. The desired oligomer series P_nD_{n+1} is formed by the reaction of an oxazolonium functionality with an OH endgroup (pathway A in figure 7.3). Oligomer series P_nD_{n+2} and P_nD_{n+3} are formed by the reaction of the oxazolonium ion with an amine that is also present in the polymerisation mixture (pathway B in figure 7.3).^{231,232} The polymerisation conditions were chosen such that the concentration of amine groups during the polymerisation is low and the relative amount of P_nD_{n+2} and P_nD_{n+3} in the final polymer is lower than P_nD_{n+1} .^{231,232}

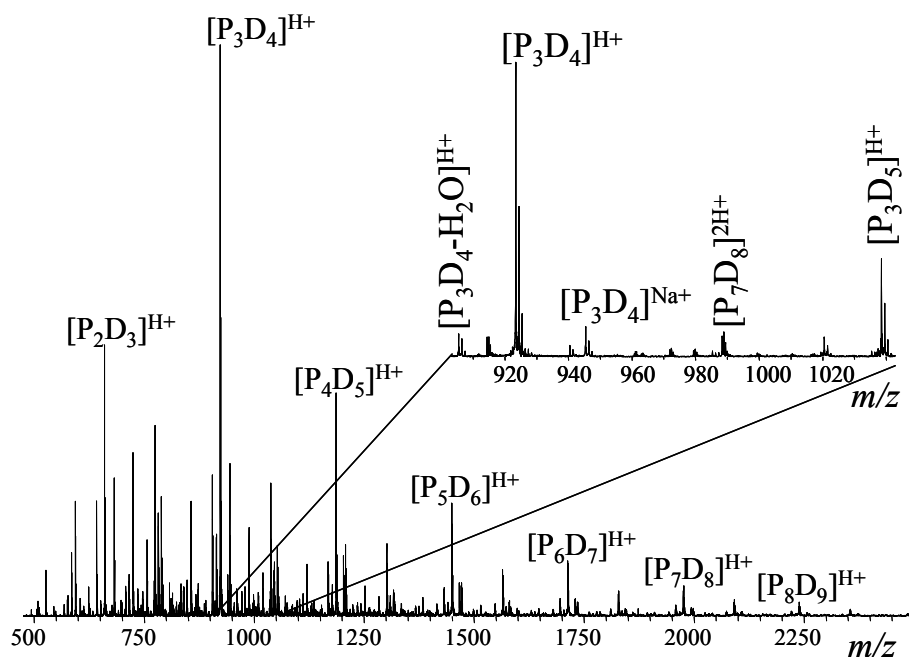


Figure 8.1 ESI FT-ICR MS spectrum of hyperbranched polyesteramides based on phthalic acid anhydride and di-isopropanolamine with an average molecular weight of 1000 Da.

The fragmentation behaviour of the hyperbranched polyesteramides synthesised with the anhydrides of 1,2-cyclohexane dicarboxylic acid, phthalic acid, succinic acid and glutaric acid has been discussed in chapter 7.⁹⁵ However,

these MS² and MS³ studies did not lead to an understanding of the isomeric composition of the hyperbranched polymers. Oligomer [P₃D₄+H]⁺ with $m/z = 923.46$ can have, for example, several isomeric structures, of which four examples are shown in figure 8.2. The P₃D₄ oligomer can have an alternating branched structure (I) although alternating linear structures (II and III) are possible as well. Note that the difference between structures II and III is the inverted orientation of one of the di-isopropanolamine groups. Structure III is symmetrical whereas structure II is not. Although the structures are very different, they all contain OH endgroup functionalities only. In principle, P₃D₄ can also have an isomer with a non-alternating structure due to pathway B in figure 7.3 (structure IV). This has so far not been considered in the literature.^{95,134,145,231-233} Structure IV contains an amine functionality which is not present in the alternating structures. More important, structure IV contains one COOH endgroup functionality. It is important from a polymer chemistry point of view to know whether oligomer series with these functionalities is formed in the polymerisation process.

8.3.1. *Dissociation of Depleted Ion Populations (DoDIP) for isomer analysis*

The MS/MS spectrum of [P₃D₄+H]⁺ resulting from on-resonance CAD with Argon and a laboratory frame kinetic energy $E_{\text{kin,lab}} = 129$ eV is presented in figure 8.3a. Many fragments are formed but it is not possible to retrieve the presence of different isomeric structures of P₃D₄, because the MS/MS behaviour of the pure isomers is not known. Fractionation prior to MS analysis has not been performed but could be an alternative way to obtain the MS/MS spectra of the pure isomers. Fractionation would however be very difficult due to the high number of possible linear, branched, alternating and non-alternating isomers. Reactions leading to the fragments in figure 8.3a will be discussed briefly based on the fragmentation pathways described in chapter 7,⁹⁵ although results that will be described later demonstrate that the mechanisms for the cleavage of the ester and amide bonds (mechanisms 7.2 and 7.3) are not correct. For reasons of clarity, we will first use the ‘old’ notation for the fragments as introduced in chapter 7 and demonstrate later that exclusively amide bonds are rearranged for which we will propose another mechanism.

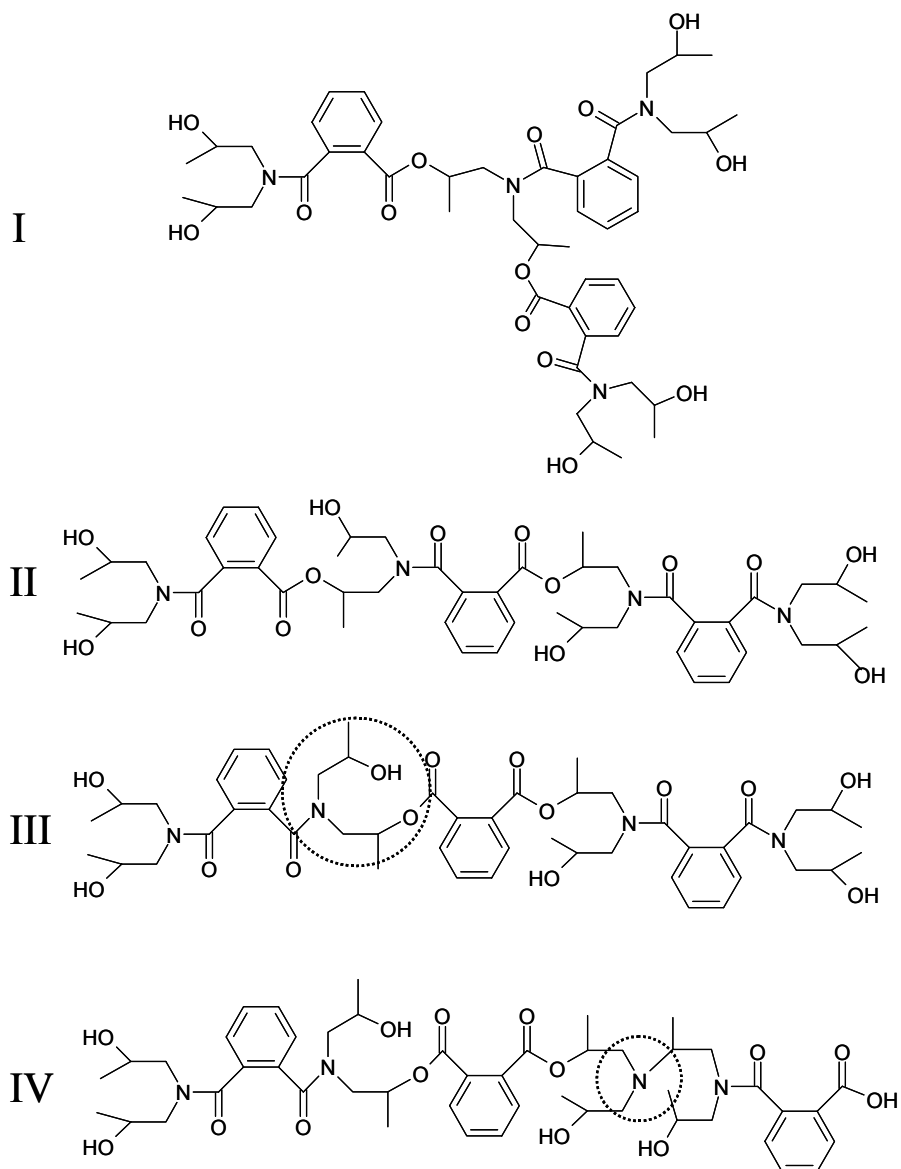


Figure 8.2 Four possible isomeric structures of oligomer P_3D_4 . The first three structures are alternating oligomers whereas the fourth is non-alternating (two di-isopropanolamines connected by an amine bond, see circle).

Fragment $[P_3D_4-H_2O]^{ox+}$ has been proposed to be due to the loss of H_2O from one of the OH endgroups (mechanism 7.1) forming oxazolonium ions denoted by the superscript $^{ox+}$. Ester and amide bond cleavages also lead to oxazolonium ions $^e[PD_2-H_2O]^{ox+}$, $^e[P_2D_3-H_2O]^{ox+}$, $^b[PD-H_2O]^{ox+}$, $^b[P_2D_2-H_2O]^{ox+}$ and $^b[P_3D_3-H_2O]^{ox+}$, in which the superscripts e and b correspond to an ester and amide cleavage, respectively. An additional H_2O loss is observed leading to $^e[PD_2-2H_2O]^{ox+}$, $^e[P_2D_3-2H_2O]^{ox+}$, $^b[PD-2H_2O]^{ox+}$, $^b[P_2D_2-2H_2O]^{ox+}$ and

$^b[P_3D_3-2H_2O]^{ox+}$. These fragments have been explained by an ester or amide bond rearrangement followed by the loss of H_2O . Finally, fragment $^{\gamma}[P_3D_4+H]^+$, due to a γ -Hydrogen rearrangement, is observed.

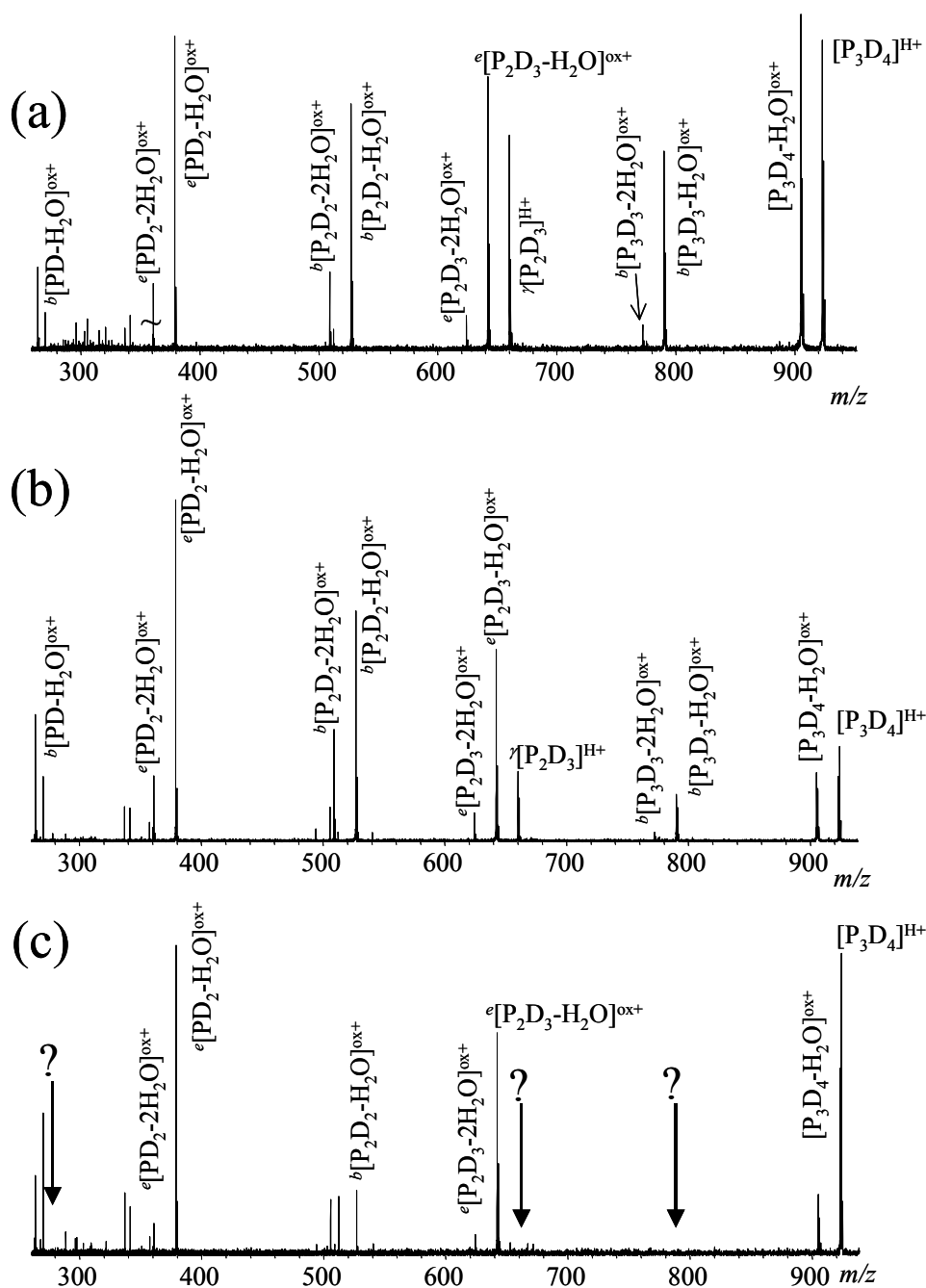


Figure 8.3 MS^2 spectrum of $[P_3D_4+H]^+$ with $E_{kin,lab} = 129$ eV (a) DoDIP mass spectrum of $[P_3D_4+H]^+$ with $E_{kin,lab} = 70$ eV ($\sim 75\%$ survival yield) for MS^2 followed by $E_{kin,lab} = 129$ eV for the second MS/MS step (b) DoDIP mass spectrum of $[P_3D_4+H]^+$ with $E_{kin,lab} = 129$ eV ($\sim 30\%$ survival yield) for MS^2 followed by 129 eV collision energy for the second MS/MS step (c).

The survival yield of the ions is plotted in the breakdown diagram as a function of the collision energy. The survival yield of the parent ion is defined as the intensity of the parent ion divided by the sum of the intensities of the parent ion and all fragments. To obtain the survival yield of the fragments, the intensity of a particular fragment is divided by the sum of the intensity of the parent ion and all fragment ions. Several fragmentation pathways are distinguished from the breakdown diagram of $[P_3D_4+H]^+$ (figure 8.4). A loss of H_2O had the lowest appearance energy followed by the rearrangement of the ester and amide bonds as discussed in chapter 7. Rearrangement of the ester and amide bond with an additional loss of H_2O to allylic or morpholine endgroups had the highest appearance energy. For reasons of clarity, only 4 of the 13 fragments that were observed and the parent ion are plotted in figure 8.4. All fragments have been included in the calculation of the breakdown diagram, however.

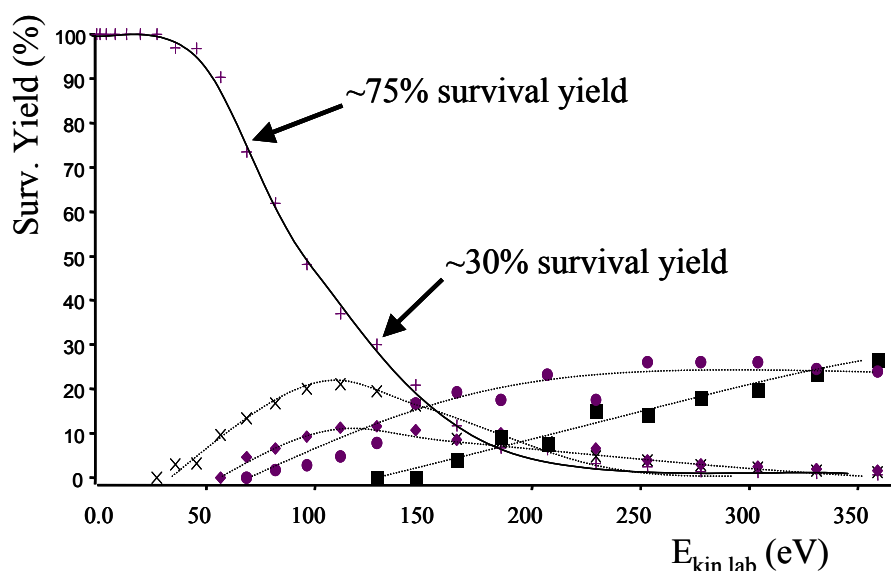


Figure 8.4 Breakdown diagram of $[P_3D_4+H]^+$. Only four fragments are shown in the figure with $\times [P_3D_4-H_2O]^{ox+}$, $\blacklozenge [P_2D_3]^{ox+}$, $\bullet [PD_2-H_2O]^{ox+}$, $\blacksquare [PD]^{ox+}$ and parent ion + $[P_3D_4]^{H+}$.

The breakdown diagram of $[P_3D_4+H]^+$ shows that the intensity of the different fragments changes with the collision energy (figure 8.4) resulting in a different composition of the MS/MS spectra with the collision energy. This effect can be explained by different appearance energies for the different fragmentation pathways of the parent ion. On the other hand, the effect may be caused by different isomeric structures that start fragmenting at different appearance energies.

The reconstructed breakdown diagram does not allow distinguishing between the isomers because the MS/MS spectrum at each collision energy is a summation of all fragments of all isomers.

A way to determine whether P_3D_4 contains different isomeric structures that have different appearance energies for fragmentation is by performing a novel CAD experiment on parent ion $[P_3D_4+H]^+$ where depleted ion populations are fragmented. Approximately 25% of the parent ion $[P_3D_4+H]^+$ population is fragmented in the first MS/MS step (to ~75% survival yield see figure 8.4) with $E_{kin,lab}$ of 70 eV. After a thermalisation delay with an Argon gas pulse of 5 seconds, the remaining ~75% of $[P_3D_4+H]^+$ is isolated and fragmented with $E_{kin,lab} = 129$ eV. This thermalisation delay is required to cool down the ion population to room temperature and release the kinetic energy and coherence of the remaining parent ions. Note that this is not a regular MS^3 experiment but a novel MS^n approach called Dissociation of Depleted Ion Populations (DoDIP). The spectrum that is obtained is presented in figure 8.3b. An experiment where the depleted ion population is fragmented using 70 eV has not been performed.

A similar DoDIP experiment is performed when ~70% of the parent ion population is fragmented (~30% survival yield) in the first MS/MS step with $E_{kin,lab} = 129$ eV. The DoDIP mass spectrum is shown in figure 8.3c. All other conditions are the same as the DoDIP experiment described in figure 8.3b. The basic idea behind this experiment is that isomers with relatively high appearance energy for fragmentation have not fragmented in the first low energy MS/MS step. The relative abundance of the isomeric ions that have relatively high appearance energy for fragmentation is increased before fragmentation in the DoDIP experiment at higher collision energy. Comparing the two DoDIP mass spectra provides information about isomeric structures if any are present. Note that this procedure relies on isomers that have a relatively large difference in their appearance energy.

All fragments observed in figure 8.3c are also observed in figure 8.3b. This is because the first MS/MS step in figure 8.3b involves fragmentation to only ~75% survival yield but the appearance of the DoDIP mass spectrum could be due to the fragmentation of multiple isomeric structures. The DoDIP mass spectrum in figure 8.3c is most probably due to only one type of isomeric structure with relatively high appearance energy for fragmentation. Figures 8.3b and 8.3c clearly demonstrate that P_3D_4 consists of at least two isomeric structures or two types of isomeric structures.

The question arises which (type of) isomeric structures are responsible for the differences in the DoDIP mass spectra. One possibility is that the polymer consists of a branched structure and a linear structure. However, similar results as

shown in figure 8.3 were obtained when parent ion $[P_2D_3+H]^+$ was studied with DoDIP experiments. This oligomer is too small to have a branched structure. The difference in figures 8.3b and 8.3c can therefore not be attributed to branching. Another possibility is that one (type of) isomeric structure is alternating like I, II and/or III (figure 8.2) and the other is non-alternating like IV. To test whether one of the isomers has a non-alternating sequence, an ion with a non-alternating structure, $[P_2D_4+H]^+$, is fragmented. The MS/MS spectrum of ion $[P_2D_4+H]^+$ with $E_{\text{kin,lab}} = 154 \text{ eV}$ is shown in figure 8.5.

Fragments ${}^b[P_2D_2]^{\text{ox}+}$ and ${}^b[PD]^{\text{ox}+}$ were expected to appear in figure 8.5, based on fragmentation studies discussed in chapter 7, but are not observed. Also, the loss of H_2O to $[P_2D_4-H_2O]^{\text{ox}+}$ and a γ -hydrogen rearrangement leading to ${}^i[P_2D_3+H]^+$ are absent. The two most intense fragments that are observed, ${}^e[PD_2-H_2O]^{\text{ox}+}$ and ${}^e[P_2D_3-H_2O]^{\text{ox}+}$, are explained by ester rearrangements (mechanism 7.3).⁹⁵ However, these fragments can also originate from cleavages of the amine bonds making the interpretation of the MS² spectra more complex. The intensity profile of the fragments did not change dramatically when the collision energy was varied indicating that probably only one (type of) isomeric structure is present (breakdown diagram not shown).

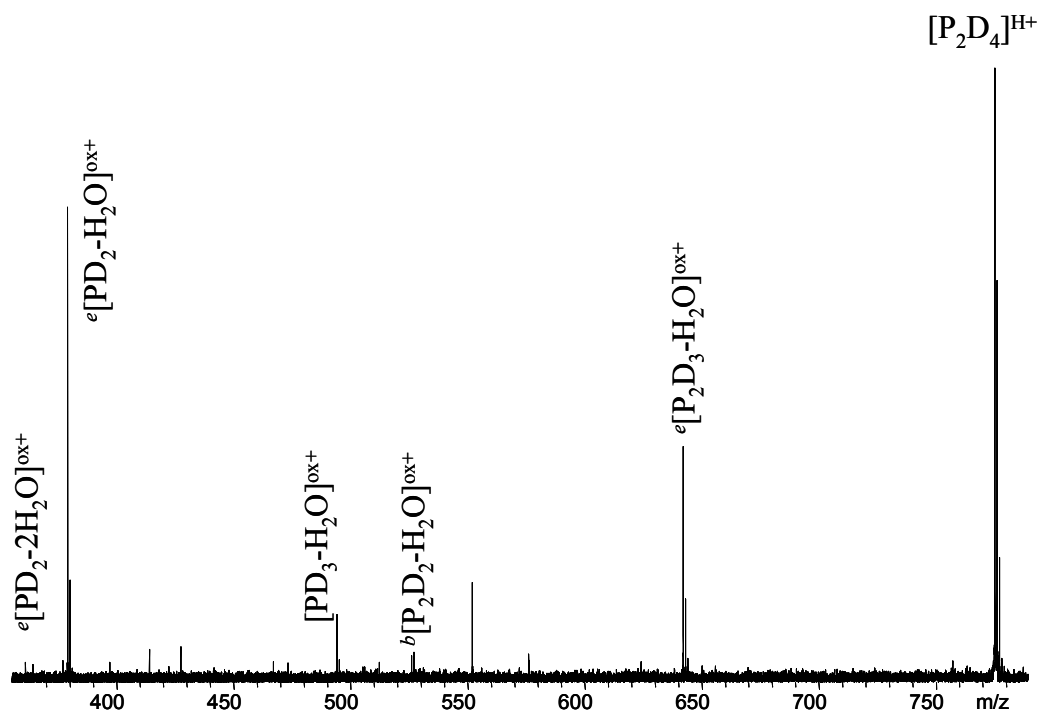


Figure 8.5 MS/MS spectrum of non-alternating oligomer $[P_2D_4+H]^+$ with a collision energy of 154 eV.

The DoDIP behaviour of the P₃D₄ isomer in figure 8.3c shows similar fragmentation behaviour as [P₂D₄+H]⁺. However, the DoDIP behaviour of the P₃D₄ isomer in figure 8.3c does not result in fragment [PD₃-H₂O]^{ox+}, which is observed upon fragmentation of [P₂D₄+H]⁺ and is a sequence specific fragment for non-alternating sequences. The intensity of this fragment was however low for the MS/MS of [P₂D₄+H]⁺ shown in figure 8.5. All fragments of the DoDIP of [P₃D₄+H]⁺ in figure 8.3c are of low intensity due to a reduction of the precursor ion in the first MS/MS step to 30% survival yield. The intensity of [PD₃-H₂O]^{ox+} is therefore probably below the detection limit. The MS/MS spectrum of [P₂D₄+H]⁺ does also not show the loss of H₂O, which is observed for the MS/MS of [P₃D₄+H]⁺ shown in figure 8.3c but the intensity profile of the other fragments of [P₂D₄+H]⁺ is very similar to the intensity profile of the fragments of [P₃D₄+H]⁺ in figure 8.3c.

The absence of fragment [P₂D₃+H]⁺ in both spectra (figure 8.3c and 8.5) and the similar fragment intensity profile both indicate that figure 8.3c is due to an isomer of P₃D₄ with a non-alternating sequence. The non-alternating isomer of P₃D₄ has at least one carboxylic acid endgroup, which might be the cause for the loss of one H₂O. P₂D₄ does not contain carboxylic acid endgroups.

A difference in the fragmentation behaviour can be accounted for by a difference in the proton affinity between the alternating and non-alternating structures. Absolute proton affinities (PA) of the molecules studied here have not been measured or reported in the literature but table 8.1 shows the literature values of the absolute proton affinities (PA in kJ/mol) of four small esters, three amides and three tertiary amines that have structural similarities with the molecules studied here.²⁶¹ The tertiary amines have a proton affinity that is ~60 kJ/mol higher than the amides and ~135 kJ/mol higher than the esters. It is assumed that a similar behaviour of the PA will occur for the molecules studied here. The non-alternating structure of P₃D₄ contains a tertiary amine, which has a higher proton affinity than an amide or ester bond. Therefore the proton will be more strongly bound to the tertiary amine bond of P₂D₄ and non-alternating P₃D₄. If the proton is involved in the fragmentation of the parent ion, a higher collision energy will be required to fragment isomers with a relatively high PA.

A hydrogen rearrangement leading to fragment ^y[P₂D₃+H]⁺ requires a higher internal energy than the other fragmentation pathways whereas in case of the alternating ion [P₃D₄+H]⁺, the proton will be adjacent to the amide carbonyl oxygens and a hydrogen rearrangement requires a relatively low collision energy.

8.3.2. Combined hydrogen/deuterium (H/D) exchange and MS² for isomer analysis

Gas phase hydrogen/deuterium (H/D) exchange experiments were performed with the entire polymer MWD without isolation of a specific ion to determine in one analysis, which of the ions exhibit H/D exchange activity. The D₂O background pressure was 5·10⁻⁷ mbar for 120 seconds. Some of the observations are summarised in figure 8.6 where the original isotopic patterns of the parent ion (due to ¹³C, ²H, ¹⁵N and ¹⁸O) are compared with the isotopic patterns after H/D exchange. Figure 8.6 demonstrates that only protonated species exhibit H/D exchange activity. Sodiated species, like [P₃D₄+Na]⁺, are present in the spectra but have not been observed to exchange hydrogen with deuterium. This is in agreement with the relay mechanism^{247,252} that was introduced to explain the H/D exchange mechanism. The relay mechanism requires a mobile proton for H/D exchange.

Proton affinities in kJ/mol	
Esters	
CH ₃ COOCH ₃	821.6
C ₂ H ₅ COOCH ₃	830.2
CH ₃ COOC ₂ H ₅	835.7
C ₆ H ₅ COOCH ₃	850.5
Amides	
(CH ₃) ₂ NCHO	887.5
(CH ₃) ₂ NCOCH ₃	908.0
C ₆ H ₅ CON(CH ₃) ₂	932.7
Tertiary amines	
(CH ₃) ₂ (C ₂ H ₅)N	960.1
(CH ₃)(C ₂ H ₅) ₂ N	971.0
(C ₂ H ₅) ₃ N	981.8

Table 8.1 Proton affinities (kJ/mol) of molecules with structural similarities to the hyperbranched polyesteramides studied in this work.

Ion series [P_nD_{n+1}+H]⁺ shows H/D exchange activity, see for example [P₃D₄+H]⁺ in figure 8.6, while the ion series that has a non-alternating monomer sequence, [P_nD_{n+2}+H]⁺, does not (for example [P₃D₅+H]⁺). Even after a longer exchange time of 30 min, no hydrogens of ion series [P_nD_{n+2}+H]⁺ were exchanged by deuterium (results not shown) although this ion series contains many exchangeable hydroxyl hydrogens. This phenomenon is explained by the difference in the proton affinity between structures P_nD_{n+1} and P_nD_{n+2}. Oligomer

series P_nD_{n+1} consist of amide and ester bonds only, if the polymerisation conditions are optimal. Oligomer series P_nD_{n+2} on the other hand consist of amide and ester bonds with an additional tertiary amine bond between two diisopropanolamines. A tertiary amine has a higher proton affinity (see table 8.1) than an amide or ester bond as discussed in the previous section. Therefore the proton will be relatively strongly bound to the tertiary amine bond (proton is less mobile) of $[P_nD_{n+2}+H]^+$ making H/D exchange more difficult. In case of alternating ion series $[P_nD_{n+1}+H]^+$, the proton will most probably be mobile and adjacent to the amide carbonyl oxygens that have a relatively low PA and therefore exhibit a higher H/D exchange activity.

Ion series P_nD_{n+2} does exhibit H/D exchange behaviour when the charge state is 2, see for example $[P_6D_8+2H]^{2+}$. This is explained by one proton being fixed at the tertiary amine whereas the other proton is mobile and responsible for the H/D exchange behaviour. Similar results as shown in figure 8.6 were obtained when mono-isotopic peaks were isolated prior to H/D exchange.

An interesting feature is the bimodal nature of the isotopic pattern of $[P_3D_4+H]^+$ after the H/D exchange event. This has been observed for all oligomers from the ion series $[P_nD_{n+1}+H]^+$. Several studies have shown that such bimodal distributions can be correlated to the secondary structure of the molecule (mostly biomolecules).^{246,248,250,253} For the molecules studied here, it could be possible that the two distributions are due to the presence of branched and non-branched oligomers. However, the isotopic pattern of oligomer $[P_2D_3+H]^+$ is also split into two distributions after the H/D exchange event (see figure 8.6), but this oligomer is too small to be branched. It is therefore unlikely that the two distribution of $[P_3D_4+H]^+$ are due to branched and linear structures.

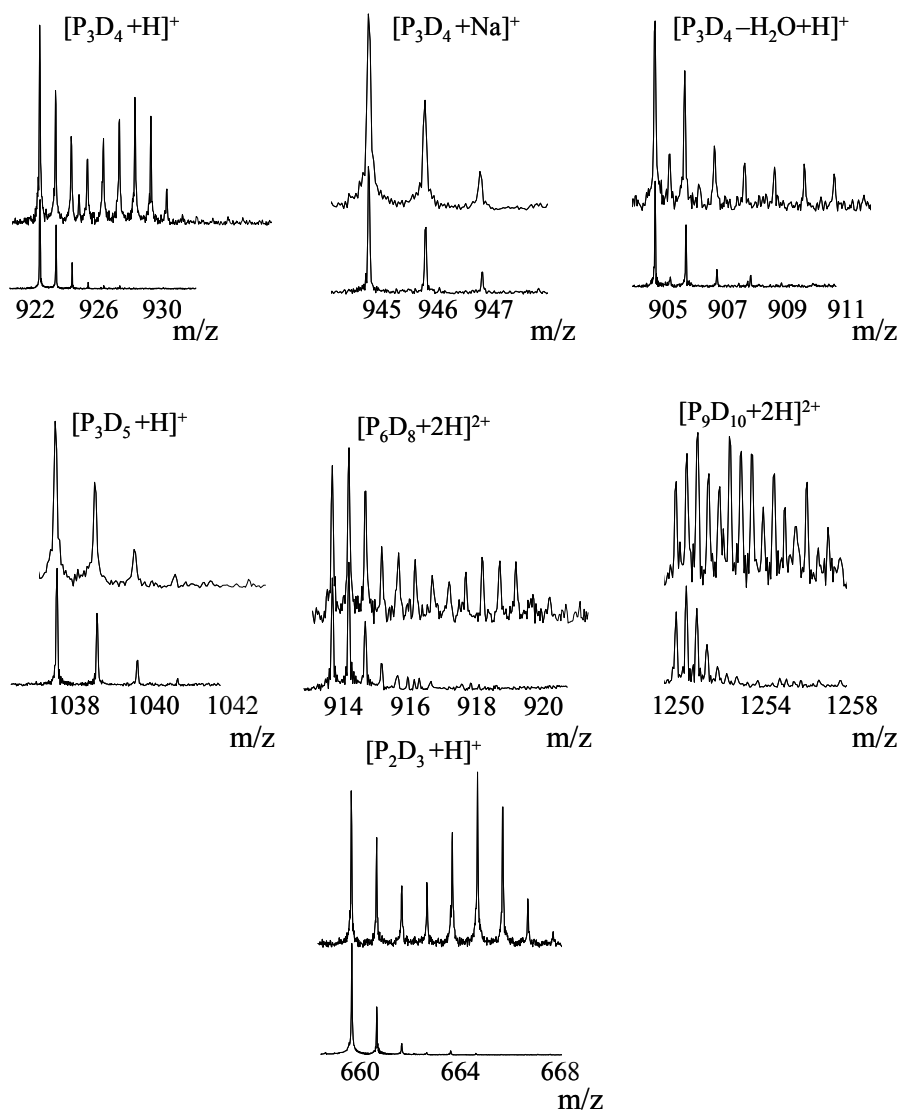


Figure 8.6 *Isotopic profiles of some oligomers before (lower) and after (top) H/D exchange at $5 \cdot 10^{-7}$ mbar D_2O for 120 seconds.*

Here, the two distributions are due to the presence of alternating and non-alternating isomeric structures. The ion series contain isomers that do exhibit H/D exchange behaviour and isomers that do not. Based on the observations discussed above, it is most likely that the $[P_3D_4+H]^+$ isomer with H/D exchange behaviour has an alternating sequence with a relatively low PA like structures I, II or III in figure 8.2. The $[P_3D_4+H]^+$ isomer that does not exhibit H/D exchange behaviour is a non-alternating oligomer resulting from an error during the polymerisation reaction, which contains a tertiary amine with a high proton affinity (structure IV). Additional MS² experiments were performed to confirm these structures. The H/D

exchange experiment was repeated after isolation of the first two isotopic peaks of $[P_3D_4+H]^+$ at $5 \cdot 10^{-7}$ mbar for 2 minutes. Two MS² experiments were performed after the H/D exchange event; 1) isolation of the first two isotopic peaks (non H/D exchanging) followed by CAD (figure 8.7a) and 2) isolation of all isotopic peaks with more than ⁵D (≥ 5 H/D exchanges) followed by CAD (figure 8.7b). Although all experimental conditions were the same, figures 8.7a and 8.7b clearly show differences. The most important differences are the absence of fragments $^a[P_2D_3+H]^+$ and $^b[P_3D_3-H_2O]^{ox+}$ in figure 8.7a. This has been observed earlier in figure 8.3 for the DoDIP experiments. Figure 8.7a shows similarities with figure 8.3c, which is a result of a non-alternating sequence. Figure 8.7b shows similarities with figure 8.3b resulting from an alternating sequence. These results clearly demonstrate that alternating and non-alternating isomers can be separated using both gas phase H/D exchange and DoDIP experiments.

An experiment is performed to check whether the separation of the isomers by H/D exchange is complete. After the first H/D exchange event on the monoisotopic peak of $[P_3D_4+H]^+$ (results not shown), the monoisotopic peak (containing non-alternating $[P_3D_4+H]^+$) is isolated again followed by a second H/D exchange event of 2 minutes. No hydrogens were exchanged during the second H/D exchange event indicating that only non-alternating isomers were present in the ICR cell, or at least below the detection threshold.

If the H/D exchange of, for example, mono-isotopic $[P_3D_4+H]^+$ would be complete, only two peaks should be obtained: one for the alternating and one for the non-alternating isomers. The H/D experiments described above show, however, a broad (bimodal) distribution, which does not change much with an increasing H/D exchange reaction time. Several authors have described earlier that extensive backexchange can occur (deuterium exchanged by hydrogen). This is due to collisions of the deuterated agent with the wall of the ICR cell, which is saturated with hydrogen containing molecules, for example H₂O.^{249,252,254} Deuterium will be exchanged by hydrogen resulting in the gas phase molecules HDO and H₂O. A way to overcome this problem is by prior saturation of the cell wall with D₂O. These experiments have not been performed here, which is most probably the cause of the broad distributions observed.

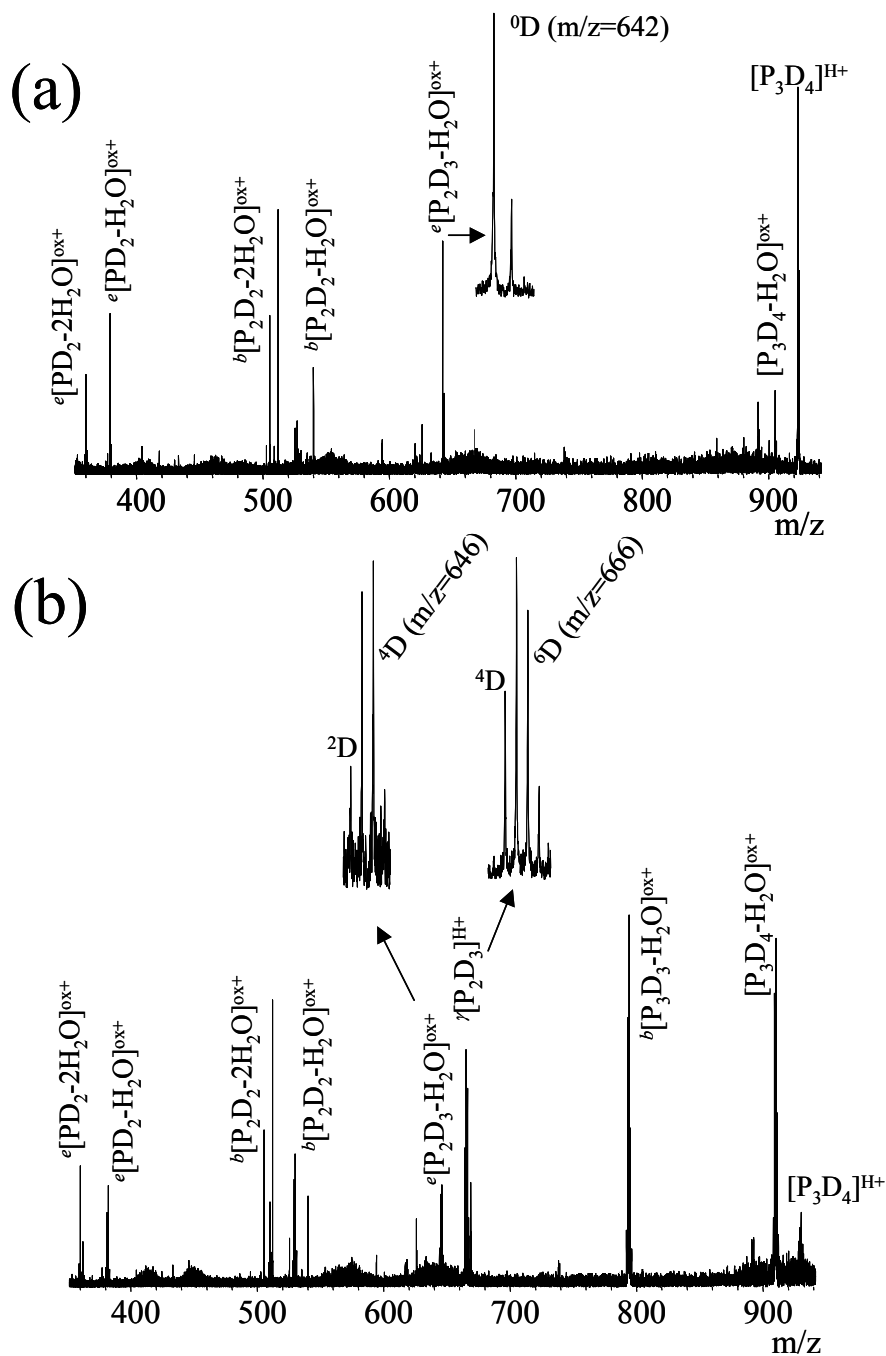


Figure 8.7 *H/D exchange experiment on the first two isotopic peaks of parent ion $[P_3D_4+H]^+$ with D_2O for 120 seconds at $5 \cdot 10^{-7}$ mbar. The experiment was followed by MS/MS after isolation of the first two isotopic peaks (a) and MS/MS after isolation of the isotopic peaks with more than 5D (≥ 5 H/D exchanges) (b).*

8.3.3. Combined MS² and hydrogen/deuterium (H/D) exchange for the study of the fragmentation mechanism

Mechanisms 7.2 and 7.3 have been proposed that explain the fragmentation behaviour of the ester and amide bonds of hyperbranched polyesteramides.⁹⁵ Both mechanisms lead to the formation of oxazonium ions. An oxazonium ion has, in contrast to a protonated fragment, a charge fixed on the molecule by a quaternary ammonium ion. Because it was not possible to confirm the mechanisms and structure of these ions, we performed an experiment to find out whether the fragments contain a ‘mobile’ proton or a fixed charge (oxazonium ion), see also the addendum of chapter 7. The mono-isotopic parent ion $[P_3D_4+H]^+$ was isolated and fragmented using collisionally activated dissociation ($E_{kin,lab}=185$ eV) followed by H/D exchange to establish if a mobile proton is present. All fragments and the remaining parent ion were exposed to D₂O for 2 minutes at $5 \cdot 10^{-7}$ mbar. The result is presented in figure 8.8. Using only the mono-isotopic parent ion for this purpose ensures that all isotopic peaks that are observed are due to H/D exchange and not due to the natural abundance of other isotopes (¹³C, ¹⁷O, ¹⁸O and ¹⁵N). The fragment $[P_3D_4-H_2O]^{ox+}$ (**1**) resulting from the loss of H₂O does not exhibit H/D exchange behaviour, which proves that this fragment does not contain a mobile proton. Scheme 7.1 was proposed to rationalise the formation of an oxazonium ion. Many of the other fragments (**2**, **4** and **7**) do show H/D exchange behaviour. Mechanisms 7.2 and 7.3 lead to oxazonium fragment ions that should *not* exhibit H/D exchange behaviour because they do *not* contain mobile protons. However, many ions exhibit H/D exchange behaviour, as can be seen from the inserts in figure 8.8, and should therefore be protonated. Our findings indicate that mechanisms 7.2 and 7.3⁹⁵ are not correct.

A nice feature of mechanisms 7.2 and 7.3 is that each cleavage of an ester or amide bond lead to only *one* charged fragment (oxazonium ion).⁹⁵ When introducing new mechanisms for the rearrangement of the ester and amide bonds that lead to protonated fragments, one should be aware that each rearrangement can lead to *two* charged fragments depending on the proton affinity of the fragments. This has as consequence that the interpretation of the MS/MS spectra becomes more complex.

If one assumes that only amide bonds are rearranged for which we propose scheme 8.1, the following protonated fragments will be obtained: $[PD-H_2O+H]^+$, $[P_2D_2-H_2O+H]^+$ (**7**), $[P_3D_3-H_2O+H]^+$ (**2**), $[D+H]^+$, $[PD_2+H]^+$ and $[P_2D_3+H]^+$ (**4**). These fragments have all been observed, except for $[PD-H_2O+H]^+$, $[D+H]^+$ and $[PD_2+H]^+$, and all exhibit H/D exchange activity. If an ester bond is rearranged it is likely that this will lead to a fragment with a carboxylic acid endgroup and a fragment with an allylic endgroup. Such rearrangements have been observed

earlier, for example mechanism 6.1.²²⁴⁻²²⁶ This rearrangement of the ester bond results in protonated fragments $[D-H_2O+H]^+$, $[PD_2-H_2O+H]^+$, $[P_2D_3-H_2O+H]^+$, $[PD+H]^+$, $[P_2D_2+H]^+$ and $[P_3D_3+H]^+$. Fragments $[PD+H]^+$, $[P_2D_2+H]^+$ and $[P_3D_3+H]^+$ have not been observed. Moreover, fragments $[PD_2-H_2O+H]^+$ (**9**) and $[P_2D_3-H_2O+H]^+$ (**5**) are observed in the MS/MS spectrum but do not exhibit H/D exchange activity. It is therefore more likely that fragments $[PD_2-H_2O+H]^+$ (**9**) and $[P_2D_3-H_2O+H]^+$ (**5**) are the result of an amide rearrangement (scheme 8.1) followed by the loss of H_2O from one of the endgroups to an oxazolonium ion in scheme 7.1. These results indicate that only amide bonds are rearranged upon CAD of these polymers and not ester bonds.

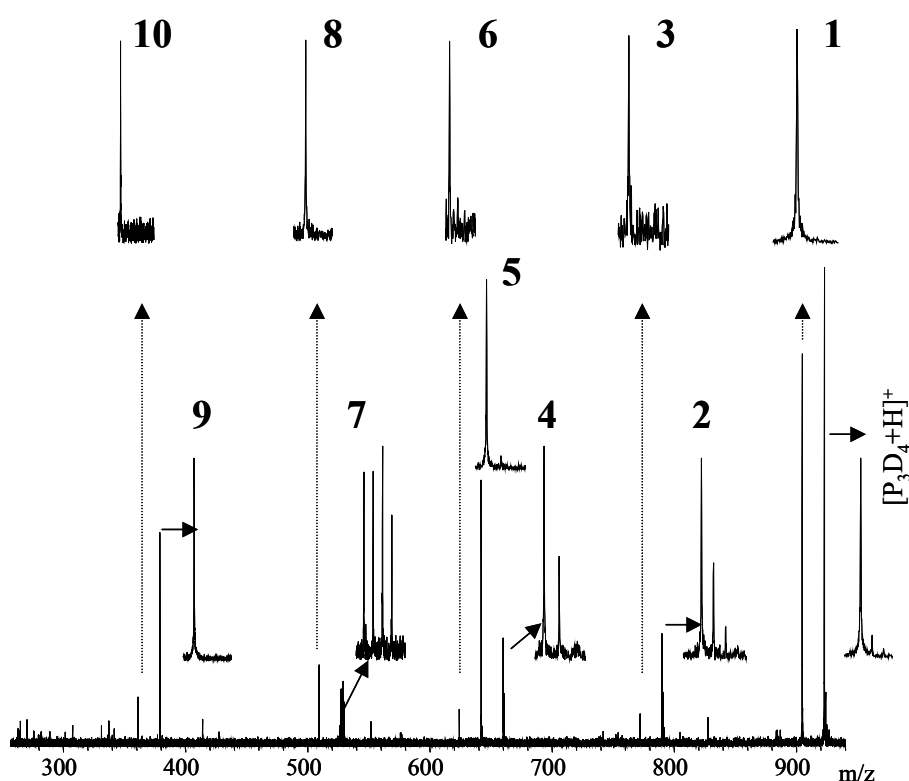
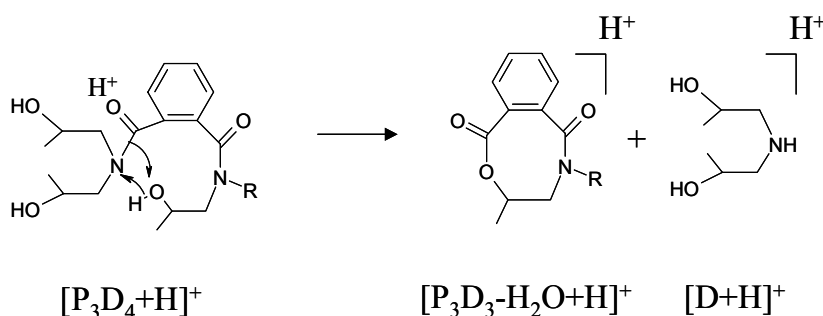


Figure 8.8 MS/MS of mono-isotopic parent ion $[P_3D_4+H]^+$ with $E_{kin,lab}=180$ eV followed by 2 minutes H/D exchange at $5 \cdot 10^{-7}$ mbar. The numbered fragments are $[P_3D_4-H_2O]^{ox+}$ (**1**), $[P_3D_3-H_2O+H]^+$ (**2**), $[P_3D_3-2H_2O]^{ox+}$ (**3**), $[P_2D_3+H]^+$ (**4**), $[P_2D_3-H_2O]^{ox+}$ (**5**), $[P_2D_3-2H_2O]^{ox+}$ (**6**), $[P_2D_2-H_2O+H]^+$ (**7**), $[P_2D_2-2H_2O]^{ox+}$ (**8**), $[PD_2-H_2O]^{ox+}$ (**9**) and $[PD_2-2H_2O]^{ox+}$ (**10**).

Isomer separation of hyperbranched polyesteramides



Scheme 8.1 Newly proposed rearrangement of the amide bond leading to protonated fragments.

8.3.4. Other hyperbranched polyesteramides

H/D exchange experiments have also been performed with hyperbranched polyesteramide polymers based on 1,2-cyclohexane dicarboxylic acid anhydride (see figure 7.1 for the structure). The polymer shows similar DoDIP and H/D exchange behaviour as the phthalic acid containing polymer described in the previous sections indicating that this polymer also contains alternating and non-alternating oligomers. Schemes 7.1 and 8.1 are therefore also valid for the hyperbranched polyesteramide based on 1,2-cyclohexane dicarboxylic acid anhydride. The oxazolonium ions of the 1,2-cyclohexane dicarboxylic acid based polymers can have a protonated structure as shown in scheme 7.4. However, the H/D exchange experiments and the MS³ experiments described in chapter 7 demonstrate that these ions are not formed.

Hyperbranched polymers based on succinic acid and glutaric acid anhydride (see figure 7.1 for their structure) do not exhibit H/D exchange activity. Additionally, their MS² behaviour shows similarities with the MS² behaviour of the non-alternating oligomers for which an example of the phthalic acid containing polymer is shown in figure 8.5. Fragments due to the loss of one D are very low in intensity. The fragment that is structurally similar as fragment $[P_2D_3+H]^+$ is not observed. This indicates that the hyperbranched polyesteramides based on succinic acid and glutaric acid contain a much higher fraction of non-alternating oligomers (i.e. contain many amine bonds with high proton affinity). DoDIP experiments have not been performed.

The results described above indicate that the synthesis of hyperbranched polyesteramides results in polymers containing an isomeric composition that depends on the monomers used in the polymerisation reaction. Two types of polymers are being formed of which one contains a mixture of oligomers with an

alternating and non-alternating monomer sequence (phthalic acid and 1,2-cyclohexane dicarboxylic acid anhydride). The other contains mainly oligomers with a non-alternating monomer sequence (succinic acid and glutaric acid anhydride).

8.4. Conclusions

A novel MSⁿ approach is used to determine whether oligomers from the hyperbranched polyesteramides based on phthalic acid anhydride and 1,2-cyclohexane dicarboxylic acid anhydride studied in this work consist of different isomeric structures. The method is called DoDIP: Dissociation of Depleted Ion Populations. The experiment starts with MS/MS to increase the relative abundance of isomeric structure that fragments at relatively high appearance energy followed by a second MS² experiment on the same parent ion. This approach was used to demonstrate that oligomers that were expected to have an alternating sequence consist of a mixture of isomers with an alternating and non-alternating monomer sequence. The method requires that the isomeric structures have a difference in the appearance energy. The same conclusion was drawn from another experimental approach that uses gas phase H/D exchange experiments. Gas phase H/D exchange experiments lead to a bimodal isotopic distribution of $[P_nD_{n+1}+H]^+$ and $[C_nD_{n+1}+H]^+$ indicating the presence of at least two isomeric structures. One of the isomeric structures does exhibit H/D exchange behaviour and the other does not. The non-exchanging isomer is a result of the non-alternating sequence of the oligomer that contains a tertiary amine with a relatively high proton affinity. Oligomers with alternating sequences only consist of amide and ester bonds with a relatively low proton affinity. Functional groups with high proton affinity reduce the mobility of protons making H/D exchange less facile. The structures of the alternating and non-alternating oligomers were confirmed with additional MS² experiments after separation with gas phase H/D exchange.

Hyperbranched polyesteramides based on succinic acid and glutaric acid did not exhibit H/D exchange behaviour. Their MS/MS behaviour is very similar to oligomers with a non-alternating monomer sequence, which indicates that these polymers contain a high fraction of non-alternating oligomers.

Mechanisms 7.2 and 7.3 that were proposed for the cleavage of the ester and amide bond⁹⁵ need to be revised. It is concluded that two types of fragments are being formed upon CAD based on gas phase H/D exchange experiments on the fragments that are obtained after MS². One type of ions is *protonated* and is proposed to result from a rearrangement of the amide bond. The other fragments

are due to amide bond rearrangements with an additional loss of H₂O from the endgroups, which leads to an *oxazolonium* ion.

The oligomer series $[P_nD_{n+1}+H]^+$ and $[C_nD_{n+1}+H]^+$ consist of alternating and non-alternating oligomers. Consequently, the non-alternating oligomers must contain OH and COOH endgroup functionalities. The presence of carboxylic acid endgroups will have an influence on, for example, cross-linking when used as cross-linkers for powder coatings.

Chapter 9

Electron capture dissociation MS of doubly charged hyperbranched polyesteramides

Electron capture dissociation (ECD) of doubly protonated or sodiated hyperbranched polyesteramide oligomers (1100-1900 Da) was examined and compared with the structural information obtained by low energy collisionally activated dissociation (CAD). Both the ester and amide bonds of the protonated and sodiated species were cleaved easily upon ECD with the formation of odd electron (OE^{+}) or even electron (EE^{+}) fragment ions. In total 13 different schemes are proposed that describe the complex fragmentation behaviour of the charged oligomers. In contrast to studies of biomolecules, the present results indicate that consecutive cleavages induced by intramolecular proton shifts are significant for ECD and of less importance for low energy CAD. The capture of an electron by the ionised species results in fragmentation associated with a distribution of the excess internal energy over the products and the subsequent cleavage of a second bond. CAD is found to be a more selective dissociation method than ECD in view of the observation that only amide bonds are cleaved for most of the tested polymers. ECD appears not to be complementary to CAD for the study of the structure of hyperbranched polymers due to the complex fragmentation behaviour. However, ECD can be of use for the structural characterisation of large oligomers that may not dissociate upon low energy CAD because ECD transfers much more energy to the hyperbranched oligomers.

9.1. Introduction

Dissociative recombination (DR) has been used for over 50 years in the physics community for the study of mainly di- and tri-atomic molecules.^{262,263} It was serendipitously discovered by McLafferty and coworkers²⁶⁴ that DR can work for large multiply charged molecules as well, and termed the process electron capture dissociation (ECD). In contrast to dissociation techniques like collisionally

activated dissociation (CAD), blackbody infrared dissociation (BIRD), infrared multiphoton dissociation (IRMPD) and surface induced dissociation (SID), ECD is a non-ergodic dissociation process. Large biomolecules have been studied (> 10 kDa) with ECD and the results demonstrate that more sequence specific product ions and less internal fragment ions are formed as compared to the other dissociation methods.²⁶⁵⁻²⁷² Internal fragment ions are defined as fragment ions that originate from the consecutive cleavage of two or more bonds leading to a fragment ion that does not contain one of the endgroups of the parent ions. CAD, BIRD and IRMPD often lead to dissociation pathways that are lowest in energy. These fragmentation pathways are often sequence unspecific and involve the loss of H₂O or the losses of H₃PO₄ and HPO₃ from phosphorylated ions.²⁶⁹

An advantage of the non-ergodic nature of ECD is that the secondary and tertiary structure of gas-phase biomolecules can be studied.^{270,273} ECD can be a powerful tool for the determination of the primary and secondary structure of synthetic polymers as well. Cerda *et al.* used ECD for the characterisation of the secondary structure of poly(ethylene glycol).²⁷⁴ Successful ECD was obtained with doubly protonated, ammoniated and sodiated species. In contrast to biomolecules, the ions formed by ECD of doubly charged oligomers are not odd-electron species OE⁺⁺, (e.g. no PEG_x+2H)⁺⁺, but are EE⁺ ions (e.g. PEG_x+H)⁺ generated by the loss of a hydrogen atom, NH₃ or a sodium atom. Single cleavages of the backbone with the formation of EE⁺ ions were the only dissociation products, whereas fragment ions with an additional H₂O loss were observed with CAD. The fragmentation behaviour of the doubly sodiated oligomer indicated that the secondary structure of the oligomers was correct and in agreement with results by Bowers *et al.* based on molecular mechanics and dynamics calculations in combination with ion mobility analysis.^{192-194,275} The primary structure (sequence) of the copolymer PEG-block-PPG-block-PEG was analysed successfully with ECD and CAD. The ECD results indicated that approximately 80% of the isomeric structures have a di-block rather than a tri-block structure. Only ~70% of the isomeric structures are di-block when measured with CAD. This discrepancy was attributed to internal fragmentation, which is absent upon ECD.¹¹⁴

A complication for the determination of the primary structure of polymers with CAD is the presence of oligomers with different sequences in the same sample. The resulting CAD mass spectra can only indicate whether the copolymer has a block or random sequence. A partially block/random sequence cannot be distinguished as described in chapter 6. In addition, information about partially block/random sequences can only be obtained if bonds can be cleaved with a high specificity. Another complication is the presence of isomeric structures with different functional groups, as is the case for hyperbranched polyesteramides described in chapter 8. Gas-phase H/D exchange experiments were used to

successfully separate isomeric structures of hyperbranched polyesteramides based on a difference in their gas-phase basicity. Different isomeric structures could also be distinguished by using the MS²/MS³ approach ‘Dissociation of Depleted Ion Populations’ (DoDIP).

In this chapter, ECD is used for the characterisation of hyperbranched polyesteramides to examine whether ECD is a complementary tool to low energy CAD for the determination of the primary structure. ECD produces more cleavages for biomolecules than CAD, and could thus be thought to provide more structural information of the hyperbranched polymers. It is for example investigated whether ECD can be used to distinguish between isomeric structures that contain different functional groups or to distinguish branched from linear oligomers. Three different polymers were studied with ECD and CAD that contain mixtures of isomers with amide, ester and amine bonds. Another hyperbranched polymer, which contains only one possible isomeric structure, was used to test whether internal fragmentations occur.

9.2. *Experimental*

The experiments described in this chapter were performed with a modified Bruker Fourier transform ion cyclotron resonance mass spectrometer (FT-ICR MS) 7T with an in-house constructed electrospray ionisation (ESI) source.^{54,212} Ions were isolated with SWIFT isolation pulses¹⁷⁷ using an in-house constructed arbitrary waveform generator.¹⁸³ The ECD experiments were performed with an electrically heated Rhenium filament (10×3 mm) on axis in the ICR cell. The open cell was in-house constructed.¹⁸² The duration of the ECD event and kinetic energy of the electrons was chosen such that the intensity of the fragment ions was maximal. In our experiments, the best ECD performance was obtained by exposure of the ions for 1-3 seconds with electrons. The kinetic energy of the electrons depends on the potential drop over the Rhenium filament and corresponds to electrons with a kinetic energy ranging from 0.4 to 2.2 eV.

Low energy CAD experiments were performed with on-resonance CAD. Argon was used as collision gas ($P_{Ar}=5.2\cdot 10^{-6}$ mbar). The geometry factor α of the open cell necessary for the calculation of the kinetic energy of the ions was estimated to be 2.26 based on a comparison between room temperature breakdown diagrams of several peptides. The peak-to-peak voltage of the RF excitation signal was 17.6 V in all CAD experiments. More details can be found in chapter 2.

The hyperbranched polyesteramides are synthesised by the polycondensation of the trifunctional di-isopropanolamine (D) and a difunctional

anhydrides of phthalic acid (P), glutaric acid (G) or 1,2-cyclohexane dicarboxylic acid (C), see figure 7.1 for their structures. The polymer that contains only one isomeric structure was made of D and C with bis(3-dimethylamino-propyl)amide (E) endgroups. The synthesis of the polymers has been described in chapter 7 and in more detail elsewhere.²³¹ The polymers were sprayed in a 0.1-0.5 mg/ml solution of 74:24:2 methanol (Merck, Darmstadt, Germany):H₂O:HAc (Biosolve, Valkenswaard, The Netherlands).

9.3. Results and discussion

9.3.1. CAD

The CAD fragmentation behaviour of the singly charged protonated hyperbranched polyesteramide ions has been discussed in chapter 7, 8 and elsewhere.⁹⁵ The present chapter describes the ECD behaviour of hyperbranched polymers, which will be compared with their CAD behaviour. Since ECD requires multiply charged ions, both the CAD and ECD behaviour of doubly charged hyperbranched oligomers is discussed. The low energy CAD behaviour is discussed first in this section and the ECD behaviour in section 3.2. A selection of three hyperbranched polyesteramides is used for this study that are mixtures of several isomers. The polymers differ only in the structure of the di-acid i.e. phthalic, glutaric and 1,2-cyclohexane dicarboxylic acid. This allows studying the influence of the di-acid structure on the CAD and ECD behaviour. A fourth hyperbranched polyesteramide that contains only one isomeric structure is used for this study, to ensure that all dissociation products originate from one type of parent ion. This should in turn result in a more facile interpretation of the CAD and ECD spectra.

9.3.1.1. CAD behaviour of the phthalic acid based polymer

Figure 9.1 shows the CAD mass spectrum of $[P_6D_7+2H]^{2+}$ (m/z 856.90 with $E_{kin,lab} = 158$ eV). P denotes the phthalic acid and D the di-isopropanolamine units. A detail of the oligomeric structure with three phthalic acids and four di-isopropanolamines is presented in figure 9.2a. To obtain one of the possible isomeric structures of P_6D_7 , three R-groups must be replaced by PD units connected by ester bonds. The other three R groups must be replaced with hydrogens. The collision energy was chosen such that almost the complete amount of parent ions were fragmented. This was done because different types of isomers

have a different appearance energy as described in chapter 8. Using this relatively high collision energy ensures that all isomers are fragmented. Singly and doubly charged fragment ions are observed of which only a few have been labelled in figure 9.1. All fragment ions can be explained by amide cleavages (scheme 9.1) to yield protonated fragment ions or amide cleavages with an additional loss of one H₂O with the formation of oxazolonium ions as discussed in chapter 7 and 8. Other fragmentation pathways of the amide bond can be proposed that lead to non-cyclic fragment ions. Fragment ions due to the loss of one and two molecules of H₂O were also observed. The *m/z* values of the fragment ion series are shown in table 9.1.

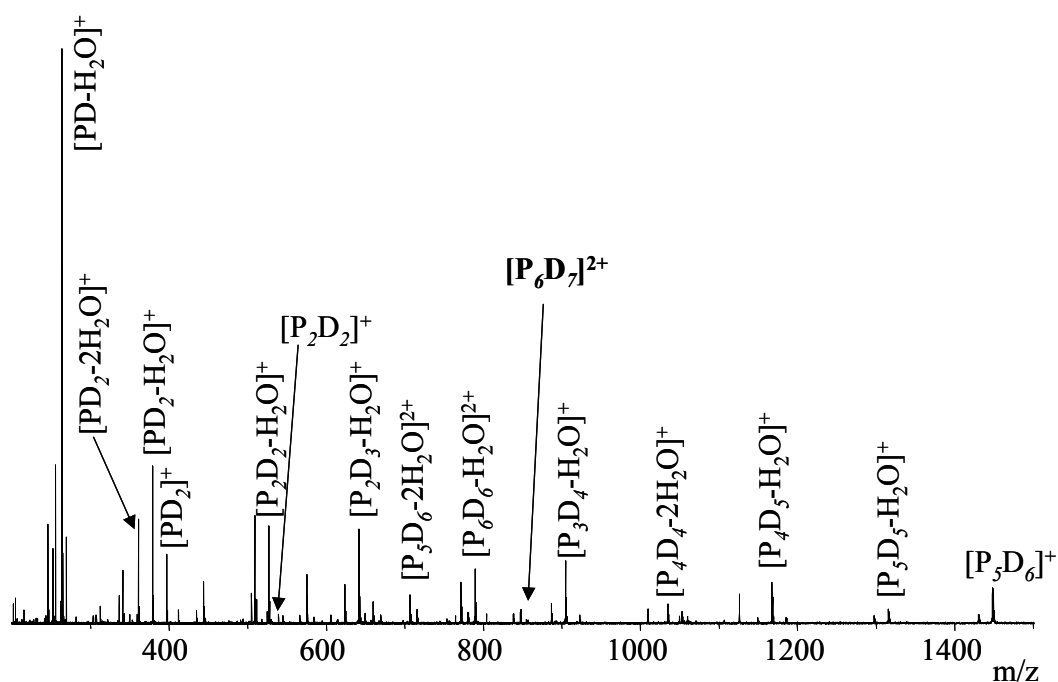
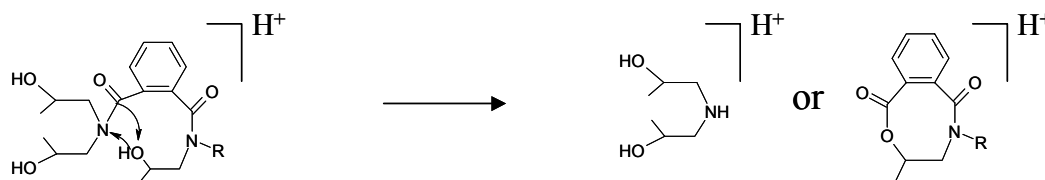


Figure 9.1 Low energy CAD of $[P_6D_7+2H]^{2+}$ ($E_{kin,lab}=158$ eV, *m/z* 856.90). *P* and *D* denote the phthalic acid and di-isopropanolamine units.



Scheme 9.1 Proposed cleavage of the amide bond of a doubly protonated oligomer under low energy CAD conditions.

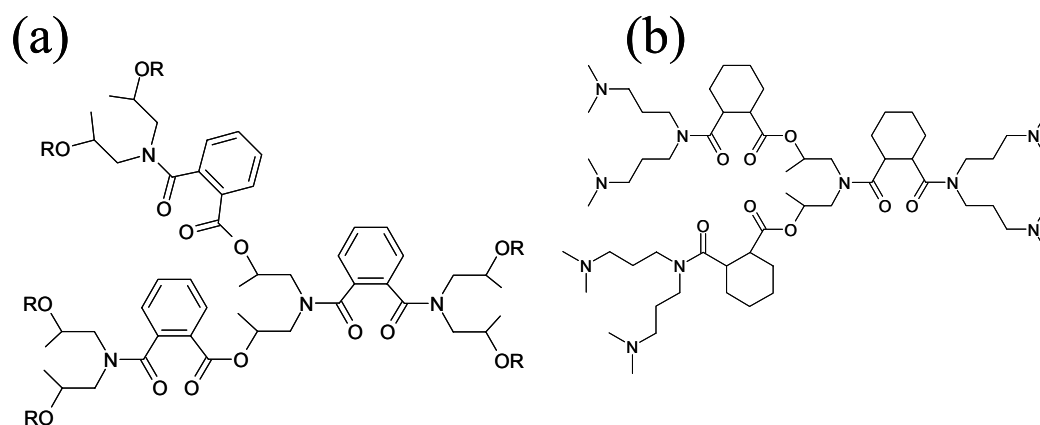


Figure 9.2 Detail of a possible isomeric structure of a phthalic acid containing oligomer (a) and the structure C_3DE_3 (b). P, D, C and E denotes phthalic acid, di-isopropanolamine, 1,2-cyclohexane dicarboxylic acid and bis(3-dimethylamino-propyl)amide units. R can be replaced by other PD units or hydrogen to obtain other isomeric structures.

	n=1	n=2	n=3	n=4	n=5	n=6
1+ fragments						
P_nD_{n+1}	397.233	660.348	923.472	1186.582	1449.695	-
$P_nD_{n+1}-H_2O$	379.224	642.336	905.454	1168.570	1431.655	-
$P_nD_{n+1}-2H_2O$	361.213	624.328	887.443	1150.459	-	-
P_nD_n	282.128	545.239	808.370	-	-	-
$P_nD_n-H_2O$	264.123	527.239	*790.354	1053.477	1316.583	-
$P_nD_n-2H_2O$	246.113	509.230	772.344	1035.438	1298.576	-
2+ fragments						
$P_nD_{n+1}-H_2O$	-	-	-	584.796	716.348	847.897
$P_nD_{n+1}-2H_2O$	-	312.667	444.225	575.785	707.343	838.904
$P_nD_{n+1}-3H_2O$	-	303.661	435.231	566.779	-	-
$P_nD_n-H_2O$	-	-	-	-	-	*790.354
$P_nD_n-2H_2O$	-	-	-	-	649.789	781.347
Total number of fragments	41					

Table 9.1 Fragment ions observed upon low energy CAD of $[P_6D_7+2H]^{2+}$ ($E_{kin,lab}=158$ eV, $m/z=856.90$). P and D denotes the phthalic acid and di-isopropanolamine units and n the degree of polymerisation. The fragment ions highlighted with * appear at the same m/z and are therefore not distinguishable.

9.3.1.2. CAD behaviour of the glutaric and 1,2-cyclohexane dicarboxylic acid based polymer

CAD was performed with $[G_7D_8+2H]^{2+}$ and $[C_6D_7+2H]^{2+}$ with m/z 869.52 and 875.05 and a $E_{kin,lab}$ of 156 and 155 eV, respectively (spectra not shown). The structure of these oligomers is similar to the structure of the oligomer presented in figure 9.2a with the exception that the phthalic acids are replaced with glutaric acid and 1,2-cyclohexane dicarboxylic acid, respectively (see figure 7.1 for their structures). Table 9.2 shows the m/z values of the fragment ions in a concise manner. To obtain the monomer composition of the CAD fragment ions, the X used in table 9.2 for the notation of the fragment ions must be replaced with C or G for the 1,2-cyclohexane dicarboxylic acid or glutaric acid containing oligomers, respectively. The printed values in table 9.2 are the combined masses of the endgroup (M_{end}) and a proton. The masses of the fragment ions can be calculated by summing $n \cdot M_{mon}$ and the mass printed in table 9.2 where M_{mon} is the monomer mass and n the degree of polymerisation (between brackets). For example, the fragment ion series X_nD_{n+1} observed for the glutaric acid anhydride based polymer, 134.116 ($n=1,2,6$), are the fragment ions $[GD_2+H]^+$, $[G_2D_3+H]^+$ and $[G_6D_7+H]^+$ with m/z values 363.247, 592.378 and 1508.902. The monomer masses of the glutaric acid and 1,2-cyclohexane dicarboxylic acid containing oligomers are 229.131 and 269.163 Da, respectively.

The fragment ions that are observed are similar to the fragment ions observed for the CAD of $[P_6D_7+2H]^{2+}$. The fragment ion series $[X_nD_n+H]^+$ was observed for the 1,2-cyclohexane dicarboxylic acid anhydride based polymer and not for the glutaric acid based polymer. Ion series $[P_nD_n+H]^+$ was also observed in figure 9.1 for the CAD of $[P_6D_7+H]^+$. These ion series cannot be explained by an amide cleavage of an alternating oligomer because this leads to ion series $[X_nD_n-H_2O+H]^+$. However, results based on gas-phase H/D exchange experiments described in chapter 8 demonstrated that the oligomer series P_nD_{n+1} and C_nD_{n+1} consist of alternating and non-alternating oligomers. The origin of the $[C_nD_n+H]^+$ and $[P_nD_n+H]^+$ ions can be explained by a cleavage of an amide bond following scheme 9.1 of a non-alternating oligomer. Fragment ions $[C_nD_n+H]^+$ and $[P_nD_n+H]^+$ contain amine endgroups.

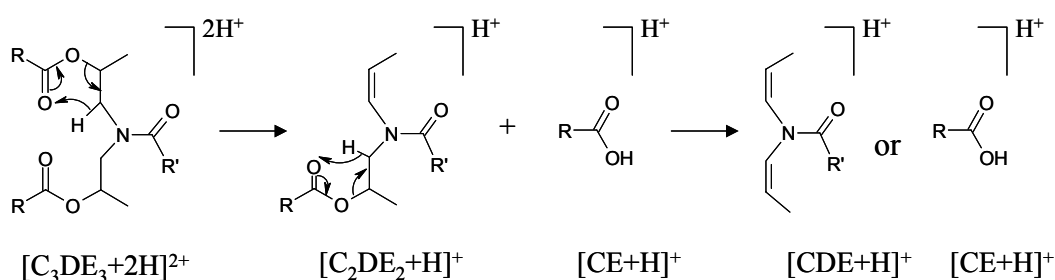
	$[G_7D_8+2H]^{2+}$	$[C_6D_7+2H]^{2+}$
+1 fragment ions		
X_nD_{n+1}	134.116 (n= 1,2,6)	134.124 (n=1-5)
$X_nD_{n+1}-H_2O$	116.108 (n= 1-6)	116.112 (n= 1-5)
$X_nD_{n+1}-2H_2O$	98.097 (n= 1-6)	98.101 (n= 1-4)
X_nD_n	-	288.184 (n= 0-4)
$X_nD_n-H_2O$	230.139 (n= 0-5)	270.173 (n= 0-4)
$X_nD_n-2H_2O$	212.129 (n= 1-5)	252.169 (n= 1-4)
+2 fragment ions		
$X_nD_{n+1}-H_2O$	58.551 (n= 4-6)	58.574 (n= 4-6)
$X_nD_{n+1}-2H_2O$	49.551 (n= 2,4-6)	49.555 (n= 2-6)
$X_nD_{n+1}-3H_2O$	40.544 (n= 3-6)	40.554 (n= 3-5)
$X_nD_n-H_2O$	-	-
$X_nD_n-2H_2O$	106.574 (n= 4-6)	126.596 (n= 3-5)
Total number of fragment ions	40	42

Table 9.2 *Fragment ions observed upon CAD of $[G_7D_8+2H]^{2+}$ ($E_{kin,lab}=156$ eV, $m/z=869.52$) and $[C_6D_7+2H]^{2+}$ ($E_{kin,lab}=155$ eV, $m/z=875.05$). The X must be replaced with G or C to obtain the composition of the fragment ions. Printed values include the masses of the endgroup and a proton. The masses of the fragment ions can be calculated by summing $n \cdot M_{mon}$ and the printed mass. M_{mon} and n are the monomer mass and degree of polymerisation, respectively (see text).*

9.3.1.3. CAD of the 1,2-cyclohexane dicarboxylic acid based polymer with bis(3-dimethylamino-propyl)amide endgroups

The hyperbranched polyesteramide oligomers studied so far have in common that multiple isomeric structures can exist, but the exact isomeric composition is unknown. Less complicated spectra can be obtained if an oligomer of a hyperbranched polyesteramide with only one isomeric structure was selected for the CAD experiments. Figure 9.2b shows the structure of the hyperbranched polyesteramide oligomer C_3DE_3 based on 1,2-cyclohexane dicarboxylic acid (C) and di-isopropanolamine (D) with bis(3-dimethylamino-propyl)amide (E) endgroups. A structural difference between this oligomer and the oligomers described in the previous sections is that it also contains amine bonds and no OH endgroups.

One of the most important fragmentation pathways is the cleavage of the ester bond shown in scheme 9.2, which leads to fragment ion $[CE+H]^+$ and its complement $[C_2DE_2+H]^+$, see figure 9.3 for the CAD spectrum of $[C_3DE_3+2H]^{2+}$ with $m/z=552.29$ at $E_{kin,lab}=162$ eV. Fragment ion $[CDE+H]^+$ is due to a consecutive cleavage of an additional ester group from fragment ion $[C_2DE_2+H]^+$. Although two covalent bonds have to be broken to obtain this fragment ion, $[CDE+H]^+$ is the base peak in the spectrum. The high intensity of this fragment ion indicates that consecutive cleavages complicate the determination of the structure of hyperbranched polymers because this implies the occurrence of internal fragment ions. Internal fragment ions do not contain one of the endgroups from the parent ion. That ester bonds are easily cleaved is a surprising result because the fragmentation behaviour of the oligomers described in sections 3.1.1 and 3.1.2 were all explained by amide bond ruptures. Ester cleavages were also observed when a relatively low collision energy (47 eV) was used to fragment ion $[C_3DE_3+2H]^{2+}$. The $[C_2DE_2+2H]^{2+}$, $[CDE+H]^+$ and $[CE+H]^+$ fragment ions lose an additional $NH(CH_3)_2$ from the endgroup indicated with an arrow in figure 9.3. More fragment ions have been observed that can only be explained by consecutive cleavages. Fragment ions that were attributed to consecutive fragmentations are denoted by an **i** in figure 9.3.



Scheme 9.2 *Consecutive cleavage of two ester bonds of doubly protonated C_3DE_3 upon low energy CAD.*

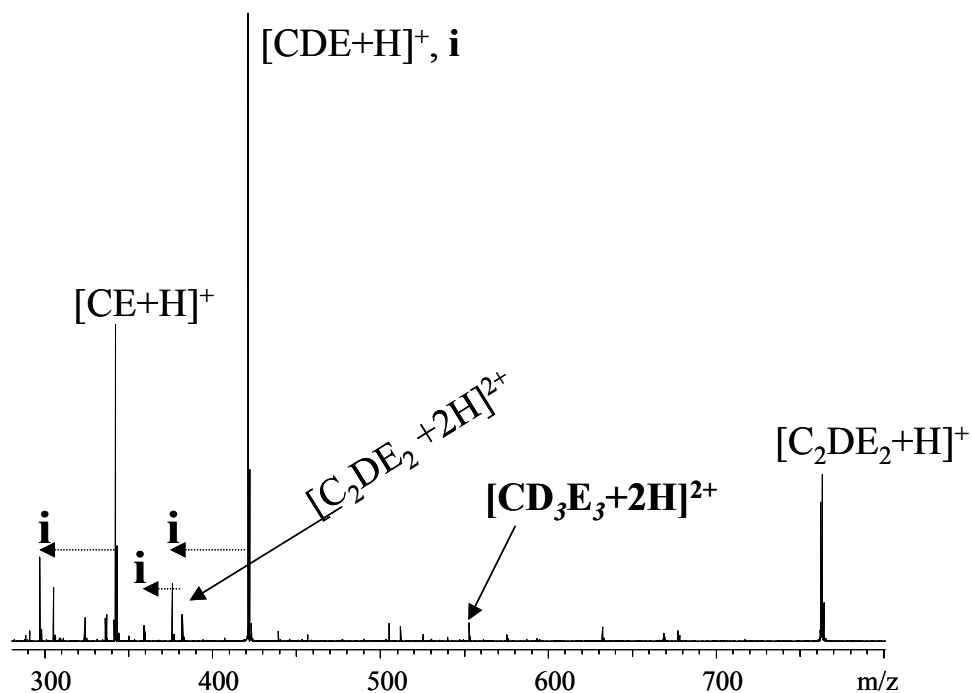


Figure 9.3 Low energy CAD of $[C_3DE_3+2H]^{2+}$ ($E_{kin,lab}=162$ eV, m/z 552.29). The **i** indicates that the fragment ions are due to consecutive fragmentations.

9.3.1.4. CAD behaviour of doubly charged hyperbranched oligomers: discussion

The CAD mass spectra of doubly charged oligomer ions $[P_6D_7+2H]^{2+}$, $[C_6D_7+2H]^{2+}$ and $[G_7D_8+2H]^{2+}$ are explained by amide bond cleavages and additional H_2O losses. The nature of the di-acid does not have a significant influence on the appearance of the CAD MS/MS spectra. In contrast with these oligomers, the ester bonds of oligomer $[C_3DE_3+2H]^{2+}$ are also cleaved. Additionally, consecutive cleavages have been observed for $[C_3DE_3+2H]^{2+}$, which make the interpretation of the MS/MS spectra more difficult. Consecutive cleavages leading to internal fragment ions were not observed for $[P_6D_7+2H]^{2+}$, $[C_6D_7+2H]^{2+}$ and $[G_7D_8+2H]^{2+}$ because this should lead to ion series $X_nD_{n-1}-2H_2O$ (two amide bonds cleaved). This implies that CAD is a very selective dissociation method for the study of the sequence of hyperbranched polyesteramides. However, branched polymers could so far not be distinguished from linear polymers using CAD. Distinguishing isomeric structures with CAD was only possible with the DoDIP procedure described in chapter 8.

9.3.2. ECD

The ECD behaviour of the same ions used for the CAD studies is discussed in the next sections to compare ECD with low energy CAD for the characterisation of hyperbranched polyesteramide oligomers. ECD has the potential to lead to more structural specific fragmentation for larger molecules as has been shown for several biomolecules. Less internal fragmentation, compared with low energy CAD, is expected due to the non-ergodic nature of ECD. These different dissociation mechanisms of ECD, compared with CAD, open the possibility for the distinction between isomeric structures and branched and linear structures. In addition, the influence of the structure of the di-acid on the ECD process is investigated.

9.3.2.1. ECD behaviour of the phthalic acid based polymer

The ECD spectrum of $[P_6D_7+2H]^{2+}$ is presented in figure 9.4a. The ions were exposed to electrons for 2 seconds. All of the 39 fragment ions that are observed are singly charged, contrary to CAD, as expected from the ECD mechanism.

Table 9.3 gives an overview of all fragment ions and their m/z values that have been observed. The table has the same structure as table 9.2. Scheme 9.3 shows how the cleavage of the amide bond results in $[1+H]^+$ and $[1^{\bullet}+H]^+$ fragment ions. R, R', R'' and R''' are hydrogens or polyesteramide chains and X is a phenyl group. Amide bonds are also cleaved as shown in scheme 9.4 leading to $[2^{\bullet}+H]^+$ ions. Its counterpart, the $[2+H]^+$ ion, was not observed. Fragment ions due to the cleavage of the ester bonds are the most intense peaks in the spectrum and are likely to involve the capture of an electron followed by homolytic cleavage of the CO bond (scheme 9.5). Two fragment ions are formed, which we call $[3+H]^+$ and $[3^{\bullet}+H]^+$. A fragment ion appears in the spectrum that is 1 Da lower than fragment ion $[3^{\bullet}+H]^+$. This fragment ion can be explained by the loss of an additional R'' from ion $[3^{\bullet}+H]^+$ to $[3'+H]^+$ via a 1,5-hydrogen shift followed by homolytic cleavage of a CO bond (scheme 9.6). This leads to internal fragment ions. R'' is likely to be a proton or a polyesteramide chain. The appearance of the fragment ion that is 1 Da lower than $[3^{\bullet}+H]^+$ can also be explained by the loss of H₂O from the $[1+H]^+$ ion. Fragment ions $[2^{\bullet}+H]^+$ and $[3+H]^+$ also lose an additional H₂O. Fragment ion $[3^{\bullet}+H]^+$ loses up to two H₂O molecules. An explanation for the additional loss of H₂O is that not all energy gained by the molecule upon electron capture is consumed in the cleavage of a bond. The remaining internal energy is ergodically distributed over the fragment ions and may lead to a subsequent loss of

H₂O from one of the fragment ion endgroups. Note that this is different to the observations published in the literature, where such consecutive cleavages do not appear to occur. Another possibility for the formation of these ion series could be the cleavage of an amide bond. However, a loss of H₂O is more likely to be responsible for these ion series because it has a lower appearance energy than the cleavage of the amide bond as was observed for collisionally activated dissociation of hyperbranched polyesteramide oligomers described in chapters 7 and 8.

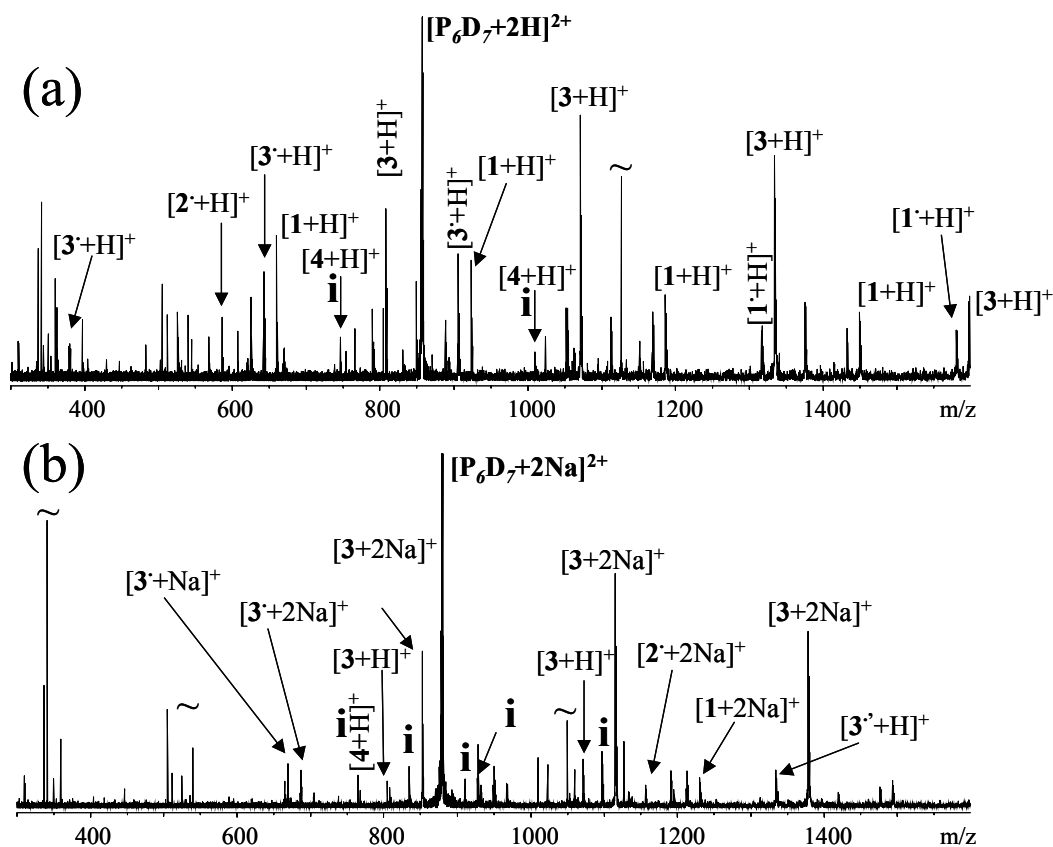
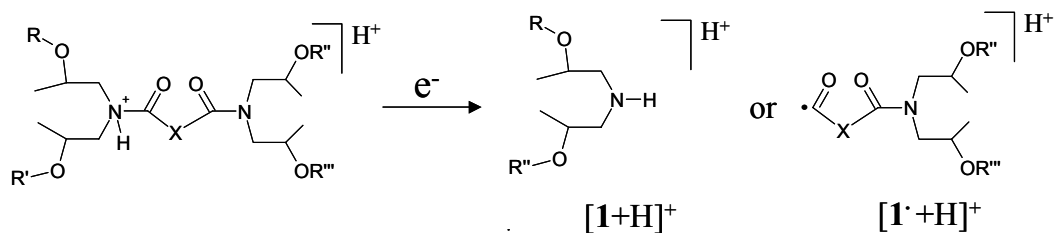
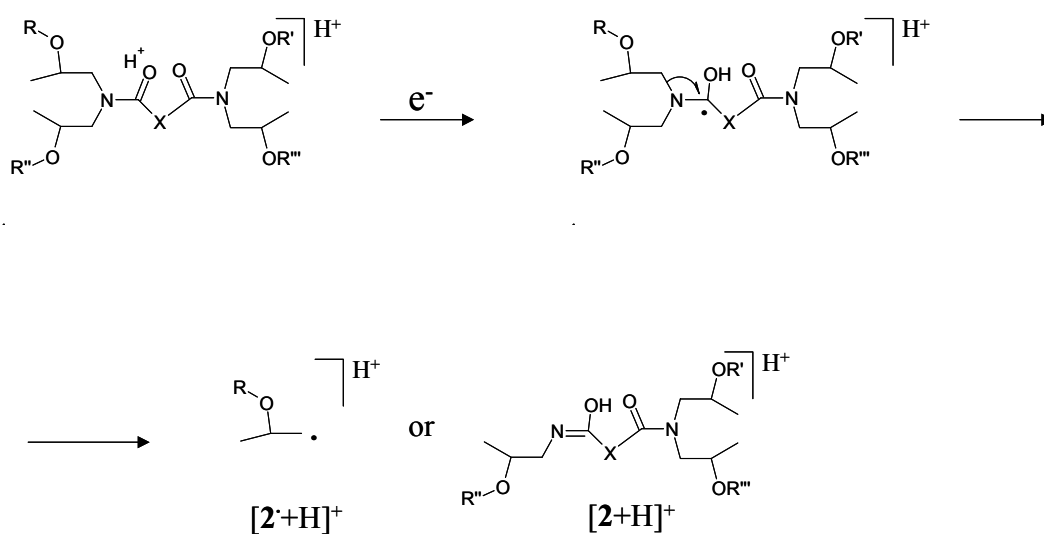


Figure 9.4 ECD of $[P_6D_7+2H]^{2+}$ (2 sec.) (a) and $[P_6D_7+2Na]^{2+}$ (1 sec.) (b). Additional losses of $NH(CH_3)_2$ are indicated with an arrow. The ~ and i denote electronic noise and internal fragment ions, respectively.

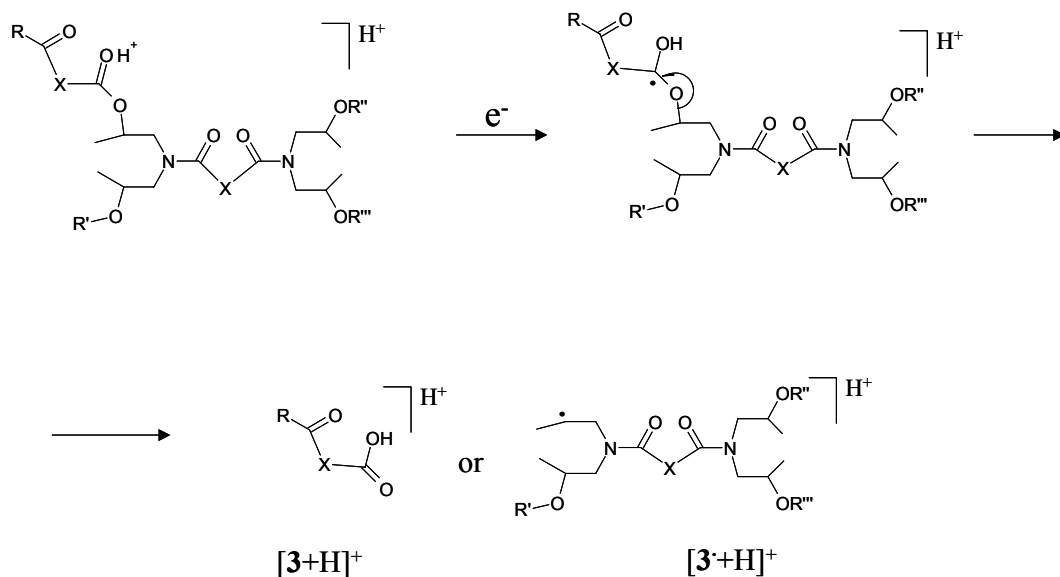
Electron capture dissociation of hyperbranched polyesteramides



Scheme 9.3 Proposed scheme for the cleavage by ECD of the amide bond of a doubly protonated oligomer leading to $[1+H]^+$ and $[1^\bullet+H]^+$ ions. R, R' R'' and R''' can be replaced by PD units or polyesteramide chains.

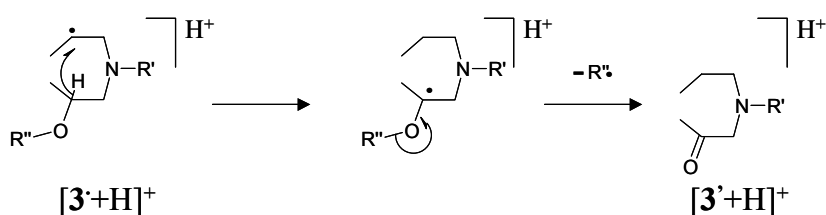


Scheme 9.4 Proposed scheme for the cleavage by ECD of the amide bond of a doubly protonated oligomer leading to $[2+H]^+$ and $[2^\bullet+H]^+$ ions.



Scheme 9.5 Proposed scheme for the cleavage by ECD of the ester bond of a doubly protonated oligomer leading to fragment ions $[3+H]^+$ and $[3'+H]^+$.

Finally, a fragment ion is observed which is a direct product of two consecutive cleavages induced by an intramolecular proton shift. Scheme 9.7 shows the capture of an electron by the amide group followed by a cleavage of a N-CO bond and loss of CO. A 1,5 proton shift precedes the cleavage of the second bond, which is an ester. The fragment ion that is formed is indicated by $[4+H]^+$ and is an internal fragment ion (denoted with an **i** in figure 9.4).



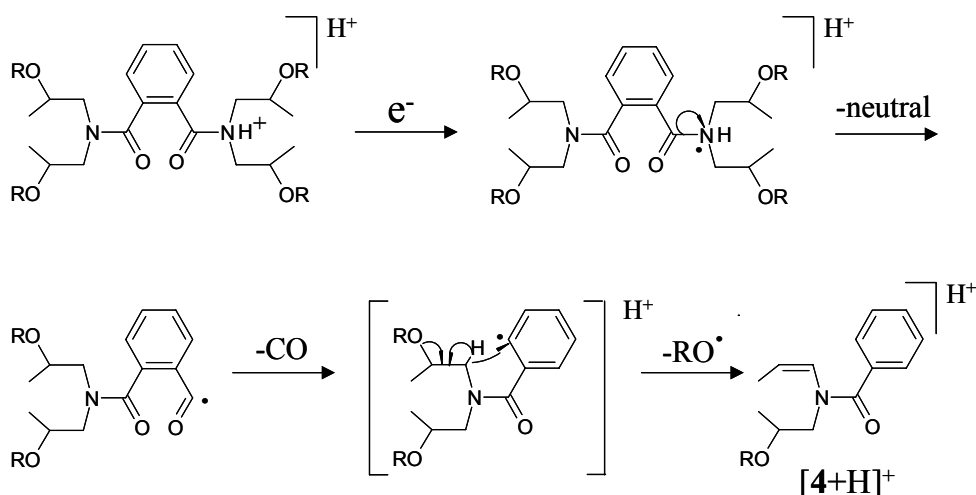
Scheme 9.6 Proposed scheme for the cleavage by ECD of an additional ester bond of a doubly protonated oligomer from $[3'+H]^+$ fragment ions leading to $[3'+H]^+$ fragment ions, which are internal fragment ions.

Electron capture dissociation of hyperbranched polyesteramides

Fragment ions	$[P_6D_7+2H]^{2+}$	$[G_7D_8+2H]^{2+}$	$[C_6D_7+2H]^{2+}$
$[1+H]^+$	134.116 ($n=1-5$)	134.097 ($n=2-6$)	134.124 ($n=2-6$)
$[1'+H]^+$	265.133 ($n=4-5$)		
$[2+H]^+$		75.968 ($n=5-7$)	76.097 ($n=4-6$)
$[2'+H]^+$	60.083 ($n=2-5$)	60.014 ($n=3-6$)	60.083 ($n=2-5$)
$[2'-H_2O+H]^+$	42.073 ($n=2-4$)		42.084 ($n=5$)
$[3'+H]^+$	19.019 ($n=2-6$)	18.985 ($n=4-6$)	19.023 ($n=2-6$)
$[3-H_2O+H]^+$	1.012 ($n=2-5$)		1.048 ($n=3-6$)
$[3'+H]^+$	117.116 ($n=1-5$)		
$[3'-H_2O+H]^+$	99.105 ($n=1-5$)		
$[3'-2H_2O+H]^+$	81.091 ($n=1-4$)		
$[4+H]^+$	220.144 ($n=2-3$)		226.180 ($n=2-4$)
$[5+H]^+$		232.015 ($n=5-6$)	272.189 ($n=1-5$)
$[6+H]^+$			118.117 ($n=2-5$)
unknown		146.032 ($n=5-6$) 87.937 ($n=6$)	99.114 ($n=2-4$) 186.150 ($n=2-4$)
Total nr. of fragment ions	39	20	40

Fragment ions	$[P_6D_7+2Na]^{2+}$	$[G_7D_8+2Na]^{2+}$	$[G_7D_8+H/Na]^{2+}$
$[1+2Na]^+$	178.015 ($n=2-5$)		
$[2'+Na]^+$		82.014 ($n=4-6$)	82.019 ($n=3-6$)
$[2'+2Na]^+$	103.993 ($n=4-5$)		
$[3'+H]^+$	18.954 ($n=3-5$)		
$[3'+Na]^+$			40.912 ($n=4-6$)
$[3+2Na]^+$	62.932 ($n=3-5$)	62.936 ($n=4-6$)	
$[3-H_2O+2Na]^+$	44.879 ($n=3-4$)		
$[3'+Na]^+$	139.074 ($n=2-4$)		
$[3'+2Na]^+$	161.039 ($n=2-5$)		
$[3'-H_2O+Na]^+$	120.996 ($n=3$)		
$[3'-H_2O+2Na]^+$	142.983 ($n=3-4$)		
$[4+Na]^+$	242.074 ($n=2$)		
unknown		177.956($n=5,6$)	
Total nr. of fragment ions	26	8	7

Table 9.3 *Fragment ions observed upon ECD of $[P_6D_7+2H]^{2+}$, $[P_6D_7+2Na]^{2+}$, $[G_7D_8+2H]^{2+}$, $[G_7D_8+H+Na]^{2+}$, $[G_7D_8+2Na]^{2+}$ and $[C_6D_7+2H]^{2+}$. The masses of the fragment ions can be obtained as described for table 9.2.*

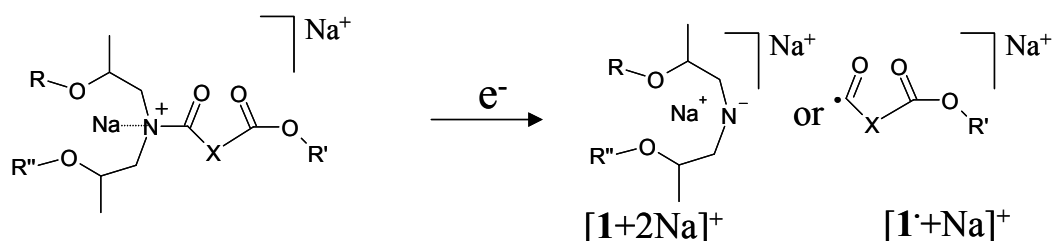


Scheme 9.7 *Proposed scheme for the consecutive cleavage by ECD of two bonds induced by an intramolecular proton shift. This leads to fragment ion $[\mathbf{4}+\text{H}]^+$ which is an internal fragment ion.*

The interpretation of the ECD spectra of these doubly protonated oligomers is very complex because many bonds are cleaved through different mechanisms. Four factors influence this complex ECD behaviour: 1) the proton involved in the capture of the electron is not necessarily localised on a specific site with a higher proton affinity than other sites. The polymers studied here contain amide and ester bonds. The difference in proton affinity of these functional groups over the entire polymer chain will be small. This is probably true for other polymers as well; 2) the polymer is a mixture of different isomeric structures that each will have a different ECD pattern; 3) an excess of internal energy after ECD leads to consecutive fragmentations. Such processes are well known from electron impact ionisation; 4) ECD gives rise to a very complex ion chemistry that involves free radical chemistry.

An experiment was performed with doubly sodiated oligomers in order to attempt to reduce the complexity of the ECD spectra. Sodium cations are probably located on specific positions on the oligomers, which could lead to less complicated ECD spectra and more structurally significant fragmentation. The ECD spectrum of $[\text{P}_6\text{D}_7+2\text{Na}]^{2+}$ (1 second) is presented in figure 9.4b. Similar fragment ions as the protonated $[\text{P}_6\text{D}_7+2\text{H}]^{2+}$ are observed, although the counter part of fragment ion $[\mathbf{1}+2\text{Na}]^+$, $[\mathbf{1}^++\text{Na}]^+$, was not observed. This is probably due to the difference in the relative sodium affinity between fragment ions $\mathbf{1}$ and $\mathbf{1}^+$. The formation of $[\mathbf{1}+2\text{Na}]^+$ is explained by the capture of an electron by the positively charged nitrogen atom due to the interaction with a sodium cation or due to the

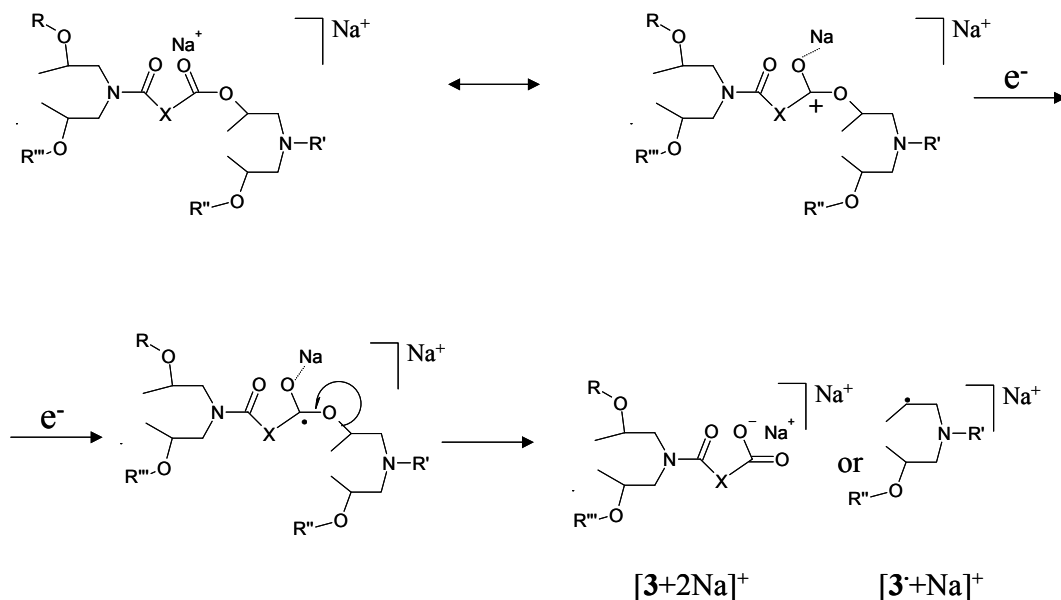
capture of the electron by the sodium cation itself. The Na^+ forms a salt with a negatively charged amine after homolytic cleavage of the C-N bond, as shown in scheme 9.8, and the second Na^+ is responsible for the +1 charge of the ion. The most intense peaks in the spectrum are due to cleavages of the ester bond resulting in $[\mathbf{3}+2\text{Na}]^+$, $[\mathbf{3}^{\bullet}+\text{Na}]^+$, $[\mathbf{3}^{\bullet}+2\text{Na}]^+$ and $[\mathbf{3}^{\bullet}+\text{H}]^+$ fragment ions. Ions $[\mathbf{3}+2\text{Na}]^+$ and $[\mathbf{3}^{\bullet}+\text{Na}]^+$ are explained by scheme 9.9 where the positively charged carbon atom, due to an interaction of the carbonyl oxygen with the sodium cation, captures an electron followed by homolytic cleavage of a C-O bond. The sodium that was involved in the interaction with the carbonyl oxygen forms a salt with the carboxylic acid endgroup of the fragment ion. Fragment ion $[\mathbf{3}^{\bullet}+2\text{Na}]^+$ has most probably the same structure as $[\mathbf{3}^{\bullet}+\text{Na}]^+$ but with an additional sodium atom. ECD fragment ion $[\mathbf{3}^{\bullet}+\text{H}]^+$ cannot be explained by single or consecutive cleavages. Scheme 9.10 demonstrates that the product ion becomes a protonated species, although the parent ion is sodiated. The exact mechanism, however, is not understood. Another ion series was observed that is identified as $[\mathbf{2}^{\bullet}+2\text{Na}]^+$. The origin of this ion series is also not clear. It cannot originate from the pathway in scheme 9.4 because that would require the formation of a salt. Internal fragment ion $[\mathbf{4}+\text{Na}]^+$ is formed by the consecutive cleavage of two bonds shown in scheme 9.7 for the protonated species.



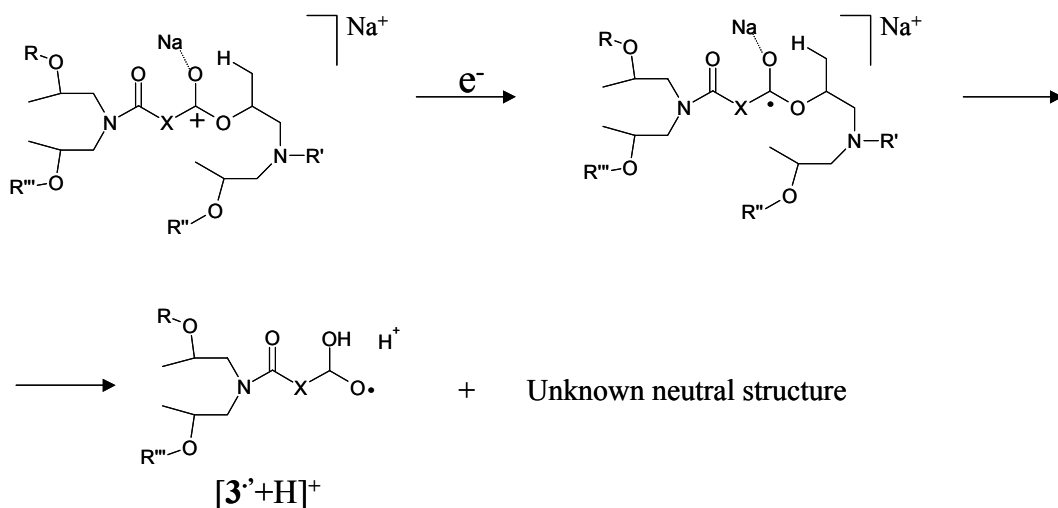
Scheme 9.8 *Proposed scheme for the cleavage by ECD of the amide bond of a doubly sodiated oligomer leading to $[\mathbf{1}+2\text{Na}]^+$.*

It seems as if most of the fragment ions lose an additional H_2O , as described for the ECD of the doubly protonated ion. However, it is unlikely that the ions lose H_2O because this requires a proton leading to an oxazolonium ion as described in chapters 7 and 8. Here, it is more likely that these ions originate by a cleavage of the amide or ester bond. Such cleavages lead to internal fragment ions (indicated with an **i** in figure 9.4) demonstrating that internal fragmentation is pronounced for hyperbranched polyesteramides using ECD. On the other hand, internal fragment ions in ECD experiments with biomolecules have never been observed in our laboratory.²⁷⁶ McLafferty and coworkers demonstrated earlier for

biomolecules that ECD leads to minimal internal fragment ions.^{270,277} These results indicate that for hyperbranched polyesteramides more excess internal energy is still available after ECD.



Scheme 9.9 Proposed scheme for the cleavage by ECD of the ester bond of a doubly sodiated oligomer leading to $[3+2Na]^+$ and $[3'+Na]^+$.



Scheme 9.10 Proposed scheme for the cleavage by ECD of the ester bond of a doubly sodiated oligomer followed by charge exchange leading to $[3'+H]^+$.

Studying the ECD of sodiated oligomers instead of protonated oligomers lead to a lower number of fragment ions (26 versus 39 fragment ions) but does not result in a reduced complexity of the spectra. The reasons for this can be explained by the same four reasons as described for the protonated oligomer.

9.3.2.2. ECD behaviour of the glutaric acid based polymer

The ECD spectrum of $[G_7D_8+2H]^{2+}$ is presented in figure 9.5a. The ions are exposed to electrons for 1 second. In total 20 fragment ions of the type $[1+H]^+$, $[2^{\bullet}+H]^+$, $[2+H]^+$ and $[3+H]^+$, are observed. Fragment ion $[2+H]^+$ (scheme 9.4) is present in figure 9.5a but was not observed for the phthalic acid based polyesteramide polymer. The fragment ions $[3^{\bullet}+H]^+$, $[2^{\bullet}+H]^+$ and fragment ions due to a loss of H_2O (or amide/ester cleavage) are not present in the spectra whereas these ions were observed for the phthalic acid based polymer. It can be hypothesised that ECD of $[G_7D_8+2H]^{2+}$ results in fragment ions either with less excess internal energy or a higher energetic barrier for consecutive cleavage compared to the phthalic acid containing polymers.

A new type of fragment ion series appears in the spectra that were not observed for the phthalic acid anhydride based polyesteramide. The possible mechanism for the formation and structure of these ions, which are denoted by $[5+H]^+$ fragment ions, is presented in scheme 9.11. The positively charged carbonyl carbon captures an electron followed by a 1,4-hydrogen shift and homolytic cleavage of the amide bond. The $[5+H]^+$ ion with a ketene endgroup is observed whereas its counterpart, the $[5^{\bullet}+H]^+$ ion, a secondary amine radical cation is not.

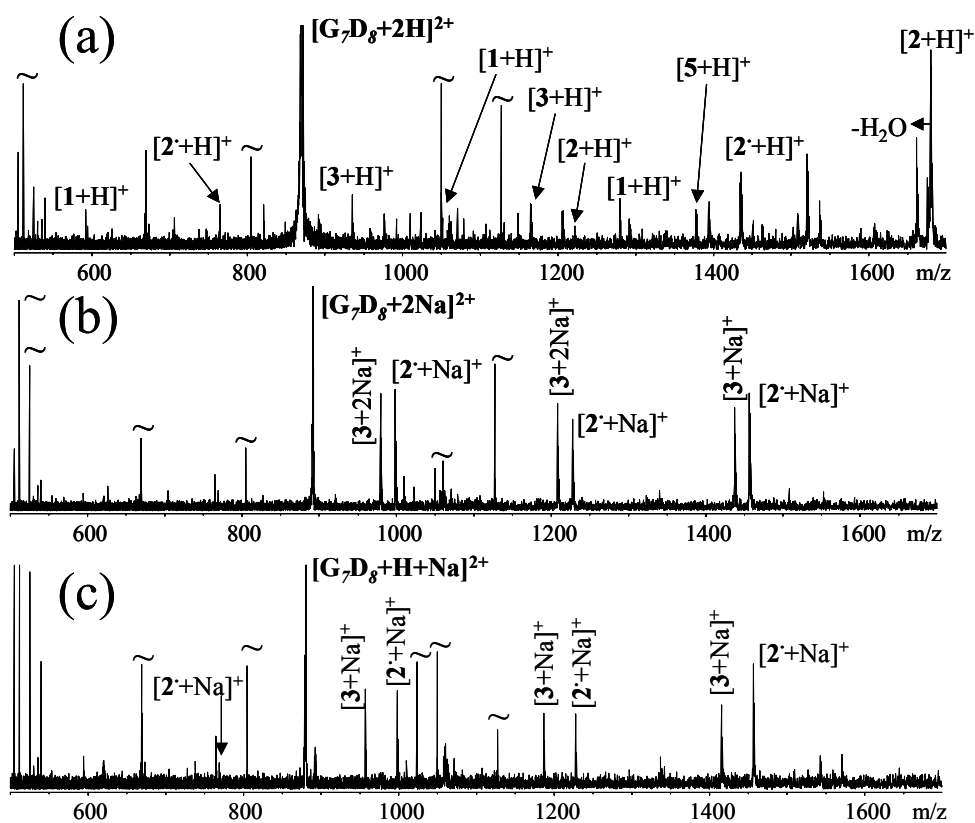
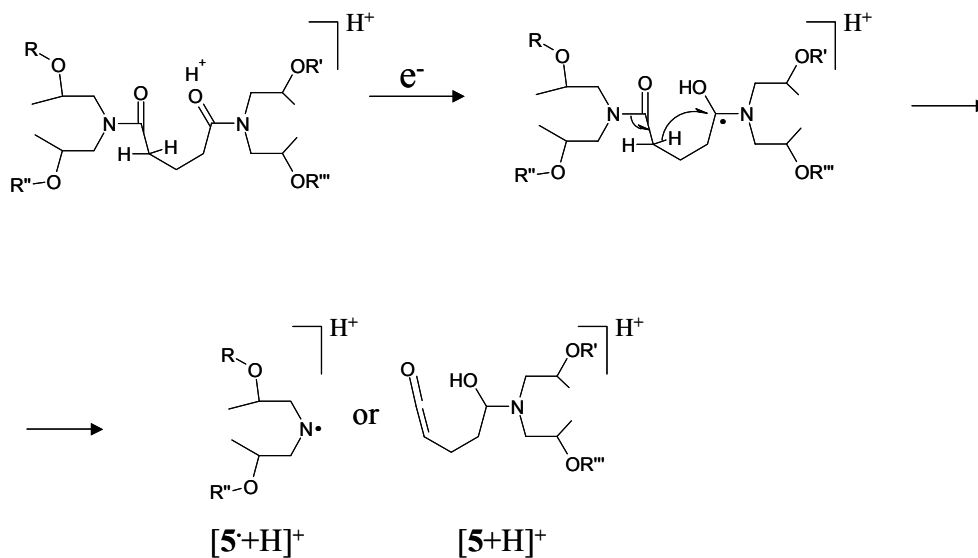


Figure 9.5 ECD of $[G_7D_8+2H]^{2+}$ (1 sec.) (a), $[G_7D_8+2Na]^{2+}$ (3 sec.) (b) and $[G_7D_8+H+Na]^{2+}$ (3 sec.) (c). The ~ is electronic noise.



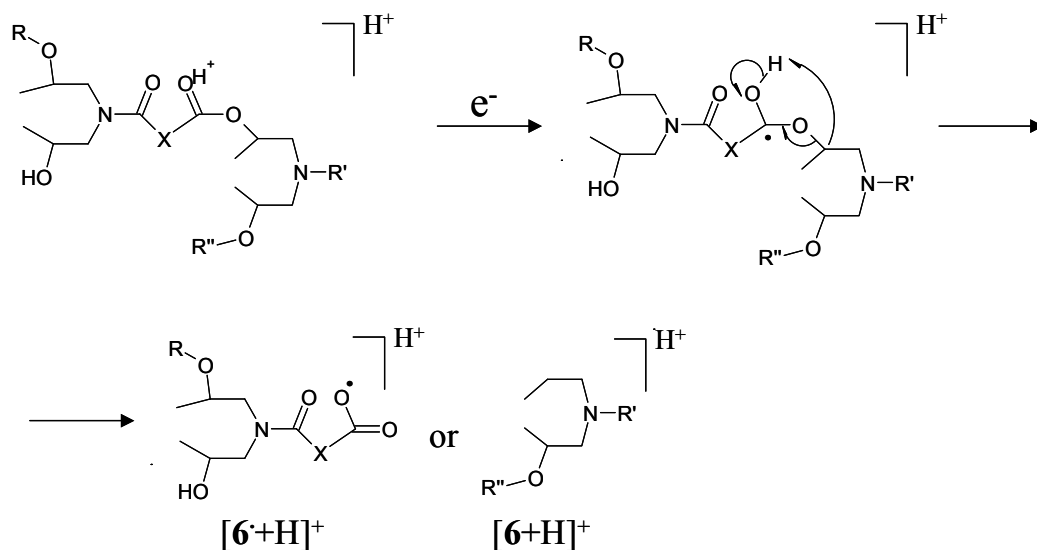
Scheme 9.11 Proposed scheme for the cleavage by ECD of the amide bond of a doubly protonated oligomer via a 1,4-hydrogen rearrangement leading to $[5+H]^+$ and $[5+H]^+$ ions.

ECD was performed with the same oligomer (3 seconds) but ionised by two sodium cations. The ECD spectrum of $[G_7D_8+2Na]^{2+}$ is shown in figure 9.5b. Only $[2^{\bullet}+Na]^+$ and $[3+2Na]^+$ ions and an ion series with a low intensity was observed (table 9.3) leading to 8 fragment ions.

The oligomer exhibits a similar ECD behaviour when ionised by one proton and one sodium cation, $[G_7D_8+H+Na]^{2+}$, as can be seen from the ECD spectrum in figure 9.5c that reveals 7 fragment ions. The only difference with the ECD spectrum of the doubly sodiated oligomer is that $[3+Na]^+$ instead of $[3+2Na]^+$ ions are formed. Note that internal fragment ions are not observed in figure 9.5b and 9.5c. The similar fragment ions observed for the ECD of $[G_7D_8+H+Na]^{2+}$ and $[G_7D_8+2Na]^{2+}$ suggest that the sodium is involved in the capture of the electron when at least one sodium is present on the molecule. ECD of protonated and sodiated P_6D_7 and G_7D_8 lead to different types of fragment ions although the structure of the polymers is similar. This demonstrates that a different structure of the di-acid has a large influence on the ECD behaviour. Note that this provides a tool to study the structure of the di-acid, which cannot be performed with low energy CAD where only labile amide bonds are cleaved.

9.3.2.3. ECD behaviour of the 1,2-cyclohexane dicarboxylic acid based polymer

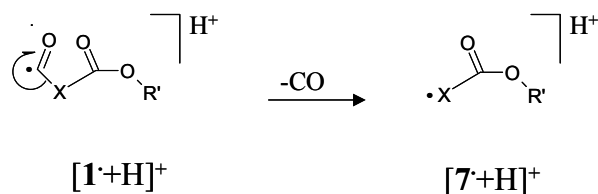
ECD was performed with $[C_6D_7+2H]^{2+}$ for 2 seconds (spectrum not shown). Most of the fragment ions that were observed in the previous sections appeared in the ECD spectrum of the 1,2-cyclohexane dicarboxylic acid based polyesteramide (40 fragment ions) as well. Fragment ions of the type $[1+H]^+$, $[2^{\bullet}+H]^+$, $[2^{\bullet}-H_2O+H]^+$, $[2+H]^+$, $[3+H]^+$, $[3-H_2O+H]^+$, $[4+H]^+$ and $[5+H]^+$ due to schemes 9.3, 9.4, 9.5, 9.7 and 9.11 have been observed. The formation of $[5+H]^+$ ions can proceed by a ring opening of the cyclohexane. A new type of fragment ion appears in the spectrum that can be explained by a cleavage of the ester bond by scheme 9.12. The fragment ions involve the capture of an electron by the positively charged carbonyl carbon followed by homolytic cleavage of the C-O bond leading to fragment ion $[6+H]^+$. Fragment ion $[6^{\bullet}+H]^+$ was not observed. Two other fragment ion series appeared in the spectrum with an unknown origin (table 9.3).



Scheme 9.12 Proposed scheme for the cleavage by ECD of the ester bond of a doubly protonated oligomer leading to $[6+H]^+$ and $[6^*+H]^+$ ions.

9.3.2.4. ECD behaviour of the 1,2-cyclohexane dicarboxylic acid based polymer with bis(3-dimethylamino-propyl)amide endgroups

The complexity of the ECD spectra described above can partly be explained by the unknown isomeric composition of the parent ion. To investigate the effect of isomers, ECD experiments were performed with C_3DE_3 with only one isomeric structure. Figure 9.6a shows the ECD spectrum (3 seconds) of the doubly protonated oligomer $[\text{C}_3\text{DE}_3+2\text{H}]^{2+}$. Although the oligomer consists of only one isomer, 26 fragment ions are observed. Fragment ions that appear in the spectrum are $[1+H]^+$ (low intensity), $[2+H]^+$, $[3+H]^+$, $[3^*+H]^+$ and $[5+H]^+$ according to reactions in schemes 9.3, 9.4, 9.5 and 9.11. Other fragment ions arise due the loss of a H^\bullet , and the formation of $[7^*+H]^+$ ions from $[1^*+H]^+$ ions as a result of a homolytic cleavage of a C-C bond and loss of a carbonyl shown in scheme 9.13. A 1,5 hydrogen shift and the consecutive cleavage of an ester bond to fragment ion $[4+H]^+$ via scheme 9.7 has also been observed.



Scheme 9.13 Loss of CO from $[1^*+H]^+$ ions by homolytic cleavage.

Fragment ions due to the cleavage of two ester bonds were also observed. The first ester bond is cleaved to $[3^{\bullet}+H]^+$ ions according to scheme 9.5 followed by the cleavage of the second ester bond leading to a fragment ion with a 3,4-dimethyl pyrrolidine endgroup. A fragment ion with an m/z 1 lower than the m/z of fragment ion $[3+H]^+$ is due to the formation of a $[2^{\bullet}+H]^+$ ion followed by propene loss (scheme 9.14) or due to a fragmentation mechanism outlined in scheme 9.12 to $[6^{\bullet}+H]^+$ ions. Most interesting is the appearance of an intense fragment ion ($m/z=818.589$) that cannot be explained by one of the mechanisms described above but is probably due to consecutive cleavages of two or even more bonds. An explanation for the relatively high intensity of fragment ions that are due to the cleavage of multiple bonds, compared with the oligomers studied earlier, is that C_3DE_3 does not contain OH endgroups. The fragment ions formed upon ECD of $[P_6D_7+2H]^{2+}$ lose their excess internal energy by a loss of H_2O . The fragment ions of $[C_3DE_3+2H]^{2+}$ cannot lose H_2O and have to release their excess internal energy by an consecutive cleavage of an ester bond.

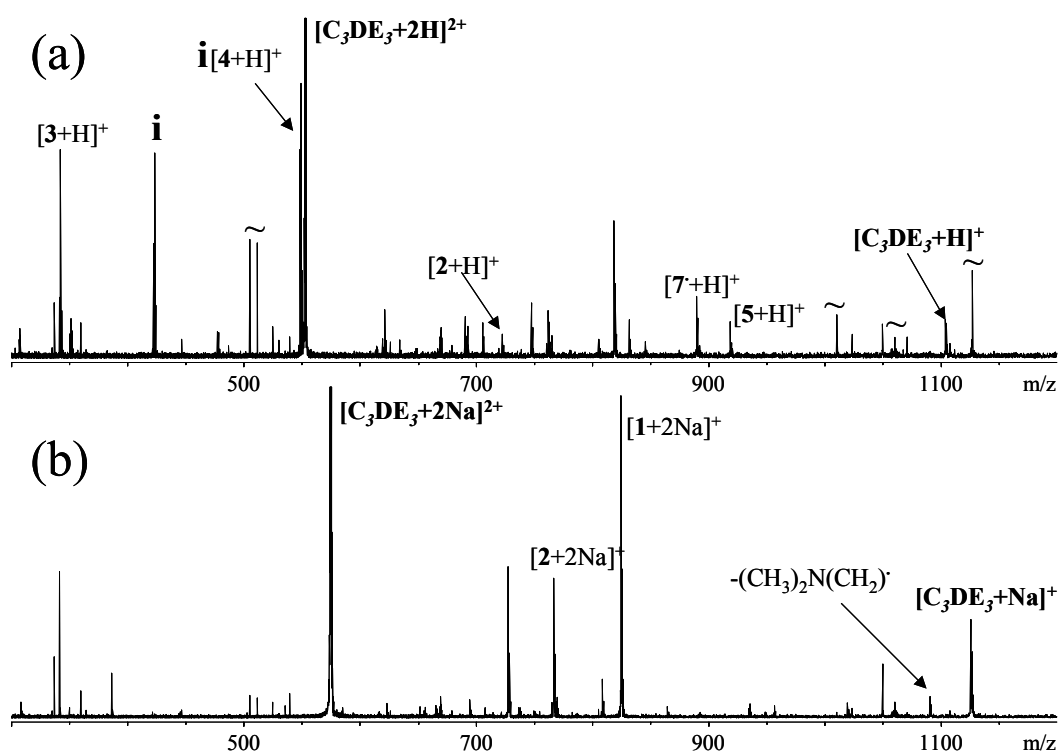
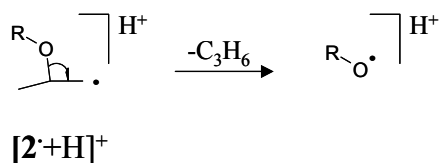
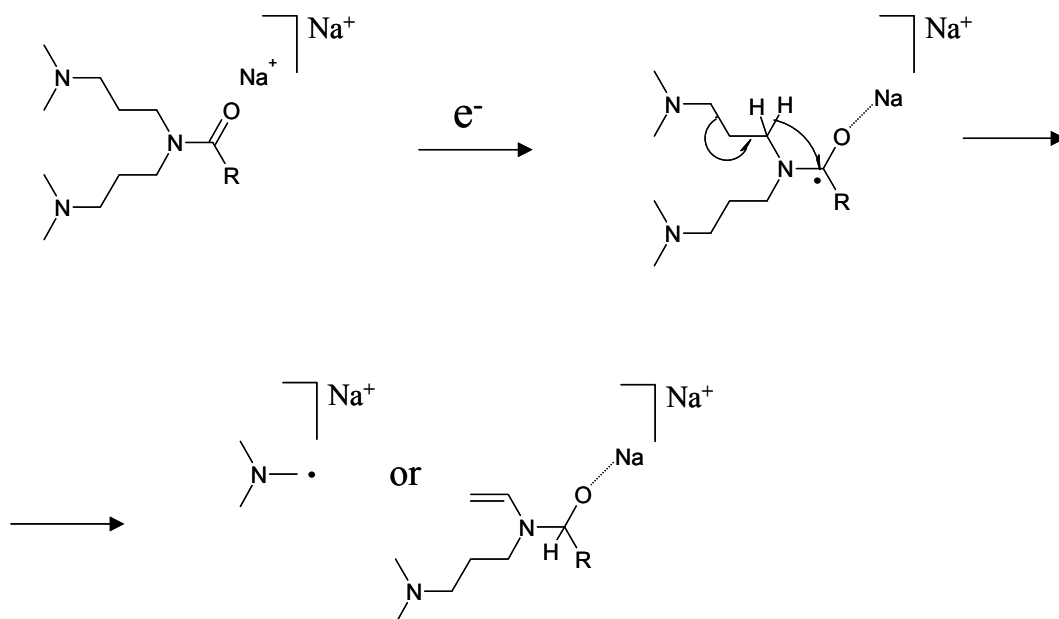


Figure 9.6 ECD of $[C_3DE_3+2H]^{2+}$ (3 sec.) (a), $[C_3DE_3+2Na]^{2+}$ (1 sec.) (b). The ~ and *i* denote electronic noise and consecutive fragmentations, respectively. Note that the origin of most peaks is unknown but they are probably a result of complex internal rearrangements.

Scheme 9.14 Loss of propene from $[\mathbf{2}^{\cdot} + \text{H}]^+$ ions by homolytic cleavage.

The ECD spectrum (1 second) of the doubly sodiated oligomer is presented in figure 9.6b and contains 21 fragment ions. A loss of a sodium atom is observed leading to the ion $[\text{C}_3\text{DE}_3 + \text{Na}]^+$. Fragment ions $[\mathbf{1} + 2\text{Na}]^+$, $[\mathbf{2} + 2\text{Na}]^+$, $[\mathbf{3} + 2\text{Na}]^+$, $[\mathbf{6} + 2\text{Na}]^+$, $[\mathbf{7}^{\cdot} + 2\text{Na}]^+$ according to schemes 9.3, 9.4, 9.5, 9.12 and 9.13 are observed. The doubly sodiated oligomer gives additional structural information about the endgroups because the parent ion loses a small radical $((\text{CH}_3)_2\text{NCH}_2)^{\cdot}$ via scheme 9.15. As observed for the doubly protonated oligomer, many fragment ions are observed that cannot be explained by cleavage of a single bond and are probably due to consecutive cleavages.

Scheme 9.15 Loss of $((\text{CH}_3)_2\text{NCH}_2)^{\cdot}$ by a homolytic cleavage.

The ECD fragment ions in the spectra, in particular the doubly protonated and doubly sodiated C_3DE_3 , give direct evidence that consecutive cleavages occur. This clearly demonstrates that internal fragment ions upon ECD of hyperbranched

polyesteramides are intense making the interpretation of the ECD spectra less straightforward.

9.4. Comparison of CAD with ECD of doubly charged hyperbranched polymers and concluding remarks

Both low energy CAD and ECD are successful methods for dissociation of doubly protonated or sodiated hyperbranched polyesteramide oligomers. Low energy CAD is a more selective dissociation method in view of the observation that only amide bonds are cleaved. ECD of doubly protonated or sodiated hyperbranched polyesteramides results in an unexpectedly high number of different types of cleavages of the ester and amide bond leading to OE^{+} and EE^{+} ions. A significant influence of the nature of the di-acid on the appearance of the ECD spectra has been observed, although the structure of the polymers is very similar. This provides complimentary structural information on the di-acid in comparison with CAD where only amide bonds are cleaved. Four factors can explain the complexity of the ECD spectra: 1) The proton or sodium cation that is involved in the capture of the electron is not located on a specific site with a higher proton or sodium affinity than other sites. The polymers studied here contain the same type of functional groups along the polymer chain, which will have only a small difference in proton or sodium affinity. 2) The polymer is a mixture of different isomeric structures that can have a different ECD pattern. 3) An excess of internal energy after ECD leads to internal fragmentation. This may be due to the energetic and non-ergodic nature of the capture of an electron (~ 6 eV) by the parent ion leading to fragmentation and a distribution of the excess internal energy over the fragment ions, which is sufficient to cleave an additional bond. This must lead to internal fragment ions that complicate the interpretation of the ECD spectra. Such consecutive cleavages are well known from electron impact ionisation. 4) ECD gives rise to a very complex chemistry that may involve free radical chemistry. Additionally, the origin of many fragment ions, especially from oligomer C_3DE_3 , cannot be explained by the 13 ECD schemes proposed above and are most probably due to complicated internal rearrangements. Complex ECD spectra and internal fragment ions can partly be overcome by performing ECD on sodiated oligomers.

The results described in this chapter demonstrate that ECD is a very useful method to obtain cleavages that are not observed upon CAD. Such cleavages can provide structural information for many classes of compounds. Additionally, an ECD analysis is ~ 10 times faster than the CAD experiments described here. However, for these relatively small oligomers of hyperbranched polyesteramides,

ECD does not provide complementary sequence information, as is the case for biomolecular analyses.²⁶⁵⁻²⁷² A number of limitations of the ECD method for these polymers may be mentioned here: 1) With the exception of C_3DE_3 , low energy CAD cleaves the amide bonds selectively, providing the sequence of the mixture of different isomers. The cleavages of the ester bonds and other types of cleavages observed with ECD do not provide additional information about the polymer monomer sequence. 2) Isomers could not be distinguished using ECD only, although this was possible with DoDIP. A combination of CAD with ECD or a combination of different ECD experiments with varying electron capture energy (for example HECD vs. ECD) can be a possible approach to obtain additional isomeric information. Note that both dissociation methods are not able to distinguish between branched and non-branched oligomers. 3) CAD leads to smaller fragment ions, which can give more information about the endgroups. 4) ECD leads to more internal fragmentation than CAD.

It will be interesting to extend this research to larger oligomers where CAD does not transfer enough energy to induce fragmentation. ECD will probably be useful for such oligomers because the excess energy must be distributed over many more degrees of freedom leading to minimal internal fragment ions. It will also be of interest to study the ECD behaviour with different cations since this leads to less fragmentation as was observed for sodiated oligomers. A study of hyperbranched polyesteramides that contain different di-acids but only one type of isomeric structure is required to confirm the ECD mechanisms proposed in this chapter.

Bibliography

- 1 Reinhold, M.; Meier, R. J.; de Koster, C. G. *Rapid Comm. Mass Spectrom.* **1998**, *12*, 1962-1966.
- 2 Flory, P. J. *Principles of polymer chemistry*, 1 ed.; Cornell University Press: Ithaca, 1953.
- 3 Shortt, D. W. *J. Liq. Chrom.* **1993**, *16*, 3371-3391.
- 4 Lloyd, P. M.; Suddaby, K. G.; Varney, J. E.; Scrivener, E.; Derrick, P. J.; Haddleton, D. M. *Eur. Mass Spectrom.* **1995**, *1*, 293-300.
- 5 Lattimer, R. P. *Int. J. Mass Spectrom. Ion Proc.* **1983/1984**, *55*, 221-232.
- 6 Parees, D. M.; Hanton, S. D.; Clark, P. A. C.; Willcox, D. A. *J. Am. Soc. Mass Spectrom.* **1998**, *9*, 282-291.
- 7 Lattimer, R. P.; Harmon, D. J.; Hansen, G. E. *Anal. Chem.* **1980**, *52*, 1808-1811.
- 8 Guo, X.; Fokkens, R. H.; Peeters, H. J.; Nibbering, N. M. M.; de Koster, C. G. *Rapid Comm. Mass Spectrom.* **1999**, *13*, 2223-2226.
- 9 Lattimer, R. P.; Hansen, G. E. *Macromolecules* **1981**, *14*, 776-780.
- 10 Simonsick, W. J., Jr. *J. Appl. Polym. Sci.* **1989**, *43*, 257-274.
- 11 Simonsick, W. J., Jr. *Progr. Org. Coat.* **1992**, *20*, 411-423.
- 12 Cotter, R. J.; Honovich, J. P.; Olthoff, J. K.; Lattimer, R. P. *Macromolecules* **1986**, *19*, 2996-3001.
- 13 Mattern, D. E.; Hercules, D. M. *Anal. Chem.* **1985**, *57*, 2041-2046.
- 14 Brown, R. S.; Weil, D. A.; Wilkins, C. L. *Macromolecules* **1986**, *19*, 1255-1260.
- 15 Hogan, J. D.; Laude, D. A. *J. Anal. Chem.* **1992**, *64*, 763-769.
- 16 Lai, S. T. F.; Chan, K. W.; Cook, K. D. *Macromolecules* **1980**, *13*, 953-956.
- 17 Bletsos, I. V.; Hercules, D. M.; van Leyen, D.; Hagenhoff, B.; Niehuis, E.; Benninghoven, A. *Anal. Chem.* **1991**, *63*, 1953-1960.
- 18 Chait, B. T.; Shpungin, J.; Field, F. H. *Int. J. Mass Spectrom. Ion Proc.* **1984**, *58*, 121-137.
- 19 Bahr, U.; Deppe, A.; Karas, M.; Hillenkamp, F.; Giessmann, U. *Anal. Chem.* **1992**, *64*, 2866-2869.
- 20 Danis, P. O.; Karr, D. E.; Mayer, F.; Holle, A.; Watson, C. H. *Org. Mass Spectrom.* **1992**, *27*, 843-846.
- 21 Danis, P. O.; Karr, D. E.; Simonsick, W. J. J.; Wu, D. T. *Macromolecules* **1995**, *28*, 1229-1232.
- 22 Nielen, M. W. F.; Malucha, S. *Rapid Comm. Mass Spectrom.* **1997**, *11*, 1194-1204.
- 23 Montaudo, G.; Montaudo, M. S.; Puglisi, C.; Samperi, F. *Rapid Comm. Mass Spectrom.* **1995**, *9*, 1158-1163.
- 24 Schriemer, D. C.; Li, L. *Anal. Chem.* **1996**, *68*, 2721-2725.
- 25 Montaudo, G.; Montaudo, M. S.; Puglisi, C.; Samperi, F. *Rapid Comm. Mass Spectrom.* **1995**, *9*, 453-460.

- 26 Lee, S.; Winnik, M. A.; Whittal, R. M.; Li, L. *Macromolecules* **1996**, *29*, 3060-3072.
- 27 Martin, K.; Spickermann, J.; Rader, H. J.; Mullen, K. *Rapid Comm. Mass Spectrom.* **1996**, *10*, 1471-1474.
- 28 Axelsson, J.; Scrivener, E.; Haddleton, D. M.; Derrick, P. J. *Macromolecules* **1996**, *29*, 8875-8882.
- 29 Montaudo, G.; Garozzo, D.; Montaudo, M. S.; Puglisi, C.; Samperi, F. *Macromolecules* **1995**, *28*, 7983-7989.
- 30 Garozzo, D.; Impallomeni, G.; Spina, E.; Sturiale, L.; Zanetti, F. *Rapid Comm. Mass Spectrom.* **1995**, *9*, 937-941.
- 31 Jackson, C.; Larsen, B.; McEwen, C. *Anal. Chem.* **1996**, *68*, 1303-1308.
- 32 Lehrle, R. S.; Sarson, D. S. *Rapid Comm. Mass Spectrom.* **1995**, *9*, 91-92.
- 33 Guttman, C. M.; Wetzel, S. J.; Blair, W. R.; Fanconi, B. M.; Girard, J. E.; Goldschmidt, R. J.; Wallace, W. E.; VanderHart, D. L. *Anal. Chem.* **2001**, *73*, 1252-1262.
- 34 Weidner, S.; Kuhn, G.; Friedrich, J. *Rapid Comm. Mass Spec.* **1998**, *12*, 1373-1381.
- 35 Linnemayr, K.; Vana, P.; Allmaier, G. *Rapid Comm. Mass Spec.* **1998**, *12*, 1344-1350.
- 36 Hunt, S. M.; Sheil, M. M.; Derrick, P. J. *Eur. Mass Spectrom.* **1998**, *4*, 475-486.
- 37 Rashidzadeh, H.; Wang, Y.; Guo, B. *Rapid Comm. Mass Spectrom.* **2000**, *14*, 439-443.
- 38 Schriemer, D. C.; Li, L. *Anal. Chem.* **1997**, *69*, 4169-4175.
- 39 Blais, J. C.; Tessier, M.; Bolbach, G.; Remaud, B.; Rozes, L.; Guittard, J.; Brunot, A.; Maréchal, E.; Tabet, J. C. *Int. J. Mass Spectrom. Ion Proc.* **1995**, *144*, 131-138.
- 40 Dogruel, D.; Nelson, R. W.; Williams, P. *Rapid Comm. Mass Spectrom.* **1996**, *10*, 801-804.
- 41 Lloyd, P. M.; Scrivener, E.; Maloney, D. R.; Haddleton, D. M.; Derrick, P. J. *J. Polym. Prep., Am. Chem. Soc. Div. Polym. Chem* **1996**, *37*, 847-848.
- 42 Poehlein, S. K.; Dormady, S. J.; McMillin, D. R.; Regnier, F. E. *Rapid Comm. Mass Spectrom.* **1999**, *13*, 1349-1353.
- 43 Hoberg, A.-M.; Haddleton, D. M.; Derrick, P. J.; Jackson, A. T.; Scrivens, J. H. *Eur. Mass Spectrom.* **1998**, *4*, 435-440.
- 44 Knochenmuss, R.; Lehmann, E.; Zenobi, R. *Eur. Mass Spectrom.* **1998**, *4*, 421-427.
- 45 Chen, H.; Guo, B. *Anal. Chem.* **1997**, *69*, 4399-4404.
- 46 Axelsson, J.; Hoberg, A.-M.; Waterson, C.; Myatt, P.; Shield, G. L.; Varney, J.; Haddleton, D. M.; Derrick, P. J. *Rapid Comm. Mass Spectrom.* **1997**, *11*, 209-213.
- 47 Sakurada, N.; Fukuo, T.; Arakawa, R.; Ute, K.; Hatada, K. *Rapid Comm. Mass Spectrom.* **1998**, *12*, 1895-1898.
- 48 Shimada, K.; Lusenkova, M. A.; Sato, K.; Saito, T.; Matsuyama, S.; Nakahara, H.; Kinugasa, S. *Rapid Comm. Mass Spectrom.* **2001**, *15*, 277-282.
- 49 Schriemer, D. C.; Li, L. *Anal. Chem.* **1997**, *69*, 4176-4183.
- 50 Fei, X.; Murray, K. K. *Anal. Chem.* **1996**, *68*, 3555-3560.

- 51 van Rooij, G. J.; Duursma, M. C.; de Koster, C. G.; Heeren, R. M. A.; Boon, J. J.; Schuyl, P. J. W.; van der Hage, E. R. E. *Anal. Chem.* **1998**, *70*, 843-850.
- 52 O'Connor, P. B.; Duursma, M. C.; van Rooij, G. J.; Heeren, R. M. A.; Boon, J. J. *Anal. Chem.* **1997**, *69*, 2751-2755.
- 53 Dey, M.; Castoro, J. A.; Wilkins, C. L. *Anal. Chem.* **1995**, *67*, 1575-1579.
- 54 Heeren, R. M. A.; Boon, J. J. *Int. J. Mass Spectrom. Ion Processes* **1996**, *157/158*, 391-403.
- 55 Pastor, S. J.; Wilkins, C. L. *J. Am. Soc. Mass Spectrom.* **1997**, *8*, 225-233.
- 56 Easterling, M. L.; Mize, T. H.; Amster, I. J. *Int. J. Mass Spectrom. Ion Proc.* **1997**, *169/170*, 387-400.
- 57 Sze, T.-P. E.; Chan, T.-W. D. *Rapid Comm. Mass Spectrom.* **1999**, *13*, 398-406.
- 58 Dole, M.; Mack, L. L.; Hines, R. L.; Mobley, R. C.; Ferguson, L. D.; Alice, M. B. *J. Chem. Phys.* **1968**, *49*, 2240-2249.
- 59 Craig, A. G.; Derrick, P. J. *Aust. J. Chem.* **1986**, *39*, 1421-1434.
- 60 Yamashita, M.; Fenn, J. B. *J. Phys. Chem.* **1984**, *88*, 4451-4459.
- 61 Yamashita, M.; Fenn, J. B. *J. Phys. Chem.* **1984**, *88*, 4671-4675.
- 62 Wong, S. F.; Meng, C. K.; Fenn, J. B. *J. Phys. Chem.* **1988**, *92*, 546-550.
- 63 Nohmi, T.; Fenn, J. B. *J. Am. Chem. Soc.* **1992**, *114*, 3241-3246.
- 64 O'Connor, P. B.; McLafferty, F. W. *J. Am. Chem. Soc.* **1995**, *117*, 12826-12831.
- 65 McEwen, C. N.; Simonsick, J., W.J.; ; Larsen, B. S.; Ute, K.; Hatada, K. *J. Am. Soc. Mass Spectrom.* **1995**, *6*, 906-911.
- 66 Tolic, L. P.; Anderson, G. A.; Smith, R. D.; Brothers, H. M. I.; Spindler, R.; Tomalia, D. A. *Int. J. Mass Spectrom. Ion Proc.* **1997**, *165/166*, 405-418.
- 67 Maziarz III, E. P.; Baker, G. A.; Mure, J. V.; Wood, T. D. *Int. J. Mass Spectrom.* **2000**, *202*, 241-250.
- 68 Jasieczek, C. B.; Buzy, A.; Haddleton, D. M.; Jennings, K. R. *Rapid Comm. Mass Spectrom.* **1996**, *10*, 509-514.
- 69 Kelly, M. A.; Vestling, M. M.; Fenselau, C. C.; Smith, P. B. *Org. Mass Spectrom.* **1992**, *27*, 1143-1147.
- 70 Chapeaurouge, A.; Bigler, L.; Schafer, A.; Bienz, S. *J. Am. Soc. Mass Spectrom.* **1995**, *6*, 207-211.
- 71 Wang, G.; Cole, R. B. , Solvent and counterion effects on observed charge states of diquatery ammonium salts in electrospray ionization mass spectrometry, Portland, Oregon, 12-16 may 1996; 1016.
- 72 Loo, J. A.; Udseth, H. R.; Smith, R. D. *Rapid Comm. Mass Spectrom.* **1988**, *2*, 207-210.
- 73 Cody, R. B.; Tamura, J.; Musselman, B. D. *Anal. Chem.* **1992**, *64*, 1561-1570.
- 74 Sherrard, K. B.; Marriott, P. J.; McCormick, M. J.; Colton, R.; Smith, G. *Anal. Chem.* **1994**, *66*, 3394-3399.
- 75 Hunt, S. M.; Sheil, M. M.; Belov, M.; Derrick, P. J. *Anal. Chem.* **1998**, *70*, 1812-1822.
- 76 Shi, S. D.-H.; Hendrickson, C. L.; Marshall, A. G.; Simonsick, W. J., Jr.; Aaserud, D. J. *Anal. Chem.* **1998**, *70*, 3220-3226.
- 77 Nielen, M. W. F. *Rapid Comm. Mass Spectrom.* **1996**, *10*, 1652-1660.
- 78 Simonsick, W. J., Jr.; Ross, C. W. I. *Polym. Prep.* **1996**, *37(1)*, 286-287.

- 79 Prokai, L.; Simonsick, W. J., Jr. *Rapid Comm. Mass Spectrom.* **1993**, *7*, 853-856.
- 80 Nielen, M. W. F. *Anal. Chem.* **1998**, *70*, 1563-1568.
- 81 Nielen, M. W. F.; Buijtenhuijs, F. A. *Anal. Chem.* **1999**, *71*, 1809-1814.
- 82 Aaserud, D. J.; Prokai, L.; Simonsick, W. J., Jr. *Anal. Chem.* **1999**, *71*, 4793-4799.
- 83 Aaserud, D. J.; Simonsick, W. J., Jr. *Progr. Org. Coatings* **1998**, *34*, 206-213.
- 84 Mengerink, Y.; Peters, R.; de Koster, C. G.; van der Wal, S.; Claessens, H. A.; Cramers, C. A. *J. Chrom. A* **2001**, *914*, 131-145.
- 85 Matsuo, T.; Matsuda, H.; Katakuse, I. *Anal. Chem.* **1979**, *51*, 1329-1331.
- 86 Neumann, G. M.; Cullis, P. G.; Derrick, P. J. *Z. Naturforsch.* **1980**, *35a*, 1090-1097.
- 87 Ballistreri, A.; Garozzo, D.; Giuffrida, M.; Impallomeni, G.; Montaudo, G. *Macromolecules* **1989**, *22*, 2107-2111.
- 88 Ballistreri, A.; Garozzo, D.; Giuffrida, M.; Montaudo, G. *Anal. Chem.* **1987**, *59*, 2024-2027.
- 89 Montaudo, G.; Scamporrino, E.; Vitalini, D. *Macromolecules* **1989**, *22*, 627-632.
- 90 Vitalini, D.; Scamporrino, E. *Polymer* **1992**, *33*, 4597-4604.
- 91 Urakami, K.; Akimoto, N.; Nishijima, K.; Kitanaka, Y.; Echigoya, M.; Hashimoto, K. *Chem. Pharm. Bull* **1999**, *47(8)*, 1068-1072.
- 92 de Koster, C. G.; Duursma, M. C.; van Rooij, G. J.; Heeren, R. M. A.; Boon, J. *J. Rapid Comm. Mass Spectrom.* **1995**, *9*, 957-962.
- 93 van Rooij, G. J.; Duursma, M. C.; Heeren, R. M. A.; Boon, J. J.; de Koster, C. G. *J. Am. Soc. Mass Spectrom.* **1996**, *7*, 449-457.
- 94 He, F.; Hendrickson, C. L.; Marshall, A. G. *Anal. Chem.* **2001**, *73*, 647-650.
- 95 Muscat, D.; Henderickx, H.; Kwakkenbos, G.; van Benthem, R.; de Koster, C. G.; Fokkens, R.; Nibbering, N. M. M. *J. Am. Soc. Mass Spectrom.* **2000**, *11*, 218-227.
- 96 Meyer, T.; Kunkel, M.; Frahm, A. W.; Waidelich, D. *J. Am. Soc. Mass Spectrom.* **2001**, *12*, 911-925.
- 97 Selby, T. L.; Wesdemiotis, C.; Lattimer, R. P. *J. Am. Soc. Mass Spectrom.* **1994**, *5*, 1081-1092.
- 98 Jackson, A. T.; Yates, H. T.; Scrivens, J. H.; Critchley, G.; Brown, J.; Green, M. R.; Bateman, R. H. *Rapid Comm. Mass Spectrom.* **1996**, *10*, 1668-1674.
- 99 Jackson, A. T.; Jennings, K. R.; Scrivens, J. H. *J. Am. Soc. Mass Spectrom.* **1997**, *8*, 76-85.
- 100 Jackson, A. T.; Yates, H. T.; Scrivens, J. H.; Green, M. R.; Bateman, R. H. *J. Am. Soc. Mass Spectrom.* **1998**, *9*, 269-274.
- 101 Przybilla, L.; Rader, H.-J.; Mullen, K. *Eur. Mass Spectrom.* **1999**, *5*, 133-143.
- 102 Pastor, S. J.; Wilkins, C. L. *Int. J. Mass Spectrom. Ion Proc.* **1998**, *175*, 81-92.
- 103 Shan, L.; Murgasova, R.; Hercules, D. M.; Houalla, M. *J. Mass Spectrom.* **2001**, *36*, 140-144.
- 104 Murgasova, R.; Hercules, D. M. *J. Mass Spectrom.* **2001**, *36*, 1098-1107.
- 105 Nielen, M. W. F. *Rapid Comm. Mass Spectrom.* **1999**, *13*, 826-827.
- 106 Mahon, A.; Kemp, T. J.; Buzy, A.; Jennings, K. R. *Polymer* **1996**, *37*, 531-535.

- 107 Jedlinski, Z.; Adamus, G.; Kowalczyk, M.; Schubert, R.; Szewczuk, Z.; Stefanowicz, P. *Rapid Comm. Mass Spectrom.* **1998**, *12*, 357-360.
- 108 Arslan, H.; Adamus, G.; Hazer, B.; Kowalczyk, M. *Rapid Comm. Mass Spectrom.* **1999**, *13*, 2433-2438.
- 109 Stolarzewicz, A.; Neugebauer, D.; Silberring, J. *Rapid Comm. Mass Spectrom.* **1999**, *13*, 2469-2473.
- 110 Maziarz, E. P. I.; Baker, G. A.; Wood, T. D. *Macromolecules* **1999**, *32*, 4411-4418.
- 111 Yalcin, T.; Gabryelski, W.; Li, L. *Anal. Chem.* **2000**, *72*, 3847-3852.
- 112 Cerda, B.; Horn, D. M.; Breuker, K.; McLafferty, F. W. , Electron capture dissociation of multiply charged polymers, Long Beach, California, June 11-15 2000; 987-988.
- 113 Cerda, B. A.; Breuker, K.; Horn, D. M.; McLafferty, F. W. *J. Am. Soc. Mass Spectrom.* **2001**, *12*, 565-570.
- 114 Cerda, B. A.; Horn, D. M.; Breuker, K.; McLafferty, F. W. *submitted to J. Am. Chem. Soc.* **2001**.
- 115 Lattimer, R. P. *J. Am. Soc. Mass Spectrom.* **1994**, *5*, 1072-1080.
- 116 Jackson, A. T.; Scrivens, J. H.; Simonsick, W. J.; Green, M. R.; Bateman, R. H. , Generation of structural information from copolymers using tandem mass spectrometry, Dallas, Texas, June 13-17 1999; 713-714.
- 117 Scrivens, J. H.; Jackson, A. T. *Int. J. Mass Spectrom.* **2000**, *200*, 261-276.
- 118 Przybilla, L.; Francke, V.; Räder, H. J.; Müllen, K. *Macromolecules* **2001**, *34*, 4401-4405.
- 119 Montaudo, M. S.; Ballistreri, A.; Montaudo, G. *Macromolecules* **1991**, *24*, 5051-5057.
- 120 Montaudo, M. S.; Montaudo, G. *Macromolecules* **1992**, *25*, 4264-4280.
- 121 Price, F. P. *J. Chem. Phys.* **1962**, *36*, 209-218.
- 122 Randall, J. C. *Polymer sequence determination; carbon-13 NMR method*; Academic press: New York, 1977.
- 123 Montaudo, M. S.; Samperi, F. *Eur. Mass Spectrom.* **1998**, *4*, 459-465.
- 124 Chen, G.; Cooks, R. G.; Jha, S. K.; Oupicky, D.; Green, M. M. *Int. J. Mass Spectrom. Ion. Processes* **1997**, *165/166*, 391-404.
- 125 Montaudo, G.; Montaudo, M. S.; Scamporrino, E.; Vitalini, D. *Macromolecules* **1992**, *25*, 5099-5107.
- 126 Montaudo, M. S.; Puglisi, C.; Samperi, F.; Montaudo, G. *Macromolecules* **1998**, *31*, 8666-8676.
- 127 Nedeá, M. E.; Morin, F. G.; Marchessault, R. H. *Polymer Bulletin* **1991**, *26*, 549-556.
- 128 Ranasinghe, A.; Lu, L.; Majumdar, T. K.; Cooks, R. G.; Fife, W. K.; Rubinsztajn, S.; Zeldin, M. *Talanta* **1993**, *40*, 1233-1243.
- 129 Zoller, D. L.; Johnston, M. V. *Anal. Chem.* **1997**, *69*, 3791-3795.
- 130 Wang, F. C.-Y. *Macromolecules* **2000**, *33*, 2437-2445.
- 131 Wang, F. C.-Y. *J. Chrom. A* **1999**, *843*, 413-423.
- 132 Chen, G.; Cooks, R. G.; Jha, S. K.; Green, M. M. *Anal. Chim. Acta* **1997**, *356*, 149-154.
- 133 Mehl, J. T.; Murgasova, R.; Dong, X.; Hercules, D. M.; Nefzger, H. *Anal. Chem.* **2000**, *72*, 2490-2498.

- 134 van Benthem, R. A. T. M. *Prog. Org. Coat.* **2000**, *40*, 203-214.
- 135 Puapairoon, U.; Taylor, R. T. *Rapid Comm. Mass Spectrom.* **1999**, *13*, 508-515.
- 136 Puapairoon, U.; Taylor, R. T.; Jai-nhuknan, J. *Rapid Comm. Mass Spectrom.* **1999**, *13*, 516-520.
- 137 Walker, K. L.; Kahr, M. S.; Wilkins, C. L.; Xu, Z.; Moore, J. S. *J. Am. Soc. Mass Spectrom.* **1994**, *5*, 731-739.
- 138 Leon, J. W.; Frechet, J. M. J. *Polymer Bulletin* **1995**, *35*, 449-455.
- 139 Sahota, H. S.; Lloyd, P. M.; Yeates, S. G.; Derrick, P. J.; Taylor, P. C.; Haddleton, D. M. *J. Chem. Soc., Chem. Commun.* **1994**, 2445-2446.
- 140 Mowat, I. A.; Donovan, R. J.; Bruce, M.; Feast, W. J.; Stainton, N. M. *Eur. Mass Spectrom.* **1998**, *4*, 451-458.
- 141 Gooden, J. K.; Gross, M. L.; Mueller, A.; Stefanescu, A. D.; Wooley, K. L. *J. Am. Chem. Soc.* **1998**, *120*, 10180-10186.
- 142 de Maaijer-Gielbert, J.; Gu, C.; Somogyi, A.; Wysocki, V. H.; Kistemaker, P. G.; Weeding, T. L. *J. Am. Soc. Mass Spectrom.* **1999**, *10*, 414-422.
- 143 Hunt, S. M.; Binns, M. R.; Sheil, M. M. *J. Appl. Polym. Sci.* **1995**, *56*, 1589-1597.
- 144 Kim, Y. L.; Hercules, D. M. *Macromolecules* **1994**, *27*, 7855-7871.
- 145 Geladé, E. T. F.; Goderis, B.; de Koster, C. G.; Meijerink, N.; van Benthem, R. A. T. M.; Fokkens, R.; Nibbering, N. M. M.; Mortensen, K. *Macromolecules* **2001**, *34*, 3552-3558.
- 146 Wilczek-Vera, G.; Danis, P. O.; Eisenberg, A. *Polym. Prep.* **1996**, *37*, 294-295.
- 147 Wilczek-Vera, G.; Danis, P. O.; Eisenberg, A. *Macromolecules* **1996**, *29*, 4036-4044.
- 148 Schriemer, D. C.; Whittal, R. M.; Li, L. *Macromolecules* **1997**, *30*, 1955-1963.
- 149 Taylor, G. *Proc. Roy. Soc. London A* **1964**, *280*, 383-397.
- 150 Blades, A. T.; Ikonomou, M. G.; Kebarle, P. *Anal. Chem.* **1991**, *63*, 2109-2114.
- 151 Rayleigh, L. *Philos. Mag.* **1882**, *14*, 184.
- 152 Iribarne, J. V.; Thomson, B. A. *J. Chem. Phys.* **1976**, *64*, 2287-2294.
- 153 Thomson, B. A.; Iribarne, J. V. *J. Chem. Phys.* **1979**, *71*, 4451-4463.
- 154 Dole, R. B. *Electrospray Ionization mass spectrometry: Fundamentals instrumentation & application*; John Wiley & Sons, Inc.: New York, 1997.
- 155 Kebarle, P.; Peschke, M. *Analytica Chimica Acta* **2000**, *406*, 11-35.
- 156 Kebarle, P.; Ho, Y. In *Electrospray ionization mass spectrometry: Fundamentals instrumentation & application*; Cole, R. B., Ed.; John Wiley & Sons Inc.: New York, 1997, pp 3-63.
- 157 Kebarle, P. *J. Mass Spectrom.* **2000**, *35*, 804-817.
- 158 Cole, R. B. *J. Mass Spectrom.* **2000**, *35*, 763-772.
- 159 Lawrence, E. O.; Livingston, M. S. *Phys. Rev.* **1932**, *40*, 19-35.
- 160 Comisarow, M. B.; Marshall, A. G. *Chem. Phys. Lett.* **1974**, *26(4)*, 489-499.
- 161 Comisarow, M. B.; Marshall, A. G. *Chem. Phys. Lett.* **1974**, *25(2)*, 282-283.
- 162 Comisarow, M. B.; Marshall, A. G. *Can. J. Chem.* **1974**, *52*, 1997-1999.
- 163 Marshall, A. G.; Verdun, F. R. *Fourier Transforms in NMR, optical, and mass spectrometry: A user's handbook*; Elsevier: Amsterdam, 1990.

- 164 Marshall, A. G.; Hendrickson, C. L.; Jackson, G. S. *Mass Spec. Rev.* **1998**, *17*, 1-35.
- 165 Marshall, A. G. *Int. J. Mass Spectrom.* **2000**, *200*, 331-356.
- 166 Amster, I. J. *J. Mass Spectrom.* **1996**, *31*, 1325-1337.
- 167 McIver, R. T. *J. Rev. Sci. Instr.* **1970**, *41(4)*, 555-558.
- 168 Comisarow, M. B. *Int. J. Mass Spectrom. Ion Phys.* **1981**, *37*, 251-257.
- 169 Comisarow, M. B. *Adv. Mass Spectrom.* **1980**, *8*, 1698-1706.
- 170 Comisarow, M. B.; Marshall, A. G. In *USA Patent No. 3,937,955*: USA, 1976.
- 171 Caravatti, P.; Allemann, M. *Org. Mass Spectrom.* **1991**, *26*, 514-518.
- 172 Gabrielse, G.; Haarsma, L.; Rolston, S. L. *Int. J. Mass Spectrom. Ion Proc.* **1989**, *88*, 319-332.
- 173 Beu, S. C.; Laude, D. A., Jr. *Int. J. Mass Spectrom. Ion Proc.* **1992**, *112*, 215-230.
- 174 Beu, S. C.; Laude, D. A., Jr.; *Anal. Chem.* **1992**, *64*, 177-180.
- 175 Sievers, H. L.; Grutzmacher, H.-F.; Caravatti, P. *Int. J. Mass Spectrom. Ion Processes* **1996**, *157/158*, 233-247.
- 176 Marshall, A. G.; Wang, T. C.; Ricca, T. L. *J. Am. Chem. Soc.* **1985**, *107*, 7893-7897.
- 177 Guan, S.; Marshall, A. G. *Int. J. Mass Spec. Ion Proc.* **1996**, *157/158*, 5-37.
- 178 Sommer, H.; Thomas, H. A.; Hipple, J. A. *Phys. Rev.* **1951**, *82*.
- 179 Francl, T. J.; Sherman, M. G.; Hunter, R. L.; Locke, M. J.; Bowers, W. D.; McIver, R. T., Jr. *Int. J. Mass Spectrom. Ion Proc.* **1983**, *54*, 189-199.
- 180 Easterling, M. L.; Mize, T. H.; Amster, I. J. *Anal. Chem.* **1999**, *71*, 624-632.
- 181 Heeren, R. M. A.; Vekey, K. *Rapid Comm. Mass Spectrom.* **1998**, *12*, 1175-1181.
- 182 Heeren, R. M. A.; Duursma, M. C.; Drahos, L.; Vekey, K. *Proceedings of the 48th ASMS conference and allied topics*, ESI-FTICR tandem mass spectrometry in the determination of internal energy relaxation rates of macromolecules, Long Beach, CA, June 11-15 2000; 804-805.
- 183 van Rooij, G. J., Laser desorption analysis in trapped ion mass spectrometry systems, Thesis, University of Amsterdam, Amsterdam, the Netherlands, 1999.
- 184 Young, R. J.; Lovell, P. A. *Introduction to polymers*, 2nd ed.; Chapman & Hall: London, 1991.
- 185 Rashidzadeh, H.; Guo, B. *Anal. Chem.* **1998**, *70*, 131-135.
- 186 Mize, T. H.; Pitsenberger, C. C.; Easterling, M. L.; Danis, P.; Amster, I. J. , Copolyester characterization by MALDI FTICR-MS, *Proceedings 45th ASMS conference and allied topics* Palm Springs, California, 1-5 june 1997; 542.
- 187 Pastor, S. J.; Wilkins, C. L. , Structural analysis of polymers using MALDI-FTMS, *Proceedings 45th ASMS conference and allied topics* Palm Springs, California, 1-5 june 1997; 537.
- 188 van der Hage, E. R. E.; Duursma, M. C.; Heeren, R. M. A.; Boon, J. J.; Nielen, M. W. F.; Weber, A. J. M.; de Koster, C. G.; de Vries, N. K. *Macromolecules* **1997**, *30*, 4302-4309.
- 189 de Koster, C. G.; Duursma, M. C.; Arisz, P. W.; Heeren, R. M. A.; Boon, J. J. , Analysis of the substituent distribution in O-methyl celluloses by MALDI-FT-

- ICR-MS, *Proceedings 43th ASMS conference and allied topics* Atlanta, Georgia 1995; 812.
- 190 Easterling, M. L.; Amster, I. J.; van Rooij, G. J.; Heeren, R. M. A. *J. Am. Soc. Mass Spectrom.* **1999**, *10*, 1074-1082.
- 191 Chan, K. W. S.; Cook, K. D. *Macromolecules* **1983**, *16*, 1736-1740.
- 192 von Helden, G.; Wyttenbach, T.; Bowers, M. T. *Science* **1995**, *267*, 1483-1485.
- 193 von Helden, G.; Wyttenbach, T.; Bowers, M. T. *Int. J. Mass Spectrom. Ion Processes* **1995**, *146/147*, 349-364.
- 194 Gidden, J.; Wyttenbach, T.; Jackson, A. T.; Scrivens, J. H.; Bowers, M. T. *J. Am. Chem. Soc.* **2000**, *122*, 4692-4699.
- 195 Yoshida, S.; Yamamoto, S.; Takamatsu, T. *Rapid Comm. Mass Spectrom.* **1998**, *12*, 535-544.
- 196 Wilczek-Vera, G.; Yu, Y.; Waddell, K.; Danis, P. O.; Eisenberg, A. *Rapid Comm. Mass Spectrom.* **1999**, *13*, 764-777.
- 197 Shard, A. G.; Volland, C.; Davies, M. C.; Kissel, T. *Macromolecules* **1996**, *29*, 748-754.
- 198 Cole, R. B.; Harrata, A. K. *J. Am. Soc. Mass Spectrom.* **1993**, *4*, 546-556.
- 199 Wang, G.; Cole, R. B. *J. Am. Soc. Mass Spectrom.* **1996**, *7*, 1050-1058.
- 200 Blair, S. M.; Kempen, E. C.; Brodbelt, J. S. *J. Am. Soc. Mass Spectrom.* **1998**, *9*, 1049-1059.
- 201 Enke, C. G. *Anal. Chem.* **1997**, *69*, 4885-4893.
- 202 Tang, L.; Kebarle, P. *Anal. Chem.* **1993**, *65*, 3654-3668.
- 203 Johnstone, R. A.; Lewis, I. A. S.; Rose, M. E. *Tetrahedron* **1983**, *39*, 1597.
- 204 Langley, G. J.; Hamilton, D. G.; Grossel, M. C. *J. Chem. Soc. Perkin Trans.* **1995**, *2*, 929-933.
- 205 Goolsby, B. J.; Brodbelt, J. S.; Adou, E.; Blanda, M. *Int. J. Mass Spectrom.* **1999**, *193*, 197-204.
- 206 Leize, E.; Jaffrezic, A.; van Dorsselaer, A. *J. Mass Spectrom.* **1996**, *31*, 537-544.
- 207 Young, D.-S.; Hung, H.-Y.; Liu, L. K. *J. Mass Spectrom.* **1997**, *32*, 432-437.
- 208 Young, D.-S.; Hung, H.-Y.; Liu, L. K. *Rapid Comm. Mass Spectrom.* **1997**, *11*, 769-773.
- 209 Kempen, E. C.; Brodbelt, J. S.; Bartsch, R. A.; Jang, Y.; Kim, J. S. *Anal. Chem.* **1999**, *71*, 5493-5500.
- 210 Brodbelt, J. S.; Kempen, E.; Reyzer, M. *Structural Chemistry* **1999**, *10*, 213-220.
- 211 Cech, N. B.; Enke, C. G. *Anal. Chem.* **2000**, *72*, 2717-2723.
- 212 Heeren, R. M. A.; de Koster, C. G.; Boon, J. J. *Anal. Chem.* **1995**, *67*, 3965-3970.
- 213 Philipsen, H. J. A.; Wubbe, F. P. C.; Klumperman, B.; German, A. L. *J. Appl. Polym. Sc.* **1999**, *72*, 183-201.
- 214 Philipsen, H. J. A., Mechanisms of gradient polymer elution chromatography and its application to (co)polyesters, Thesis, Technical University Eindhoven, Eindhoven, the Netherlands, 1998.
- 215 Cools, P. J. C. H.; van Herk, A. M.; German, A. L.; Staal, W. *J. Liq. Chrom.* **1994**, *17(14&15)*, 3133-3143.

- 216 De la Mora, J. F. *J. Fluid Mech.* **1992**, *243*, 561-574.
- 217 Cole, R. B. *Electrospray Ionization mass spectrometry: Fundamentals, Instrumentation, and applications*, 1st ed.; John Wiley & Sons, Inc.: New York, 1997.
- 218 Chen, R.; Zhang, N.; Tseng, A. M.; Li, L. *Rapid Comm. Mass Spectrom.* **2000**, *14*, 2175-2181.
- 219 Ibbett, R. N. *NMR Spectroscopy of polymers*, 1st ed.; Blackie Academic & Professional: New York, 1993.
- 220 van der Maeden, F. P. B.; Biemond, M. E. F.; Janssen, P. C. G. M. *J. Chrom.* **1978**, *149*, 539-552.
- 221 Scrivens, J. H.; Jackson, A. T.; Yates, H. T.; Green, M. R.; Critchley, G.; Brown, J.; Bateman, R. H.; Bowers, M. T.; Gidden, J. *Int. J. Mass Spectrom. Ion Proc.* **1997**, *165/166*, 363-375.
- 222 Heck, A. J. R.; de Koning, L. J.; Pinkse, F. A.; Nibbering, N. M. M. *Rapid Comm. Mass Spectrom.* **1991**, *5*, 406-414.
- 223 Yan, W.; Ammon, D. M., Jr.; Gardella, J. A., Jr.; Maziarz, E. P., III; Hawkrigde, A. M.; Grobe, G. L., III; Wood, T. D. *Eur. Mass Spectrom.* **1998**, *4*, 467-474.
- 224 Buxbaum, L. H. *Angew. Chem. Internat. Edit.* **1968**, *7*, 182-190.
- 225 Lüderwald, I.; Urrutia, H. *Makromol. Chem.* **1976**, *177*, 2079-2091.
- 226 Adams, R. E. *J. Polym. Sc.: Polym. Chem. Ed.* **1982**, *20*, 119-129.
- 227 Garozzo, D.; Giuffrida, M.; Montaudo, G. *Macromolecules* **1986**, *19*, 1643.
- 228 Montaudo, G.; Puglisi, C.; Scamporrino, E.; Vitalini, D. *Macromolecules* **1986**, *19*, 870-882.
- 229 Gidden, J.; Wyttenbach, T.; Batka, J. J.; Weis, P.; Jackson, A. T.; Scrivens, J. H.; Bowers, M. T. *J. Am. Chem. Soc.* **1999**, *121*, 1421-1422.
- 230 *The notation A is used by Muscat et al. 2000 for di-isopropanolamine and D for 1,2-cyclohexane dicarboxylic acid anhydride. In this chapter we used a notation which is consistent with van Benthem et al. (Macromolecules, 2001). D is used to denote di-isopropanolamine and C for 1,2-cyclohexane dicarboxylic acid anhydride.*
- 231 van Benthem, R. A. T. M.; Meijerink, N.; Geladé, E.; de Koster, C. G.; Muscat, D.; Froehling, P. E.; Hendriks, P. H. M.; Vermeulen, C. J. A. A.; Zwartkruis, T. J. G. *Macromolecules* **2001**, *34*, 3559-3566.
- 232 Muscat, D.; van Benthem, R. A. T. M. *Topics in Current Chemistry* **2001**, *212*, 41-80.
- 233 Geladé, E.; Meijerink, N.; van Benthem, R.; Henderickx, H.; de Koster, C. G., Molecular characterisation of hyperbranched polymers by SEC with multiple detectors, *Proceedings 48th ASMS conference and allied topics* Long Beach, California, June 11-15 2000; 166-167.
- 234 Harrison, A. G.; Csizmadia, I. G.; Tang, T.-H.; Tu, Y.-P. *J. Mass Spectrom.* **2000**, *35*, 683-688.
- 235 Nold, M. J.; Cerda, B. A.; Wesdemiotis, C. *J. Am. Soc. Mass Spectrom.* **1999**, *10*, 1-8.
- 236 Morgan, D. G.; Bursey, M. M. *Org. Mass Spectrom.* **1994**, *29*, 354-359.
- 237 de Koster, C.G. *private communication.*
- 238 Ingemann, S., *private communication.*

- 239 Nibbering, N. M. M. *Recl. Trav. Chim. Pays-Bas* **1986**, *105*, 245.
- 240 Nibbering, N. M. M. *Adv. Phys. Org. Chem.* **1988**, *24*, 1-55.
- 241 Meot-Ner, M.; Hunter, E. P.; Field, F. H. *J. Am. Chem. Soc.* **1979**, *101*, 686-689.
- 242 Locke, M. J.; McIver, R. T. J. *J. Am. Chem. Soc.* **1983**, *105*, 4226-4232.
- 243 Locke, M. J.; Hunter, R. L.; McIver, R. T. J. *J. Am. Chem. Soc.* **1979**, *101*, 272-273.
- 244 Gard, E.; Willard, D.; Bregar, J.; Green, M. K.; Lebrilla, C. B. *Org. Mass Spectrom.* **1993**, *28*, 1632-1639.
- 245 Green, M. K.; Lebrilla, C. B. *Mass Spectrom. Rev.* **1997**, *16*, 53-71.
- 246 Wood, T. D.; Chorush, R. A.; Wampler, F. M. I.; Little, D. P.; O'Connor, P. B.; McLafferty, F. W. *Proc. Natl. Acad. Sci. USA* **1995**, *92*, 2451-2454.
- 247 Wyttenbach, T.; Bowers, M. T. *J. Am. Soc. Mass Spectrom.* **1999**, *10*, 9-14.
- 248 Schaaff, T. G.; Stephenson, J. L. J.; McLuckey, S. A. *J. Am. Soc. Mass Spectrom.* **2000**, *11*, 167-171.
- 249 Gard, E.; Green, M. K.; Bregar, J.; Lebrilla, C. B. *J. Am. Soc. Mass Spectrom.* **1994**, *5*, 623-631.
- 250 Freitas, M. A.; Hendrickson, C. L.; Emmett, M. R.; Marshall, A. G. *Int. J. Mass Spectrom.* **1999**, *185/186/187*, 565-575.
- 251 Campbell, S.; Rodger, M. T.; Marzluff, E. M.; Beauchamp, J. L. *J. Am. Chem. Soc.* **1994**, *116*, 9765-9766.
- 252 Campbell, S.; Rodgers, M. T.; Marzluff, E. M.; Beauchamp, J. L. *J. Am. Chem. Soc.* **1995**, *117*, 12840-12854.
- 253 Freitas, M. A.; Hendrickson, C. L.; Emmett, M. R.; Marshall, A. G. *J. Am. Soc. Mass Spectrom.* **1998**, *9*, 1012-1019.
- 254 Green, M. K.; Gard, E.; Bregar, J.; Lebrilla, C. B. *J. Mass Spectrom.* **1995**, *30*, 1103-1110.
- 255 Green-Church, K. B.; Limbach, P. A.; Freitas, M. A.; Marshall, A. G. *J. Am. Soc. Mass Spectrom.* **2001**, *12*, 268-277.
- 256 Freiser, B. S.; Woodin, R. L.; Beauchamp, J. L. *J. Am. Chem. Soc.* **1975**, *97*(23), 6893-6894.
- 257 Ranasinghe, A.; Cooks, R. G.; Sethi, S. K. *Org. Mass Spectrom.* **1992**, *27*, 77-88.
- 258 Hunt, D. F.; Yates, J. R. I.; Shabanowitz, J.; Winston, S.; Hauer, C. R. *Proc. Natl. Acad. Sci. USA* **1986**, *83*, 6233-6237.
- 259 Johnson, R. S.; Martin, S. A.; Biemann, K. *Int. J. Mass Spectrom. Ion Proc.* **1988**, *86*, 137-154.
- 260 Schwartz, B. L.; Bursery, M. M. *Biol. Mass Spectrom.* **1991**, *21*, 92.
- 261 Hunter, E. P. L.; Lias, S. G. *J. Phys. Chem. Ref. Data* **1998**, *27*(3), 413-656.
- 262 Biondi, M. A.; Brown, S. C. *Phys. Rev.* **1949**, *75*, 1700.
- 263 Bates, D. R. *Phys. Rev.* **1950**, *78*, 492.
- 264 Zubarev, R. A.; Kelleher, N. L.; McLafferty, F. W. *J. Am. Chem. Soc.* **1998**, *120*, 3265-3266.
- 265 Kruger, N. A.; Zubarev, R. A.; Horn, D. M.; McLafferty, F. W. *Int. J. Mass Spectrom.* **1999**, *185/186/187*, 787-793.
- 266 Zubarev, R. A.; Kruger, N. A.; Fridriksson, E. K.; Lewis, M. A.; Horn, D. M.; Carpenter, B. K.; McLafferty, F. W. *J. Am. Chem. Soc.* **1999**, *121*, 2857-2862.

- 267 Kelleher, N. L.; Zubarev, R. A.; Bush, K.; Furie, B.; Furie, B. C.; McLafferty, F. W.; Walsh, C. T. *Anal. Chem.* **1999**, *71*, 4250-4253.
- 268 Kruger, N. A.; Zubarev, R. A.; Carpenter, B. K.; Kelleher, N. L.; Horn, D. M.; McLafferty, F. W. *Int. J. Mass Spectrom.* **1999**, *182/183*, 1-5.
- 269 Shi, S. D.-H.; Hemling, M. E.; Carr, S. A.; Horn, D. M.; Lindh, I.; McLafferty, F. W. *Anal. Chem.* **2001**, *73*, 19-22.
- 270 McLafferty, F. W.; Horn, D. M.; Breuker, K.; Ge, Y.; Lewis, M. A.; Cerda, B.; Zubarev, R. A.; Carpenter, B. K. *J. Am. Soc. Mass Spectrom.* **2001**, *12*, 245-249.
- 271 Olsen, J. V.; Haselmann, K. F.; Nielsen, M. L.; Budnik, B. A.; Nielsen, P. E.; Zubarev, R. A. *Rapid Comm. Mass Spectrom.* **2001**, *15*, 969-974.
- 272 Ge, Y.; Lawhorn, B. G.; ElNaggar, M.; Strauss, E.; Park, J.-H.; Begley, T. P.; McLafferty, F. W. *submitted to J. Am. Chem. Soc.* **2001**.
- 273 Horn, D. M.; Ge, Y.; McLafferty, F. W. *Anal. Chem.* **2000**, *72*, 4778-4784.
- 274 Cerda, B. A.; Horn, D. M.; Breuker, K.; Carpenter, B. K.; McLafferty, F. W. *Eur. Mass Spectrom.* **1999**, *5*, 335-338.
- 275 Wyttenbach, T.; G., v. H.; Bowers, M. T. *Int. J. Mass Spectrom. Ion Proc.* **1997**, *165/166*, 377-390.
- 276 Kleinnijenhuis, A.; Duursma, M. C.; Breukink, E.; Heck, A.J.R.; Heeren, R. M. A. *In preparation*.
- 277 Zubarev, R. A.; Horn, D. M.; Fridriksson, E. K.; Kelleher, N. L.; Kruger, N. A.; Lewis, M. A.; Carpenter, B. K.; McLafferty, F. W. *Anal. Chem.* **2000**, *72*, 563-573.
- 278 Koster, S.; de Koster, C.G.; van Benthem, R.A.T.M.; Duursma, M.C.; Boon, J.J.; Heeren, R.M.A. *Int. J. Mass Spectrom.* **2001**, *210/211*, 591-602.

Glossary of symbols and abbreviations

amu	Atomic mass unit
AWG	Arbitrary waveform generator
CAD	Collisional activated dissociation
CRM	Charge residue model
D	Polydispersity
Da	Dalton
ECD	Electron capture dissociation
EO	Polyoxyethylene
ESI	Electrospray ionisation
FAB	Fast atom bombardment
FD	Field desorption
FT-ICR MS	Fourier transform ion cyclotron resonance mass spectrometry
GPEC	Gradient polymer elution chromatography
H/D	Hydrogen/deuterium
IE	Electrospray ionisation efficiency
IEM	Ion evaporation model
LCCC	Liquid chromatography at the critical point of adsorption
MALDI	Matrix-assisted laser desorption/ionisation
MeOH	Methanol
MWD	Molecular weight distribution
NMR	Nuclear magnetic resonance spectroscopy
PA	Proton Affinity
PEG	Polyethylene glycol
PET	Polyethylene terephthalate
PMMA	Polymethyl methacrylate
PO	Polyoxypropylene
PPG	Polypropylene glycol
PS	Polystyrene
PSD	Post source decay
PTHF	Polytetrahydrofurane
SEC	Size exclusion chromatography
SIMS	Secondary ion mass spectrometry
SORI	Sustained off resonance irradiation
THF	Tetrahydrofurane
TOF	Time-of-flight
$\nu(z)$	Statistical degree of freedom
σ_a^2	Uncertainty in the slope
σ_b^2	Uncertainty in the centre of gravity
σ_{data}^2	Uncertainty in the mass measurement
σ_{end}^2	Accuracy of the endgroup mass

σ_{data}	Uncertainty in the experimental data
$\sigma_{data,all}$	Weighted average of σ_{data} values over the different charge states
$\sigma_{end,regression}$	Uncertainty of endgroup mass determined with linear regression
$\Delta m_{mon,regression}$	Accuracy of monomer mass determination with linear regression
$\sigma_{mon,average}$	Uncertainty of monomer mass determined with averaging meth.
$\sigma_{mon,regression}$	Uncertainty of monomer mass determined with linear regression
\bar{n}	Transformed average degree of polymerisation
A	Peak area
B	Magnetic field
d	Diameter of the ICR cell
E	Electrical field
$E_{kin,com}$	Centre of mass collision energy
$E_{kin,lab}$	Laboratory frame kinetic energy
eV	Electronvolt
F_C	Centrifugal force
F_L	Lorentz force
I	Peak intensity
$I_{n,z}$	Intensity of an oligomer in charge state z
$I_{n,z}^{corr}$	Corrected intensity of an oligomer for number of charges z
m/z	Mass over charge ratio
m_{cat}	Mass of the cation
m_{elec}	Mass of an electron
m_{end}	Mass of the endgroup
$m_{end,average}$	Mass of endgroup determined with averaging method
$m_{end,exact}$	Exact endgroup mass
$m_{end,regression}$	Mass of endgroup determined with linear regression
$m_{end-cation,regression}$	Mass of the endgroup without the cation(s)
m_{exact}	Exact mass
m_{meas}	Measured mass
m_{mon}	Mass of the monomer unit
$m_{mon,exact}$	Exact monomer mass
$m_{mon,regression}$	Monomer mass determined with linear regression
M_n	Number average molecular weight
M_w	Weight average molecular weight
n	Degree of polymerisation
N	Number of data points
$n(M)$	Number fraction of a specific oligomer in the MWD
$N(M)$	Calculated molar fraction of adipic acid
$P(I)$	Calculated molar fraction of isophthalic acid
$P(n)$	Probability of finding an oligomer containing only ^{12}C
P_n	Number average degree of polymerisation
q	Charge
r	Radius of the ions in the ICR cell
t_{exc}	Excitation time
v	Velocity of the ion
V_{pp}	Peak-to-peak voltage
V_T	Trapping potential

Glossary of symbols and abbreviations

$w(M)$	Weight fraction of a certain oligomer
z	Charge state
α	Geometry constant of the ICR cell
τ_i	Damping constant of time domain signal
ω_c	Cyclotron frequency
ω_T	Trapping frequency

Summary

Synthetic polymers are generally very complex mixtures of molecules that vary in length, monomer, endgroup, chemical composition, sequence and branched structure. Many of the techniques that are used for polymer characterisation provide invaluable information about the *average* composition of polymers. However, for a more detailed structural analysis of the individual polymer molecules, a separation of most molecules in the complex polymer mixtures is necessary. Although a limited number of techniques is available that can separate the many components that constitute synthetic polymers, Fourier transform ion cyclotron resonance mass spectrometry (FT-ICR MS) would be very suitable for this purpose. This thesis reports studies on the electrospray ionisation (ESI) FT-ICR MS applied to characterise synthetic polymers. An overview of the literature published in the last decade on polymer characterisation with matrix-assisted laser desorption/ionisation (MALDI) and ESI mass spectrometry is given in chapter 1. The theoretical concepts and operating principles of the ESI FT-ICR MS used for the investigation in this thesis are described in chapter 2. It will be demonstrated that ESI FT-ICR MS contributes significantly to an improved characterisation of synthetic polymers. The unsurpassed resolution, mass accuracy and ion storage possibilities of FT-ICR MS enables the determination of structural characteristics of polymers with a molecular weight up to 10.000 Da.

Most polymers have a broad molecular weight distribution (MWD) as a result of the statistical nature of the polymerisation process. Complex mass spectra are often obtained when a polymer is analysed with ESI MS because ESI generates multiple charge states. A MWD that is observed in multiple charge states will result in many overlapping peaks in the mass spectrum. Many of these overlapping peaks can be resolved for polymer molecules up to a molecular weight of 10.000 by high resolution mass spectrometry such as FT-ICR MS as described in chapter 3. Mass spectra acquired with a high resolution give insight into the shape and molecular weight of the polymer distribution. Calculating the number average molecular weight (M_n) for each charge state separately leads to an increase of the calculated M_n with the charge state. Despite this effect, an M_n can be determined with a reasonable accuracy (<10%) for polymers with a molecular weight <8.000 Da and polydispersity <1.1 by combining all charge states that are observed with ESI compared with the M_n obtained with MALDI TOF.

A high resolution as well as a high mass accuracy can be achieved with FT-ICR MS as demonstrated in chapter 4 for the same poly(oxyalkylene)s as described in chapter 3. Isotopically resolved analysis, as obtained with FT-ICR MS, is required for the accurate determination of the monomer and endgroup mass using linear regression. By combining the multiple charge states generated by ESI, the endgroup and monomer masses can be determined with a high precision. The precision of this procedure is higher than using the single charge state observed with MALDI FT-ICR MS because more data points are available. Endgroup and monomer masses can be deduced directly from a mass spectrum. The procedure does however not provide the mass of both endgroups separately. A way to determine the mass of the two endgroups separately is by fragmentation of the polymer molecules into smaller fragments with for example collisionally activated dissociation (CAD). This research was not further pursued in this thesis.

The polymers discussed in chapter 3 and 4 consist of one type of monomer. Copolymers on the other hand consist of different types of monomers, which can be arranged on polymer molecules in a specific sequence, for example a block sequence. A major complication in the analysis of copolymers is that copolymer molecules with a given mass can be constituted of a series of isomeric molecules, i.e. with the same mass but a different arrangement of the monomers along the linear chain. This makes the structural determination of such polymers much more complex. Several studies are reported in the literature that apply Bernoullian and Markovian chain statistics to mass spectra to obtain information on the possible arrangement of monomers in a copolymer. Chapter 5 shows that this method is very sensitive to variations in the structure of the monomer, the endgroup, the type of solvent, the spray conditions and other parameters using well-defined mixtures of homopolymers. It is almost impossible to determine the influence of each of these parameters on the mass spectrometric response. Without this knowledge, the sequence analysis using chain statistics cannot be done. To obtain information on the linear arrangement of the monomers, the polymer molecules can be selectively fragmented using collisionally activated dissociation (CAD) as discussed in chapter 6 and 7 for copolyesters and hyperbranched polyesteramides. Due to the many different permutations of the monomers along chains, such fragmentation studies do not provide enough sequence specific fragments to identify all possible isomeric structures. Synthetic polymers differ fundamentally in this way from proteins, which have only one isomeric structure. It should be possible to determine whether the copolymer has a block sequence by CAD fragmentation studies provided that internal fragmentation is absent. The MS/MS spectrum of such copolymer sequences is expected to contain a high number of fragment ions with a block structure. Such a study could however not be pursued in this thesis, because the copolymers studied in this thesis do not have a block sequence, as was

deduced from the MS² spectra. The results of the investigations presented in chapter 6 point out that polymers with a random or partly random/block structure cannot be distinguished with CAD fragmentation studies.

A polymer mass spectrum generated with MALDI or ESI is often considered to be a reflection of the molecular distribution. That this is not always true became clear from a MALDI study of hyperbranched polyesteramides reported in the literature. This study demonstrated that MALDI did induce fragmentation during the ionisation process. Ions with the same mass as the fragments observed with MALDI were observed with ESI FT-ICR MS analysis of the same polymers described in chapter 7. It was not possible to determine *directly* from the mass spectrum whether the ions originate from fragmentation in the ESI source or from the polymer sample. The MS³ study reported in chapter 7 demonstrates that the ion series is not due to mass spectrometric fragmentation but due to molecules formed during the polymerisation reaction.

Identification of isomeric structures poses a problem because isomers have the same mass but can have a completely different structure. Hyperbranched polymers are examples of isomers that can be linear or branched but still have the same mass. The novel MSⁿ methodology, Dissociation of Depleted Ion Populations (DoDIP), introduced in chapter 8 allows the distinction between different isomeric structures. The ion mixture that consists of different isomeric structures is fragmented in a first MS/MS step with relatively low collision energy. Structurally more stable isomeric ions that fragment at higher appearance energy are concentrated in the gas phase. A second MS/MS step is used to fragment the preconcentrated parent ion to see whether different isomeric structures are present by comparing the first MS/MS spectrum with the second. DoDIP experiments made it possible to distinguish between isomeric structures of hyperbranched polyesteramides with an alternating and non-alternating sequence. Chapter 8 introduces also another methodology that allows the study of different isomeric structures using gas phase hydrogen/deuterium (H/D) exchange. Isomeric structures are separated in the gas phase on the basis of a difference in the proton affinity of the different isomers. Isomeric structures with a non-alternating sequence have a relatively high proton affinity and will not exhibit H/D exchange behaviour. Isomeric structures with an alternating sequence have a relatively low proton affinity and exchange their exchangeable hydrogen's with deuterium. This enables the separation of the two isomeric structures. Both methods, DoDIP and H/D exchange, provide information about alternating and non-alternating isomeric structures.

The last chapter in this thesis, chapter 9, concerns the fragmentation behaviour of hyperbranched polyesteramides with electron capture dissociation (ECD) in the ICR cell. Several studies on biomolecules have shown that ECD is a

complementary method to CAD for the determination of the arrangement of amino acids along a peptide chain. Chapter 9 shows that ECD is not complementary to CAD for the sequence analysis of relatively small hyperbranched polyesteramide oligomers mainly because internal fragmentation processes are pronounced. The ion fragments after an electron is captured but this process results in fragments with an excess internal energy. This excess internal energy causes the fragment ion to undergo consecutive cleavages resulting in internal fragments. Such internal fragments make the interpretation of ECD spectra less straightforward compared to the ECD spectra of, for example, proteins. The different type of fragmentation process that is observed upon ECD can be used to obtain information about other structural characteristics of polymers.

Samenvatting

Synthetische polymeren zijn over het algemeen zeer complexe mengsels van moleculen die verschillen in lengte, type monomeer en eindgroep, chemische samenstelling, sequentie en vertakkingsgraad. Veel van de technieken die gebruikt worden voor het karakteriseren van polymeren leveren informatie over de gemiddelde samenstelling. Voor een gedetailleerde analyse van alle bovengenoemde structurele eigenschappen is een scheiding van de meeste moleculen in het complexe polymeermengsel nodig. Er is daartoe maar een beperkt aantal technieken beschikbaar waarmee men in staat is om de meeste componenten van een polymeer te scheiden. Fourier transformatie ionen cyclotron resonantie massaspectrometrie (FT-ICR MS) is hiervoor zeer geschikt. In dit proefschrift wordt de studie van synthetische polymeren met behulp van electrospray ionisatie (ESI) FT-ICR MS beschreven. Een overzicht van de literatuur gepubliceerd gedurende de laatste tien jaar over polymeerkarakterisering, met matrix geassisteerde laserdesorptie/ionisatie (MALDI) en ESI massaspectrometrie, is beschreven in hoofdstuk 1. De theorie achter ESI FT-ICR MS en de experimentele opstelling zijn beschreven in hoofdstuk 2. In dit proefschrift wordt aangetoond dat ESI FT-ICR MS een significante bijdrage levert aan de karakterisering van synthetische polymeren. De onovertroffen resolutie, massanauwkeurigheid en de mogelijkheid om ionen voor langere tijd op te slaan in de ionenval dragen ertoe bij dat structurele eigenschappen van polymeren met een moleculaire massa tot 10.000 Da kunnen worden bepaald.

De meeste polymeren hebben een breed verdeelde moleculaire gewichtsdistributie (MWD) die een gevolg is van de statistische aard van het polymerisatie proces. Een massaspectrum, gemeten met ESI massaspectrometrie, is zeer complex omdat tijdens het ESI proces de MWD geconvolveerd is met de verschillende ladingstoestanden, hetgeen resulteert in veel overlappende pieken in het massaspectrum. De meeste van deze overlappende pieken kunnen worden onderscheiden door gebruik te maken van een massaspectrometer met een hoog oplossend vermogen zoals de FT-ICR MS. Met deze techniek kunnen ionen van verschillende polymeermoleculen met een massa tot 10.000 Da nog van elkaar worden onderscheiden, zoals is gebleken in deze studie beschreven in hoofdstuk 3. Massaspectra, die worden gemeten met een hoge resolutie, leveren inzage in de vorm en het gewicht van de polymeerdistributie. Als het zogenoemde aantalgemiddelde moleculaire gewicht (M_n) wordt berekend, blijkt dat deze

toeneemt met de waargenomen ladingstoestand. Dit wordt veroorzaakt door het aantal beschikbare zuurstofatomen van de polymeermoleculen waarmee het cation een interactie kan hebben. In hoofdstuk 3 wordt gedemonstreerd hoe een redelijk nauwkeurige M_n waarde kan worden berekend (<10%) voor polymeren met een moleculair gewicht <8.000 Da en polydispersiteit <1.1 door de metingen van alle waargenomen ladingstoestanden met elkaar te combineren.

Met FT-ICR MS kan een hoge resolutie en hoge massanauwkeurigheid behaald worden, zoals beschreven in hoofdstuk 4. Een hoge massanauwkeurigheid, waarmee de polymeermoleculen met FT-ICR MS gemeten kunnen worden, is nodig om de monomeer- en eindgroepmassa nauwkeurig te kunnen bepalen met behulp van lineaire regressie. De nauwkeurigheid van deze bepaling kan worden verhoogd door de verschillende ladingstoestanden, die worden gegenereerd met ESI, te combineren in één procedure. De nauwkeurigheid is hoger dan wanneer gebruik gemaakt wordt van MALDI FT-ICR MS waarbij maar één ladingstoestand wordt gegenereerd. Dit komt door het grotere aantal datapunten dat beschikbaar is met ESI om de lineaire regressieprocedure toe te passen. Het is niet mogelijk met deze procedure de massa van de beide eindgroepen afzonderlijk te bepalen. Een potentiële manier om die informatie toch te krijgen is, door de ionen van polymeermoleculen in kleinere fragment ionen te fragmenteren, met bijvoorbeeld botsing geïnduceerde dissociatie (CAD).

De polymeren, beschreven in hoofdstuk 3 en 4, bestaan uit één type monomeer. Co-polymeermoleculen zijn opgebouwd uit twee verschillende types monomeren. Deze monomeren kunnen op verschillende manieren zijn gerangschikt in het co-polymeer molecuul: de sequentie. Een voorbeeld is een blok co-polymeer, waarbij dezelfde type monomeren zich naast elkaar bevinden. Een complicatie van een massaspectrometrische analyse aan co-polymeren is dat er co-polymeermoleculen bestaan die dezelfde massa hebben, maar een verschillende rangschikking van monomeren. Dit maakt de analyse veel ingewikkelder. Verschillende onderzoeken zijn in de literatuur beschreven waarbij Bernoulliaanse en Markoviaanse statistiek wordt toegepast op massaspectra, teneinde informatie over de mogelijke typen rangschikkingen van monomeren te bepalen. Hoofdstuk 5 laat zien dat, in het geval van mengsels van homo-polymeren, deze methode zeer gevoelig is voor variaties in de structuur van het monomeer, de eindgroep, het type oplosmiddel, de ESI condities en andere parameters. Het is dan bijna onmogelijk om de invloed van elk van deze parameters op een massaspectrometrisch signaal te bepalen. Zonder de wetenschap van al deze invloeden kan de rangschikking van de monomeren op co-polymeermoleculen niet berekend worden. Er is een andere methode om een indruk te krijgen van de rangschikking van de monomeren op een co-polymeermolecuul. Met deze methode wordt gebruik gemaakt van botsing geïnduceerde dissociatie (CAD), zoals beschreven in hoofdstuk 6 en 7, voor

copolyesters en hoogvertakte polyesteramides. Zulke ion fragmentatiestudies leveren, als gevolg van het grote aantal mogelijke permutaties van de monomeren over de polymeermoleculen, niet genoeg sequentiespecifieke fragmenten om alle mogelijke isomere structuren aan te tonen. Dit is in tegenstelling tot biomoleculen die maar één mogelijke sequentie hebben. Wel moet het mogelijk zijn om met CAD te bepalen of de monomeren een blokstructuur hebben. Van de fragmenten, die na CAD gemeten worden in een massaspectrum, zullen er een groot aantal een blokstructuur hebben. In hoofdstuk 6 en 7 is aangetoond dat de in dit proefschrift onderzochte co-polymeren géén blokstructuur hebben. De resultaten die zijn beschreven in hoofdstuk 6 laten zien dat polymeren met een random of gedeeltelijke random/blokstructuur niet van elkaar te onderscheiden zijn met CAD fragmentatiestudies.

Een massaspectrum van een polymeer, dat met MALDI en ESI wordt verkregen, wordt vaak beschouwd als een afbeelding van de moleculaire polymeerdistributie. Dat dit niet altijd het geval is, blijkt duidelijk uit een onderzoek aan hoogvertakte polyesteramides met MALDI en ESI, wat beschreven is in de recente literatuur. Deze studie toont aan dat fragmentatie van de polymeermoleculen plaatsvindt tijdens het MALDI proces. Ionen, met dezelfde massa als de fragmenten die met MALDI werden waargenomen, werden tevens tijdens de ESI FT-ICR MS analyse van dezelfde polymeren waargenomen zoals beschreven in hoofdstuk 7. Het is niet mogelijk om direct uit het massaspectrum te bepalen of deze ionen het gevolg zijn van fragmentatie tijdens het ESI proces of dat ze in het oorspronkelijke polymeer aanwezig waren. De MS^3 experimenten, beschreven in hoofdstuk 7, bewijzen dat deze ionen niet het gevolg zijn van fragmentatie tijdens het ESI proces, maar dat ze tijdens de polymerisatiereactie gevormd worden.

Identificatie van isomere structuren met massaspectrometrie kan een probleem zijn daar dit soort moleculen weliswaar dezelfde massa hebben, maar volledig anders van structuur kunnen zijn. Een illustratief voorbeeld van isomere structuren treedt op bij hoogvertakte polyesteramides die zowel lineair als vertakt kunnen zijn maar toch dezelfde massa hebben. Zowel de lineaire als vertakte isomeren kunnen nog meer typen isomere structuren bevatten. De nieuwe MS^n methode, dissociatie van uitgedunde ionenpopulaties (DoDIP) geïntroduceerd in hoofdstuk 8, maakt het mogelijk om verschillende isomere structuren van elkaar te onderscheiden op basis van een verschil in stabiliteit tijdens laagenergetische botsingen. Met laagenergetische CAD wordt het ionenmengsel gefragmenteerd dat bestaat uit verschillende isomere structuren. Isomere ionen, die een stabielere structuur hebben, zullen pas bij een hogere botsingsenergie fragmenteren. Deze ongefragmenteerde, stabielere isomeren worden in de gasfase geconcentreerd. Een tweede CAD experiment, met iets hogere botsingsenergie, wordt toegepast op de

geconcentreerde ionenpopulatie om te zien of dezelfde of andere fragmenten worden gevormd. Door de resultaten van twee experimenten met elkaar te vergelijken, kan worden geconcludeerd of er verschillende isomere structuren aanwezig zijn. Met deze DoDIP experimenten was het mogelijk om onderscheid te maken tussen isomeren met een alternerende en niet-alternerende sequentie. In hetzelfde hoofdstuk wordt een andere methode beschreven die het mogelijk maakt om verschillende isomere structuren van elkaar te onderscheiden. Met deze methode wordt gebruik gemaakt van waterstof/deuterium (H/D) uitwisseling in de gasfase. Isomere structuren kunnen worden gescheiden door een verschil in protonaffiniteit. Isomere structuren met een niet-alternerende sequentie hebben een relatief hoge protonaffiniteit en zullen zeer langzaam H/D uitwisselingsgedrag vertonen. Daarentegen zullen isomere structuren met een alternerende sequentie een relatief lage protonaffiniteit hebben en wel H/D uitwisselingsgedrag vertonen, waardoor de twee isomere structuren van elkaar gescheiden kunnen worden. Beide methoden, DoDIP en H/D uitwisseling, laten zien dat verschillende isomeren gescheiden kunnen worden en geven daarnaast elkaar aanvullende informatie over alternerende en niet-alternerende isomere structuren.

Het laatste hoofdstuk in dit proefschrift, hoofdstuk 9, is een studie naar het fragmentatiegedrag van hoogvertakte polyesteramides door de invangst van een elektron (ECD). Verschillende studies met biomoleculen hebben aangetoond dat ECD complementair is aan CAD voor het bepalen van de sequentie van de aminozuren van een biomolecuul. Het hier beschreven onderzoek laat zien dat ECD in het geval van kleine hoogvertake polymeren niet complementair is aan CAD indien men alleen geïnteresseerd is in de sequentie. Dit wordt voornamelijk veroorzaakt door de vorming van interne fragmenten die de interpretatie van de ECD massaspectra bemoeilijken, wat niet het geval is voor biomoleculen. De vorming van interne fragmenten kan verklaard worden door de hoge hoeveelheid interne energie die achterblijft in de fragmenten na invangst van het elektron. Dit resulteert in het verbreken van een extra binding op één van de fragmenten ionen waarbij een zo genoemd intern fragment wordt gevormd. Desondanks wordt er met ECD een heel ander type fragmentatieproces waargenomen welke, naast CAD, additionele informatie oplevert over andere structurele eigenschappen van polymeren.

Dankwoord

Hoogst waarschijnlijk heb ik de indruk gewekt, dat dit boekje het resultaat is van mijn geploeter alleen. Dat is zeer zeker niet het geval, aangezien velen mij hebben geholpen. Allereerst wil ik mijn promotor Ron Heeren bedanken, die een regelmatig door Marc en mij ‘dood verklaarde’ FT-MS weer springlevend maakte. Ron heeft een grote wetenschappelijke bijdrage geleverd aan mijn werk.

Dit proefschrift zou kop noch staart hebben gehad als mijn andere promotor, Jaap Boon, niet zo kritisch was geweest. Ik wil hem, voornamelijk voor de hulp bij het schrijfwerk, hartelijk bedanken.

Marc Duursma heeft mij de afgelopen vier jaar enorm geholpen met mijn experimenten op de FT-MS. Volgens mij kwam hij die bewuste maandag niet toevallig op het lab, terwijl hij vrij was, maar wist hij gewoon dat ik de stikstof was vergeten. Anderen, die ik wil bedanken voor de hulp met de FT-MS, zijn Ton Vijftigschild, Sjoerd Wouda, Ad de Snaijer, Xinghua Guo en Ilja Stavenuiter.

De sponsors van mijn project, Akzo Nobel Chemicals Research Arnhem en DSM Research in Geleen, dank ik voor de extra financiële ondersteuning om dit project mogelijk te maken. Chris de Koster, Michel Nielen en in het laatste jaar Pieter van Woerkom dank ik voor hun wetenschappelijke bijdragen aan dit project. De halfjaarlijkse bijeenkomsten waren voor mij zeer nuttig. En toch denk ik nog steeds, dat die (bio)polymeren een goede tussenzet waren.

Harry Philipsen wil ik bedanken voor de interessante discussies en de polyesters, die hij beschikbaar stelde. Overigens heb ik die polymeren met behulp van Jan van Velde van de Akzo kunnen GPEC ESI-TOF'en. Mijn dank daarvoor. Steen Ingemann wil ik danken voor de bijdrage aan de mechanistische interpretatie van het ECD werk in dit proefschrift. Steen is nu typisch zo iemand die ik eigenlijk eerder bij mijn werk betrokken zou moeten hebben. De discussies die ik met hem heb gehad waren zeer nuttig.

De afgelopen vier jaren is mij gebleken dat er binnen de muren van het AMOLF heel veel mogelijk is. Dat werd voor mij extra duidelijk toen ik met Bela Mulder in gesprek raakte over MS aan co-polymeren. Dit leidde tot een aantal discussies waardoor een opzet is gemaakt voor vervolgonderzoek. Nu alleen de experimenten nog!

Gedurende twee jaar ben ik (gebombardeerd) voorzitter geweest van het IRC, waar ik heb mogen kijken achter de schermen van AMOLF en de FOM organisatie. Deze periode heb ik als zeer nuttig en plezierig ervaren, waarvoor ik Wim, Ben, Hans, Bela, Martijn, Lenneke, Piet, Yumna, Christiaan, Dirk en Gerbrand wil bedanken.

Mijn mede kippenhokbewoners en de overige Macromollers dank ik voor de gezellige tijd in o.a. de brouwerij: Jorrit, Georgiana, Nick, Gies, Oscar, Bea, Stefan (ook voor de filosofische gesprekken ?), Frank, Jerre, Klaas-Jan, Jaap, Linda, Ad, Liz, Annebeth (tevens voor het carpoolen samen met Marc), Pete, Laszlo, Krisztina, Vincent, Marcel, Janine, Leo, Muriël, Jan, Ron, Jaap, Theo, Marc, Gert, Gerard, Tina, Lidwien, Donna, Han, Katrien, Petra, Wim, Dominique, Bea, Frans, Anne, Annelies, Ahmed, Piet en Krista. Iliya Cerjak wil ik bedanken voor de hulp bij het ontwerpen van de cover.

Zowel mijn ouders als Tamara wil ik bedanken voor de onvoorwaardelijke steun en stimulans die ze mij tijdens mijn studie en promotieonderzoek hebben gegeven. Zonder hen was dit boekje nooit verschenen.

Sander, 3 december 2001